CO_2-Selective Thin-Film Polymer Composite Membranes: Improvement of Thermal Stability and Role of Amine Carriers

A Thesis
Submitted in Partial
Fulfillment of the Requirements for the Degree of

DOCTOR OF PHILOSOPHY

by

Arijit Mondal

Department of Chemical Engineering
Indian Institute of Technology Guwahati
Guwahati 781039, Assam, India

July 2014

Dedicated

To

My parents and my mentor

Department of Chemical Engineering
Indian Institute of Technology Guwahati
Guwahati 781039, Assam, India

CERTIFICATE

It is certified that the work contained in this thesis entitled **"CO_2-Selective Thin-Film Polymer Composite Membranes: Improvement of Thermal Stability and Role of Amine Carriers"** submitted by **Mr. Arijit Mondal** for the award of the degree of Doctor of Philosophy has been carried out in Department of Chemical Engineering, Indian Institute of Technology Guwahati under my supervision and this work has not been submitted elsewhere for the award of any other degree or diploma.

This thesis in my opinion, has reached the standard fulfilling the requirements for the award of the degree of Doctor of Philosophy in accordance with the regulations of the institute.

(**Dr. Bishnupada Mandal**)
Professor
Department of Chemical Engineering
Indian Institute of Technology Guwahati
Guwahati 781039, India

ACKNOWLEDGEMENTS

I express my sincere thanks to my research supervisor **Prof. Bishnupada Mandal** for his valuable guidance towards the completion of my research work. His continuous support towards research and given me enough freedom to think, plan and execute my ideas towards my work, which has provided a good basis for the present thesis. I would like to thank him for spending his precious time for discussion by which I have gained immense skills of knowledge in terms of research. I am also indebted to Prof. Bishnupada Mandal for instilling in me a craving for perfection. I believe, it will always remain with me in my future life. It has really been a notable working experience with him.

Besides my supervisor, I would like to thank my doctoral committee members, **Prof. A.K. Ghoshal, Dr. Mihir Kumar Purkait,** Department of Chemical Engineering and **Dr. Parameswar K. Iyer,** Department of Chemistry, for their valuable suggestion and effort which made my thesis successful. I am also grate full to the **Staffs** of Department of Chemical Engineering for providing me necessary facilities.

My special thanks to **Dr. Sasidhar Gumma** of Chemical Engineering Department for his experience and helping nature in several ways of my Ph.D life.

I acknowledge with thanks to the **Central Instruments Facility**, Department of **Chemistry** of IIT Guwahati for providing me the necessary instrument facility which has been very important in this research work.

ACKNOWLEDGEMENTS

I was fortunate enough to get excellent and close friends like**, Mahesh Kumar Gagrai, Mriganka Sekhar Manna, Sanjib Barma** and **Swarnadeep Acharyya** for their friendly support and helping nature during my stay in IITG.

I would like to thank all my **seniors**, **juniors**, **friends** and other **well-wishers** whoever making my stay in IITG memorable.

Finally, I express my gratitude to my beloved **parents, sister, auntie** and **Gargi Deb** for showering their love, care, sacrifice and encouragement which have made it possible for me to come so for.

Arijit Mondal

July 2014

Vitae

Arijit Mondal

Permanent Address 22, Garfa Sitala Mondir Road, Kolkata – 700075, West Bengal, India.

Email ari.info4u@gmailcom
a.mondal@iitg.ernet.in

Date of birth 02/04/1983

Education

- ***Ph.D Student (Research Scholar)***
  Department of Chemical Engineering
  Indian Institute of Technology Guwahati
  Guwahati, Assam, India
  (2008-2014)
- ***M.E (Chemical Engineering)***
  (First Class)
  Department of Chemical Engineering
  Jadavpur University, West Bengal, India
  (2006-2008)
- ***B.Tech (Chemical Engineering)***
  (First Class)
  Department of Chemical Engineering
  Haldia Institute of Technology, West Bengal, India
  (2002-2006)

Achievements *Qualified in GATE 2006*

LIST OF PUBLICATIONS

Published/Accepted Articles in International Refereed Journals

1. **Mondal, A**. **a**nd Mandal, B. **(2014)**. CO_2 separation using thermally stable crosslinked poly(vinyl alcohol) membrane blended with polyvinylpyrrolidone / polyethyleneimin / tetraethylenepentamine. ***Journal of Membrane Science,*** 460, 126-138. Impact Factor: 4.093 **(Elsevier)**.

2. **Mondal, A**. **a**nd Mandal, B. **(2013)**. Synthesis and characterization of crosslinked poly(vinyl alcohol)/poly (allylamine)/2-amino-2-hydroxymethyl-1,3-propanediol/polysulfone composite membrane for CO_2/N_2 separation. ***Journal of Membrane Science***, 446, 383-394. Impact Factor: 4.093 **(Elsevier)**.

3. Muraleedharan, R., **Mondal, A**. and Mandal, B. **(2012)**. Absorption of Carbon Dioxide into Aqueous Blends of 2-Amino-2-hydroxymethyl-1,3-propanediol and Monoethanolamine. ***Separation and Purification Technology***, 94, 92-96. Impact Factor: 2.894 **(Elsevier)**.

Communicated/Under Review in Refereed International Journals

4. **Mondal, A**. and Mandal, B. A novel CO_2-Selective crosslinked poly(vinyl alcohol) / polyvinylpyrrolidone blend membrane containing amine carrier for CO_2/N_2 separation: synthesis, characterization and gas permeation study. **(under review)**.

Conference Presentations (National and International)

1. **Mondal, A**., Mandal, A., Barooah, M. and Mandal. B. (2013). Synthesis and characterization of crosslinked poly(vinylalcohol) / polyethyleneimine / tetraethylenepentamine / polyvinylpyrrolidone / polysulfone composite membrane. **Indian Chemical Engineering Congress (CHEMCON 2013),** Dec 27-30, Mumbai, INDIA.
2. **Mondal, A.** and Mandal, B. (2013). Synthesis and characterization of crosslinked poly(vinylalcohol)/polyethyleneimine/pentaethylenehexamine/polyvinylpyrrolidone/polysulfone composite membrane for CO_2/N_2 separation. **The Energy System Modeling and Optimization Conference (ESMOC 2013)**, Dec 9-11, Durgapur, INDIA.
3. Deogam, B., Das, B., **Mondal, A.**, Barma, S. and Mandal, B. (2013). Absorption of Carbon Dioxide into Piperazine Activated Aqueous Diethanolamine. The **Energy System Modeling and Optimization Conference (ESMOC 2013)**, Dec 9-11, Durgapur, INDIA.
4. Gupta, N., Das, B., Deogam, B., **Mondal, A.**, Barma, S. and Mandal, B. (2013). Modelling and simulation for post-combustion carbon dioxide capture from power plant flue gas with economic analysis. **The Energy System Modeling and Optimization Conference (ESMOC 2013)**, Dec 9-11, Durgapur, INDIA.
5. **Mondal, A.,** Mandal, A., Barooah, M. and Mandal. B. (2013). Facilitated transport of CO_2 in novel crosslinked poly(vinylalcohol) / polyethyleneimine / tetraethylenepentamine / polyvinylpyrrolidone/polysulfone composite membrane. **"International Symposium on Membranes and Applications", CSIR-Central Glass and Ceramic Research Institute, Govt. of India (ICMA 2013),** Nov 22-23, Kolkata, INDIA.

6. **Mondal, A**., Barma, S. and Mandal, B. (2012). Synthesis and Characterization of thin-film-composite polymeric membranes containing Amine carrier. To be presented in the Indian Chemical Engineering Congress (**CHEMCON 2012**), Dec 27-30, Jalandhar, INDIA.
7. Barma, S., **Mondal, A**. and Mandal, B. (2012). Synthesis and Characterization of MCM-48 Materials at different Aging Time. To be presented in the Indian Chemical Engineering Congress (**CHEMCON 2012**), Dec 27-30, Jalandhar, INDIA
8. **Mondal, A**. and Mandal, B. (2012). Improvement of thermal stability of poly(vinyl alcohol) membrane by using crosslinking agent and polymer blending. **International Symposium on Processing and Fabrication of Advanced Materials (PFAM-21)**, Dec 10-13, IIT Guwahati, INDIA.
9. **Mondal, A**. and Mandal, B. (2010). Synthesis and Characterization of Crosslinked poly (vinyl alcohol) membrane containing blended amine carrier. The Indian Chemical Engineering Congress (**CHEMCON 2010**), Dec 27-29, Annamalainagar, INDIA.
10. Muraleedharan, R., **Mondal, A**. and Mandal, B. (2010). Kinetics of reaction of carbon dioxide with aqueous blends of 2-amino 2-hydroxymethyl 1,3-propanediol and monoethanolamine. The Indian Chemical Engineering Congress (**CHEMCON 2010**), Dec 27-29, Annamalainagar, INDIA.
11. Muraleedharan, R., **Mondal, A**. and Mandal, B. (2010). Density and viscosity of aqueous blends of 2-Amino 2-hydroxymethyl 1,3-propanediol and monoethaanmine. The Indian Chemical Engineering Congress (**CHEMCON2010),** Dec 27-29, Annamalainagar, INDIA.

12. **Mondal, A**. and Mandal, B. (2010). Synthesis and Characterization of Crosslinked poly (vinyl alcohol) membrane containing sterically hindered amine carrier. **Frontiers in Chemical Sciences (FICS 2010)**, Dec 3-4, IIT Guwahati, INDIA.

ABSTRACT

The overall objective of this work is to develop a simple process to separate carbon dioxide (CO_2) from a fossil fuel combustion gases using thin-film composite dense polymeric membrane containing amine carrier. Main focus of this project is to improve the membrane permeability along with high CO_2/N_2 selectivity at elevated temperature (> 100^oC) against low pressure difference (ΔP is around 1 atm) which is essentially close to the flue gas emitting condition from thermal power plant. Poly(vinyl alcohol) (PVA) was used as basic polymeric material due to its excellent hydrophilic nature and good film-forming ability. Thermal stability of PVA has been improved by crosslinking with formaldehyde (HCHO) and polymer blending with thermally stable polymer like polyvinylpyrrolidone (PVP). The optimum degree of crosslinking of PVA with formaldehyde was 60 mole%. The PVA/PVP weight percent ratio was chosen as 1:0.2. Different combinations of single and blended amines were introduced into the polymer hydrogel to enhance the CO_2 transport property through the membrane. These amines were polyethyleneimine (PEI), tetraethylenepentamine (TEPA), pentaethylenehexamine (PEHA), poly(allylamine) (PAA) and 2-amino-2-hydroxymethyl-1,3-propanediol (AHPD).

The synthesized dry membranes were characterized with TGA, DSC, FTIR and XRD. All the characterizations were done for active layer only which was found to be optically transparent to visible light and mechanically stable to be handled. Each TGA curve showed three main steps of weight loss. The first weight loss was due to the evaporation

of absorbed moisture from the atmosphere. The second weight loss was presumably due to the removal of hydroxyl groups or amine. The final weight loss was due to decomposition of the polymer backbones. The melting temperature (T_m) and glass transition temperature (T_g) were determined by using DSC analysis. T_g and T_m were improved after crosslinking and polymer blending. But after addition of the amine carrier to the polymer hydrogel the T_g was slightly reduced. The X-ray diffraction pattern for all the amine doped membranes obtained by XRD analysis displayed a semi-crystalline structure with peaks at 2Θ angles of 20^o.

Gas stream containing 20% CO_2 and 80% N_2 by volume was used to study the transport properties (CO_2 and N_2 fluxes, CO_2 and N_2 permeabilities, and CO_2/N_2 selectivity) across the membrane. The effects of active layer thickness, feed absolute pressure (1.7 to 6.2 atm), temperature (90 to 125^oC), and sweep side water flow rate (0.02 to 0.075 cm^3/min) on transport properties across the membrane were analyzed. The dense layer containing amine carrier displays both high selectivity and permeability. Several membrane have been synthesized for the gas permeation. The crosslinked-PVA-PVP membrane containing 25wt% PAA and 15wt% AHPD with 44 μm active layer thickness showed maximum CO_2/N_2 selectivity of 432 and CO_2 permeability of 1825 Barrer at 1.3 atm absolute pressure difference (ΔP), 100^oC temperature and 0.03/0.04 ml/min feed/sweep water flow rate.

CONTENTS

LIST OF TABLES

LIST OF FIGURES

Chapter 1

CO_2 CAPTURE AND EMISSIONS OVERVIEW, LITERATURE REVIEW AND OBJECTIVES

This chapter presents a discussion on emission of CO_2 and its impact on environmental pollution and greenhouse effect. It also discusses the features of different membrane based technologies for CO_2 separation. It elaborates the background of the research work. Importance and objectives of the present work are highlighted in this chapter. The chapter subsequently presents detailed literature review that includes facilitated transport of CO_2 through dense polymeric membrane containing different single and blended amine carriers.

1.1 INTRODUCTION AND OVERVIEW OF CO_2 EMISSIONS

Global warming, a subject of increased emphasis for the recent years, is believed to be caused by the emission of greenhouse gases. Greenhouse gases (GHGs) trap the heat radiating from the surface of earth when solar energy is being transmitted through the atmosphere and thus, increase the global surface temperature. As estimated by the

researchers, the global average surface temperature has increased between 0.6 and 1.0^{o}C during the last 150 years [1]. As a result of global warming, melting icebergs in polar oceans causes sea level to rise globally [2]. The Intergovernmental Panel on Climate Change (IPCC) predicts that the sea level will rise by 0.09 to 0.88 meters from 1990 to 2100 [1], which is a matter of extreme concern as 25% of world's population is living less than 1.1 meters above sea at present. Other alarming consequences of global warming includes drought, expansion of desert, heat wave, disrupted ecosystem, increasingly severe weather and loss of agricultural productivity.

GHGs include carbon dioxide (CO_2), water vapor (H_2O), ozone (O_3), methane (CH_4), nitrous oxide (N_2O), and chlorofluorocarbons (CFCs) [2, 3]. The concentrations of the anthropogenic GHGs (CO_2, CH_4, N_2O, CFC-11 (CCl_3F) and CFC-12 (CCl_2F_2)) have been increased since the beginning of the industrial phase [2]. Among those gases, CO_2 is considered with more interest for "its large current greenhouse forcing, its substantial projected future forcing and its long persistence in the atmosphere" [2]. The concentration of CO_2 in the atmosphere has been increased from 280 ppmv in the preindustrial era to about 400 ppmv in 2014 [2, 4]. According to the researchers, a doubling of the atmospheric CO_2 concentration may increase global temperature by 5^{o}C [5]. In the preindustrial era, the concentration of CO_2 in the atmosphere was comparatively stable, which indicates that the amount of CO_2 generated by natural processes was almost equal to the amount of CO_2 absorbed by the nature itself. Among numerous human activities, the burning of fossil fuels can alone produce about 24 billion tons of CO_2 per year while only half of it is being absorbed by nature [2-5].

For reducing GHG emissions, non-carbon energy sources can be most effective in short term. To accomplish this objective, four salient areas are to be considered: (i) improvement in thermo-electric energy conversion efficiency of power generating plants, by using technology like natural gas combined cycle systems (NGCC); (ii) refinement in fuel efficiency in transportation, particularly in automobiles by introducing hybrid cars, fuel cell vehicles (FCV) and electric vehicles; (iii) generating more energy efficient heating process and hot water supplies in buildings and houses; and (iv) development of small scale power sources i.e. fuel cells [6].

Though the above methods might be effective for reducing CO_2 emissions, these are not applicable to the large number of existing fossil fuel fired power plants. However, CO_2 capture and sequestration to reduce the CO_2 concentration in the atmosphere is a continual process to be followed for next several decades. Concentration of CO_2 can be reduced from the air by enhancing natural sinks, i.e. growing more algae by ocean fertilization, plantation and by the process of man-made reclamation of deserts [3]. These ideas might have long-term significance, but are not viable enough in view of present scenario; therefore CO_2 capture from the sources like burning of fossil fuel must receive the current research emphasis.

1.2 CO_2 CAPTURE AND SEQUESTRATION

Currently fossil fuel is the source of 90% of global energy consumption; therefore it can't be phased out rapidly for the next several decades [5, 6]. So, for reducing CO_2 from the atmosphere which is released from stationary sources i.e. fossil fuel fired power plants, carbon capture and sequestration is of immense importance. The idea beyond carbon

sequestration is to find large reservoirs for storing CO_2 rather than allowing it to discharge in the atmosphere. The process is followed by separation and compression of CO_2 from combustion stack gases to generate liquid CO_2, which can be transported for discharging into the bottom of the ocean; can be stored in geological formations or in the form of dry ice [3]; can be converted to benign solid materials or fuels through biological or chemical methods [7]. Current emphasis is put mostly on geologic sequestration (GEO-SEQ). As the first step, separation and compression (i.e. capture), is relatively costlier than transportation and sequestration at present. Thus, to develop a new technology for reducing the CO_2 capture cost is the matter of principal concern.

1.3 AVAILABLE TECHNIQUES FOR CO_2 CAPTURE

There are generally three steps in the process of CO_2 capture and storage (CCS): (1) capture and compression from combustion exhaust (i.e. flue gas), (2) transportation, usually via pipeline, and (3) utilization (e.g., urea production, underground storage, uses in food and beverage industry, enhanced oil recovery, dry ice production, etc.) [8, 9]. As per estimation, the cost of capture stage includes 70-90% of the total operating costs of a CCS system [10]. Most of the research has been conducted in the area of CO_2 capture to find a way out for reducing this high amount of cost. Currently, CO_2 capture technology for fossil fuel fired power plants can be divided into four categories such as (i) post-combustion, (ii) pre-combustion, (iii) oxy-combustion and (iv) chemical looping combustion, each of which requires a distinctly different approach to CO_2 capture.

The major technologies for CO_2 capture from fossil fuel fired power plants within each of the four aforementioned categories are discussed critically. Depending upon the

combustion approach taken, the CO_2 capture technology applicable to each category varies distinctly. By providing benefits and limitations of each technology, this discussion aimed at choosing the most suitable technology for a particular process.

1.3.1 Post-Combustion Techniques for CO_2 Capture

Post combustion capture of CO_2 refers to CO_2 capture from flue gases (a mixture of gases such as CO_2, O_2, N_2, H_2O, SO_x and NO_x etc.) produced by fuel combustion [8, 11] using suitable processes such as absorption, adsorption, gas separation membranes, and cryogenic distillation. As the post combustion technologies can be retrofitted to existing fossil fueled power plants and might be applied to other industrial emitters of CO_2 as well (e.g., cement, iron and steel production industries), it is widely believed that this technology may present the greatest potential for reduction of CO_2 emissions. During the process of post combustion capture, CO_2 is captured from a low pressure (1 bar) and low CO_2 content (3-20%) gas stream often at high temperatures (120-180^oC) containing the impurities SO_x and NO_x [12]. The high temperature and low partial pressure of CO_2 present in post combustion gas streams requires large equipment and cooling system which are considered as major design constraints. Till date**,** these problems were tried to be resolved by absorption of CO_2 using chemical solvents.

1.3.2 Pre-Combustion Techniques for CO_2 Capture

Pre-combustion capture of CO_2 refers to CO_2 capture from a synthesis gas (syngas) stream before combustion and power production occurs. It applies to integrated gasification combined cycle (IGCC) power plants. The primary fuel (coal, natural gas, crude oil, etc.) is first ‘‘gasified’’ to produce a syngas consisting primarily of carbon

monoxide (CO) and hydrogen (H_2). The CO is then converted to CO_2, to create a gas stream consisting of CO_2 and H_2 from which the CO_2 is separated. The remaining H_2 gas stream is used as the fuel source for energy production. Pre-combustion gas streams contain 15-40% CO_2 at elevated pressures (200-600 psi). Due to the increase in the partial pressure of the CO_2 it can be captured by contact with physical solvents in an absorption column or by the use of membranes.

1.3.3 Oxy-Combustion for CO_2 Capture

Oxy-combustion technology is a relatively new approach to reducing CO_2 emissions, originally developed in 1982 to produce high purity CO_2 (>99%) for enhanced oil recovery (EOR). Due to the concerns over global climate change and CO_2 emissions [13], this technology is again in the point of interest. In oxy-combustion the fuel is burnt in a stream of pure oxygen as opposed to ordinary air. Thus, the flue gas stream contains no nitrogen and CO_2 can be captured more efficiently with lower cost by simple condensation process. Although this pathway looks very simple, the challenge lies in obtaining pure oxygen without adversely affecting the economics of the existing process.

1.3.4 Chemical Looping Combustion for CO_2 Capture

Chemical looping combustion (CLC) was first proposed in 1983 as an alternative approach to traditional fuel combustion, though later was found to possess benefits related to CO_2 capture [14, 15]. In CLC, the oxygen needed for combustion is transferred from the combustion air to the fuel by use of an oxygen carrier; most commonly an oxidized metal is used as the oxygen carrier. In a typical CLC system the oxygen carrier (the metal oxide) is transported between two fluidized bed reactors - an air and a fuel

reactor. Thus a system is created in which the fuel and combustion air never comes into contact with one another, creating a CO_2 exhaust gas stream not diluted with N_2, which is made for relatively easy CO_2 capture [16-18].

Compared to previously discussed technologies, CLC is least beneficial in terms of commercial development. For CLC to be a viable option for reducing CO_2 emissions several areas must still be addressed, i.e. large scale chemical looping operation and conversion/retrofitting of existing facilities [19].

1.4 REQUIREMENT OF ALTERNATIVE TECHNIQUE

Current CO_2 separation technology is not applicable for the entire range of separation applications. For post combustion technology, absorption of CO_2 in aqueous alkanolamine solutions and adsorption of CO_2 onto a solid such as zeolite and activated carbon are the most common technique of CO_2 capture. However, scientific community is actively involved in search for alternate technologies due to high energy requirement for the amine absorption process in addition to corrosive nature of the solvents as well as costly equipment used for absorption. Amongst these processes, membrane based separation has received considerable focus in recent years for CO_2 separation.

The focus of this thesis is to investigate the potential of membrane processes for the energy-efficient and effective separation of CO_2 and N_2. Membrane processes are frequently used for gas separation due to its light weight and space efficiency as well as compact modular design. Also, it does not require a separating agent and hence no regeneration is required [20, 21]. Membrane systems discussed here can be classified into six categories: Zeolite Membranes, Carbon Molecular Sieves Membranes, Silica

Membranes, Mixed-matrix Membranes, Supported Ionic Liquid Membranes and Polymeric Membranes.

Zeolites are crystalline aluminosilicates with a well-defined repeating pore structure. Thin zeolite layer deposited on different types of support (porous α-alumina or stainless steel) is called zeolite membranes which have numerous advantages on the field of gas separation application compared to traditional polymeric membranes due to their excellent thermal and mechanical stabilities and chemical resistance [22]. Gas separation through the zeolite membranes is governed by molecular sieving accompanied by surface diffusion. In application of CO_2 separation at low temperature, zeolite membranes are very useful due to their preferential adsorption [23] which helps to get both high permeance and selectivity. At high temperature application, selectivity of zeolite membranes starts decreasing with temperature because the selective adsorption of CO_2 decreases. Additionally, zeolite membranes are very expensive, difficult to process and handle.

Carbon membranes are prepared by pyrolysis of thermosetting polymers under controlled conditions which provides the porous random networks throughout the membrane. The pore sizes of the carbon membranes vary from 0.35 to 1 nm depending on preparation conditions [24]. Here the gas transport mechanism is molecular sieving [25]. Two types of carbon membranes are normally available i.e supported or unsupported. Unsupported carbon membranes are brittle in nature. Few limitations of carbon membranes are poor selectivity due to defective thin active layer, expensive, hard to process and difficult to handle.

Two types of silica membranes normally reported according to their morphology are mesoporous and microporous silica membranes for gas separation application. Different techniques are available to prepare silica membranes like hydrothermal synthesis, sol-gel method etc. There are certain issues associated with the preparation of silica membranes like defect formation due to preparation, thermal cracking during heat treatment which affect membrane reproducibility [26]. Another type of problem associated with the silica membrane is hydrothermal instability at elevated temperatures. Permeance and selectivity are drastically decreased when the membranes are exposed to water vapor [26].

Composite organic-inorganic membranes consist of inorganic particles incorporated into a polymer matrix called mixed-matrix membranes. Gases are transported through both polymeric and inorganic phases. There are lots of inorganic materials like zeolites [27], silica particles [28], metal organic frameworks [29] and carbon nanotubes [30] which are incorporated in the polymer matrix. At low loadings of the inorganic phase in mixed-matrix membranes, the gas transport primarily governs through the polymeric phase. Overall, the mixed-matrix membranes cannot show a significant improvement in gas permeance or selectivity over conventional polymeric membranes.

In case of supported ionic liquid membranes (SILMs), ionic liquids are impregnated into polymeric or inorganic supports which help to transport gas molecule through the membrane by solution-diffusion mechanism or facilitated transport mechanism. Ionic liquids normally treated as organic salts are liquid at room temperature, nonflammable and thermally stable salt [31]. Traditional SILMs suffer from stability problems under

pressurized conditions or under vacuum [32] which disrupts performance. The instability is possibly caused by carrier washout and carrier degradation [21].

Organic polymers are the most widely used materials in membrane based gas separation applications [33]. Conventional polymers are classified in two different categories, one is rubbery polymer (used above their glass transition temperature) and the other is glassy polymers (used below their glass transition temperature). The sorption of gases in rubbery polymers and glassy polymers follows Henry's law and complex sorption isotherms, respectively. Commercial polymeric membranes generally have an asymmetric structure with a very thin selective layer supported on a thicker porous layer. A thin selective layer allows gas separation through the membrane while the thick support layer provides mechanical strength.

The main limitation of existing conventional polymeric membranes is low CO_2 permeability as well as low CO_2/N_2 selectivity. Wind et al. [34] studied the CO_2/N_2 separation using cellulose acetate membrane. The values of CO_2 permeability and CO_2/N_2 selectivity have been reported as 4 Barrers and 26, respectively. Selectivity of conventional polymeric membrane is limited by relative solubility and diffusivity of the components in the gas mixture. Hence, the fixed-site carrier membranes should be favorable when membranes stability and high selectivity as well as high permeance play an important role for gas separation application. CO_2-selective membranes can be obtained by incorporating the amines in the polymer backbone. Blending of amines in different polymers is very useful for the improvement of CO_2 transport properties through the membrane. Several investigations have been reported in the literature for polymers

containing amine blends due to their useful applications in the field of CO_2 removal and gas separation [35-48]. Less energy requirements on the other hand plays significant benefit for the use of membrane technology over other technologies. Membrane based technology uses 70-75 kWh energy per ton of recovered CO_2 compared to significantly higher values for pressure swing adsorption (160-180 kWh), cryogenic distillation (600-800 kWh) or amine absorption (330-340 kWh) [49], making membrane technology an attractive alternative.

1.5 LITERATURE REVIEW ON MEMBRANE BASED CO_2 SEPARATION

The important literatures on CO_2 separation by facilitated transport membranes are discussed below.

Ward et al. [50] introduced the idea of preparing defect free ultra-thin (0.015 micron) membrane using silicone/polycarbonate. Composite membranes were readily handled and may provide the basis for practical gas separation processes. Two such processes are (1) the production of 30% oxygen-enriched air and (2) the on-board generation of nitrogen-enriched air. They observed that with increasing the dimethyl siloxane content in the membrane, the O_2/N_2 selectivity start decreasing with increasing O_2 permeability and 50-60% dimethyl siloxane was selected as optimum.

Matsuyama et al. [51] prepared CO_2 selective facilitated transport membrane using perfluorosulfonic acid ionomer. Monoprotonated ethylenediamine was used as a carrier. The effects of the membrane thickness and temperature were investigated. CO_2 permeability and the selectivity decreased with decreasing membrane thickness and with increasing temperature but the permeability of N_2 was almost constant. The cast

membrane with thickness 22 micron showed much higher CO_2 permeance than the commercial Nafion-117 membrane of thickness 186 micron. However, CO_2/N_2 selectivity was lower in the cast membrane.

Matsuyama et al. [40] prepared a polyethylenimine (PEI)/poly(vinyl alcohol) (PVA) blend membranes for the facilitated transport of CO_2. The polymeric carrier PEI was blended with membrane by the entanglement with PVA chains. They analyzed the stability of membrane and also studied the effect of CO_2 partial pressure, wt% of PEI, heat treatment effect on CO_2 permeation test. The highest selectivity obtained as 230 when the CO_2 partial pressure was 0.065 atm. They had tested the stability over one week. It had been reported that the selectivity was roughly constant but the CO_2 and N_2 permeance decreased slightly.

Kim et al. [39] worked with cation-exchange polysaccharide membranes and used diamine (EDA) as a carrier. This membrane basically used as facilitated transport membranes with fixed carrier. The effect of CO_2 partial pressure, carrier (EDA) content and crosslinking temperature was investigated. They reported that the CO_2 permeability as well as CO_2/N_2 selectivity of the EDA carrier membranes increased with increasing carrier (EDA) content in the membrane. CO_2 permeability decreased with increase in CO_2 partial pressure of feed gas. The ion-exchange capacity of the membrane was high. This high ion-exchange capacity led to higher CO_2 permeability and selectivity.

Kim et al. [52] synthesized facilitated transport membranes for propylene / propane separation containing $AgBF_4$ which dissolved in poly(2-ethyl-2-oxazoline) (POZ). They observed that facilitated propylene transport through these membranes depends on their

thickness. As the membrane thickness increases, the propylene permeability increases whereas the propane permeability remains almost constant. So the selectivity of propylene over propane was increased through the membranes.

Zou and Ho [47] worked with poly (vinyl alcohol) crosslinked with formaldehyde. The amine salt like potassium carbonate-potassium bicarbonate, 2-aminoisobutyric acid potassium salt and poly(allylamine) used as the carriers. The crosslinking of PVA by formaldehyde was confirmed by FTIR and it showed the good improvement of thermal stability of membrane. The membranes showed good CO_2/H_2 selectivity and high CO_2 permeability up to 170^oC. At 120^oC, CO_2 permeability was 1800 Barrer and CO_2/H_2 selectivity was 450. The effects of feed pressure, water content, and temperature on transport properties were investigated. The decrease in CO_2 permeability and CO_2/H_2 selectivity with increasing feed pressure at constant temperature of 110^oC with constant water flow rates of 0.03/0.03 cm^3/min (feed/sweep) was reported. Both CO_2 and H_2 permeability and CO_2/H_2 selectivity reduced as temperature increased from 110^oC to 170^oC for fixed water flow rates in both feed and sweep with constant feed pressure at 2.0 atm. This was explained by the reduction of water retention in the membrane as temperature increased. Both CO_2 and H_2 permeability and CO_2/H_2 selectivity increased significantly with increasing water contents in both feed and sweep side at constant temperature (e.g. 180^oC, 150 ^oC) and feed pressure of 2.0 atm.

Wu et al. [44] worked with solid polymer electrolyte (SPE) membranes with varying composition ratios. SPE membranes were prepared from poly(vinyl alcohol) and poly(acrylic acid). The acrylic acid monomer with cross-linker was first blended with

PVA polymer. A free radical polymerization was then carried out to form an alkaline polymer electrolyte. The solution casting method was used to form the solid polymer membranes. The solid polymer membranes were then immersed in 32 wt.% KOH solution to form different types of electrolyte, and the characteristic properties were examined with differential scanning calorimetry (DSC), stress–strain test, X-ray diffraction (XRD) and SEM morphology analysis. The results showed that the highest room temperature ionic conductivity for the PVA/poly(acrylic acid)/KOH solid polymer membrane electrolyte system was 0.301 S cm^{-1}, which is a four-fold increase from that of the PVA-KOH electrolyte. These PVA/poly(acrylic acid) composite polymer membranes also exhibited excellent thermal and mechanical properties. The membranes were stable for a wide temperature range. The PVA/poly(acrylic acid) polymer membrane had good mechanical strength and ductility.

Shen et al. [41] synthesized a water-soluble co-polymeric membrane material containing tertiary amine and carboxyl groups by radical polymerization of DMAEMA (2-*N*,*N*-dimethyl aminoethyl methacrylate)-AA (acrylic acid). The composite membrane was consisting of copolymer of DMAEMA-AA as separation layer and polysulfone (PS) ultra-filtration membrane as support. The permeation rates of the membranes for pure CO_2 and CH_4 were investigated. The results show that the copolymeric membrane possesses a higher permeance of CO_2. The membrane displays a CO_2 permeance of 6.12×10^{-7} cm^3 (STP)/cm^2 s Pa and a CH_4 permeance of 2.4×10^{-9} cm^3 (STP)/ cm^2 s Pa at 26^{o}C and 0.011 atm of gas pressure. The effect of system temperature on the membrane performance was investigated, CO_2 permeation rate decreases and CO_2/CH_4 selectivity increases with increasing the operating temperature. The CO_2 permeation rate and

separation factor of the mixed gas are not as high as those of pure gas because of coupling effects.

Yi et al. [53] worked with polyvinylamine/polyethylene glycol (PEG) blend membranes. They had seen the effect of PEG content and effect on crosslinking on the performance of blend membranes. They observed that if the PEG concentration increases up to 15% the crystallinity decreases as well as increases the membrane effective permeation area and membrane effective carrier content so the CH_4 and CO_2 permeation increases up to the marked. On the other hand, crosslinking reduced the mobility of the polymer and produced a denser membrane which leads to decreases in diffusion of CO_2 and CH_4. The amino group was reduced due to the reaction between amino group and glutaraldehyde, which decreases transport of CO_2.

Du et al. [54] synthesized the poly(*N*,*N*-dimethylaminoethyl methacrylate) (PDMAEMA) from the DMAEMA monomer and coated on the synthesized micro porous polysulfone (PSF) substrate. Morphology of this composite membrane was examined under scanning electron microscopy. Different pure gases (H_2, N_2, O_2, CO_2, and CH_4) were used to examine the transport property (permeability, flux and selectivity) of the membrane with the effective membrane area of 16.6 cm^2. The permeation experiment was done in room temperature (23^oC) and the effect of feed pressure (1.9-3.9 atm) was examined for different pure gases while maintaining the sweep pressure almost atmospheric. They observed the CO_2 permeance of 30 GPU and CO_2/N_2 ideal separation factor of 53 at 23^oC and 4 atm of CO_2 feed pressure.

Zhao et al. [55] prepared the ultra-thin composite membrane with the help of interfacial polymerization between trimethylene tetramine (TETA) and trimesoyl chloride (TMC) on polyethersulfone (PES) supports. A series of the composite membranes were prepared by adopting various heat-treatment time or temperature. They varied the heat treatment temperature from 60-80^{o}C for various time (5, 10, 15, 20, 25 min). The active layer of the thin film composite membrane was around 0.2 micron. The effect of feed pressure (1.3-7.8 atm) was examined at around 32^{o}C with CO_2/CH_4 mixed gas (10/90 by volume). Effective area of the composite membranes used in the test cell was 19.26 cm^2. The membrane with 1.4 wt.% TMC concentration, 2.8 wt.% TETA concentration, 3 min interfacial polymerization and 15 min heat treatment at 65^{o}C had a performance of CO_2 permeance of 1.33×10^{-5} cm^3 (STP) cm^{-2} s^{-1} $cmHg^{-1}$ and CO_2/CH_4 selectivity of 94.1 at feed pressure of 1.1 atm.

Francisco et al. [38] synthesized facilitated transport membranes comprising of alkanolamines entrapped in poly(vinyl alcohol) matrix for CO_2/N_2 separation. Monoethanolamine (MEA), 2-amino-2-methyl-1-propanol (AMP), diethanolamine (DEA) and *N*-methyldiethanolamine (MDEA) were examined for their suitability as the facilitating agent for CO_2 permeation. DEA was found to be most effective in improving the CO_2/N_2 permselectivity. The effects of amine content, feed pressure and temperature on the membrane performance were evaluated. The facilitation in CO_2 transport became less significant at higher CO_2 pressures due to carrier saturation. The PVA/DEA membrane showed a CO_2/N_2 selectivity of more than 100, which was much higher than the plain PVA membrane.

Yegani et al. [46] worked with the membrane which was prepared by the polymer (PVA/PAA) gel consisting of 2,3-diaminopropionic acid (DAPA) as mobile carrier. The membrane performance was tested by the experiments on the selective separation of CO_2 from a mixture of 3.65% CO_2, 32.9% N_2 and 63.5% H_2O at the temperature from 125^oC to 160^oC and the feed gas pressure from 0.98 to 6.4 atm. The highest CO_2/H_2 selectivity and CO_2 permeance were observed as 1070 and I3.14×10^{-4} mol/m^2 s kPa, respectively at 125^oC temperature and 2.9 atm feed pressure. The CO_2 permeance as well as CO_2/N_2 selectivity increased with increasing pressure rapidly in the low pressure region and leveled off in the high pressure region. The membrane performance decreased with increasing temperature.

Cai et al. [35] prepared composite membranes by using polyallylamine/PVA blend polymer as the separation layer and polysulfone (PSF) ultrafiltration membranes as the support layer. The gas transport property of the membranes, including gas permeance, flux and selectivity, were investigated by using pure CO_2, N_2, CH_4 gases and CO_2/N_2 gas mixture (20 vol% CO_2 and 80 vol% N_2) and CO_2/CH_4 gas mixture (10 vol% CO_2 and 90 vol% CH_4). Effect of polyallylamine content (0-50 wt%) in the separation layer was investigated. With increasing polyallylamine content, gas permeance increases initially, reaches a maximum and then decreases gradually. For CO_2/N_2 gas mixture, the membranes with 10 wt% polyallylamine content show the highest CO_2 permeance of about 1.80×10^{-5} cm^3 (STP) cm^{-2} s^{-1} kPa^{-1} and CO_2/N_2 selectivity of 80 at 0.98 atm feed gas pressure. For CO_2/CH_4 gas mixture, the membranes with 20 wt% polyallylamine content display the highest CO_2 permeance of about 1.95×10^{-5} cm^3 (STP) cm^{-2} s^{-1} kPa^{-1} and CO_2/CH_4 selectivity of 58 at 0.98 atm feed gas pressure.

Shen et al. [42] worked with radical polymerization of DMAEMA(2-*N*,*N*-dimethyl aminoethyl methacrylate)-AA(acrylic acid). The composite membranes were prepared by casting solution of poly(2-*N*,*N*-dimethyl aminoethyl methacrylate-*co*-acrylic acid sodium) on the various support layer. The copolymeric membranes were crosslinked by heat treatment at 120°C. The result shows that CO_2/CH_4 selectivity of the composite membrane increased but the CO_2 permeation rate decreased with increasing molecular weight of the copolymer, both the CO_2/CH_4 selectivity and CO_2 permeation rate had a maximum against the carrier (tertiary amine and carboxyl groups) content of the copolymer. The permeation performance of the composite membrane for CO_2/CH_4 mixed gas was not as good as those obtained with pure CO_2 and CH_4 gas because of the coupling effects between CO_2 and CH_4. In common radical polymerization method, the increase in molecular weight for copolymer resulted in a slight decrease in permeation for CO_2 but a major decrease for CH_4, This was explained by the restricted mobility in higher molecular weight membranes.

Xing and Ho [45] synthesized crosslinked PVA/polyethylene glycol (PEG) blend membrane and characterized for CO_2/CH_4 separation and also studied the effect of crosslinking time, molecular weight of PEG, PEG (*Mw* 200) content, temperature, feed pressure on gas transport property like CO_2/CH_4 selectivity, CO_2 permeability etc. At 64 wt% PEG, the membranes showed good CO_2 permeability of 80 Barrers and CO_2/CH_4 selectivity of 33 at 30^{o}C. Effects of the zeolite 5A loading, temperature and feed pressure were also investigated for the gas separation performance of both zeolite-filled and zeolite-unfilled PVA/PEG membranes. They observed that the CO_2/CH_4 selectivity decreased as the zeolite 5A content increased.

Deng et al. [37] obtained a defect-free ultra-thin polyvinyl amine (PVAm)/PVA blend facilitated transport membrane on a porous polysulfone (PSf) support. The target membrane was prepared from commercial polyvinyl amine and PVA. Effects of experimental conditions were investigated for a CO_2/N_2 mixed gas. A CO_2/N_2 separation factor of up to 174 and a CO_2 permeance up to 0.58 m^3(STP)/(m^2 h bar) were documented. Experimental results suggest that CO_2 is being transported according to the facilitated transport mechanism through this membrane. The fixed amino groups in the polyvinyl amine matrix function as CO_2 carriers to facilitate the transport whereas the PVA adds mechanical strength to the blend by the polymeric chains. The good mechanical properties obtained from the blend of PVA with polyvinyl amine, enabled an ultra-thin selective layer (down to 0.3µm) on PSf support (with molecular weight cut-off of 50,000) and resulted in both high selectivity and permeance. The polyvinyl amine/PVA blend membrane also exhibited a good stability during a 400 h test.

Deng and Kin [36] developed a PVAm/PVA blend membrane with fixed amino groups for CO_2 transport. PVAm offers a high amount of primary amino groups with a mechanically robust polymer. PVA enhances polymeric network with good membrane forming properties. The reversible reactions of CO_2 with amino carriers in PVAm facilitate the CO_2 transport, resulting in both high CO_2 permeability and CO_2/CH_4 selectivity. The defect free ultra-thin PVAm/PVA blend membrane was obtained on porous polysulfone (PSf) supports. The selectivity of CO_2/CH_4 up to 45 and CO_2 permeance up to 0.3 m^3(STP)/m^2.h.bar were reported at 2 atm pressure. Selectivity up to 40 for CO_2/CH_4 was also recorded at 15 atm pressure. The blend membrane showed good reproducibility and stable performance.

Francisco et al. [56] developed CO_2 selective membranes at various operating conditions (i.e., temperature, feed composition and pressure) using diethanolamine (DEA) impregnated poly(vinyl alcohol). Effect of DEA content (0-50wt%), temperature (30-60^oC) and CO_2 partial pressure (0-0.24 atm) were examined using CO_2/N_2 gas mixture (15.6 mol% CO_2) with the membrane effective surface area of 13.8 cm^2 and active layer thickness of 268 micron. They observed that 20 wt% DEA exhibited the best separation performance among all the membranes. CO_2 facilitation transport was more pronounced at lower CO_2 partial pressures and the membrane exhibited a higher permselectivity at higher temperature and lower CO_2 partial pressure. At a feed pressure of 3 atm, a CO_2 permeance of 9.7 GPU and a CO_2/N_2 selectivity of 112 were achieved at ambient temperature. The membrane was shown to be stable during continuous operation over a period of over 5 weeks.

Hamouda et al. [57] introduced PVA/PEG/PEI blend membranes for CO_2 separation. They had used pure CO_2 and N_2 for the permeation experiment. All the experiment had been carried out at room temperature (25^oC). All the membranes were characterized by TGA, DSC and FTIR analysis. Effect of feed pressure (0.1-3 atm) and weight fraction of PEI (5-50 wt%) were observed. It was shown that the CO_2 permeability decreased with an increase in CO_2 partial pressure in feed gas, while the N_2 permeability remained constant. The CO_2 and N_2 permeabilities increased monotonically with the PEI content in the blend membranes, whereas the ideal selectivity of CO_2 to N_2 transport showed a maximum.

Barillas et al. [58] performed experiments using supported liquid membranes (SLM) for CO_2/H_2 separation. The support material was porous nylon under the trade name of Biodyne A (pore diameter = 0.2 micron, thickness = 152 micron and the effective membrane area = 2.2 cm^2). They used several CO_2 selective liquid polymers as a carrier such as polyethylene glycol (PEG), polypropylene glycol (PPG), glycerol triacetate (GTA), polytetramethylene ether glycol (PTMEG), polybutylene glycol (PBG), perfluoropolyether (PFPE), poly(dimethyl siloxane) (PDMS), and polyacetoxy oxetane (PAO). The permeation experiment was carried out at 1 atm total pressure in steady-state flux experiments over the temperature range of 25-150^oC. PEG based SLMs showed the highest CO_2/H_2 selectivity of 11 and CO_2 permeability of 800 Barrer at 37^oC.

Duan et al. [59] prepared crosslinked-PVA membrane doped with poly(amidoamine) (PAMAM) dendrimers for CO_2 separation at elevated pressures from CO_2/H_2 gas mixture (5/95 or 80/20 by vol). An organic metal compound (Ti) was selected as a cross-linker of PVA. The CO_2 partial pressures of the feed side were varied like 0.049 atm, 0.78 atm, 2.36 atm and 5.52 atm and the operating temperature was varied from 25-60^oC. They observed that moisture plays a very important role for the CO_2 separation performance and 80% relative humidity was required for high separation performance. The CO_2/H_2 selectivity was almost constant when the CO_2 partial pressure in feed gas was varied from 0.78 to 5.52 atm at 40^oC. CO_2/H_2 selectivity and CO_2 permeance of the membrane were 32 and 1.6×10^{-12} m^3 (STP) / (m^2 s Pa), respectively, at 5.52 atm CO_2 partial pressure in the feed gas. Both CO_2 permeance and CO_2/H_2 selectivity increased as the operation temperature of the membrane was increased from 25 to 60^oC. A membrane containing 63.3 wt% of the dendrimer showed CO_2/H_2 selectivity and CO_2 permeance of 42 and

1.2×10^{-11} m^3 (STP) / (m^2 s Pa), respectively, at 5.52 atm of CO_2 partial pressure and 60^oC.

Shamsabadi et al. [60] reported that the polymer concentration is one of the most important variables which can change membrane morphology and behavior. They prepared polyetherimide (PEI) membrane using N-methyl-2-pyrrolidone (NMP) as a solvent. After that Polydimethylsiloxane (PDMS) solution was coated on the PEI membrane. Three asymmetric PDMS/PEI membranes with different concentrations of PEI were prepared for H_2/CH_4 separation with the effective membrane surface area of 20 cm^2. The permeation experiment was carried out at room temperature (25^oC) only. Effect of feed pressure (1-10 atm) and PEI concentration on H_2/CH_4 transport properties were investigated in both pure and mixed gas (50% H_2 and 50% CH_4) experiments. The results showed that the H_2/CH_4 selectivity increased with PEI concentrations. The influence of the pressure on the H_2 and CH_4 permeance and the selectivity for a mixed binary gas showed that the permeance of both gases declined by pressure enhancement. This membrane offers the H_2/CH_4 selectivity as high as 26 for pure gas and 24.8 for mixed gas, at 1 atm and 25^oC.

Ahmad and Hagg [61] synthesized organic inorganic nano-composite membrane using polyvinyl acetate (PVAc) and titanium dioxide (TiO_2) for single gas (N_2, O_2, CO_2 and H_2) permeation. The prepared membranes were characterized by optical microscope, FESEM, XRD, DSC and TGA. Effect of feed pressure (2-8 atm) and temperature (30-50^oC) were examined with membrane effective surface area of 2.5 cm^2. They observed that the addition of TiO_2 up to 10wt% has improved both the permeability and selectivity of the

nono-composite membranes. The permeability of O_2, CO_2 and H_2 was increased by 95%, 79% and 62%, respectively. Selectivity of the gas pairs O_2/N_2, H_2/N_2, CO_2/N_2 was also increased by 38%, 26.5% and 14%, respectively. Increasing the feed pressure from 2 atm to 8 atm has no significant effect on the permeability of N_2, O_2 and H_2 resulting in almost unchanged selectivity of the gas pairs O_2/N_2 and H_2/N_2.

Duan et al. [62] reported that crosslinked poly(vinylalcohol) (PVA) membrane doped with poly(amidoamine) (PAMAM) dendrimer shows selective separation of CO_2 from a mixture of CO_2 and H_2 (80/20 vol% of CO_2/H_2). An organic metal compound, di-isopropoxy-bis (triethanol aminato) titanium was used as crosslinking agent. The effects of cross-linker concentration (0-50 wt%), membrane thickness (6-400 micron) and temperature (40-60^oC) on separation performance were discussed. The optimum concentration of Ti cross-linker was from 10 to 25 wt%. CO_2 permeance increased with decreasing thickness, but the CO_2/H_2 selectivity decreased with decreasing thickness. Both permeance and CO_2/H_2 selectivity increased with increasing temperature. The CO_2/H_2 selectivity reached a maximum of 32 with CO_2 permeance of 3.0×10^{-11} m^3 (STP) / (m^2 s Pa) at 60^oC under CO_2 partial pressure of 5.52 atm using a membrane of 6 micron thickness.

Taniguchi et al. [63] reported that Poly(amidoamine) (PAMAM) dendrimer entrap with poly(ethylene glycol)-dimethacrylate (PEGDMA) by photo-polymerization gives enormous effect on CO_2 separation over H_2. The dendrimer content, generation of the dendrimer and relative humidity are crucial factors to characterize CO_2 separation

performance of the polymeric membrane. The polymeric membranes exhibited excellent CO_2 separation properties.

Pedram et al. [64] prepared crosslinked poly(vinyl alcohol) (PVA) membrane doped with diethanolamine (DEA) on polytetrafluoroethylene (PTFE) support. Glutaraldehyde (GA) had been used as crosslinking agent and the blend composition of GA/PVA was varied like GA/PVA: 0.5, 1, 3, 5, 7 ratio%. Also, the DEA doped crosslinked PVA membranes were prepared with different DEA concentration of 5, 15, 25, 35 and 45 wt%. The effective membrane surface area was 4.9 cm^2 and the permeation experiment was carried out at room temperature (25^oC). The effects of crosslinking agent content, feed pressure (0.5-7.5 atm) and composition as well as stability on CO_2/CH_4 transport properties were investigated in both pure and mixed gas experiments. During the gas experiments, membrane containing 15 wt% of DEA showed the best performance. The best-yield CO_2-selective membranes (DEA-PVA/GA (1 wt%)) represented the best CO_2/CH_4 selectivity of 91.13 and 665 for pure and mixed gas experiments, respectively.

Saedi et al. [65] synthesized defect free asymmetric polyethersulfone membrane using a novel poly(acrylonitrile-co-N, N-dimethylaminopropyl acrylamide) [PAN-PDMAPAM]. The membranes were coated by a solution of 1.5 wt.% PVA via dip coating method. The membranes were used for CO_2 separation from CO_2/CH_4 gas mixture (30/70 vol%). Effect of feed pressure (5-30 atm) and temperature (30-70^oC) were investigated. High permeation of PES/PAN-PDMAPAM membranes at low temperature was reported.

1.6 IMPORTANCE AND OBJECTIVES OF THE PRESENT STUDY

In view of the substantial energy requirement of acid gas treating plants using alkanolamines, there is considerable incentive required for the development of more efficient and flexible methods for acid gas separation. With the advancement of membrane research, membrane based separation are getting considerable attention to be used for acid gas treatment. Therefore, researchers across the world paid considerable attention on membrane material aiming at development of potential method to capture CO_2 with reduced energy consumption. From the introductory discussion, it is apparent that the development of novel CO_2-selective and thermally stable membrane has immense industrial significant and there is huge scope of research today.

Different CO_2-selective polymeric membranes have now gained huge interest due to their advantages which have been discussed in the review of the literatures reported so far. But most of the literature reported on CO_2 selective polymeric membrane failed to describe the effect of elevated temperature (beyond 100^oC) on separation performance and simultaneous improvement of CO_2 flux and CO_2/N_2 selectivity. In this perspective, significant research work is going on worldwide to synthesize polymer based novel CO_2-selective membranes having both, high CO_2 flux and CO_2/N_2 selectivity which can operate at elevated temperature ($> 100^oC$).

This work aims at developing new polymer based CO_2-selective membranes and uses these membranes to separate CO_2 from CO_2/N_2 gas mixture. This work is combination of synthesis, characterization and permeation experimental studies and is broadly divided into two parts. In the first part, a suitable base polymer is chosen and the thermal stability

of the membrane is improved by changing degree of crosslinking and then by polymer blending. In the second part of the work, different new amine carriers are introduced into the crosslinked-polymer membrane to increase the CO_2 flux, CO_2 permeability and CO_2/N_2 selectivity.

Poly (vinyl alcohol) (PVA), a 1, 3-diglycol polymer, is chosen for the base polymer in this research due to ease of its preparation as well as its excellent physical properties and film-forming ability, good compatibility with amine, hydrophilic in nature, semi crystalline polymer consists of crystalline domain and amorphous domain and moderate thermal stability. Formaldehyde (HCHO) and polyvinylpyrrolidone (PVP) have been used as a crosslinking and polymer blending agents, respectively to improve the thermal stability of the membrane. Different new amine carriers such as polyethyleneimine (PEI), tetraethylenepentamine (TEPA), pentaethylenehexamine (PEHA), polyallylamine (PAA), 2-amino-2-hydroxymethyl-1,3-propanediol (AHPD) and there blends have been introduced into the crosslinked-PVA-PVP membrane to improve the CO_2 transport property (CO_2 flux, CO_2 permeability, CO_2/N_2 selectivity).

This research work has been undertaken with the following objectives:

- Synthesis of the new PVA-PVP blends CO_2-selective membrane using HCHO as a crosslinking agent and different amines as carrier.

- Characterization of the synthesized membranes by thermogravimetric analysis (TGA), differential scanning calorimetry (DSC) analysis, fourier transform infrared spectroscopy (FTIR) analysis, scanning electron microscope (SEM), and *X*-ray diffraction (XRD) analysis.

- Optimization of membrane composition to obtain high CO_2 flux and permeability as well as high CO_2/N_2 selectivity.

- Optimization of various operating conditions viz. temperature, pressure, moisture content of sweep gas etc. that affects the transport of CO_2 through the membrane.

- Detailed performance studies (CO_2 flux, CO_2 permeability and CO_2/N_2 selectivity) under optimized membrane composition and operating conditions by the synthesized membrane using counter flow flat sheet membrane permeation module.

1.7 THESIS OUTLINE

From the discussion in the previous section, it is apparent that the development of novel CO_2 selective membrane has immense industrial significant and there is huge scope of research. The present research work has been divided into five chapters.

Chapter 1: This chapter presents a brief overview of global warming and greenhouse gas effect. It also discusses their origin, impacts on environment structure, guidelines and need for removal of excess quantity and the available capture techniques, merits and demerits of each treatment techniques and the requirement of easiest low-cost treatment technique to capture CO_2 from fossil fuel fired emission. Also, this chapter describes the detail literatures studied for the removal of CO_2 using thin-film polymer composite membrane. The final part of this chapter highlights the importance and draws clear objectives of this research work.

Chapter 2: This chapter describes the various reaction mechanisms between CO_2 and amines such as zwitterionic mechanism, termolecular mechanism, base-catalyzed

hydration mechanism, alcohol-group bonding of CO_2, etc. This helps to understand the concept about the formation of CO_2-amine complex. Based on these reaction mechanisms the underlying principle of facilitated transport of CO_2 through the thin-film dense polymer composite membrane is also presented in this chapter.

Chapter 3: This chapter elaborates the detailed study of membrane synthesis and characterization. Formaldehyde and polyvinylpyrrolidone were used as crosslinking and polymer blending agents, respectively to enhance the thermal stability of the membrane. Different combinations of single and blended amines were introduced into the polymer hydrogel to enhance the CO_2 transport property through the membrane. These amines were polyethyleneimine, tetraethylenepentamine, pentaethylenehexamine, poly(allylamine) and 2-amino-2-hydroxymethyl-1,3-propanediol. The resulting dry membranes were characterized with TGA, DSC, FTIR and XRD. All the characterizations were done for active layer only which was found to be optically transparent to visible light and mechanically stable to be handled.

Chapter 4: This chapter presents the detailed permeation study of novel CO_2-selective crosslinked-PVA-PVP blend membranes containing different amines and their blends. Five different amines (PEI, TEPA, PEHA, PAA and AHPD) and their blends were used as carriers. In this chapter the effects of active layer thickness, feed pressure, sweep side water flow rate and temperature on the transport properties (CO_2 flux, CO_2 permeability, CO_2/N_2 selectivity) were investigated with a mixed gas stream containing 20% CO_2 and 80% N_2 by volume. The best composition for each set of combination was obtained by comparing CO_2 transport properties at a particular active layer thickness. Then the

performance of each membrane was analyzed at various operating conditions viz. temperature, feed pressure, moisture content of sweep gas etc. that affects the transport of CO_2 through the membrane.

Chapter 5: This chapter draws appropriate conclusions based on this study. This chapter also provides some useful recommendations for future research in the relevant field.

A part of the work in this thesis has been published or accepted for publication in different international journals, international and national level conference proceedings, and some more papers would be communicated in due course of time. The details of papers published/ accepted, to be communicated and conference presentations have been appended at the end.

1.8 SUMMARY

CO_2 separation is always increasing problem in the industries and environment. From the literature citations, it is clear that there is a need to find a low-cost process for the removal of CO_2 from the industrial gases like flue gas. There are three primary ways to remove CO_2 from industrial off-gases like pre-combustion, post-combustion and oxy-fuel combustion. Due to the present establishment of the different industrial process, post-combustion process might be the most economical process among others. Keeping in view the importance of CO_2 removal from the industrial off-gases, the objectives of the present study is to synthesize novel CO_2 selective membrane for post-combustion CO_2 capture.

REFERENCES

[1]. A. Berger, "The effect of greenhouse gases on climate." proceedings of the conference on the future energy systems and technology for CO_2 Abatement, Antwerp, Belgium, November 2002: 3-10.

[2]. T. S. Ledley, E. T. Sundquist, S. E. Schwartz, D. K. Hall, J. D. Fellows and T. L. Killeen, "Climate change and greenhouse gases." EOS-Transactions American Geophysical Union, 80(39), (1999), 453-458.

[3]. B. Matthews, "Climate engineering: A critical review of proposals, their scientific and political context, and possible impacts" Compiled for Scientists for Global Responsibility, November 1996, http://www.chooseclimate.org/cleng/part1b.html.

[4]. Earth's CO_2 Home Page, http://co2now.org/

[5]. E. S. Rubin, R. N. Cooper, R. A. Frosch, T. H. Lee, G. Marland, A. H. Rosenfeld and D. D. Stine, Realistic mitigation options for global warming. Science. 257 (1992) 148-266.

[6]. Y. Kaya, "A strategy for mitigating global warming." Proceedings of the Conference on the Future Energy Systems and Technology for CO_2 Abatement, Antwerp, Belgium, November 2002: 19-25.

[7]. D. A. Beecy, V. A. Kuuskraa and C. Schmidt, "A perspective on the potential role of geologic options in a national carbon management strategy." Proceedings of First National Conference on Carbon Sequestration,

Washington, D. C, May 2001.

[8]. DOE, Report of the interagency task force on carbon capture and storage, The US Department of Energy and the Environmental Protection Agency, 2010.

[9]. R. S. Haszeldine, Carbon capture and storage: how green can black be?, Science 325 (2009) 1647-1652.

[10]. H. Herzog and D. Golomb, Carbon capture and storage from fossil fuel, Use Encyclopedia Energy. 1 (2004) 1-11.

[11]. A. A. Olajire, CO_2 capture and separation technologies for end-of-pipe applications-A review, Energy. 35 (2010) 2610-2628.

[12]. S. C. Stultz, J. B. Kitto, Steam: Its generation and use, 40th ed., The Babcock and Wilcox Company, Barberton, Ohio, 1992.

[13]. B. J. P. Buhre, L. K. Elliott, C. D. Sheng, R. P. Gupta and T. F. Wall, Oxy-fuel combustion technology for coal-fired power generation, Prog. Energy Combust. Sci. 31 (2005) 283-307.

[14]. H. J. Richter and K. F. Knoche, "Reversibility of combustion processes," in efficiency and costing: second law analysis of processes, ACS Symposium Series. 235 (1983) 71-85.

[15]. M. Ishida and H. Jin, A new advanced power-generation system using chemical-looping combustion, Energy. 19 (1994) 415-422.

[16]. J. Adanez, L. F. d. Diego, F. Garcia-Labiano, P. Gayan and A. Abad, Selection of oxygen carriers for chemical-looping combustion, Energy & Fuels. 18 (2004) 371-377.

[17]. A. Lyngfelt, B. Leckner and T. Mattisson, A fluidized-bed combustion process with inherent CO_2 separation; application of chemical-looping combustion, Chem. Eng. Sci. 56 (2001) 3101-3113.

[18]. A. Cuadrat, A. Abad, L. F. de Diego, F. Garcia-Labiano, P. Gayan and J. Adanez, Prompt considerations on the design of chemical-looping combustion of coal from experimental tests, Fuel. 97 (2012) 219-232.

[19]. B. Moghtaderi, Review of the recent chemical looping process developments for novel energy and fuel applications, Energy & Fuels. 26 (2012) 15-40.

[20]. T. C. Merkel, H. Lin, X. Wei and R. Baker, Power plant post-combustion carbon dioxide capture: an opportunity for membranes, J. Membr. Sci. 359 (2010) 126-139.

[21]. Y. Zhao and W. S. W. Ho, Steric hindrance effect on amine demonstrated in solid polymer membranes for CO_2 transport, J. Membr. Sci. 415-416 (2012) 132-138.

[22]. S. Himeno, T. Tomita, K. Suzuki, K. Nakayama, K. Yajima and S. Yoshida, Synthesis and permeation properties of a DDR-type zeolite membrane for separation of CO_2/CH_4 gaseous mixtures, Ind. Eng. Chem. Res. 45 (2007) 6989-6997.

[23]. D. Shekhawat, D. R. Luebke and H. W. Pennline, A review of carbon dioxide selective membranes-A topical report, National Energy Technology Laboratory, US Department of Energy, (2003).

[24]. M. Hagg, Membranes in gas separation, in: A. K. Pabby, S. S. H. Rizvi, A. M. Sastre (Eds.), Handbook of Membrane Separations: Chemical, Pharmaceutical, Food, and Biotechnological Applications, CRC Press, Boca Raton, FL, 2009, pp. 65-105.

[25]. A. F. Ismail and L. I. B. David, A review on the latest development of carbon membranes for gas separation, J. Membr. Sci. 193 (2001) 1-18.

[26]. R. M. de Vos and H. Verweij, Improved performance of silica membranes for gas separation, J. Membr. Sci. 143 (1998) 37-51.

[27]. Y. Li and T. S. Chung, Novel Ag+-zeolite/polymer mixed matrix membranes with a high CO_2/ CH_4 selectivity, AIChE J. 53 (2007) 610-616.

[28]. T. Suzuki and Y. Yamada, Effect of end group modification on gas transport properties of 6FDATAPOB hyperbranched polyimide-silica hybrid membranes, High Perform. Polym. 19 (2007) 553-564.

[29]. Y. Zhang, I. H. Musselman, J. P. Ferraris and K. J. Balkus Jr, Gas permeability properties of Matrimid membranes containing the metal-organic framework Cu-BPY-HFS, J. Membr. Sci. 313 (2008) 170-181.

[30]. S. Kim, L. Chen, J. K. Johnson and E. Marand, Polysulfone and functionalized carbon nanotube mixed matrix membranes for gas separation: theory and experiment, J. Membr. Sci. 294 (2007) 147-158.

[31]. Y. Y. Jiang, Z. Zhou, Z. Jiao, L. Li, Y. T. Wu and Z. B. Zhang, SO_2 gas separation using supported ionic liquid membranes, J. Phys. Chem. B. 111 (2007) 5058-5061.

[32]. A. Ito, S. Duan, Y. Ikenori and A. Ohkawa, Permeation of wet CO_2/CH_4 mixed gas through a liquid membrane supported on surface of a hydrophobic microporous membrane, Sep. Purif. Technol. 24 (2001) 235-242.

[33]. V. Abetz, T. Brinkmann, M. Dijkstra, K. Ebert, D. Fritsch and K. Ohlrogge, Developments in membrane research: from material via process design to industrial application, Adv. Eng. Mater. 8 (2006) 328-358.

[34]. J. D. Wind, D. R. Paul and W. J. Koros, Natural gas permeation in polyimide membranes, J. Membr. Sci. 228 (2004) 227-236.

[35]. Y. Cai, Z. Wang, C. Yi, Y. Bai, J. Wang and S. Wang, Gas transport property of polyallylamine–poly(vinyl alcohol)/polysulfone composite membranes, J. Membr. Sci. 310 (2008) 184-196.

[36]. L. Deng, T. J. Kim and M. B. Hagg, Facilitated transport of CO_2 in novel PVAm/PVA blend membrane, J. Membr. Sci. 340 (2009) 154-163.

[37]. L. Deng, T. J. Kim, M. Sandru and M.B. Hagg, PVA/PVAm blend FSC membrane for natural gas sweetening, proceedings of the 1st annual gas processing symposium, Elsevier, Norway, 2009.

[38]. G. J. Francisco, A. Chakma and X. Feng, Membranes comprising of alkanolamines incorporated into poly(vinyl alcohol) matrix for CO_2/N_2 separation, J. Membr. Sci. 303 (2007) 54-63.

[39]. M. J. Kim, Y. I. Park, K. H. O. Youm and K. H. O. Lee, Facilitated transport of CO_2 through ethylenediamine-fixed cation-exchange polysaccharide membranes, J. Membr. Sci. 245 (2004) 79-86.

[40]. H. Matsuyama, A. Terada, T. Nakagawara, Y. Kitamura and M. Teramoto, Facilitated transport of CO_2 through polyethylenimine/poly(vinyl alcohol) blend membrane, J. Membr. Sci. 163 (1999) 221-227.

[41]. J. Shen, J. Qiu, L. Wu and C. Gao, Facilitated transport of carbon dioxide through poly (2-N,N-dimethyl aminoethyl methacrylate-co-acrylic acid sodium) membrane, Sep. Purif. Technol. 51 (2006) 345-351.

[42]. J. Shen, L. Wu, D. Wang and C. Gao, Sorption behavior and separation performance of novel facilitated transport membranes for CO_2/CH_4 mixtures, Desalination. 223 (2008) 425-437.

[43]. W. J. Ward, W. R. Browal and R. M. Salemme, Ultrathin silicone/polycarbonate membranes for gas separation processes, J. Membr. Sci. 1 (1976) 99-108.

[44]. G. M. Wu, S. J. Lin and C. C. Yang, Preparation and characterization of PVA/PAA membranes for solid polymer electrolytes, J. Membr. Sci. 275 (2006) 127-133.

[45]. R. Xing and W. S. W. Ho, Synthesis and characterization of crosslinkedpolyvinylalcohol/polyethyleneglycol blend membranes for CO_2/CH_4 separation, J. Taiw. Inst. Che. Eng. 40 (2009) 654-662.

[46]. R. Yegani, H. Hirozawa, M. Teramoto, H. Himei, O. Okada, T. Takigawa, N. Ohmura, N. Matsumiya and H. Matsuyama, Selective separation of CO_2 by using novel facilitated transport membrane at elevated temperatures and pressures, J. Membr. Sci. 291 (2007) 157-164.

[47]. J. Zou and W. S. W. Ho, CO_2-selective polymeric membranes containing amines in crosslinkedpoly(vinyl alcohol), J. Membr. Sci. 286 (2006) 310-321.

[48]. B. Mandal and W. S. W. Ho, Gas purification by polymeric membranes containing fixed and mobile carriers, Int. J. Chem. Sci. 5 (2007) 1938-1946.

[49]. H. H. Khoo and R. B. H. Tan, Life cycle investigation of CO_2 recovery and sequestration, Environ. Sci. Technol. 40 (2006) 4016.

[50]. W. J. Ward, W. R. Browall and R. M. Salemme, Ultrathin silicone/polycarbonate membranes for gas separation processes, J. Membr. Sci. 1 (1976) 99-108.

[51]. H. Matsuyama, K. Matsui, Y. Kitamura, T. Maki and M. Teramoto, Effects of membrane thickness and membrane preparation condition on facilitated transport of CO_2 through ionomer membrane, Sep. Purif. Technol. 17 (1999) 235-241.

[52]. J. H. Kim, S. M. Park, J. Won and Y. S. Kang, Dependence of facilitated olefin transport on the thickness of silver polymer electrolyte membranes, J. Membr. Sci. 236 (2004) 209-212.

[53]. C. Yi, Z. Wang, M. Li, J. Wang and S. Wang, Facilitated transport of CO_2 through polyvinylamine/polyethylene glycol blend membranes, Desalination. 193 (2006) 90-96.

[54]. R. Du, X. Feng and A. Chakma, Poly(*N*,*N*-dimethylaminoethyl methacrylate)/polysulfone composite membranes for gas separations, J. Membr. Sci. 279 (2006) 76-85.

[55]. J. Zhao, Z. Wang, J. Wang and S. Wang, Influence of heat-treatment on CO_2 separation performance of novel fixed carrier composite membranes prepared by interfacial polymerization, J. Membr. Sci. 283 (2006) 346-356.

[56]. G. J. Francisco, A. Chakma and X. Feng, Separation of carbon dioxide from nitrogen using diethanolamine-impregnated poly(vinyl alcohol) membranes, Sep. Purif. Technol. 71 (2010) 205-213.

[57]. S. B. Hamouda, Q. T. Nguyen, D. Langevin and S. Roudesli, Poly(vinylalcohol) / poly(ethyleneglycol) / poly(ethyleneimine) blend membranes-structure and CO_2 facilitated transport, C. R. Chimie. 13 (2010) 372-379.

[58]. M. K. Barillas, R. M. Enick, M. O'Brien, R. Perry, D. R. Luebke and B. D. Morreale, The CO_2 permeability and mixed gas CO_2/H_2 selectivity of membranes composed of CO_2-philic polymers, J. Membr. Sci. 372 (2011) 29-39.

[59]. S. Duan, I. Taniguchi, T. Kai and S. Kazama, Poly(amidoamine)dendrimer / poly(vinylalcohol) hybrid membranes for CO_2 capture, J. Membr. Sci. 423-424 (2012) 107-112.

[60]. A. A. Shamsabadi, A. Kargari, M. B. Babaheidari, S. Laki and H. Ajami, Role of critical concentration of PEI in NMP solutions on gas permeation characteristics of PEI gas separation membranes, J. Ind. Eng. Chem. 19 (2013) 677-685.

[61]. J. Ahmad and M. B. Hagg, Polyvinyl acetate/titanium dioxide nano-composite membranes for gas separation, J. Membr. Sci. 445 (2013) 200-210.

[62]. S. Duan, I. Taniguchi, T. Kai and S. Kazama, Development of poly(amidoamine) dendrimer/polyvinylalcohol hybrid membranes for CO_2 capture at elevated pressures, Energy Procedia. 37 (2013) 924-931.

[63]. I. Taniguchi, T. Kai, S. Duan and S. Kazama, PAMAM dendrimer containing polymeric membrane for preferential CO_2 separation over H_2 - Interplay between CO_2 separation properties and morphology, Energy Procedia. 37 (2013) 1067-1075.

[64]. M. Z. Pedram, M. Omidkhah and A. E. Amooghin, Synthesis and characterization of diethanolamine-impregnated cross-linked polyvinylalcohol/glutaraldehyde membranes for CO_2/CH_4 separation, J. Ind. Eng. Chem. 20 (2014) 74-82.

[65]. S. Saedi, S. S. Madaeni, F. Seidi, A. A. Shamsabadi, S. Laki, Fixed facilitated transport of CO_2 through integrally-skinned asymmetric polyethersulfone

membrane using a novel synthesized Poly(acrylonitrile-co-N, N-Dimethylaminopropyl acrylamide), Chem. Eng. J. 236 (2014) 263-273.

Chapter 2

CO_2 SEPARATION BY REACTIVE POLYMER MEMBRANE: REACTIONS AND TRANSPORT MECHANISMS

This chapter describes the various reaction mechanisms between CO_2 and amines such as zwitterionic mechanism, termolecular mechanism, base-catalyzed hydration mechanism, alcohol-group bonding of CO_2, etc. This helps to understand the concept about the formation of CO_2-amine complex. Based on these reaction mechanisms the underlying principle of facilitated transport of CO_2 through the thin-film dense polymer composite membrane is also presented in this chapter.

2.1 INTRODUCTION

Reactive polymer membrane based CO_2 separation involves chemical reaction of the CO_2 with the carriers. In case of acid gas separation, researchers are normally using different amines as a carrier because amines react rapidly, selectively and reversibly with CO_2 and are relatively nonvolatile. Commonly gaseous species transport through the conventional

polymeric membranes by solution-diffusion mechanism [1]. First the species dissolves in the polymer film and then diffuses across the membrane due to an imposed concentration driving force followed by the pressure difference. Gaseous species transports through reactive polymeric membrane by the combination of solution-diffusion mechanism and facilitated transport mechanism. In case of facilitated transport mechanism, target species are transported through the membrane by reversible chemical reaction between the reactive carrier and species. The mechanism is analogous to chemical absorption process at feed side (high partial pressure) of the membrane and desorption process on the permeate side (low partial pressure) of the membrane. The total flux of the facilitated transport membrane is the combination of Fickian diffusion and carrier-mediated diffusion [2]. As shown in Figure 2.1, the CO_2-amine carrier complex reaction in the membrane creates another transport mechanism in addition to solution-diffusion mechanism. After CO_2 molecule dissolves in the membrane, it can diffuse through its concentration gradient or react with carrier (amine) species. At low CO_2 partial pressure (before carriers are saturated), the reaction between CO_2 and carriers is fast, and the growing concentration of CO_2-carrier complex is much faster than the concentration of dissolved CO_2 molecules in feed side of membrane. The CO_2 transport is dominated by facilitated transport. At high CO_2 partial pressure at the feed side when the concentration of free CO_2 is much higher than CO_2-carriers complex then Fickian diffusion plays an important part. In this situation the membrane suffers more from the loss of facilitated effect. In between this two limiting regimes, the contributions of both reaction and diffusion are important.

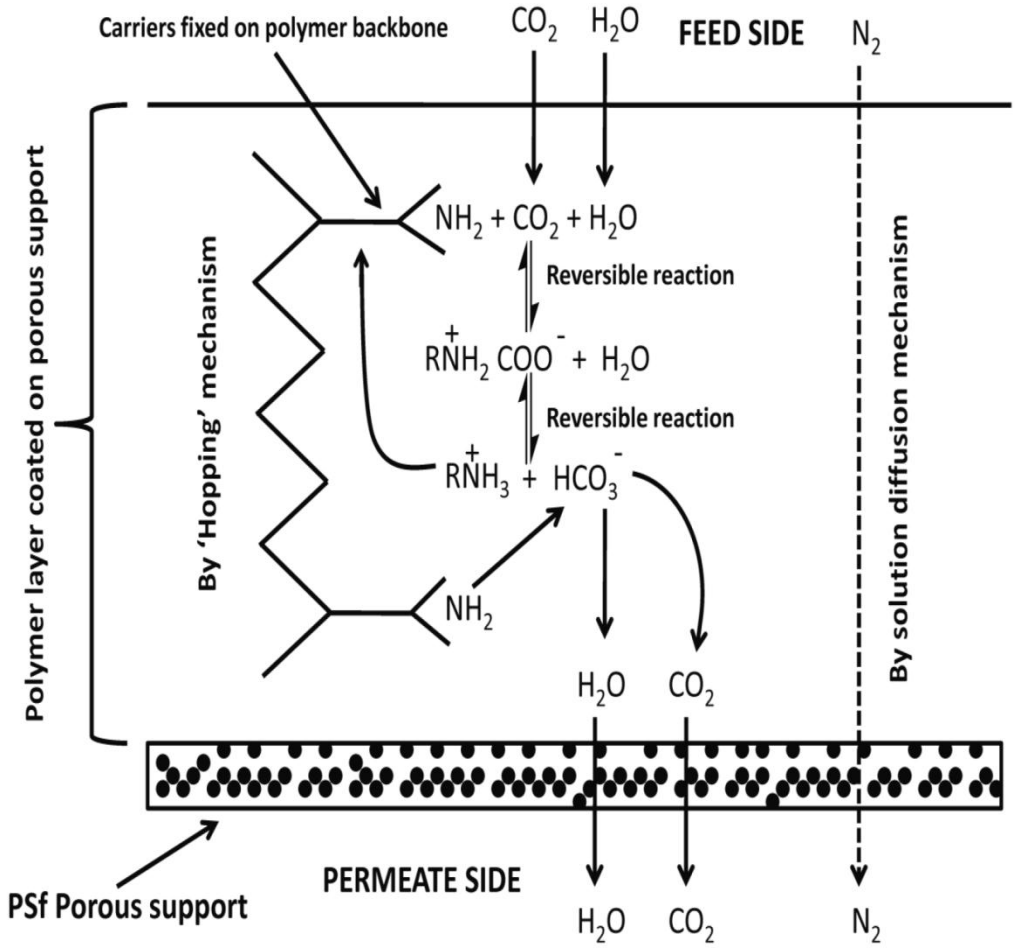

Figure 2.1 Schematic of CO_2 and N_2 transport mechanism through reactive dense polymeric membrane

2.2 CO_2-AMINE CHEMISTRY

The amines are normally distinguished as a primary, secondary and tertiary amine if one, two or three carbon containing groups are attached to the nitrogen atom, respectively. Also, the amines can be sterically hindered or sterically unhindered based on their chemical structure. A primary amine in which the amino-group is attached to a tertiary carbon atom or a secondary amine in which the amino-group is attached to at least one secondary or tertiary carbon atom is called sterically hindered amine [3, 4]. Some of the industrially useful amines are monoethanolamine (MEA), diethanolamine (DEA), di-2-propanolamine (DIPA), N-methyldiethanolamine (MDEA), 2-amino-2-methyl-1-propanol (AMP) and 2-amino-2-hydroxymethyl-1,3-propanediol (AHPD). The structural formulas of these amines are given in Figure 2.2. The reaction kinetics between CO_2 and amines has been mostly investigated for amine absorption process. The principle reaction mechanism when amine solutions are used to absorb the CO_2 may be represented as follows.

2.2.1 Zwitterionic Mechanism

Zwitterionic mechanism is one of the popular mechanisms for CO_2-amine reaction proposed by Caplow [5] and then modified by Danckwerts [6]. CO_2 with amine reaction is considered as a two-step reaction: first CO_2 makes bond with amine functionalized group then amine proton is transferred to the second molecule. This second molecule should be a base molecule. In the first step of the reaction, zwitterion has been formed. In the second step the zwitterion has been deprotonated by base catalyzed to form carbamate ion.

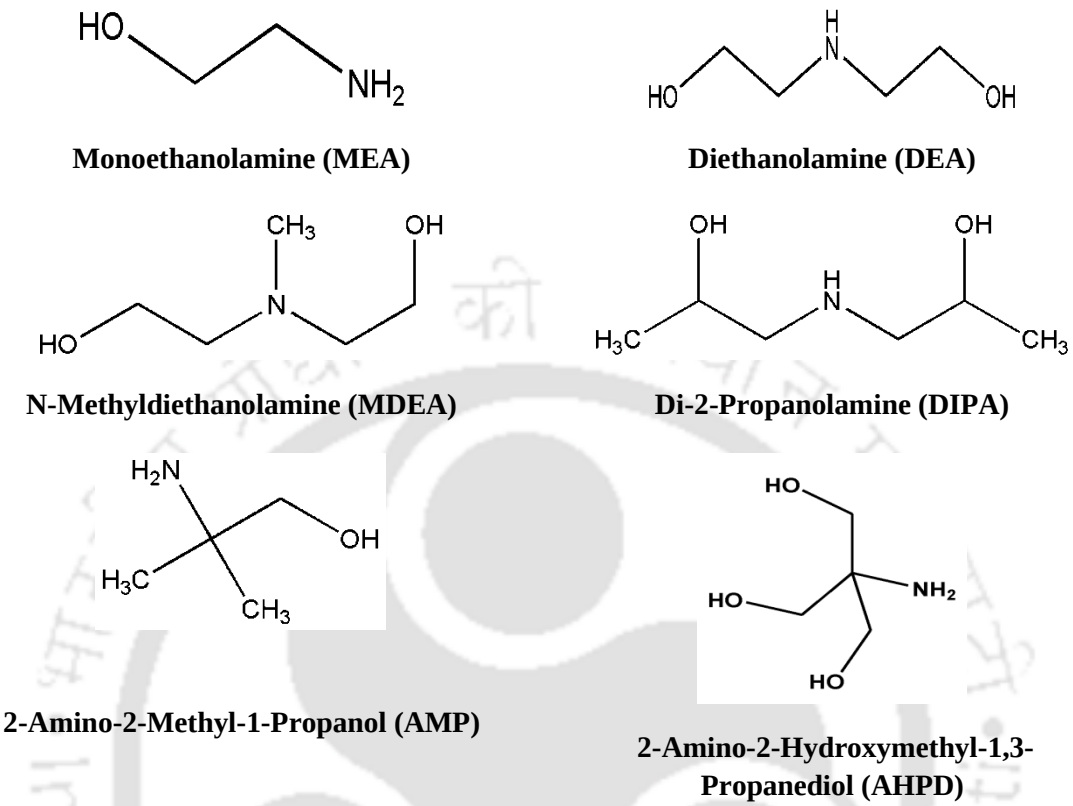

Figure 2.2 The structural formulas for some important amines

The base could be amine itself, (OH^-) ion or H_2O [7]. Initially, Caplow [5] assumed that water makes hydrogen bond with amine (shown in Figure 2.3) before amine makes zwitterion with CO_2 molecule. This concept has however been removed in the later published literature by Danckwerts [6], Versteeg et al. [8] and Kumar et al. [9]. CO_2 reacts in aqueous amine systems to form either bicarbonate or carbamate. These species are shown in the Figure 2.4. So, according to this mechanism, reaction between CO_2 and the amine proceeds through the formation of a zwitterion as mentioned below.

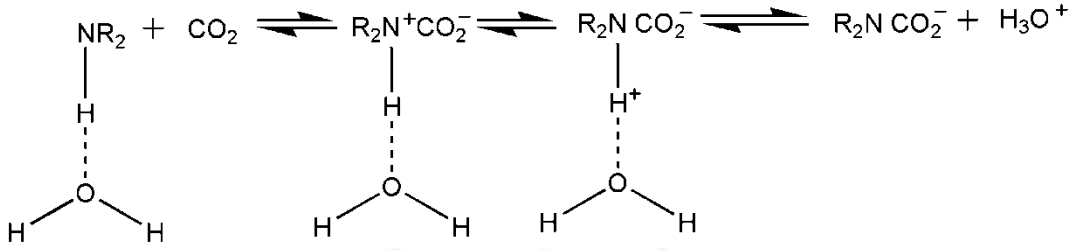

Figure 2.3 Formation of carbamate by zwitterionic mechanism

Figure 2.4 Structural formulae of bicarbonate and carbamate ions

$$CO_2 + RR'NH \leftrightarrow RR'NH^+COO^- \quad (2.1)$$

where *RR'NH* represents a primary or a secondary amine and zwitterion is deprotonated by base, b, to form carbamate ion as follows:

$$RR'NH^+COO^- + b \leftrightarrow RR'NCOO^- + bH^+ \quad (2.2)$$

The contribution of (OH^-) ion might be neglected as its concentration is very low compared with those of amine and H_2O [10]. If the base, b, in the reaction described by Equation. (2.2) is the amine itself, the carbamate formation can be represented as follows:

$$RR'NH^{+}COO^{-} + RR'NH \leftrightarrow RR'NCOO^{-} + RR'NH_2^{+} \quad (2.3)$$

In this case, the overall reaction in a solution is given by the sum of reactions represented by Equations (2.1) and (2.3):

$$CO_2 + 2RR'NH \leftrightarrow RR'NCOO^{-} + RR'NH_2^{+} \quad (2.4)$$

where $RR'NH_2^{+}$ is called protonated amine. If the amine is sterically hindered, the zwitterion reacts more easily with water and amine to form bicarbonate ion as follows:

$$RR'NH^{+}COO^{-} + H_2O \leftrightarrow HCO_3^{-} + RR'NH_2^{+} \quad (2.5)$$

In this case, the overall reaction for the formation of bicarbonate ion is given by the sum of reactions represented by Equations (2.1) and (2.5):

$$CO_2 + RR'NH + H_2O \leftrightarrow HCO_3^{-} + RR'NH_2^{+} \quad (2.6)$$

The carbamate ion of the sterically hindered amine is very unstable and may also readily undergo hydrolysis to form bicarbonates and releases free amine molecules as follows:

$$RR'NCOO^{-} + H_2O \leftrightarrow HCO_3^{-} + RR'NH \quad (2.7)$$

These free amine molecules can again react with CO_2. From the above reaction mechanism it can be visualized that the formation of bicarbonate ions is more compared to carbamate ions. Thus, bicarbonate ions will be present in larger amounts in the solution in case of sterically hindered amines. However, a certain amount of carbamate hydrolysis (Reaction (2.7)) occurs with all amines, particularly at high pressures [3]. Carbamate stability constants (K_C) can be represented as follows:

$$K_C = \frac{[RR'NCOO^-]}{[RR'NH][HCO_3^-]} \tag{2.8}$$

The reported values of carbamate stability constant of aqueous MEA, DEA and AMP measured by ^{13}C NMR at 313 K are presented in Table 2.1 [4, 11 and 12]. As observed from the Table 2.1, the carbamate stability constant of sterically hindered amine is much lower than the primary and secondary sterically unhindered amine

Table 2.1 Carbamate stability constants for hindered and conventional amines by ^{13}C NMR [4, 11 and 12]

$K_C = \frac{[RR'NCOO^-]}{[RR'NH][HCO_3^-]}$	
Amine	K_C at 313 K (m^3kmol^{-1})
MEA	12.5
DEA	2
AMP	<0.1

2.2.2 Aqueous Solution Chemistry

The effect of water on the reaction between CO_2 and amine has great importance. The most important reaction in aqueous chemistry is the water dissociation reaction.

$$H_2O \leftrightarrow H^+ + OH^- \tag{2.9}$$

In aqueous solution, CO_2 can react with water or its dissociated product like H^+ ion or OH^- ion, as follows:

$$CO_2 + H_2O \leftrightarrow H_2CO_3 \tag{2.10}$$

$$CO_2 + OH^- \leftrightarrow HCO_3^- \tag{2.11}$$

$$HCO_3^- + OH^- \leftrightarrow CO_3^{2-} + H_2O \tag{2.12}$$

$$HCO_3^- + H_3O^+ \leftrightarrow H_2CO_3 + H_2O \tag{2.13}$$

Reactions (2.10) and (2.11) are called finite rate reaction whereas reactions (2.12) and (2.13) are involved in proton transfer with instantaneous at equilibrium.

Now primary, secondary and tertiary amines might react with water to form protonated amines which further can react with hydroxide ion to revert back to the original amines as follows:

$$RR'NH + H_2O \leftrightarrow RR'NH_2^+ + OH^- \tag{2.14}$$

$$RR'NH_2^+ + OH^- \leftrightarrow RR'NH + H_2O \tag{2.15}$$

2.2.3 Termolecular Mechanism

Crooks and Donnellan [13] invented this mechanism which was modified by da Silva and Svendsen [12]. According to this mechanism one molecule of amine simultaneously react with one molecule of CO_2 and one molecule of a base (b). The bond formation among amine, CO_2 and base (b) take place simultaneously (Figure 2.5). The reaction proceeds in a single step via a loosely-bound encounter complex as the intermediate as follows:

$$CO_2 + RR'NH \cdots b \leftrightarrow RR'NCOO^- \cdots bH^+ \quad (2.16)$$

This complex further can dissociate to form reactant molecules (CO_2 and amine).

2.2.4 Base-catalyzed Hydration Mechanism

Tertiary amines (RR'R"N) can't react directly with CO_2 [14]. Such amines normally react in presence of water by hydration of CO_2. This can be represented as:

$$CO_2 + RR'R"N + H_2O \leftrightarrow RR'R"NH^+ + HCO_3^- \quad (2.17)$$

In aqueous solutions, an amine dissociation reaction may also occur:

$$RR'R"N + H_2O \leftrightarrow RR'R"NH^+ + OH^- \quad (2.18)$$

Jørgensen and Faurholt [15] reported that the direct reaction between CO_2 and tertiary amines may occur at high pH and the resulting product may be the formation of monoalkylcarbonate. However, at pH values lower than 12, the rate of this reaction can be neglected [16]. Yu et al. [17] proposed that the base-catalysis reaction could also be explained by a zwitterion-type mechanism as follows:

$$CO_2 + RR'R''N \leftrightarrow RR'R''NCOO^- \quad (2.19)$$

$$RR'R''NCOO^- + H_2O \leftrightarrow RR'R''NH^+ + HCO_3^- \quad (2.20)$$

Equation (2.19) represents a reaction of the amine with CO_2 to form an unstable complex. Equation (2.20) describes the homogeneous hydrolysis reaction in which water reacts with the zwitterion-type complex to yield bicarbonate.

2.2.5 Alcohol-group Bonding of CO_2

It has been suggested that at very high pH values, CO_2 can make bond with alcohol-groups. The mechanism is analogous to that of the carbamate formation (Figure 2.6). This reaction is however in general not expected to play a significant role in industrial CO_2 absorption processes as the pH of the system is usually not high enough.

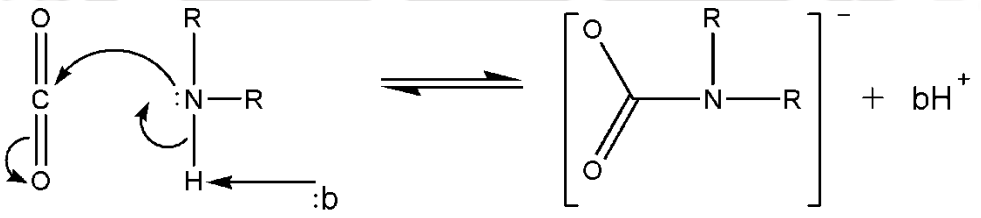

Figure 2.5 Formation of carbamate by termolecular mechanism

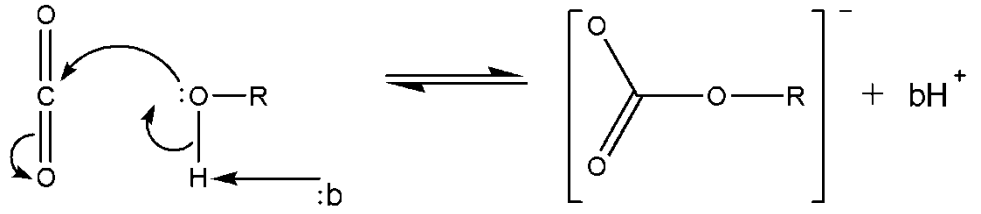

Figure 2.6 Alcohol bonding of CO_2

2.2.6 Molecules with Multiple Amine Functionalities

Molecules can have more than one amine functionality. Among the amine carriers being considered for membrane synthesis tetraethylenepentamine (TEPA), pentaethylenehexamine (PEHA), polyethyleneimine (PEI) and polyallylamine (PAA) have multiple amine functionalities. The nature of the functional groups is the same in such molecules as in simpler amines. The form of interactions with CO_2 is therefore also likely to be the same. In the case of multiple amine functionalities (Figure 2.7) there is however a greater number of species that can be formed. The reaction mechanism of CO_2 with this primary and secondary amines is similar as zwitterionic mechanism discussed above because this mechanism is widely accepted due to its versatility.

2.3 THEORY OF GAS PERMEATION THROUGH POLYMER MEMBRANES

The first polymer membrane based gas separation was observed by Thomas Graham in 1829 [18, 19]. In 1866, he first proposed the "solution-diffusion mechanism", where he said that the permeation process involved the dissolution of penetrant, followed by transmission of the dissolved species through the membrane. In 1855, Fick [20] proposed the law of mass diffusion from the analogy of Fourier's law of heat conduction. As per Fick [20], the penetrant flux, *J* (one dimensional diffusion) can be represented as:

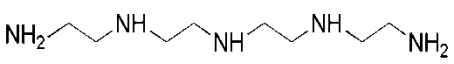

tetraethylenepentamine (TEPA)

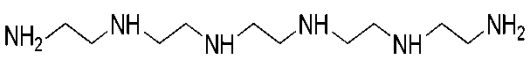

pentaethylenehexamine (PEHA)

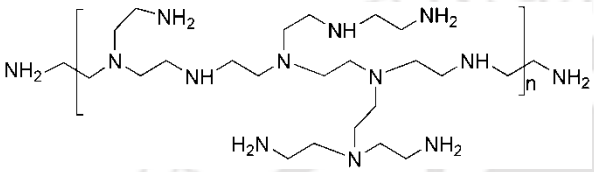

polyethyleneimine (PEI)

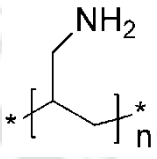

polyallylamine (PAA)

Figure 2.7 Molecular structures of multiple amine functionalities species

$$J = -D\frac{dC}{dx} \tag{2.21}$$

where D is the diffusion coefficient and the driving force, dC/dx is the concentration gradient across the membrane. Under steady-state conditions this equation can be integrated to give:

$$J_i = D_i \frac{(C_{i,\,feed} - C_{i,\,permeate})}{L} \tag{2.22}$$

where $C_{i,\,feed}$ and $C_{i,\,permeat}$ are the concentrations in the membrane on feed side and permeate side, respectively. L is the thickness of the membrane.

Henry's law states that a linear relationship exists between the concentration of the species inside the membrane C_i and the partial pressure of the gas outside of the membrane (p_i), i.e.

$$C_i = S_i \,.\, p_i \tag{2.23}$$

where S_i is the solubility coefficient of the component in the membrane. Henry's law is mainly applicable to the amorphous elastomeric polymers for the solubility behavior. Now, combining the equations (2.22) and (2.23) gives:

$$J_i = \frac{D_i \,.\, S_i \,(p_{i,\,feed} - p_{i,\,permeate})}{L} \tag{2.24}$$

where $p_{i,\,feed}$ and $p_{i,\,permeate}$ are the partial pressures of the species *i* on feed side and permeate side of the membrane, respectively

In late 1870's, Stefan and Exner [20] showed that gas permeation through soap membrane was proportional to the product of solubility coefficient (*S*) and diffusion coefficient (*D*). Later, Wroblewski [20] showed that under steady-state conditions, the diffusion and solubility coefficients are independent of concentration. The product of solubility coefficient (*S*) and diffusion coefficient (*D*) is called the permeability coefficient, *P*, i.e.

$$P = D \,.\, S \tag{2.25}$$

So the equation (2.24) can be written as:

$$J_i = \frac{P_i \,(p_{i,\,feed} - p_{i,\,permeate})}{L} = \frac{P_i}{L}\Delta p_i \tag{2.26}$$

From Equation (2.26), it has been clearly shown that the penetrant flux, J across the membrane is proportional to the partial pressure difference (Δp) and inversely proportional to the membrane thickness. The conventional unit for expressing P is Barrers, where 1 Barrer = 10^{-10} (cm^3 (STP) . cm / cm^2 . sec . cmHg).

The ideal selectivity of the membrane for gas A over gas B, α_{AB} is thus defined as the ratio of permeability values for two gases, i.e.

$$\alpha_{AB} = \frac{P_A}{P_B} \tag{2.27}$$

In case of binary gas system, the selectivity of the membrane is thus defined as:

$$\alpha_{AB} = \frac{y_A / y_B}{x_A / x_B} \tag{2.28}$$

where y_A and y_B are the mole fractions of gas A and B at permeate side, respectively and x_A and x_B are the mole fractions of gas A and B at feed side, respectively.

Although, the study of gas permeation is 150 years old, significant improvement have been made only in the last three decades. The interest in the field was generated from the developments of new synthetic polymeric materials. Morphology of the polymer plays a significant role in the case of gas transport and separation through polymer membranes.

Facilitated Transport Membranes: The first significant analysis on mathematical aspects of facilitated transport was done by Goddard et al. [21]. Their analysis was mainly based on the limit of very fast and slow reactions and they also discussed the techniques for obtaining approximate solutions. Goddard [22] provided a detailed analysis which mainly

focused on systems near the reaction equilibrium limit. Perturbation analysis was carried out by Smith et al. [23] to obtain solutions for very fast and very slow reaction limit. Yung and Probestian [24] used a similarity transform to simplify the differential equations and the numerical solution was obtained based on this transform.

The most common reaction mechanism used in modeling and analysis of facilitated transport is given by:

$$A + B \leftrightarrow AB \tag{2.29}$$

where A = solute being transported, B = carrier, AB = solute-carrier complex.

Recently a lot of interest has been arising in fixed-site carrier membranes, which are solid polymer films into which carriers are incorporated within the membrane. These membranes have a limit of facilitated transport since it does not contain liquid phase. Cussler et al. [25] had presented a theory describing facilitated transport in these membranes which is based on chained-carrier or "Tarzan swng" mechanism. According to their theory, two carriers should be close enough to each other to "pass off" a solute molecule from one carrier to another. The concentration of carriers decreases with an increasing distance between carriers. At some concentration (percolation threshold) the distance becomes too large for pass-off of solute molecules, which results in decrease of solute flux. They derived expression for solute flux for both diffusion limited and reaction limited regimes and concluded that the equations have the same form as normal facilitated transport.

Noble's theory [26] suggests that it does not require the existence of percolation threshold. According to his theory solute molecules can migrate between the carriers by moving along the polymer chains.

Facilitated transport could be affected by transfer of heat. The effect of heat on facilitation was shown by Kemp and Noble [27]. They showed that imposing a temperature gradient across the membrane could cause a significant increase or decrease in facilitation. At intense conditions, reversal in the direction of facilitated flux could take place.

REFERENCES

[1]. J. Crank and G. S. Park. 1968. Diffusion in polymers. New York: Academic press.

[2]. L. Deng, T. J. Kim and M. B. Hagg, Facilitated transport of CO_2 in novel PVAm/PVA blend membrane, J. Membr. Sci. 340 (2009) 154-163.

[3]. G. Sartori and D. W. Savage, Sterically hindered amines for CO_2 removal from gases, Ind. Eng. Chem. Fundam. 22 (1983) 239-249.

[4]. G. Sartori, W. S. W. Ho, D. W. Savage, G. R. Chludinski and S. Wiechert, Sterically hindered amines for acid gas absorption, Separ. Purify. Method. 16 (1987) 171.

[5]. M. Caplow, Kinetics of carbamate formation and breakdown, J. Am. Chem. Soc. 90 (1968) 6795-6803.

[6]. P. V. Danckwerts, The reaction of CO_2 with ethanolamines, Chem. Eng. Sci. 34 (1979) 443-446.

[7]. P. M. M. Blauwhoff, G. F. Versteeg and W. P. M. Van Swaaij, A study on the reaction between CO_2 and alkanolamines in aqueous solution, Chem. Eng. Sci. 38 (1983) 1411-1429.

[8]. G. F. Versteeg, L. A. J. Van Dijck and W. P. M. Van Swaaij, On the kinetics between CO_2 and alkanolamines both in aqueous and non-aqueous solution. An Overview, Chem. Eng. Comm. 144 (1996) 113-158.

[9]. P. S. Kumar, J. A. Hogendoorn, G. F. Versteeg and P. H. M. Feron, Kinetics of the reaction of CO_2 with aqueous potassium salt of taurine and glycine, AIChE J. 49 (2003) 203-213.

[10]. S. Xu, Y. W. Wang, F. D. Otto and A. E. Mather, Kinetics of the reaction of CO_2 with 2-amino-2-methyl-1-propanol solutions, Chem. Eng. Sci. 51 (1996) 841-850.

[11]. S. Paul, Absorption of CO_2 by single and blended amine solvents in various gas-liquid contactors, PhD Dissertation. Indian Institute of Technology Guwahati (2008).

[12]. E. F. da Silva and H. F. Svendsen, Ab initio study of the reaction of carbamate formation from CO_2 and alkanolamines, Ind. Eng. Chem. Res. 43 (2004) 3413-3418.

[13]. J. E. Crooks and J. P. Donnellan, Kinetics and mechanism of the reaction between carbon dioxide and amines in aqueous solution, J. Chem. Soc., Perkin Trans. 2: Phy. Org. Chem. 4 (1989) 331-333.

[14]. T. L. Donaldson and Y. N. Nguyen, Carbon dioxide reaction kinetics and transport in aqueous amine membranes, Ind. Eng. Chem. Fundam. 19 (1980) 260-266.

[15]. E. Jørgensen and C. Faurholt, Reactions between carbon dioxide and amino alcohols. II. triethanolamine, Acta Chem. Scand. 8 (1954) 1141-1144.

[16]. J. Benitez-Garcia, G. Ruiz-Ibanez, H. A. Al-Ghawas and O. C. Sandall, On the effect of basicity on the kinetics of carbon dioxide absorption in tertiary amines, Chem.Eng. Sci. 46 (1991) 2927-2931.

[17]. W. C. Yu, G. Astarita and D. W. Savage, Kinetics of carbon dioxide absorption in solutions of methyldiethanolamine, Chem. Eng. Sci. 40 (1985) 1585-1590.

[18]. V. Stannett, The transport of gases in synthetic polymeric membranes-an historic perspective, J. Membr. Sci. 3 (1978) 97.

[19]. K. W. Boddeker, The early history of membrane science: selected papers, J. Membr. Sci. 100 (1995) 1.

[20]. S. S. Dhingra, Mixed gas transport study through polymeric membranes: A novel technique, PhD Dissertation. Virginia Polytechnic Institute and State University (1997).

[21]. J. D. Goddard, J. S. Schultz and S. R. Suchdeo, Facilitated transport via carrier-mediated diffusion in membranes: part II. mathematical aspects and analyses, AlChE J. 20(4) (1974) 625-645.

[22]. J. D. Goddard, Further applications of carrier- mediated transport theory: a survey, Chem. Eng. Sci. 32 (1977) 795.

[23]. K. A. Smith, J. H. Meldon and C. K. Colton, An analysis of carrier-facilitated transport, AlChE J. 19(1) (1973) 102.

[24]. D. Yung and R. L. Probstein, Similarity considerations in facilitated transport, J. Phys. Chem. 77(18) (1973) 2201.

[25]. E. L. Cussler, R. Aris, and A. Bhown, On the limits of facilitated diffusion, J. Membr. Sci. 43 (1989) 149-164.

[26]. R. D. Noble, Analysis of facilitated transport in fixed site carrier membranes, J. Membr. Sci. 50 (1990) 207-214.

[27]. N. J. Kemp and R. D. Noble, Heat transfer effects in facilitated transport liquid membranes, Sep. Sci. Technol. 18 (1983) 1147-1165.

Chapter 3

SYNTHESIS AND CHARACTERIZATION OF NEW CO_2-SELECTIVE MEMBRANES

This chapter presents the procedures followed for the synthesis of different membranes. The details characterizations of the membranes are included. Materials used and their purities are also provided.

3.1 INTRODUCTION

Since most of the polymer membranes are affected by high temperature application, an attempt has been made to improve the thermal stability of the membrane by varying the degree of crosslinking and polymer blending. Poly (vinyl alcohol) (PVA) is chosen as the base polymer for this work as discussed in Chapter 1. Formaldehyde (HCHO) and polyvinylpyrrolidone (PVP) have been used as a crosslinking and polymer blending agent, respectively to improve the thermal stability of the membrane. The pyrrolidone rings in PVP contain a proton accepting carbonyl moiety, while PVA presents hydroxyl groups. Therefore, a hydrogen-bonding interaction may take place between these two chemical moieties in blends of PVA and PVP [1-4]. The same interaction is responsible

for the solubility of PVA and PVP in water [5]. Polymer blend has attracted intense interest in recent years and there had been few detailed studies dealing with PVA/PVP blends [4, 6-10].

Many single or blended amines have been utilized for the CO_2 selective membranes which are reported in the literature review section (Chapter 1). In this research, different combinations of novel single and blended amines were introduced into the polymer hydrogel to enhance the CO_2 transport property through the membrane. Miscibility between polymers and amines is a key factor, since it affects the mechanical properties such as morphology, permeability, degradation and thermal stability [11-24]. The amine compositions in the membrane have been carefully controlled so as to obtain thermally stable and highly permeable CO_2-selective membrane. The amines considered for this study were polyethyleneimine (PEI), tetraethylenepentamine (TEPA), pentaethylenehexamine (PEHA), poly(allylamine) (PAA) and 2-amino-2-hydroxymethyl-1,3-propanediol (AHPD). The synthesized membranes have been characterized to understand the morphology, thermal degradation and stability. Four different characterization techniques i.e. Thermo Gravimetric Analysis (TGA), Differential Scanning Calorimetry (DSC) Analysis, Fourier Transform Infrared (FTIR) Spectroscopy Analysis and Crystal Structure by X-ray Diffraction (XRD) have been used. All the characterizations were done for active layer only which was found to be optically transparent to visible light and mechanically stable to be handled. The main interest is in the study of glass transition temperature (T_g), melting temperature (T_m), degree of crystallinity, swelling ratio analysis and weight loss of polymer fraction of the membranes.

3.2 MATERIALS

Poly(vinyl alcohol) (98-99 mole% hydrolyzed powder, *M*w = 130,000), polyvinylpyrrolidone (*Mw* = 360,000), polyethyleneimine (average *Mw* = 25,000), tetraethylenepentamine (*Mw* = 189.3), pentaethylenehexamine (*Mw* = 232.37) and poly(allylamine hydrochloride) (*M*w = 56,000) were procured from Sigma–Aldrich, USA. Formaldehyde (37 wt. % aqueous solution), potassium hydroxide and 2-amino-2-hydroxymethyl-1,3-propanediol (*Mw* = 121.14) were purchased from Merck, India and used without further purification. Microporous polysulfone supports (thickness: about 150 micron and average pore size: 0.03 micron) were obtained from Sterlitech USA.

3.3 EXPERIMENTAL

3.3.1 Membrane Synthesis

Active layer of thin-film-composite membranes was synthesized by the solution casting methodology on the porous polysulfone support. The membrane synthesis process is mainly divided into three parts. Firstly, PVA polymer hydrogel was synthesized with different mole percent degree of crosslinking using formaldehyde as a crosslinking agent. Secondly, crosslinked-PVA polymer hydrogel was blended with polyvinylpyrrolidone at different PVA/PVP weight percentage ratio. And finally, a suitable amine carrier was introduced into the crosslinked-PVA-PVP polymer hydrogel.

3.3.1.1 Crosslinked-PVA Membrane Synthesis

The membrane was synthesized by varying the degree of crosslinking of poly (vinyl alcohol) with formaldehyde. Weight percentage of PVA (90 wt%) and KOH (10 wt%)

were kept constant for all the membranes compositions. KOH was used as a basic catalyst for aldol condensation reaction to enhance the crosslinking reaction rate. Dry compositions of the membrane were 90wt% PVA + 10 wt% KOH with 10 to 80 mole% degree of crosslinking by HCHO.

The membranes were synthesized according to the procedure published elsewhere [24, 25]. Initially, PVA was dissolved in water at 95^{o}C under vigorous stirring. A stoichiometric amount of formaldehyde and a calculated amount of potassium hydroxide (KOH) was added into the PVA aqueous solution to achieve a desired degree of crosslinking. The PVA/formaldehyde/KOH solution was heated at about 95^{o}C for the time period of 16 hours under stirring. Calculation of amount of HCHO added is shown in Appendix A1.1 and A1.2. The solution was then centrifuged at 11000 rpm for 35 min before casting. The liquid polymer hydrogel was cast onto a porous polysulfone support membrane. The thickness was controlled by using an adjustable micrometer casting knife (GARDCO, Paul N. Gardner, USA). The composite membrane was first dried at room temperature inside a fume hood overnight to remove the surface water. Then they were heated at 120^{o}C inside an oven over the time period of 8 hours to ensure complete crosslinking reaction with PVA and removal of water. To observe the mixed gas (CO_2/N_2) permeation through crosslinked-PVA composite membrane, a membrane with the active layer thickness of 44 micron on the porous polysulfone support was synthesized and discussed in Chapter 4.

To characterize the membranes, the liquid polymer hydrogel was cast onto a glass plate using casting knife and kept inside the fume hood overnight. Finally, it was peeled out carefully from the glass plate and dried in an oven at around 120^{o}C for 8 hours.

3.3.1.2 Crosslinked-PVA-PVP Membrane Synthesis

The optimum degree of crosslinking of PVA with HCHO was selected as 60 mole% among others, above which liquid polymer hydrogel agglomerate (Discussed in section 3.4.2). The ratio of PVA and PVP was then varied keeping the concentration of KOH constant at 10 wt%. Four different compositions of membranes were synthesized by varying the PVA/PVP ratio (PVA/PVP = 1/0.25, 1/0.5, 1/1, 1/2). The dry compositions of the membranes were (72 wt% PVA + 18 wt% PVP + 10 wt% KOH), (60 wt% PVA + 30 wt% PVP + 10 wt% KOH), (45 wt% PVA + 45 wt% PVP + 10 wt% KOH) and (30 wt% PVA + 60 wt% PVP + 10 wt% KOH).

The aqueous solution of PVA was prepared at 95^{o}C under vigorous stirring. A stoichiometric amount of formaldehyde and a calculated amount of potassium hydroxide (KOH) was added into the PVA aqueous solution to achieve a 60 mole% degree of crosslinking. The PVA/formaldehyde/KOH solution was heated at about 95^{o}C for the time period of 9 hours under stirring. A calculated amount of polyvinylpyrrolidone was added slowly to the PVA/formaldehyde/KOH solution and heated at same temperature for the time period of 7 hours under stirring. The viscosity of the solution increased significantly. This increase might be due to the crosslinking of PVA and addition of PVP. Calculation of amount of PVP added is shown in Appendix A1.3. The solution was then centrifuged at 11000 rpm for 35 min before casting. The liquid polymer hydrogel was

cast onto a glass plate using casting knife and kept inside the fume hood overnight. Finally, it was peeled out carefully from the glass plate and dried at oven around 120^{o}C for 8 hours. The synthesized crosslinked-PVA-PVP membranes were then used for detail characterization.

3.3.1.3 Synthesis of New Crosslinked-PVA-PVP Membrane Containing Different Single and Blended Amines

The PVA/PVP ratio was considered as 1:0.2 (Discussed in section 3.4.3). 60 mole% degree of crosslinking of PVP with HCHO was maintained. Concentration of KOH was kept constant for all the compositions at 10 wt%. Different amines and their blends were incorporated into the crosslinked-PVA-PVP polymer hydrogel. Four different sets of crosslinked-PVA-PVP membranes containing single amine and their blends were prepared. The compositions of each membrane based on the percentage of each component present in the polymer film on dry basis are given in Table 3.1. The synthesis procedure of each set of membrane doped with amine is briefly discussed below:

Table 3.1 Detailed compositions of different amine based thin-film composite membranes with 60 mole% degree of crosslinking by HCHO

Set - 1 Crosslinked-PVA-PVP with PEI and TEPA	**Set - 2 Crosslinked-PVA-PVP with PEI and PEHA**	**Set - 3 Crosslinked-PVA-PVP with PAA and PEHA**	**Set - 4 Crosslinked-PVA-PVP with PAA and AHPD**
41.66 wt% PVA + 8.33 wt% PVP + 10 wt% KOH + **40 wt% PEI**	41.66 wt% PVA + 8.33 wt% PVP + 10 wt% KOH + **15 wt% PEI + 25 wt% PEHA**	41.66 wt% PVA + 8.33 wt% PVP + 10 wt% KOH + **40 wt% PAA**	41.66 wt% PVA + 8.33 wt% PVP + 10 wt% KOH + **40 wt% PAA**
41.66 wt% PVA + 8.33 wt% PVP + 10 wt% KOH + **30 wt% PEI + 10 wt% TEPA**	41.66 wt% PVA + 8.33 wt% PVP + 10 wt% KOH + **15 wt% PEI + 25 wt% TEPA**	41.66 wt% PVA + 8.33 wt% PVP + 10 wt% KOH + **25 wt% PAA + 15 wt% PEHA**	41.66 wt% PVA + 8.33 wt% PVP + 10 wt% KOH + **25 wt% PAA + 15 wt% AHPD**
41.66 wt% PVA + 8.33 wt% PVP + 10 wt% KOH + **15 wt% PEI + 25 wt% TEPA**		41.66 wt% PVA + 8.33 wt% PVP + 10 wt% KOH + **15 wt% PAA + 25 wt% PEHA**	41.66 wt% PVA + 8.33 wt% PVP + 10 wt% KOH + **15 wt% PAA + 25 wt% AHPD**

Crosslinked-PVA-PVP membrane with PEI and TEPA (Set-1): The detailed compositions of active layer were 41.66 wt% PVA + 8.33 wt% PVP + 10 wt% KOH + 40 wt% PEI, 41.66 wt% PVA + 8.33 wt% PVP + 10 wt% KOH + 30 wt% PEI + 10 wt% TEPA and 41.66 wt% PVA + 8.33 wt% PVP + 10 wt% KOH + 15 wt% PEI + 25 wt% TEPA. The preparation procedure of crosslinked-PVA-PVP polymer hydrogel is similar as discussed

in Section 3.3.1.2. A proper amount of the aqueous solution of PEI was added into the PVA/formaldehyde/KOH/PVP solution with stirring at around 95^{o}C for about an hour. Thereafter a calculated amount of aqueous TEPA solution was added slowly into the PVA/formaldehyde/KOH/PVP/PEI solution with stirring. Calculation of amount of PEI and TEPA added are shown in Appendix A1.4. The solution was then centrifuged at 11000 rpm for 35 min before casting. The liquid polymer hydrogel was cast onto a glass plate (for characterization) or cast onto a porous polysulfone support membrane (for permeation study) using casting knife and kept inside the fume hood overnight. Then it was carefully peel off from the glass plate and dried in an oven at around 120^{o}C for 8 hours to ensure complete crosslinking reaction with PVA and removal of water.

Crosslinked-PVA-PVP membrane with PEI and PEHA (Set-2): The detailed composition of active layer was 41.66 wt% PVA + 8.33 wt% PVP + 10 wt% KOH + 15 wt% PEI + 25 wt% PEHA. Preparation techniques of crosslinked-PVA-PVP membrane doped with PEI and PEHA is exactly similar to the crosslinked-PVA-PVP membrane doped with PEI and TEPA membrane. Only, the TEPA has been replaced by PEHA. Calculation of amount of PEHA added is shown in Appendix A1.5.

Crosslinked-PVA-PVP membrane with PAA and PEHA (Set-3): The detailed compositions of active layer were 41.66 wt% PVA + 8.33 wt% PVP + 10 wt% KOH + 40 wt% PAA, 41.66 wt% PVA + 8.33 wt% PVP + 10 wt% KOH + 25 wt% PAA + 15 wt% PEHA and 41.66 wt% PVA + 8.33 wt% PVP + 10 wt% KOH + 15 wt% PAA + 25 wt% PEHA. Initially, Free poly(allylamine) was obtained by mixing poly(allylamine hydrochloride) with KOH in methanol (equimolar ratio) for 12 hours. The resulting

potassium chloride was precipitated out from the solution. The methanol was then evaporated at 50°C and water was added as the solvent. Thereafter a calculated amount of aqueous PAA solution was added slowly into the PVA/formaldehyde/KOH/PVP solution with stirring at around 95°C for one hour. Required amount of aqueous PEHA solution was added slowly into the PVA/formaldehyde/KOH/PVP/PAA solution with stirring. Calculation of amount of PAA and PEHA added are shown in Appendix A1.6. The solution was then centrifuged at 11000 rpm for 35 min before casting. After centrifuging, the liquid polymer hydrogel was cast onto a glass plate (for characterization) or onto a porous polysulfone support membrane (for permeation study) using casting knife and kept inside the fume hood overnight. After that it was peeled out carefully from the glass plate and dried at oven around 120°C for 8 hours to ensure complete crosslinking reaction with PVA and removal of water.

Crosslinked-PVA-PVP membrane with PAA and AHPD (Set-4): The detailed compositions of active layer were 41.66 wt% PVA + 8.33 wt% PVP + 10 wt% KOH + 40 wt% PAA, 41.66 wt% PVA + 8.33 wt% PVP + 10 wt% KOH + 25 wt% PAA + 15 wt% AHPD and 41.66 wt% PVA + 8.33 wt% PVP + 10 wt% KOH + 15 wt% PAA + 25 wt% AHPD. A preparation technique of crosslinked-PVA-PVP membrane containing PAA and AHPD is exactly similar to the crosslinked-PVA-PVP membrane containing PAA and PEHA membrane. Only, the PEHA has been replaced by AHPD. Calculation of amount of AHPD added is shown in Appendix A1.7. The detail composite membrane preparation units are given in the Figure 3.1. All the permeation experiments of

crosslinked-PVA-PVP membranes containing different amine mentioned above are discussed in Chapter 4.

3.3.2 Measurement of Membrane Thickness

The cross-section view of SEM photographs of crosslinked-PVA-PVP doped with different amines and their blends on porous polysulfone membrane are shown in Figure 3.2 to 3.4. The membrane has two different layers viz dense active layer and porous polysulfone support layer for all the compositions. Dense active layer helps the selective separation of CO_2 and porous polysulfone support layer provides the mechanical support to the membrane. This composite structure minimizes the mass transfer resistance while maximizing the mechanical strength.

Dense active layer thickness of thin film composite membranes was measured by using a litematic thickness gauge (Make: Mitutoyo, Model: VL-50, Measuring pressure: 0.15N, Japan) with an accuracy of about ±0.2 μm. Figure 3.5 shows the image of litematic thickness gauge instrument. Initially, the thickness of pure polysulfone support layer was measured. After complete preparation of thin-film composite membrane onto a polysulfone support, the total thickness of the composite membrane was measured. The active layer thickness was then calculated from the difference between the total thickness and the thickness of polysulfone support. The dry active layer thickness of the synthesized membranes with different amine compositions are given in Table 3.2.

Figure 3.1 Composite membrane preparation set-up

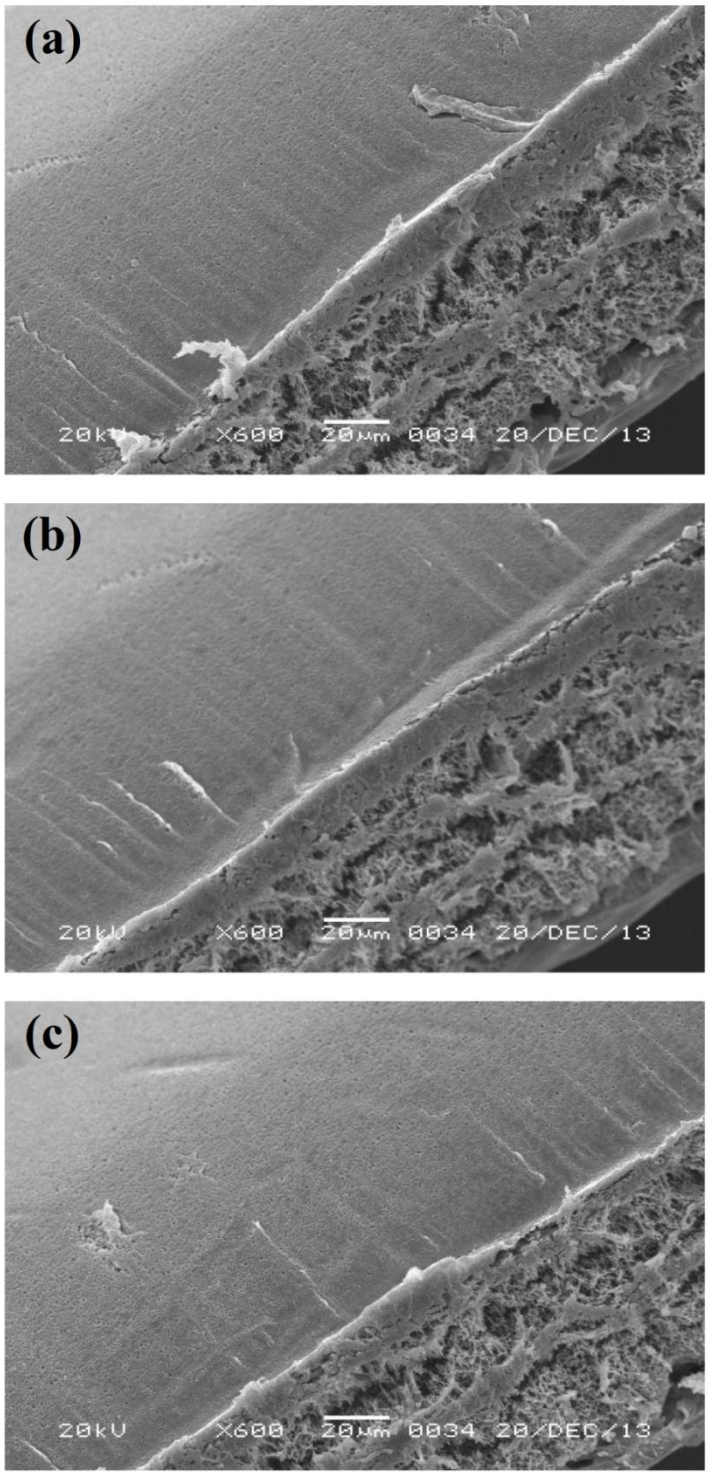

Figure 3.2 SEM image of cross-section view of crosslinked PVA-PVP with amines active layer on porous polysulfone membrane, **(a)** blended amines (15 wt% PEI + 25 wt% TEPA) active layer thickness around 73 micron **(b)** blended amines (30 wt% PEI+10 wt% TEPA) active layer thickness around 75 micron and **(c)** single amine (40 wt% PEI) active layer thickness around 69 micron

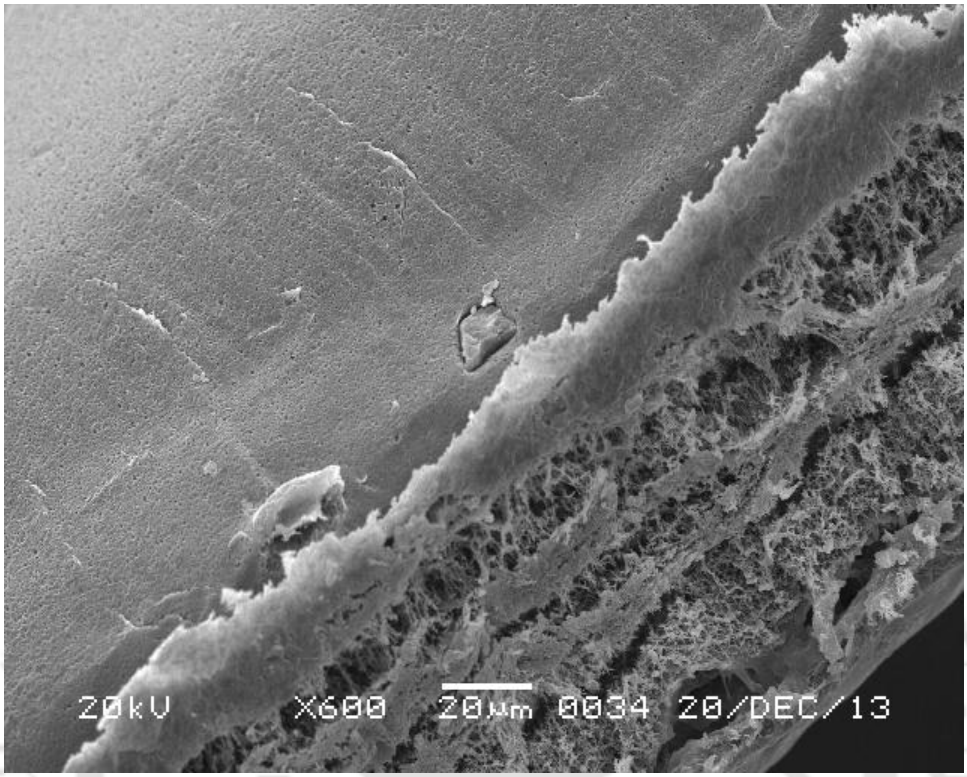

Figure 3.3 SEM image of cross-section view of crosslinked PVA-PVP with amines active layer on porous polysulfone membrane, blended amines (15 wt% PEI + 25 wt% PEHA) active layer thickness around 75 micron

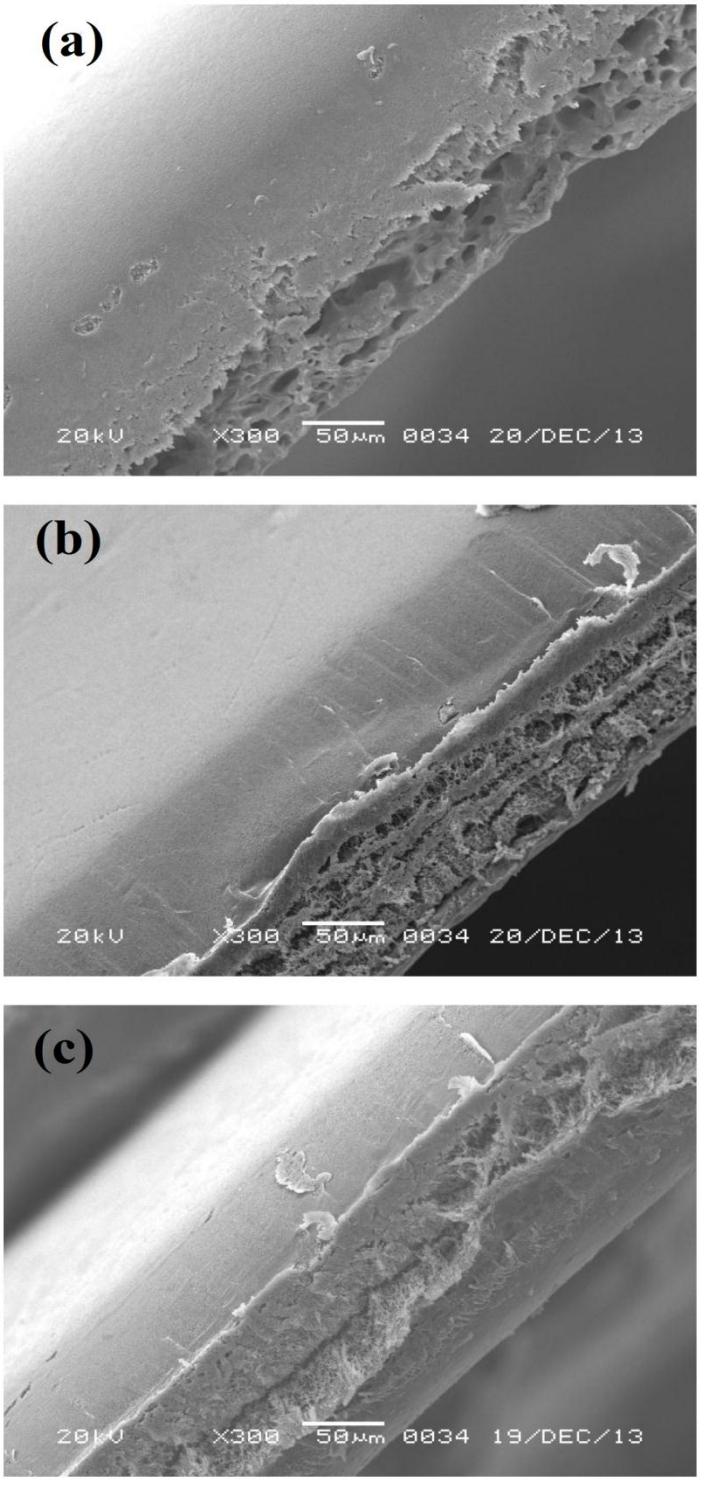

Figure 3.4 SEM image of cross-section view of crosslinked PVA-PVP with amines active layer on porous polysulfone membrane, **(a)** blended amines (25 wt% PAA + 15 wt% PEHA) active layer thickness around 55 micron **(b)** blended amines (15 wt% PAA + 25 wt% PEHA) active layer thickness around 62 micron and **(c)** single amine (40 wt% PAA) active layer thickness around 45 micron

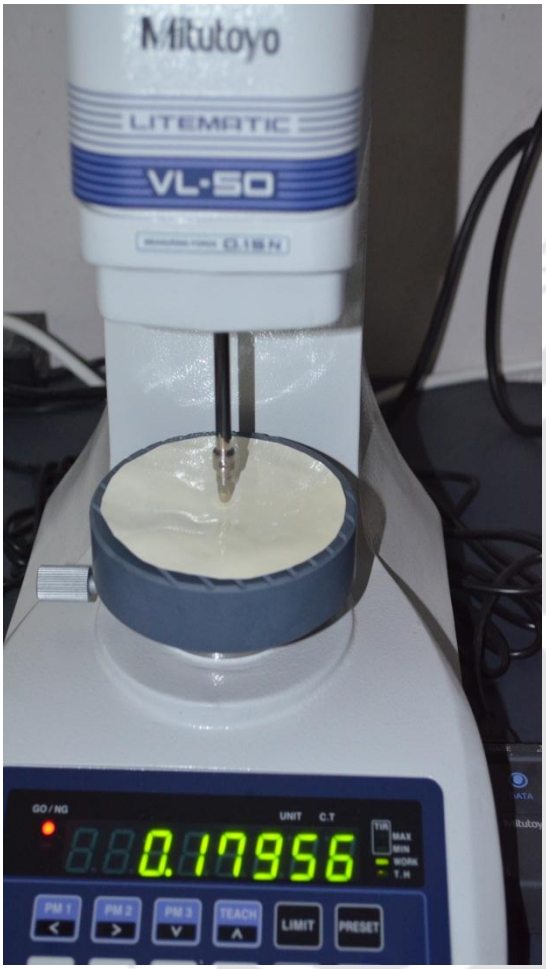

Figure 3.5 Litematic thickness gauge instrument (Make: Mitutoyo, Model: VL-50, Measuring pressure: 0.15N, Japan)

Table 3.2 Different active layer thickness of different compositions of single amine and their blends with 60 mole% degree of crosslinking by HCHO

Active layer composition (wt%)	Active layer Thickness (micron)	Active layer composition (wt%)	Active layer Thickness (micron)
41.66%PVA+8.33% PVP+10%KOH+15% PEI+25% TEPA	34 67 73	41.66%PVA+8.33% PVP+10%KOH+25% PAA+15% PEHA	42 55 78
41.66%PVA+8.33% PVP+10%KOH+15% PEI+25% PEHA	40 60 75	41.66%PVA+8.33% PVP+10%KOH+15% PAA+25% PEHA	41 62 81
41.66%PVA+8.33% PVP+10%KOH+30% PEI+10% TEPA	41 75 87	41.66%PVA+8.33% PVP+10%KOH+25% PAA+15% AHPD	44 58 80
41.66%PVA+8.33% PVP+10%KOH+40% PEI	69	41.66%PVA+8.33% PVP+10%KOH+15% PAA+25% AHPD	43 65 84
41.66%PVA+8.33% PVP+10%KOH+40% PAA	45		

3.3.3 Characterization of the Synthesized Membranes

The synthesized dry membranes were characterized via TGA, DSC, FTIR spectroscopy and XRD analysis. The characterizations were done for thin active layer only. The detailed protocols of all analysis were discussed below.

3.3.3.1 Thermo Gravimetric Analysis

The thermal stability of the synthesized active layers was carried out using TGA/SDTA 851^e system (MATTLER TOLEDO, Switzerland). About 10 mg of sample was taken in the 900 µL sample crucible and then it was allowed for heat treatment from 30^oC to 900^oC at the heating rate of 10^oC per min. All experiments were done under an inert atmosphere (N_2 flow of about 40 cm^3 min^{-1}).

3.3.3.2 Differential Scanning Calorimetry Analysis

To analyze the structural change of the polymer membrane, the glass transition temperature (T_g) and the melting temperature (T_m) of the polymers were investigated by differential scanning calorimetry (DSC) on a DSC 1/400 $STAR^e$ system with a refrigerated cooling arrangement (METTLER TOLEDO, Switzerland). Polymer samples of 3-4 mg were precisely weighed on an electronic microbalance (Sartorius, BT 224 S, Germany). DSC aluminum sample pans with a volume of 40 µL (METTLER TOLEDO, Switzerland) were used for analysis. The sample pans were sealed using the sample encapsulating press (METTLER TOLEDO, Switzerland). An empty sealed pan was used as reference for the determination of glass transition temperature (T_g) and the melting temperature (T_m). The protocol followed by Lucke et al. [26] was applied in this work.

Initially, sample and empty (reference) pans were kept at -40^{o}C for 15 min to attain equilibrium. Both the pans were then heated at the heating rate of 10^{o}C per min from -40^{o}C to 150^{o}C and kept at 150^{o}C for 5 min. The samples were cooled to -40^{o}C at the rate of -10^{o}C per min and again heated to 300^{o}C at the same heating rate. After the 1st heating and cooling cycle, the relaxation phenomena of amorphous polymers were less pronounced and hence T_g and T_m of the polymer were determined from the second heating cycle [27].

3.3.3.3 Fourier Transform Infrared Spectroscopy Analysis

FTIR spectrum analysis (SHIMADZU, IRAffinity 1, Japan) in ATR mode were carried out to resolve the organic chemical groups of the synthesized active layers. FTIR spectra were obtained in the range of wave number from 4000 to 400 cm^{-1} with a 40 scans per sample and 4 cm^{-1} resolutions.

3.3.3.4 Crystal Structure by X-ray Diffraction Analysis

The crystal structure of all active layers was examined using Bruke D8, advanced X-ray diffraction measurement with Cu Kα radiation of wavelength λ = 1.54056 Å for 2Θ angles between 10^{o} and 50^{o}.

3.3.3.5 Swelling Ratio Analysis

Swelling ratio in percentage of crosslinked-PVA-PVP membranes were measured by using four different types of acidic or basic aqueous media. Initially, all the polymeric layers were dried in the hot air oven for around 6 hours. After drying the appropriate weight of each sample (W_0) was measured and immersed in D.I water, 6 (M) CH_3OH, 2

(M) H_2SO_4 and 7 (M) KOH aqueous solution, respectively, at room temperature of about 30^oC [28]. Samples were kept for 2 days until swelling equilibrium was established. All the samples were taken out from immersion bath and excess amount of water was carefully removed from the surface. Final weights of all membranes (W_1) were measured and the percentage swelling ratio (%S) was calculated using the following equation.

$$(\%S) = \frac{W_1 - W_0}{W_0} \times 100 \quad (3.1)$$

3.4 RESULTS AND DISCUSSION

Several membranes have been synthesized as discussed before. The thin membrane layer was found to be optically transparent to visible light and mechanically stable to be handled.

3.4.1 Crosslinking Mechanism and Polymer Blending

During the intermolecular or intramolecular crosslinking, two (OH) groups of PVA react with one mole of HCHO that produces one mole of water and (-C-O-C-) linkage. Figure 3.6 illustrates the crosslinking mechanism of PVA with HCHO and Figure 3.7 shows the polymer blending between crosslinked-PVA and PVP membrane. During polymer blending, the proton accepting carbonyl moiety of PVP might make a hydrogen bond with hydroxyl groups of PVA [6-10].

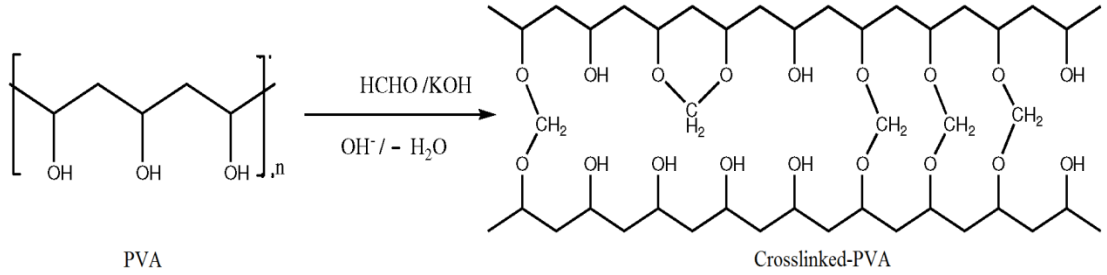

Figure 3.6 Synthesis of PVA crosslinked with formaldehyde (HCHO)

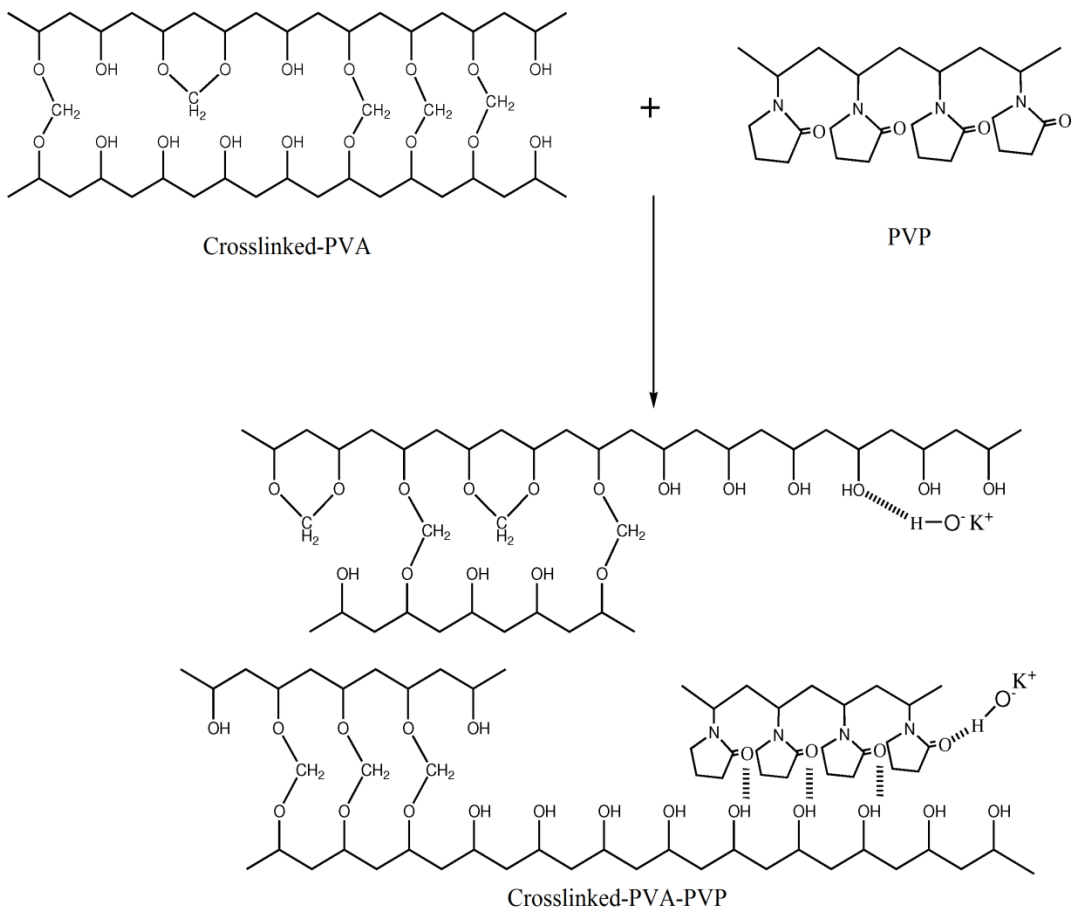

Figure 3.7 Synthesis of crosslinked-PVA blended with polyvinylpyrrolidone (PVP)

3.4.2 Optimization of Degree of Crosslinking

The thermal stabilities and weight loss of PVA membrane (90 wt% PVA and 10 wt% KOH) crosslinked with formaldehyde were determined by TGA curves (Figure 3.8). Degree of crosslinking of PVA with HCHO was varied from 10 mole% to 80 mole%. Each TGA curve showed three main steps of weight loss. The first weight loss was observed below 120^{o}C, due to loss of water which was absorbed from the atmosphere during sample preparation. The presence of KOH in the membrane makes the membrane more hygroscopic. The second weight loss (200-275^{o}C) was associated with the removal of hydroxyl groups present in the membrane. The final weight loss between 400 to 500^{o}C was related to the decomposition of the polymer backbones. With the increase of degree of crosslinking the thermal stability was marginally increased. This might be due to formation of acetal (–C–O–C–) linkage.

The melting temperature (T_m) and glass transition temperature (T_g) were determined by DSC analysis. Figure 3.9 represents the DSC curves of 90 wt % PVA and 10 wt% KOH membranes crosslinked with formaldehyde. Degree of crosslinking was varied from 10 mole% to 80 mole%. It can be seen from the Figure 3.9 that there is one endothermic peak around 248^{o}C, which is the melting temperature (T_m) of all the membranes and also it shows a temperature shift at a region of 68-82^{o}C for all the membranes which might be the glass transition temperature (T_g). It can be observed that the T_g has marginally increased with increasing the degree of crosslinking which attributed to the formation of acetal linkage (-C-O-C-) during the crosslinking reaction.

The functional groups present in the membranes (90 wt % PVA + 10 wt% KOH) with varying degree of crosslinking (10 mole% to 80 mole%) with formaldehyde were obtained using the Fourier transform infrared (FTIR) spectrometer as shown in Figure 3.10. The broad peak around 3288 cm^{-1} for all the membranes is the indication of presence of hydroxyl group (O–H). The sharp peak at 2939 cm^{-1} is assigned to the symmetric vibrations of (C–H), predominantly responsible for alkyl groups [29]. The sharp frequency at 1656 and 1556 cm^{-1} is assigned to (C=C) stretching and combination of (O-H) and (C-H) bending, respectively [30]. The vibrational band observed at around 1408 cm^{-1} and 1329 cm^{-1} refers to the combination of CH_2 bending and CH_2 out of plane bending [29, 30]. The band frequency between 1150-1085 cm^{-1} is assigned to the combination of (–C–O–C–) and (C–O) bond [31, 32]. This (–C–O–C–) bond indicates the formation of acetal linkage during the crosslinking reaction. The peak intensity at 1141 cm^{-1} is marginally increased with the increase of degree of crosslinking (Figure 3.10). The other vibrations less than 852 cm^{-1} are the finger print zone.

The thermal stability was improved with increasing the degree of crosslinking. However, the 90 wt % PVA + 10 wt% KOH with 60 mole% degree of crosslinking with HCHO was the optimum among others, above which liquid polymer hydrogel agglomerate. Hence, this membrane has been chosen for further modification via PVP doping into the polymer hydrogel.

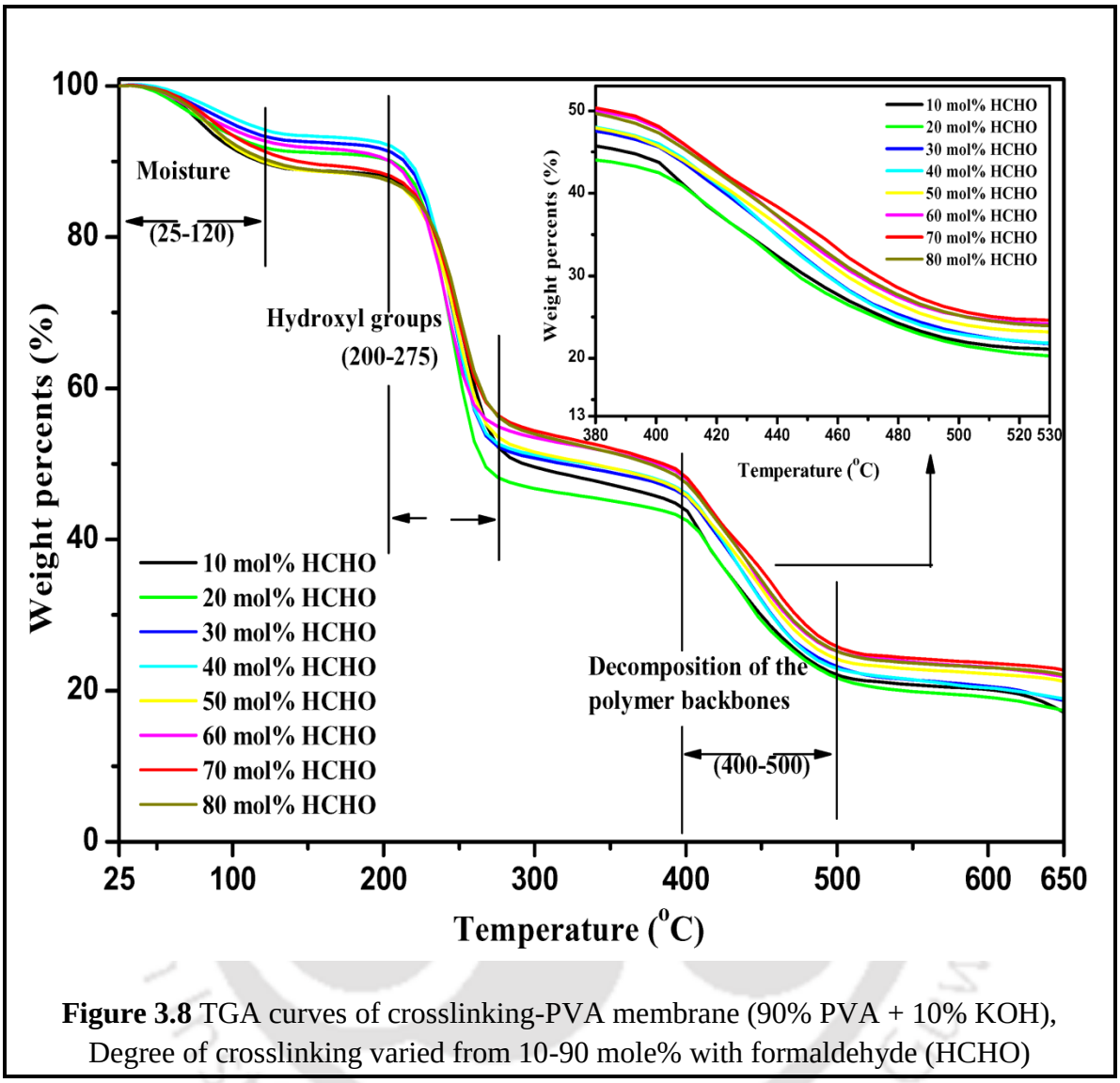

Figure 3.8 TGA curves of crosslinking-PVA membrane (90% PVA + 10% KOH), Degree of crosslinking varied from 10-90 mole% with formaldehyde (HCHO)

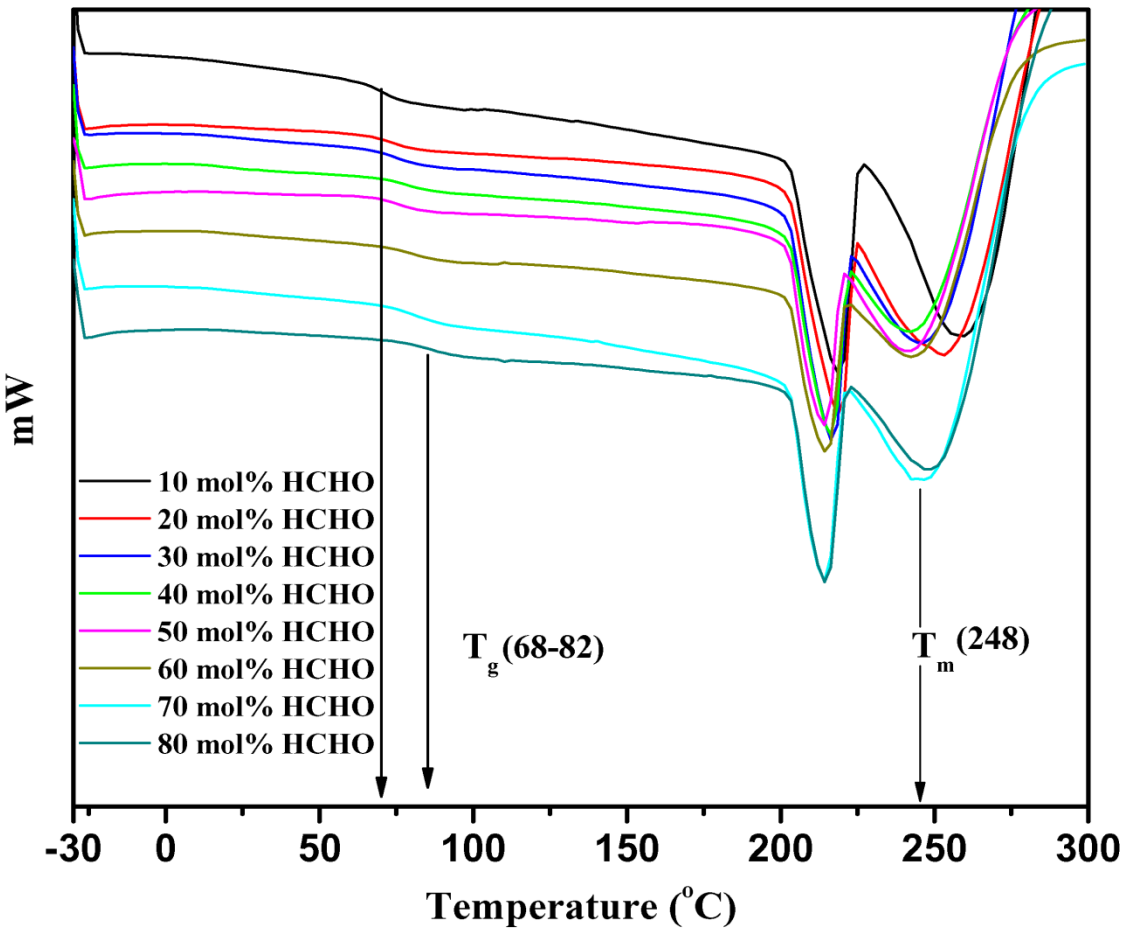

Figure 3.9 DSC curves of crosslinking-PVA membrane (90% PVA + 10% KOH), Degree of crosslinking varied from 10-90 mole% with formaldehyde (HCHO)

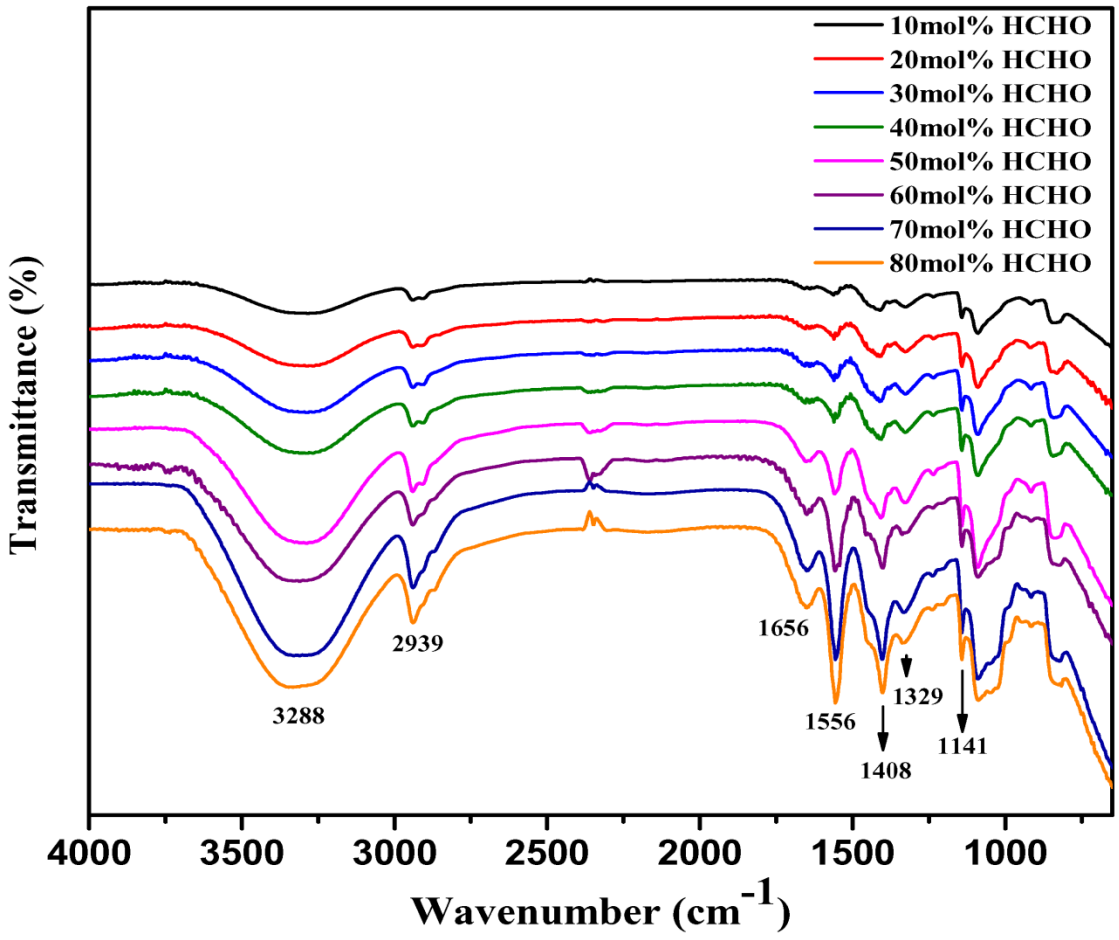

Figure 3.10 FTIR spectra of crosslinking-PVA membrane (90% PVA + 10% KOH), Degree of crosslinking varied from 10-90 mole% with formaldehyde (HCHO)

3.4.3 Optimization of PVA/PVP Ratio

Four different PVA/PVP weight percentage ratio with constant (10 wt%) weight percentage of KOH along with 60 mole% of degree of crosslinking with HCHO membrane were prepared. The detailed compositions of the membrane were (72 wt% PVA + 18 wt% PVP + 10 wt% KOH), (60 wt% PVA + 30 wt% PVP + 10 wt% KOH), (45 wt% PVA + 45 wt% PVP + 10 wt% KOH) and (30 wt% PVA + 60 wt% PVP + 10 wt% KOH). The thermal stabilities and weight loss of crosslinked-PVA-PVP blend polymers were determined by TGA curves (Figure 3.11). Each TGA curve showed three main steps of weight loss. The first weight loss was observed below 150^{o}C, due to loss of water which was absorbed from the atmosphere during sample preparation. The second weight loss (210-275^{o}C) was associated with the removal of hydroxyl groups present in the membrane. It was observed that for PVA without PVP membrane, at this temperature range, (%) wt loss is higher (about 25 wt %) as compared to other four membranes (12% to 5%). This might be due to the presences of PVP. The formation of hydrogen bonds between carbonyl group of PVP and the hydroxyl group of PVA during the polymer blending with PVP might be the probable reason for less weight loss at this temperature region. The final weight loss between 360 to 500^{o}C was related to the decomposition of the polymer backbones.

Figure 3.12 represents the DSC curves of four different membranes which have different PVA/PVP weight percentage ratio with constant (10 wt%) weight percentage of KOH along with 60 mole% of degree of crosslinking with HCHO. Figure 3.12 depicts that there is one endothermic peak at around 248^{o}C, which is the melting temperature (T_m) of

all the membranes and also a temperature shift at a region of 90-120^oC for all the membranes which might be the glass transition temperature (T_g). It can be observed that the T_g has marginally increased with increasing the PVP weight percentage.

The FTIR spectra of the crosslinked-PVA-PVP blend membrane are shown in Figure 3.13. The broad peaks around 3288 cm^{-1} for all crosslinked-PVA-PVP membrane is the indication of hydroxyl group (O–H). The sharp peaks at 2939 cm^{-1} are assigned to the symmetric vibrations of (C–H), predominantly responsible for alkyl groups. The band observed at 1647 and 1558 cm^{-1} represent the stretching vibration of (C=O) bonds. The vibrational bands observed at 1418 cm^{-1} and 1319 cm^{-1} refers to (CH_2) and (OH) bending respectively. The band frequency between 1141 cm^{-1} is assigned to the combination of (–C–O–C–) and (C–O) bond. This (–C–O–C–) bond indicates the formation of acetal linkage during the crosslinking reaction. The other vibrations less than 852 cm^{-1} are the finger print zone.

The crosslinked-PVA-PVP blend membranes have the swells behavior in different aqueous media. The percentage of swelling ratio for different PVA/PVP blend membrane with constant KOH percentage and 60 mole% crosslinked with HCHO in different aqueous medium such as D.I water, 6 (M) CH_3OH, 2 (M) H_2SO_4 and 7 (M) KOH are given in Table 3.3. It can be observed from Table 3.3 that swelling ratio increased drastically with increasing the amount of PVP in the PVA/PVP blend for all aqueous medium. This might be due to the increase of overall hydrophilicity of the blend membrane as PVP polymer is highly hydrophilic in nature. Higher swelling of membrane causes drastic drop in CO_2/N_2 selectivity at elevated temperature under humid condition.

Lower swelling was observed for PVA/PVP ratio of 1:0.25. Since lower swelling is preferred for CO_2/N_2 separation, a smaller PVA/PVP ratio of 1:0.2 was considered for further study.

Figure 3.14 shows the TGA analysis of optimum crosslinked-PVA-PVP membrane and pure PVA membrane. The drastic improvement of weight loss in 200-340^oC temperature range was observed for crosslinked-PVA-PVP membrane compared to pure PVA membrane. For pure PVA membrane, at this temperature range, percentage weight loss is higher (about 75 wt. %) compared to crosslinked-PVA-PVP membrane (25 wt. %). This might be due to the crosslinking and polymer blending of PVA with HCHO and PVP, respectively.

Figure 3.15 shows the DSC analysis of optimum crosslinked-PVA-PVP membrane and pure PVA membrane. DSC analysis shows the drastic improvement of melting temperature (T_m) and glass transition temperature (T_g) of crosslinked-PVA-PVP membrane compared to pure PVA membrane. T_m and T_g have been improved from 224 to 248^oC and 75 to 90^oC, respectively for crosslinked-PVA-PVP membrane compared to pure PVA membrane.

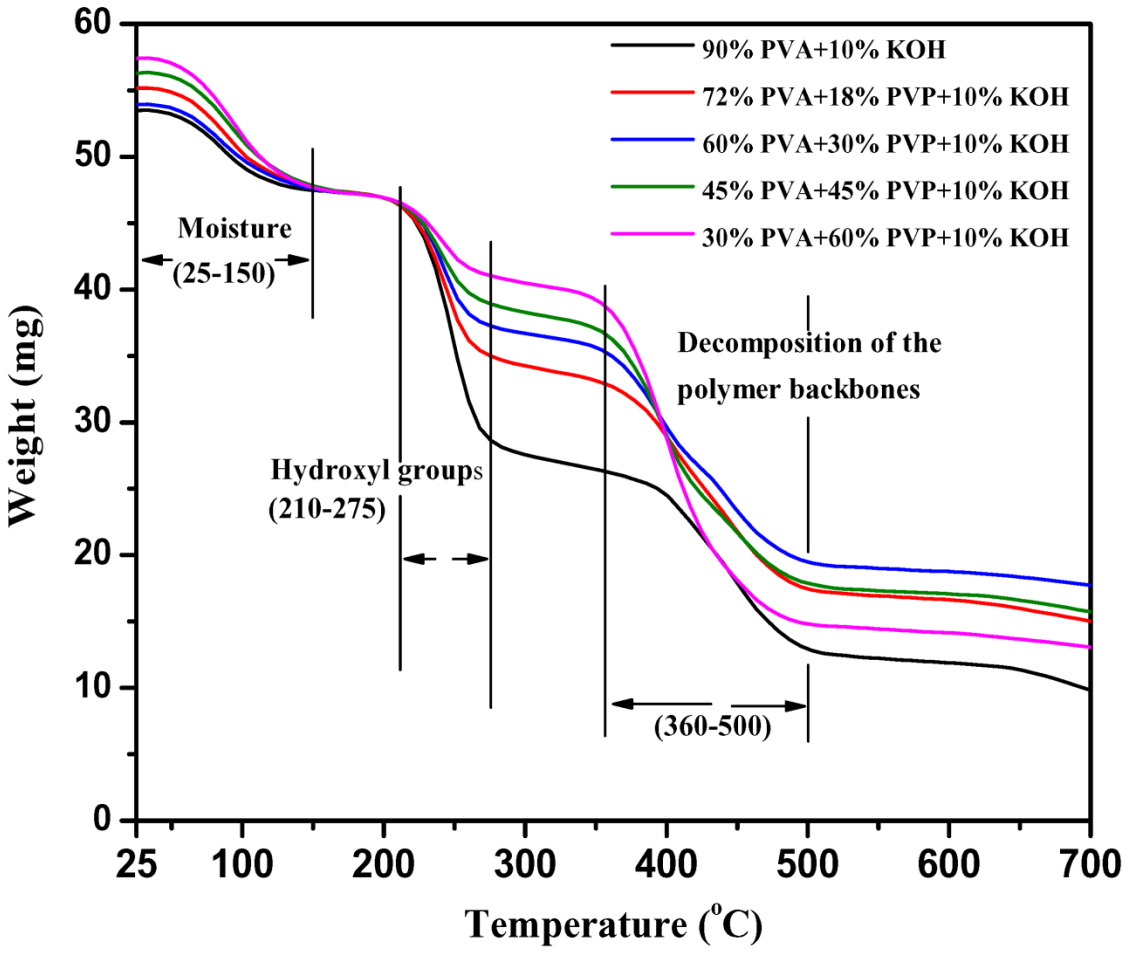

Figure 3.11 TGA curves of crosslinked-PVA membrane blended with PVP, PVA/PVP ratio varied like 1/0.25, 1/0.5, 1/1 and 1/2 with 60 mole% degree of crosslinking by HCHO

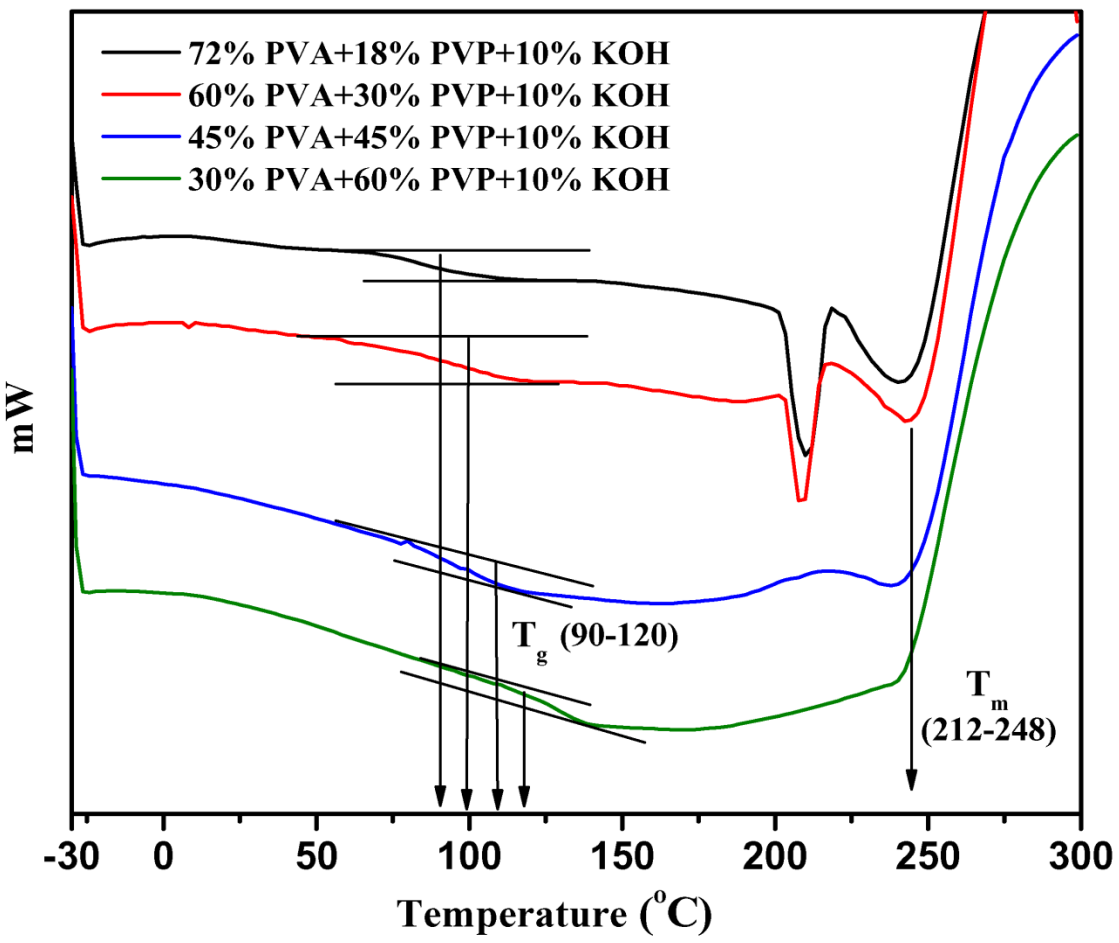

Figure 3.12 DSC curves of crosslinked-PVA membrane blended with PVP, PVA/PVP ratio varied like 1/0.25, 1/0.5, 1/1 and 1/2 with 60 mole% degree of crosslinking by HCHO

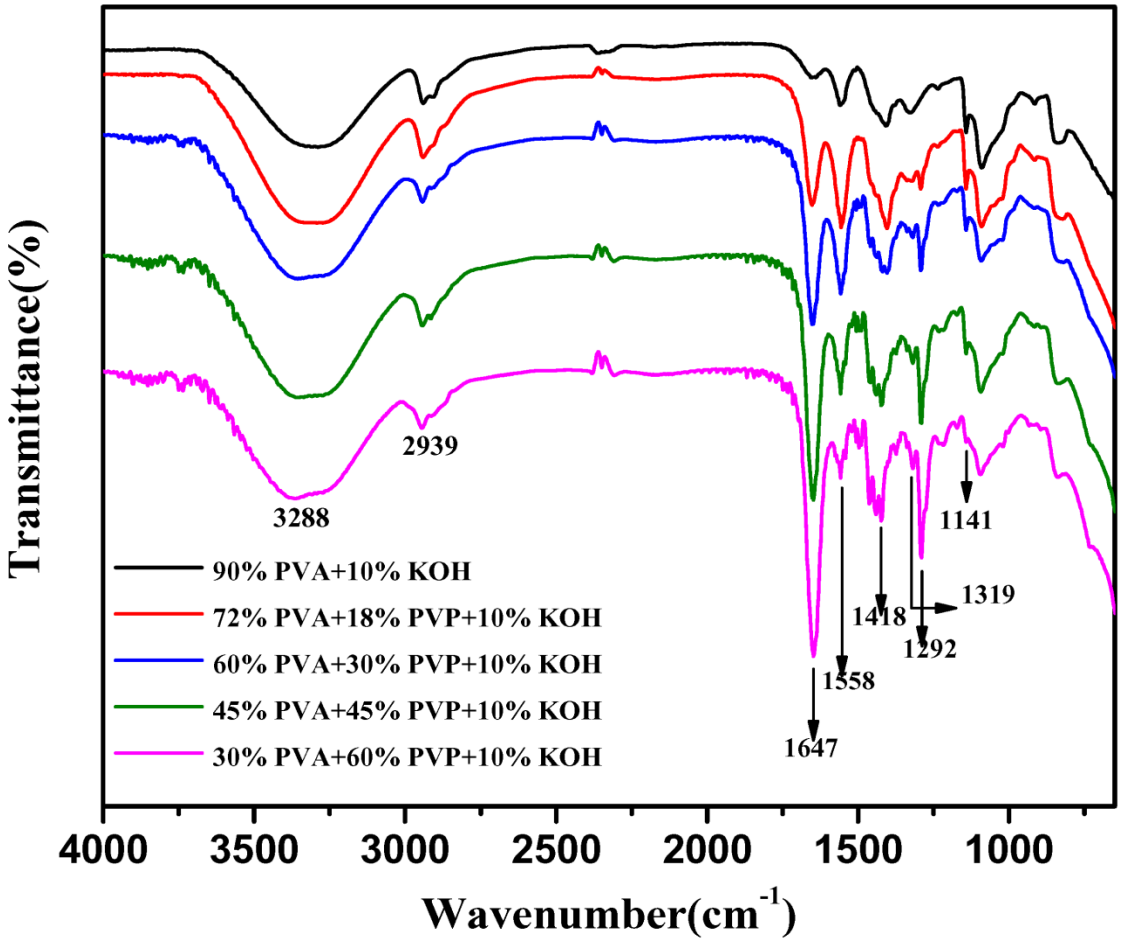

Figure 3.13 FTIR spectra of crosslinked-PVA membrane blended with PVP, PVA/PVP ratio varied like 1/0.25, 1/0.5, 1/1 and 1/2 with 60 mole% degree of crosslinking by HCHO

Table 3.3 Swelling ratio (%) result for all type of membrane with 60 mole% degree of crosslinking by HCHO at 30^{o}C

	S1	**S2**	**S3**	**S4**
	(%) Swelling	(%) Swelling	(%) Swelling	(%) Swelling
D.I H_2O	70.26	98.89	148.3	255.45
6(M) CH_3OH	55.5	82.26	131.85	204.65
2(M) H_2SO_4	89.6	118.57	177	305.09
7(M) KOH	36.66	36.73	34.22	32.38

S1 : 72% PVA + 18% PVP + 10% KOH

S2 : 60% PVA + 30% PVP + 10% KOH

S3 : 45% PVA + 45% PVP + 10% KOH

S4 : 30% PVA + 60% PVP + 10% KOH

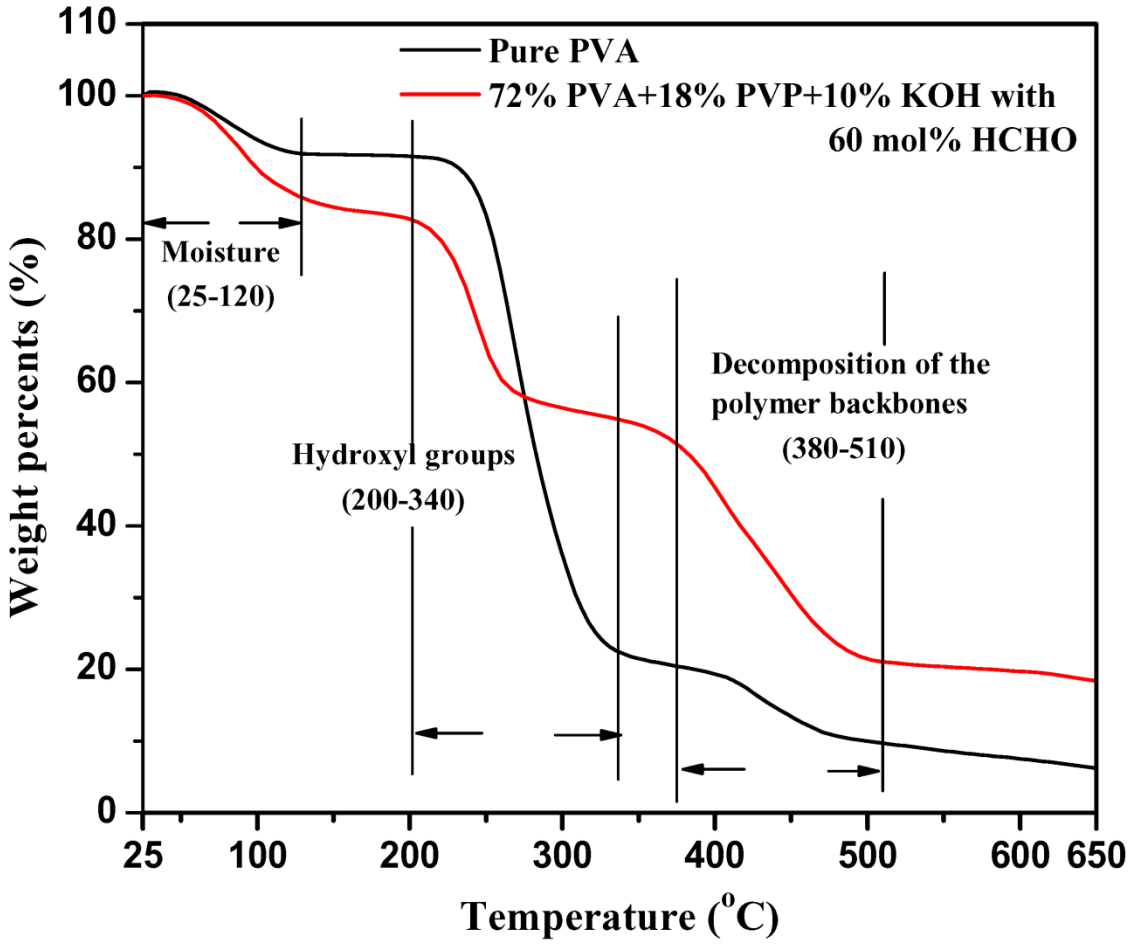

Figure 3.14 TGA curves of Pure PVA and crosslinked-PVA with PVP membranes

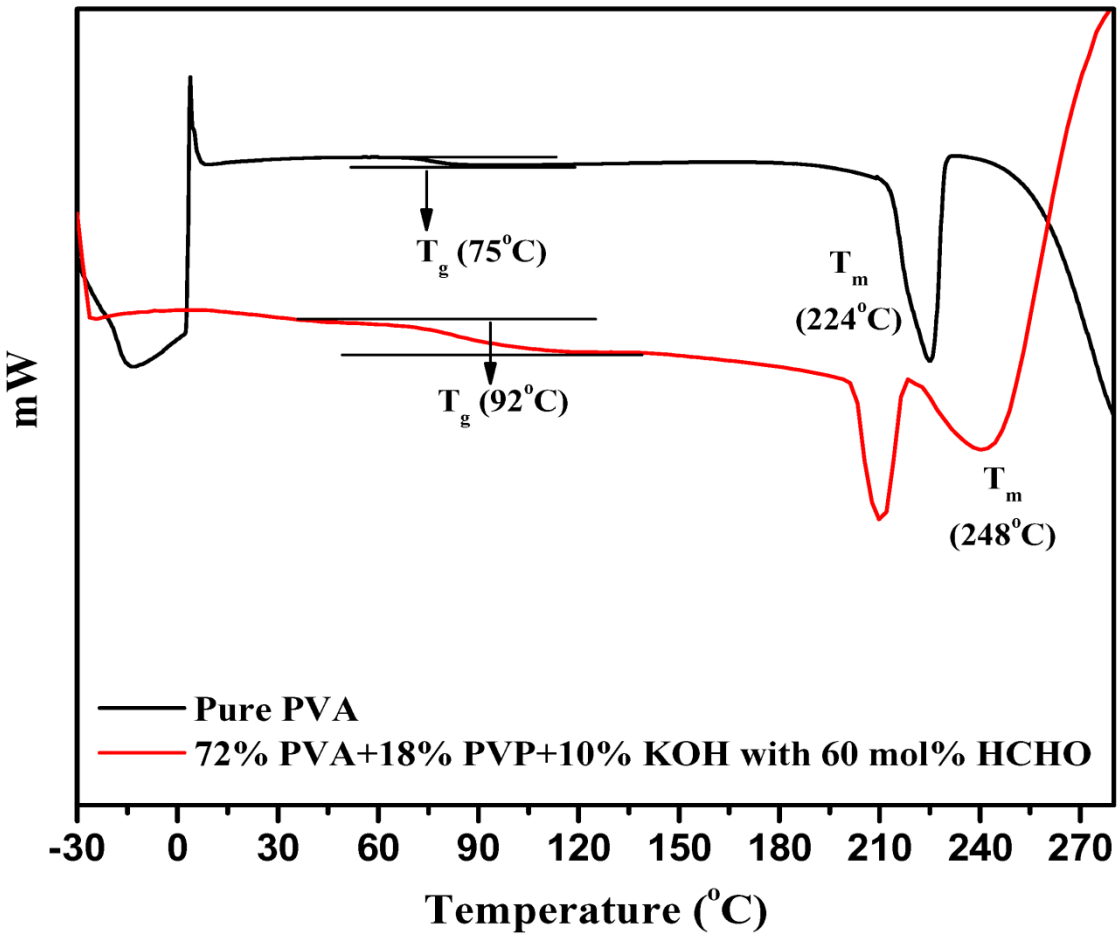

Figure 3.15 DSC curves of Pure PVA and crosslinked-PVA with PVP membranes

3.4.4 Characterization of Membranes Containing PEI, TEPA and Their Blends

The thermal stabilities and weight loss of crosslinked-PVA-PVP blended with PEI and crosslinked-PVA-PVP mixed with PEI and TEPA membrane were determined by TGA curves (Figure 3.16). Each TGA curve showed three main steps of weight loss. The first weight loss was observed below 115^{o}C, due to loss of water which was absorbed from the atmosphere during sample preparation. The second weight loss (204-275^{o}C) was associated with the removal of hydroxyl groups present in the membrane. The final weight loss between 350 to 488^{o}C was related to the decomposition of the polymer backbones. The TGA curves clearly indicated that crosslinked-PVA-PVP membrane containing amines have fairly good thermal stability for potential high temperature application.

Figure 3.17 represents the DSC curves of crosslinked-PVA-PVP blended with PEI and crosslinked-PVA-PVP mixed with PEI and TEPA membrane. An endothermic peak was observed around 240^{o}C which is the melting temperature (T_m) of all the membranes (Figure 3.17) and also a temperature shift was shown at a region of 40-60^{o}C for all the membranes. Hence, the T_g of crosslinked-PVA-PVP blended with (40 wt% PEI), crosslinked-PVA-PVP mixed with (30 wt% PEI + 10 wt% TEPA) and crosslinked-PVA-PVP mixed with (15 wt% PEI + 25 wt% TEPA) membranes were obtained as 45^{o}C, 47^{o}C and 58^{o}C, respectively.

The functional groups present in the crosslinked-PVA-PVP blended with PEI and blends of PEI and TEPA membranes were obtained using FTIR is shown in Figure 3.18. The broad peak around 3267 cm^{-1} for all the membranes is the indication of presence of

hydroxyl group (O–H). The sharp peak at 2912 cm^{-1} is assigned to the symmetric vibrations of (C–H), predominantly responsible for alkyl groups [29]. The sharp frequency at 1650 and 1580 cm^{-1} is assigned to (C=C) stretching and combination of (O-H) and (C-H) bending, respectively [30]. The band frequency between 1150-1085 cm^{-1} is assigned to the combination of (–C–O–C–) and (C–O) bond [31, 32]. This (–C–O–C–) bond indicates the formation of acetal linkage during the crosslinking reaction. In this figure it can be observed that the peak intensity at 1141 cm^{-1} is satisfactory for all three membranes (Figure 3.18). The other vibrations less than 852 cm^{-1} are the finger print zone.

The diffraction pattern for the crosslinked-PVA-PVP membrane containing single amine (PEI) and crosslinked-PVA-PVP membrane containing blended amines (PEI and TEPA) are shown in Figure 3.19. The PVA polymeric film displays a semi-crystalline structure with peaks at 2Θ angles of 20^{o}. It is apparent from Figure 3.19 that the peak intensity of all three membranes at 2Θ angles of 20^{o} was not affected by the addition of single or blended amine to the membrane.

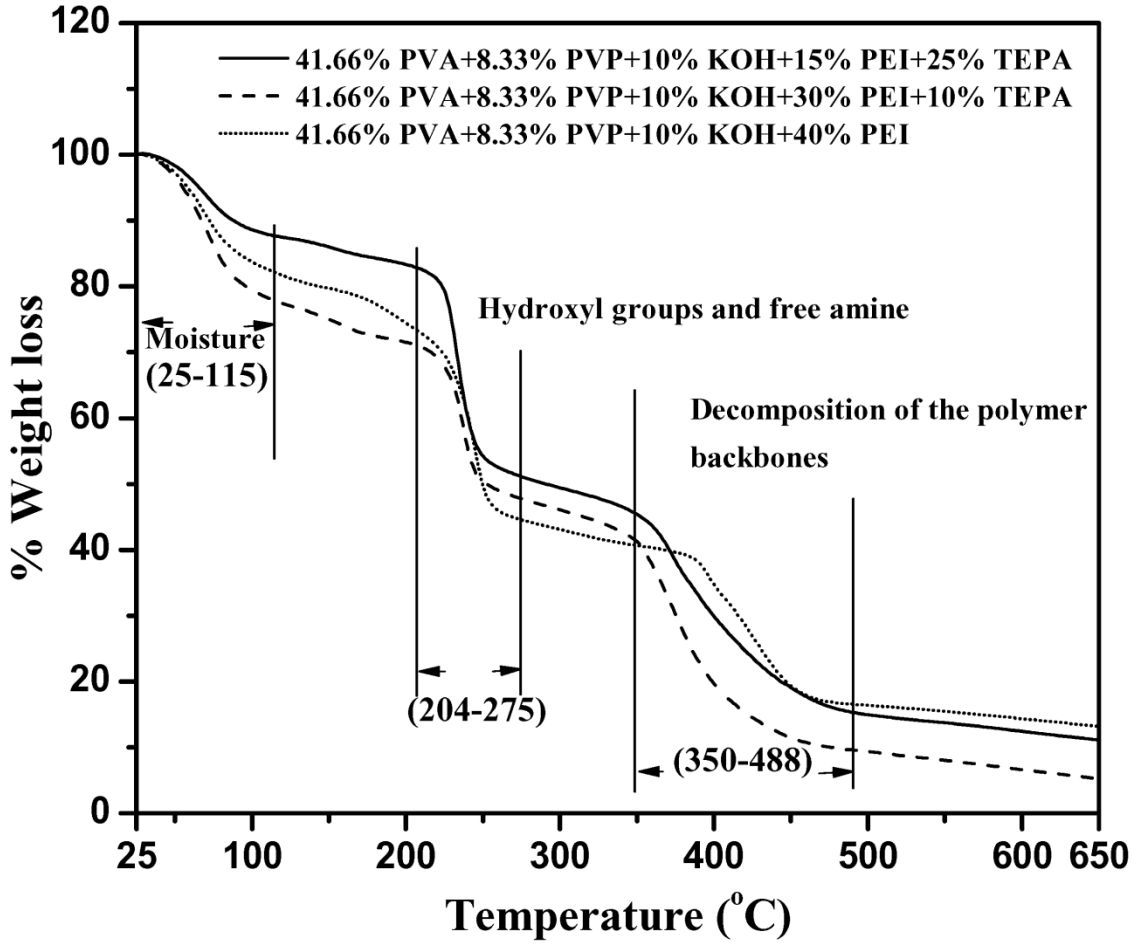

Figure 3.16 TGA curves of crosslinked-PVA-PVP membrane containing single (PEI) and blended (PEI and TEPA) amines. 60 mole% degree of crosslinking of PVA with HCHO

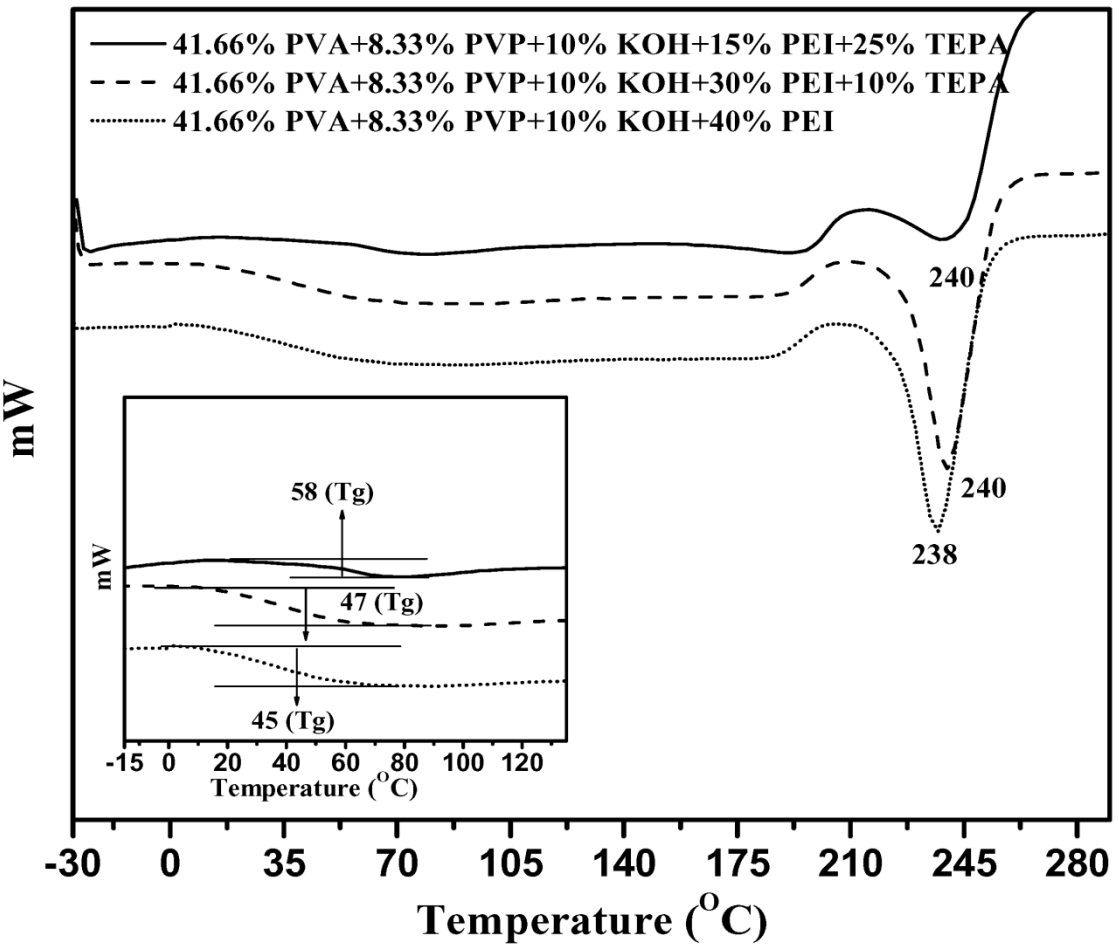

Figure 3.17 DSC curves of crosslinked-PVA-PVP membrane containing single (PEI) and blended (PEI and TEPA) amines. 60 mole% degree of crosslinking of PVA with HCHO

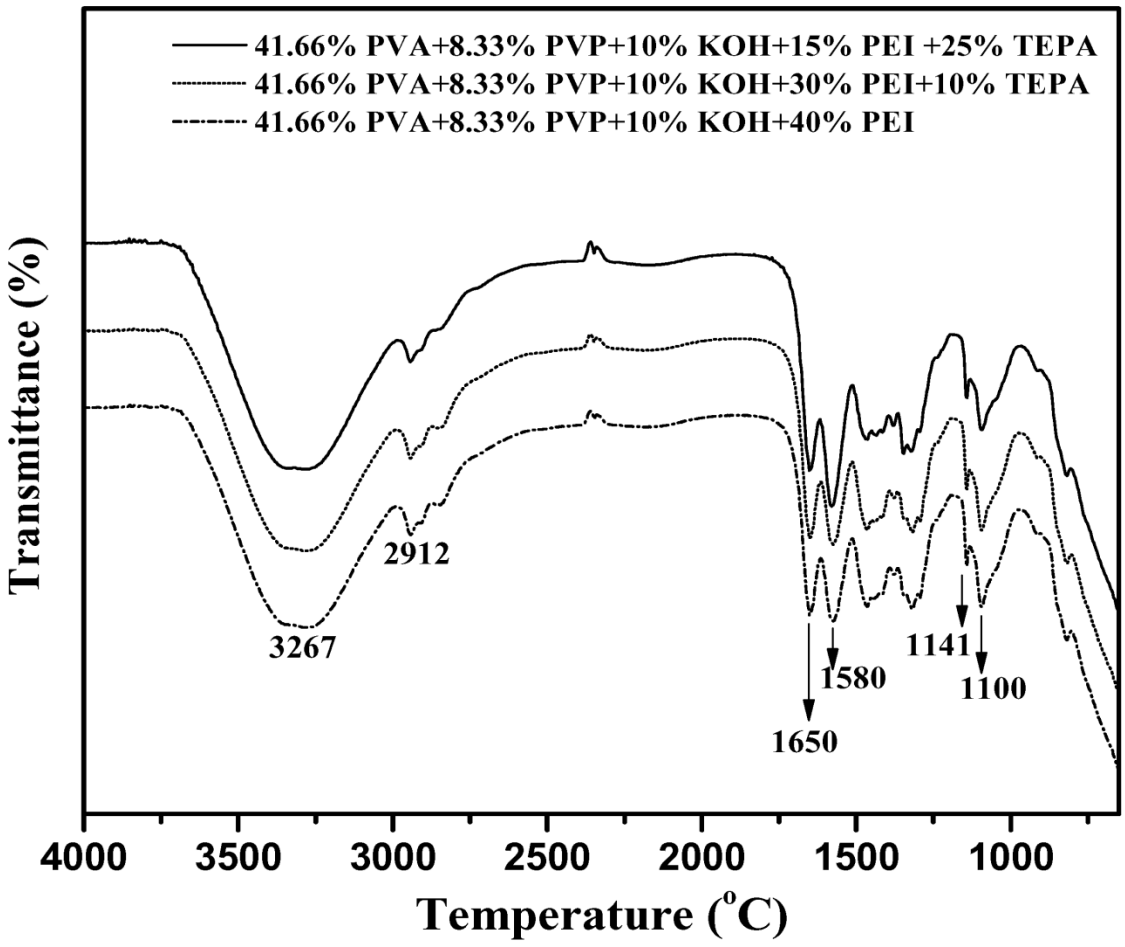

Figure 3.18 FTIR spectra of crosslinked-PVA-PVP membrane containing single (PEI) and blended (PEI and TEPA) amines. 60 mole% degree of crosslinking of PVA with HCHO

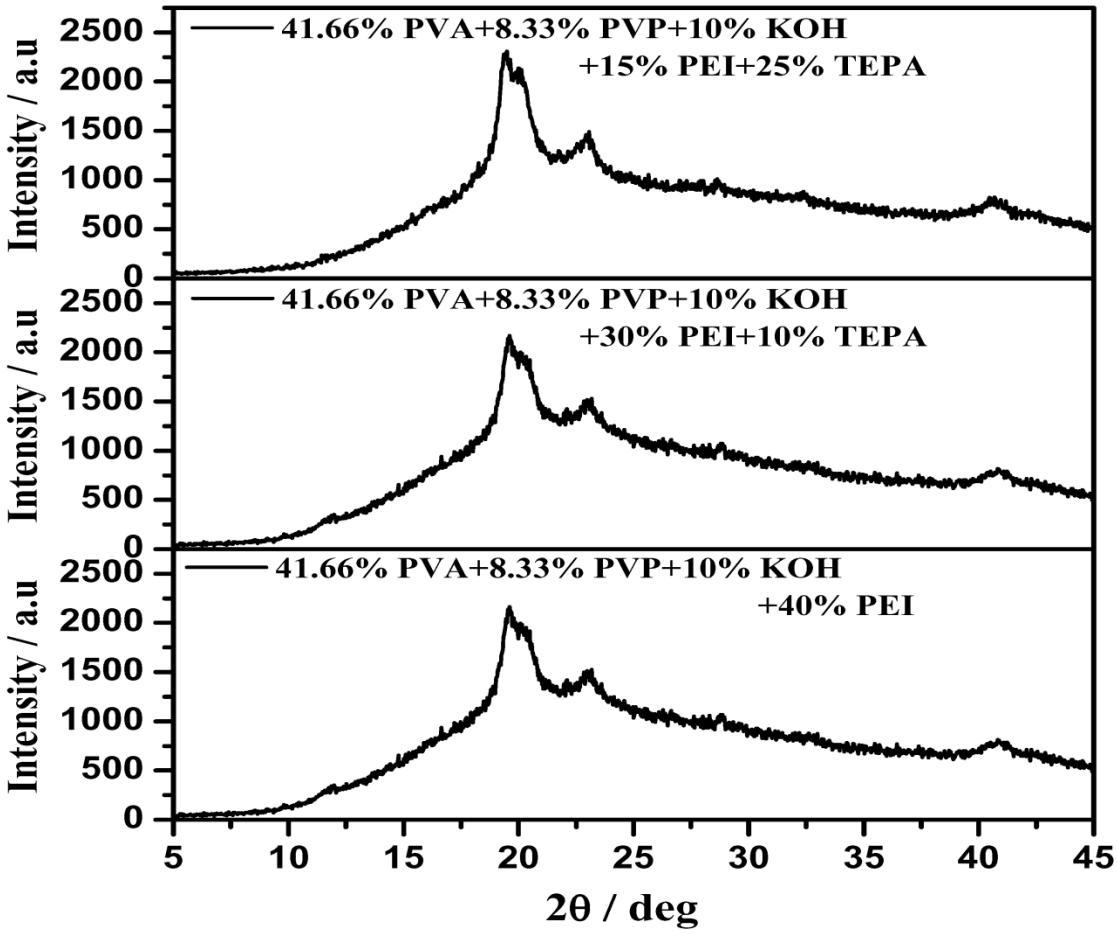

Figure 3.19 XRD spectra of FTIR spectra of crosslinked-PVA-PVP membrane containing single (PEI) and blended (PEI and TEPA) amines. 60 mole% degree of crosslinking of PVA with HCHO

3.4.5 Characterization of Membranes Containing PEI, PEHA and Their Blends

The thermal stability and weight loss of crosslinked-PVA-PVP mixed with PEI and PEHA membranes was determined by TGA curve and compared with crosslinked-PVA-PVP membranes containing PEI and blends of PEI and TEPA (Figure 3.20). Each TGA curve showed three main steps of weight loss. The first weight loss was observed below

120^{o}C, due to loss of water which was absorbed from the atmosphere during sample preparation. This is due to the presence of KOH and amine in the membrane, which makes the membrane more hygroscopic. The second weight loss (204–275^{o}C) was associated with the removal of hydroxyl groups present in the membrane. The final weight loss between 350 to 488^{o}C was related to the decomposition of the polymer backbones. The TGA curves clearly indicated that crosslinked-PVA-PVP doped with amines membrane have fairly good thermal stability for potential high temperature application.

Figure 3.21 represents the DSC curves of crosslinked-PVA-PVP membranes containing blend of PEI and PEHA and compared with crosslinked-PVA-PVP membranes containing PEI as well as blends of PEI and TEPA. It can be seen from the Figure 3.21 that there is one endothermic peak around 240^{o}C, which is the melting temperature (T_m) of all the membranes and also it shows a temperature shift at a region of 40-65^{o}C for all the membranes. Hence, the T_g of crosslinked-PVA-PVP blended with (40 wt% PEI), crosslinked-PVA-PVP mixed with (30 wt% PEI + 10 wt% TEPA), crosslinked-PVA-PVP mixed with (15 wt% PEI + 25 wt% TEPA) and crosslinked-PVA-PVP mixed with (15 wt% PEI + 25 wt% PEHA) membranes were obtained as 45^{o}C, 47^{o}C, 58^{o}C and 60^{o}C, respectively.

Figure 3.22 shows FTIR spectra of the crosslinked-PVA-PVP membranes containing PEI, blends of PEI and TEPA as well as PEI and PEHA. The broad peak around 3267 cm^{-1} for all the membranes is the indication of presence of hydroxyl group (O–H). The sharp peak at 2912 cm^{-1} is assigned to the symmetric vibrations of (C–H), predominantly

responsible for alkyl groups [29]. The sharp frequency at 1650 and 1580 cm^{-1} is assigned to (C=C) stretching and combination of (O-H) and (C-H) bending, respectively [30]. The vibrational band observed at around 1419 cm^{-1} is refers to CH_2 bending [29, 30]. The band frequency between 1150-1085 cm^{-1} is assigned to the combination of (–C–O–C–) and (C–O) bond [31, 32]. This (–C–O–C–) bond indicates the formation of acetal linkage during the crosslinking reaction. In this figure it can be observed that the peak intensity at 1141 cm^{-1} is satisfactory for all three membranes (Figure 3.22). The other vibrations less than 852 cm^{-1} are the finger print zone.

The diffraction pattern for the crosslinked-PVA-PVP membrane containing blended amines (PEI and PEHA) is shown in Figure 3.23 and compared with crosslinked-PVA-PVP membrane containing single amine (PEI) as well as blended amines (PEI and TEPA). The PVA polymeric film displays a semi-crystalline structure with peaks at 2Θ angles of 20^o. It is apparent from Figure 3.23 that the peak intensity of all four membranes at 2Θ angles of 20^o was not affected by the addition of single or blended amine to the membrane.

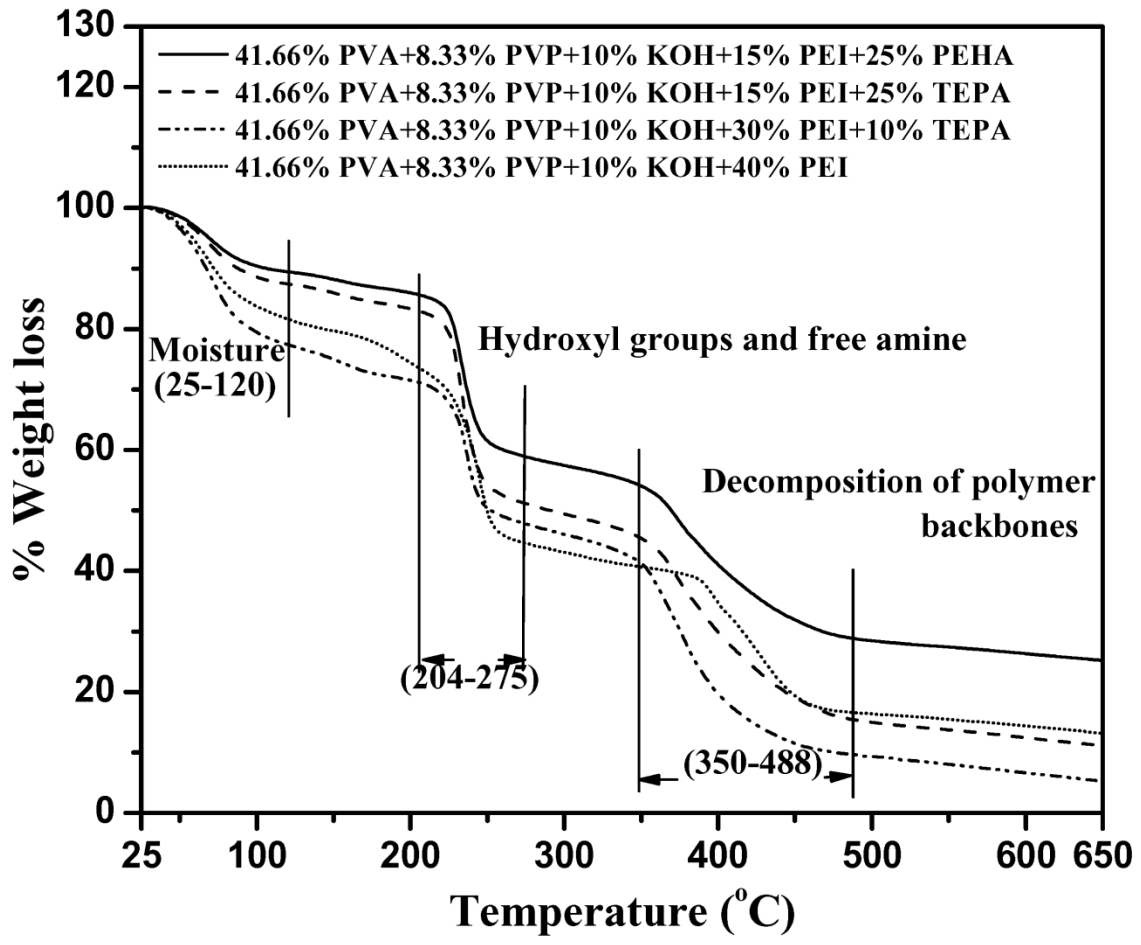

Figure 3.20 TGA curves of crosslinked-PVA-PVP membrane containing blended amines (PEI and PEHA) and also compared with previous single (PEI) and blended (PEI and TEPA) amines. 60 mole% degree of crosslinking of PVA with HCHO

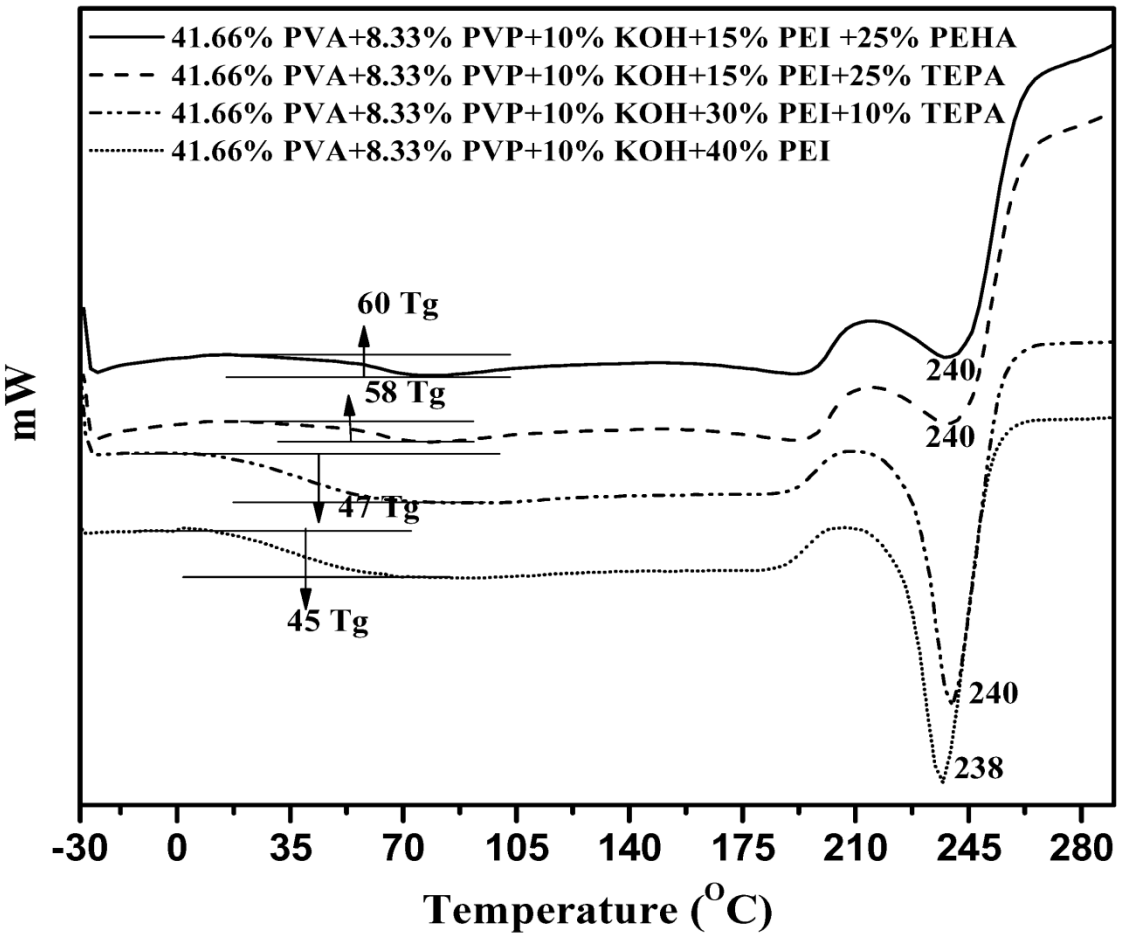

Figure 3.21 DSC curves of crosslinked-PVA-PVP membrane containing blended amines (PEI and PEHA) and also compared with previous single (PEI) and blended (PEI and TEPA) amines. 60 mole% degree of crosslinking of PVA with HCHO

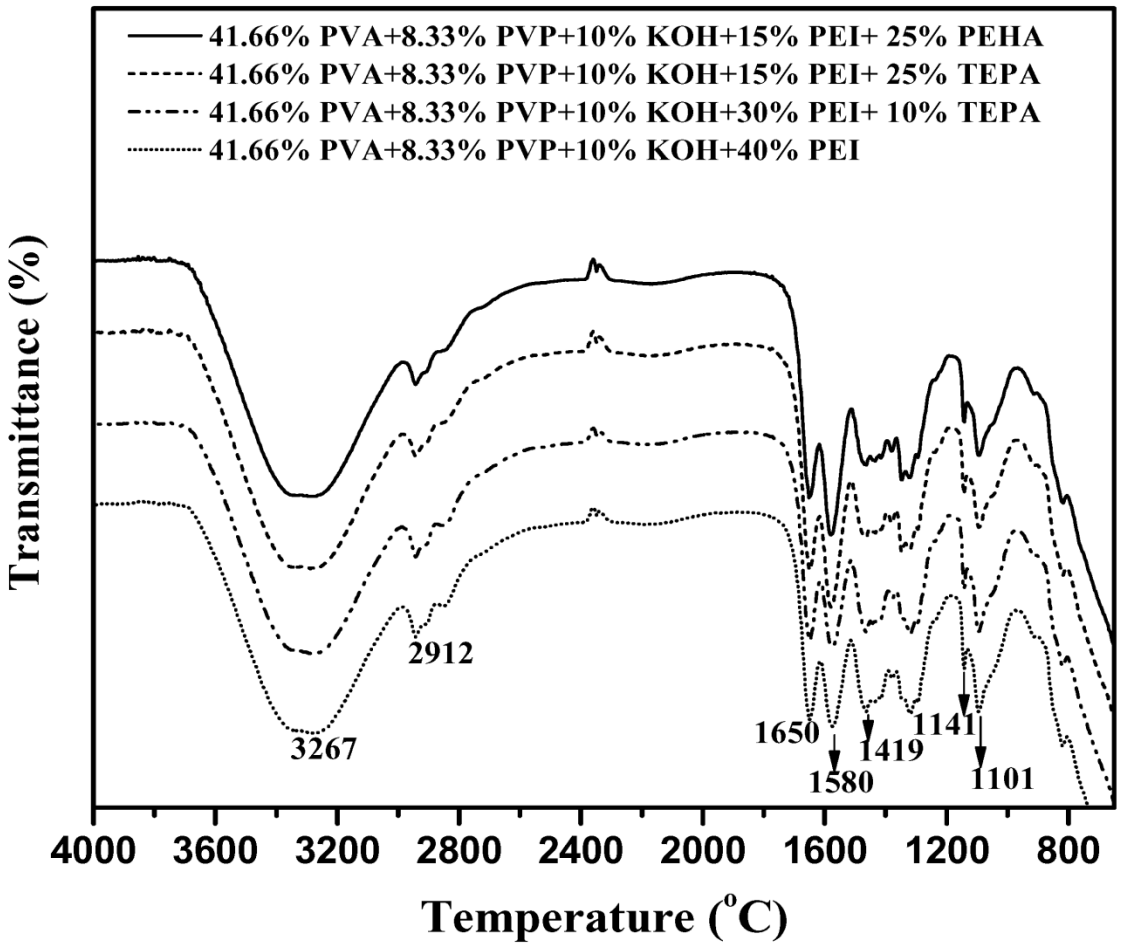

Figure 3.22 FTIR spectra of crosslinked-PVA-PVP membrane containing blended amines (PEI and PEHA) and also compared with previous single (PEI) and blended (PEI and TEPA) amines. 60 mole% degree of crosslinking of PVA with HCHO

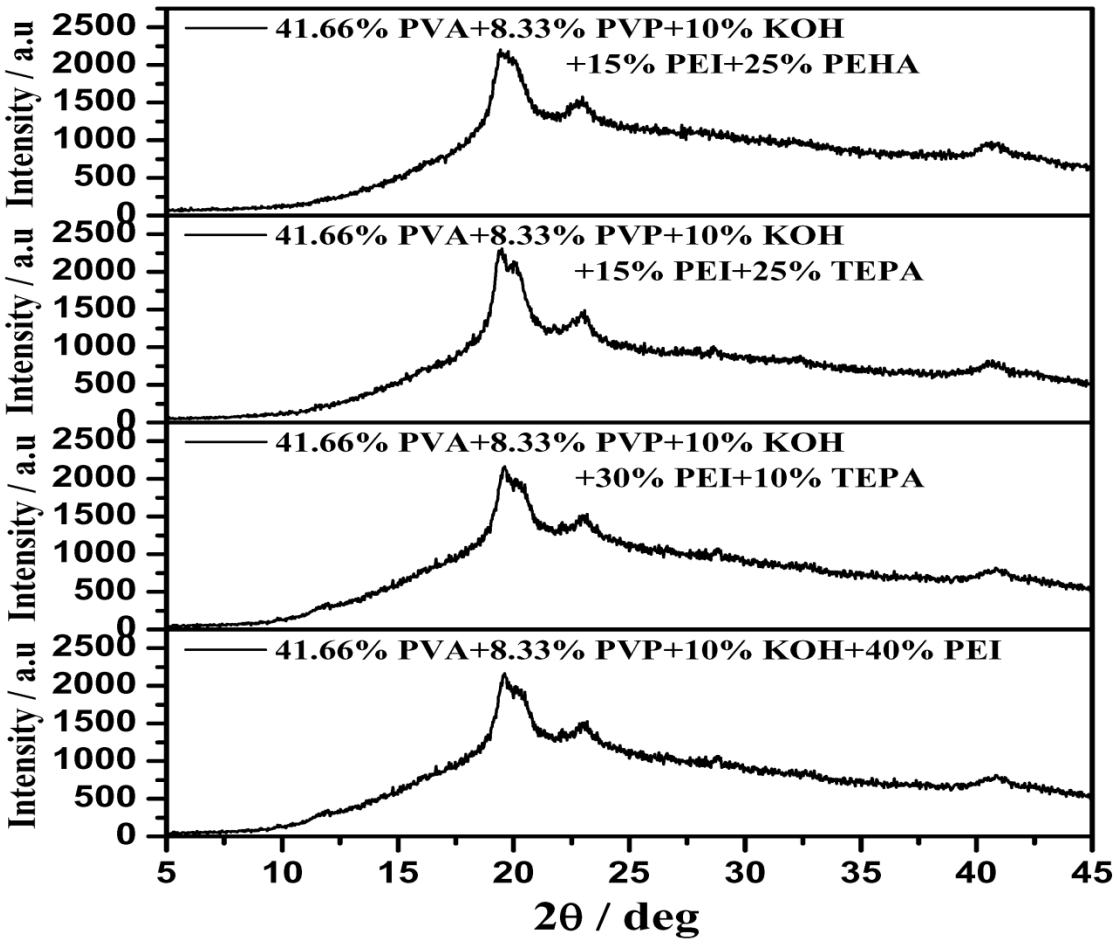

Figure 3.23 XRD spectra of crosslinked-PVA-PVP membrane containing blended amines (PEI and PEHA) and also compared with previous single (PEI) and blended (PEI and TEPA) amines. 60 mole% degree of crosslinking of PVA with HCHO

3.4.6 Characterization of Membranes Containing PEHA, PAA and Their Blends

The thermal stabilities and weight loss of crosslinked-PVA-PVP membranes containing PAA and blends of PAA and PEHA were determined by TGA curves (Figure 3.24). Each TGA curve showed three main steps of weight loss. The first weight loss was observed below 115^{o}C, due to loss of water which was absorbed from the atmosphere during sample preparation. This is due to the presence of KOH and amine in the membrane, which makes the membrane more hygroscopic. The second weight loss (204–275^{o}C) was associated with the removal of hydroxyl groups present in the membrane. The final weight loss between 350 to 488^{o}C was related to the decomposition of the polymer backbones. The TGA curves clearly indicated that crosslinked-PVA-PVP doped with amines membrane have fairly good thermal stability for potential high temperature application.

Figure 3.25 represents the DSC curves of crosslinked-PVA-PVP blended with PAA as well as PAA and PEHA membranes. It can be seen from the Figure 3.25 that there is one endothermic peak around 250^{o}C, which is the melting temperature (T_m) of all the membranes and also it shows a temperature shift at a region of 80-85^{o}C for all the membranes. Hence, the T_g of crosslinked-PVA-PVP blended with (40 wt% PAA), crosslinked-PVA-PVP mixed with (25 wt% PAA + 15 wt% PEHA) and crosslinked-PVA-PVP mixed with (15 wt% PAA + 25 wt% PEHA) membranes were obtained as 84^{o}C, 83^{o}C and 82^{o}C, respectively.

The functional groups present in the crosslinked-PVA-PVP membrane containing blends of PAA and PEHA were obtained using FTIR as shown in Figure 3.26. The broad peak

around 3267 cm^{-1} for all the membranes is the indication of presence of hydroxyl group (O–H). The sharp peak at 2912 cm^{-1} is assigned to the symmetric vibrations of (C–H), predominantly responsible for alkyl groups [29]. The sharp frequency at 1650 and 1580 cm^{-1} is assigned to (C=C) stretching and combination of (O-H) and (C-H) bending, respectively [30]. The vibrational band observed at around 1419 cm^{-1} is refers to CH_2 bending [29, 30]. The band frequency between 1150-1085 cm^{-1} is assigned to the combination of (–C–O–C–) and (C–O) bond [31, 32]. This (–C–O–C–) bond indicates the formation of acetal linkage during the crosslinking reaction. In this figure it can be observed that the peak intensity at 1141 cm^{-1} is satisfactory for all three membranes (Figure 3.26). The other vibrations less than 852 cm^{-1} are the finger print zone.

The diffraction pattern for the crosslinked-PVA-PVP doped with single amine (PAA) and blended amines (PAA and PEHA) membranes are shown in Figure 3.27. The PVA polymeric film displays a semi-crystalline structure with peaks at 2Θ angles of 20^o. It is apparent from Figure 3.27 that the peak intensity of all three membranes at 2Θ angles of 20^o was not affected by the addition of single or blended amine to the membrane.

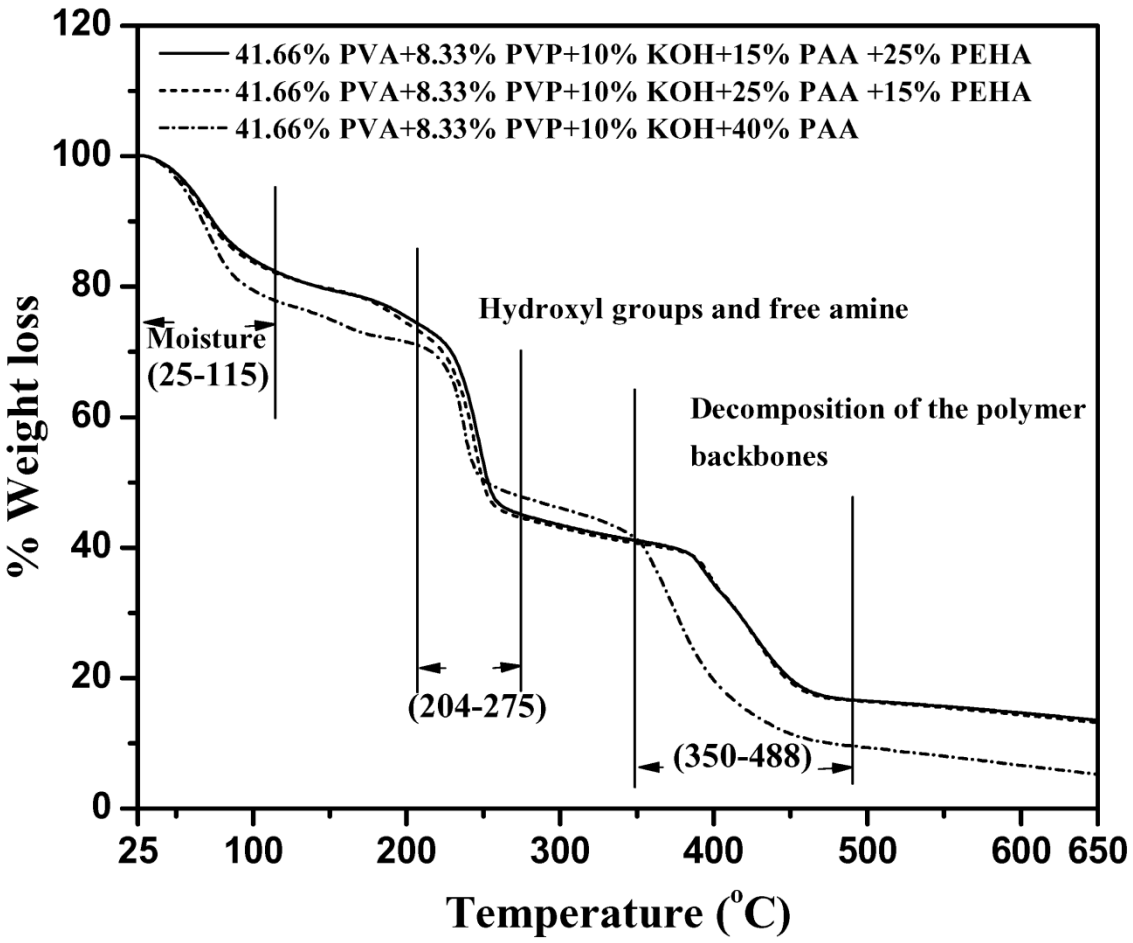

Figure 3.24 TGA curves of crosslinked-PVA-PVP membrane containing single (PAA) and blended (PAA and PEHA) amines. 60 mole% degree of crosslinking of PVA with HCHO

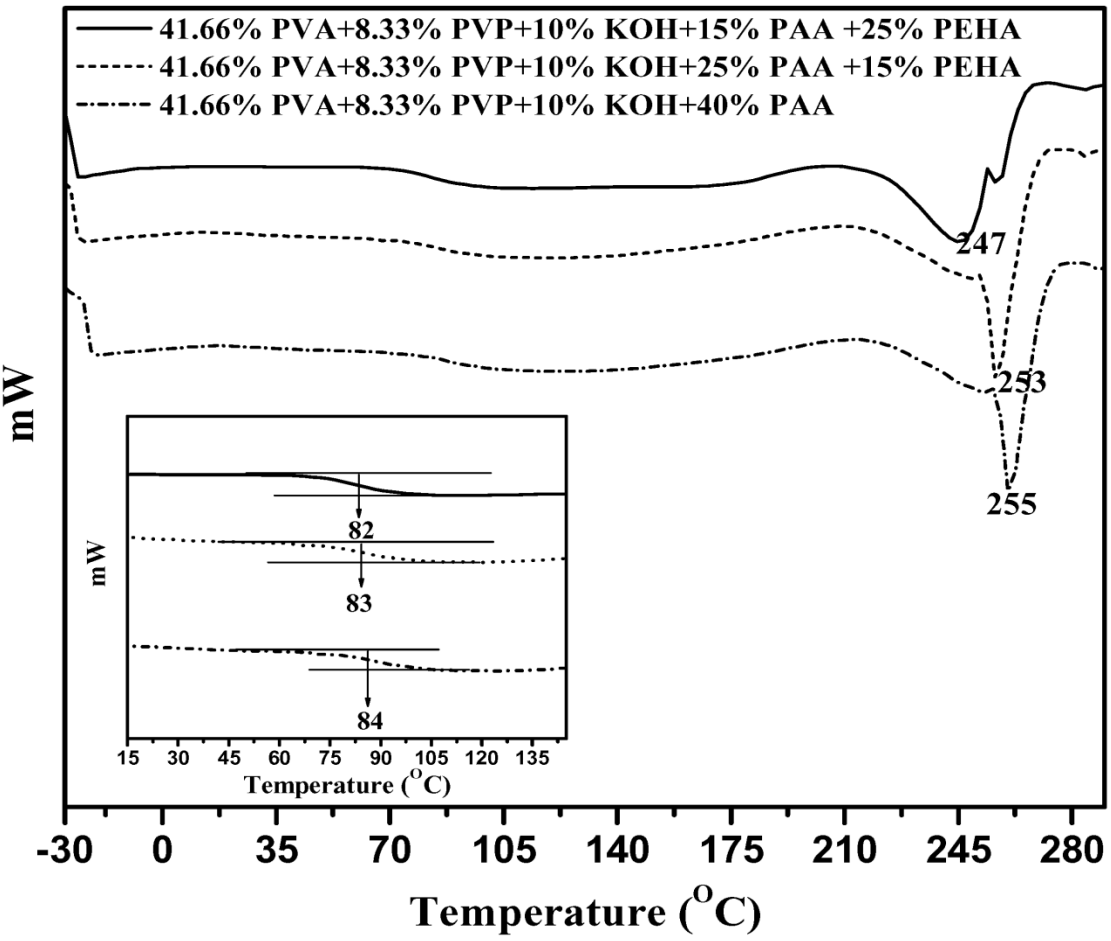

Figure 3.25 DSC curves of crosslinked-PVA-PVP membrane containing single (PAA) and blended (PAA and PEHA) amines. 60 mole% degree of crosslinking of PVA with HCHO

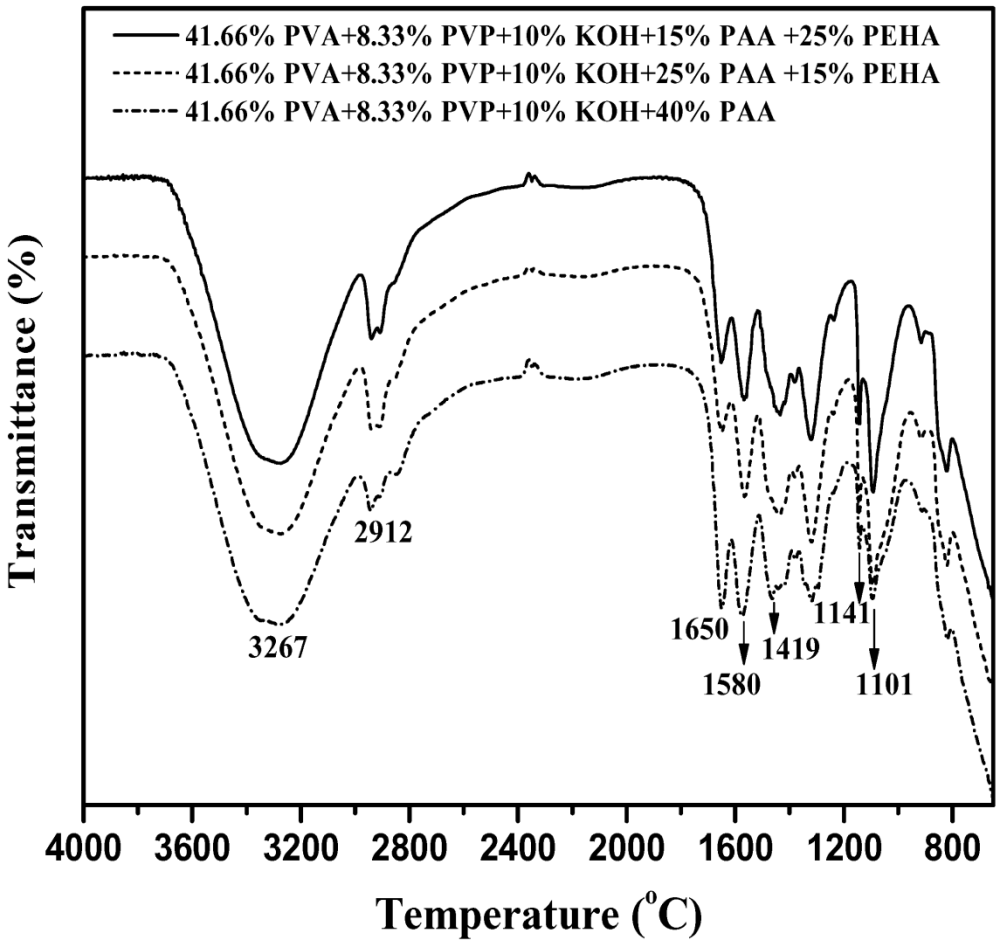

Figure 3.26 FTIR spectra of crosslinked-PVA-PVP membrane containing single (PAA) and blended (PAA and PEHA) amines. 60 mole% degree of crosslinking of PVA with HCHO

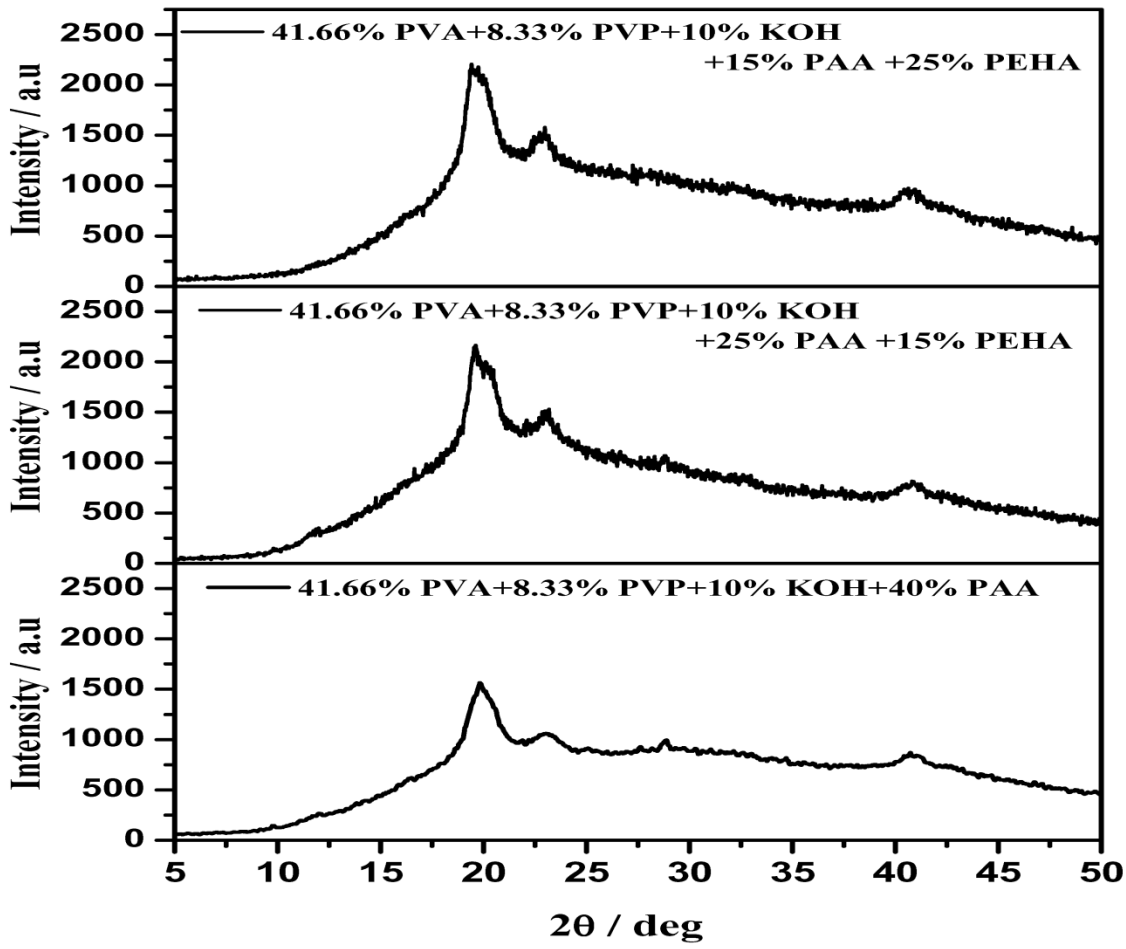

Figure 3.27 XRD spectra of crosslinked-PVA-PVP membrane containing single (PAA) and blended (PAA and PEHA) amines. 60 mole% degree of crosslinking of PVA with HCHO

3.4.7 Characterization of Membranes Containing PAA, AHPD and Their Blends

The thermal stabilities and weight loss of crosslinked-PVA-PVP membranes containing PAA and blends of PAA and AHPD were determined by TGA curves (Figure 3.28). Each TGA curve showed three main steps of weight loss. The first weight loss was observed below 115^{o}C, due to loss of water which was absorbed from the atmosphere during

sample preparation. The second weight loss (204–275^oC) was associated with the removal of hydroxyl groups present in the membrane. The final weight loss between 350 to 488^oC was related to the decomposition of the polymer backbones. The TGA curves clearly indicated that crosslinked-PVA-PVP doped with amines membrane have fairly good thermal stability for potential high temperature application.

Figure 3.29 represents the DSC curves of crosslinked-PVA-PVP blended with PAA and crosslinked-PVA-PVP mixed with PAA and AHPD membrane. It can be seen from the Figure 3.29 that there is one endothermic peak around 240-255^oC, which is the melting temperature (T_m) of all the membranes and also it shows a temperature shift at a region of 60-85^oC for crosslinked-PVA-PVP with (40 wt% PAA) and crosslinked-PVA-PVP with (25 wt% PAA + 15 wt% AHPD) membrane. Hence, the T_g of those two membranes was obtained as 85^oC and 67^oC, respectively. But after increasing the weight percentage of AHPD in the membrane composition, the T_g was obtained as 22^oC for crosslinked-PVA-PVP with (15 wt% PAA + 25 wt% AHPD) membrane.

The functional groups present in the crosslinked-PVA-PVP blended with PAA and crosslinked-PVA-PVP mixed with PAA and AHPD membrane were obtained using the Fourier transform infrared spectrometer (FTIR) as shown in Figure 3.30. The broad peak around 3267 cm^{-1} for all the membranes is the indication of presence of hydroxyl group (O–H). The sharp peak at 2912 cm^{-1} is assigned to the symmetric vibrations of (C–H), predominantly responsible for alkyl groups [29]. The sharp frequency at 1650 and 1580 cm^{-1} is assigned to (C=C) stretching and combination of (O-H) and (C-H) bending, respectively [30]. The vibrational band observed at around 1419 cm^{-1} is refers to CH_2

bending [29, 30]. The band frequency between 1150-1085 cm^{-1} is assigned to the combination of (–C–O–C–) and (C–O) bond [31, 32]. This (–C–O–C–) bond indicates the formation of acetal linkage during the crosslinking reaction. In this figure it can be observed that the peak intensity at 1141 cm^{-1} is satisfactory for all three membranes (Figure 3.30). The other vibrations less than 852 cm^{-1} are the finger print zone.

The diffraction pattern for the crosslinked-PVA-PVP doped with single amine (PAA) and crosslinked-PVA-PVP doped with blended amines (PAA and AHPD) membranes are shown in Figure 3.31. The PVA polymeric film displays a semi-crystalline structure with peaks at 2Θ angles of 20^{o}. After addition of 25 wt% of AHPD, peak intensity at 2Θ angles of 20^{o} was significantly increased. This implies that the addition of the AHPD largely decreased the domain of the amorphous region. This figure also represents that increasing the weight percentage of PAA in the membrane the peak intensity at 2Θ angles of 20^{o} was largely decreased. This signifies that the addition of blended amines greatly enhanced the domain of the amorphous region.

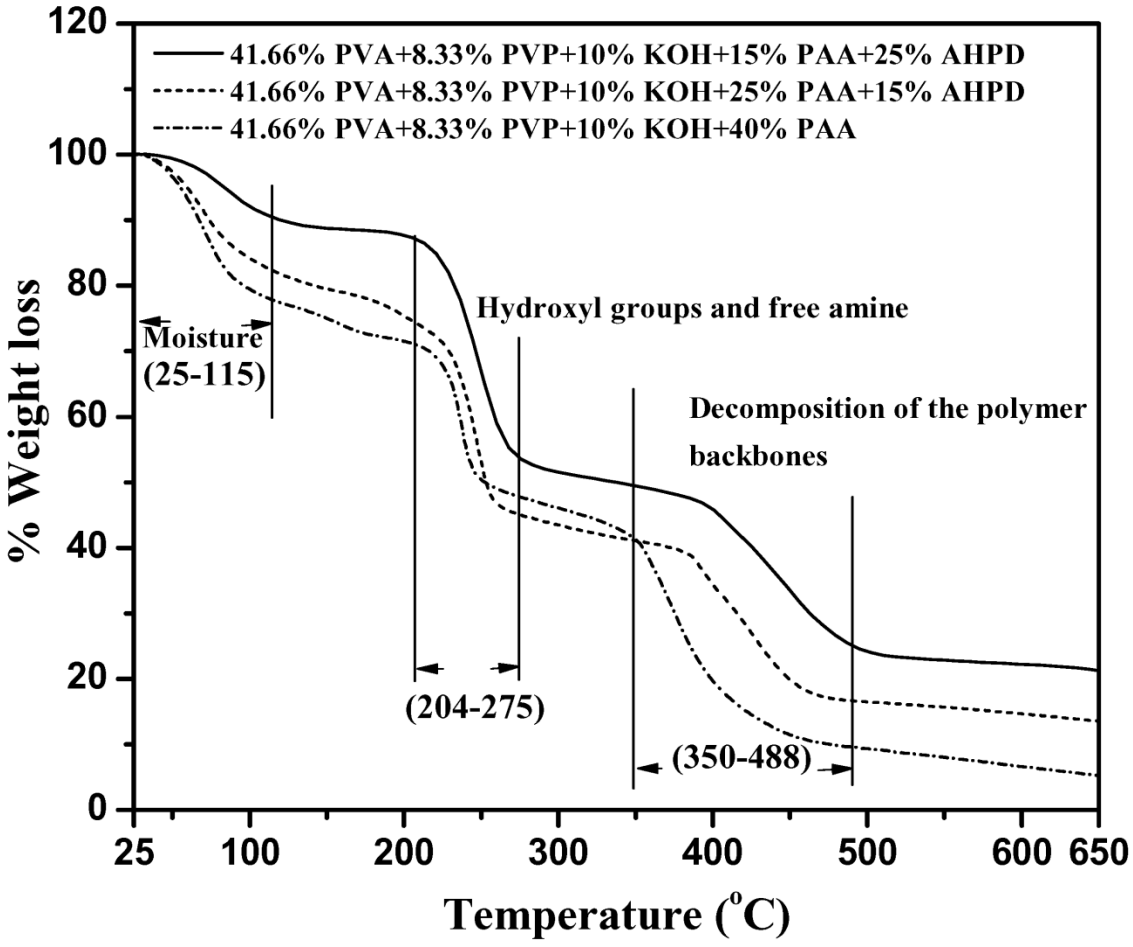

Figure 3.28 TGA curves of crosslinked-PVA-PVP membrane containing single (PAA) and blended (PAA and AHPD) amines. 60 mole% degree of crosslinking of PVA with HCHO

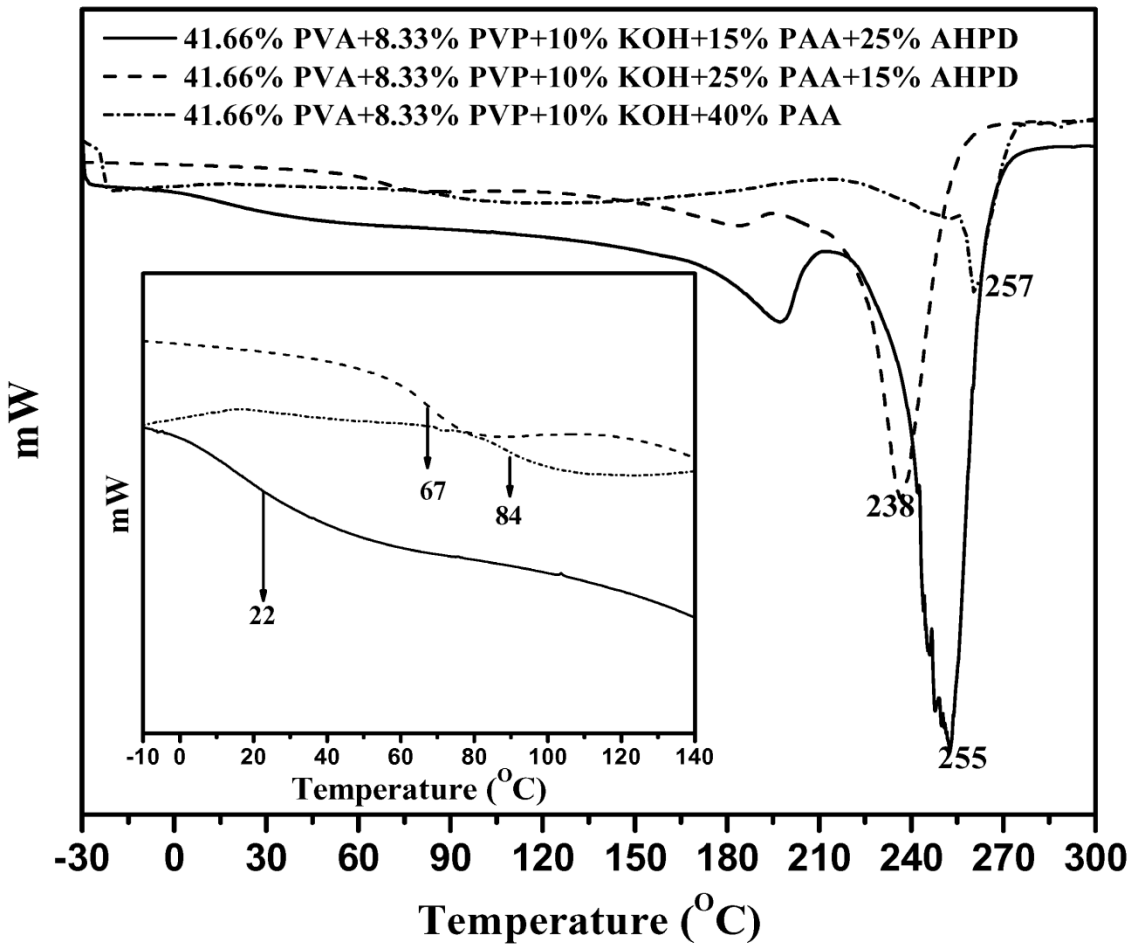

Figure 3.29 DSC curves of crosslinked-PVA-PVP membrane containing single (PAA) and blended (PAA and AHPD) amines. 60 mole% degree of crosslinking of PVA with HCHO

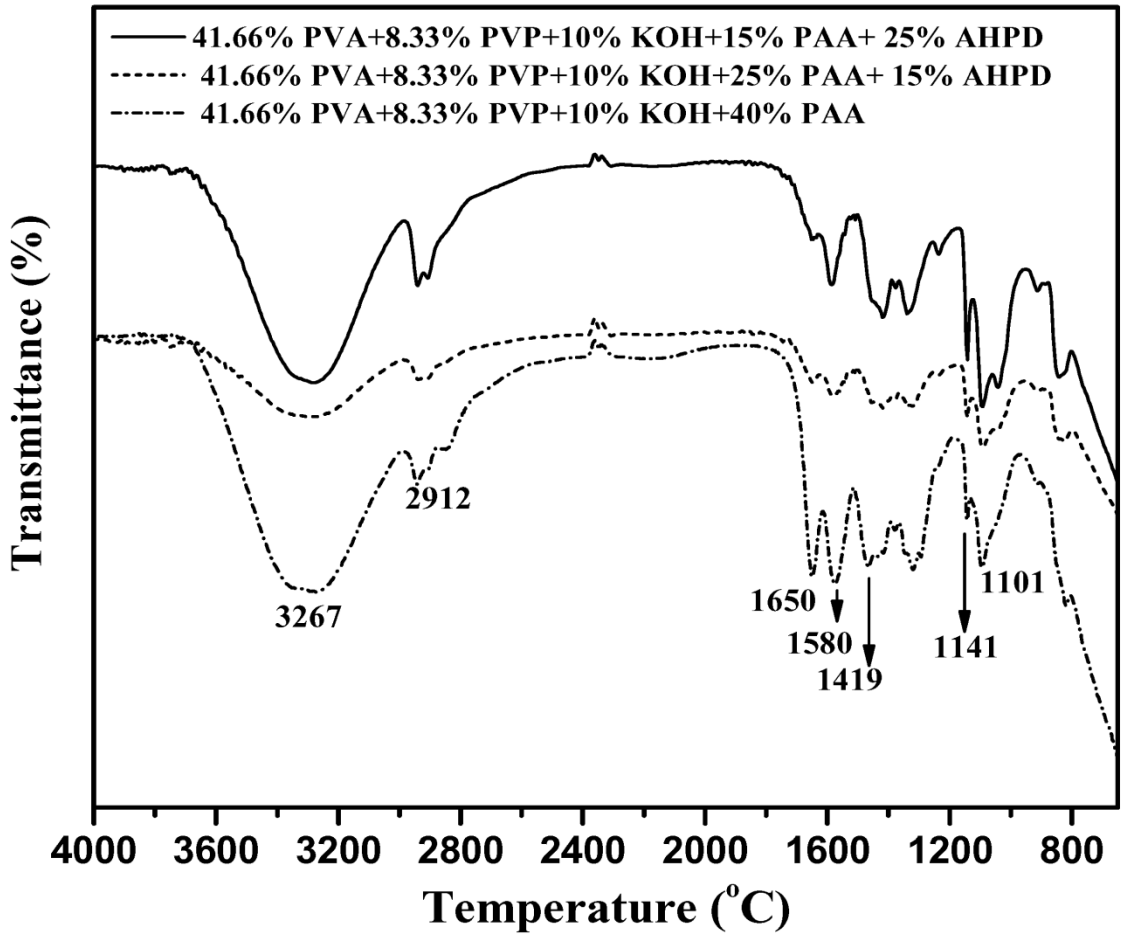

Figure 3.30 FTIR spectra of crosslinked-PVA-PVP membrane containing single (PAA) and blended (PAA and AHPD) amines. 60 mole% degree of crosslinking of PVA with HCHO

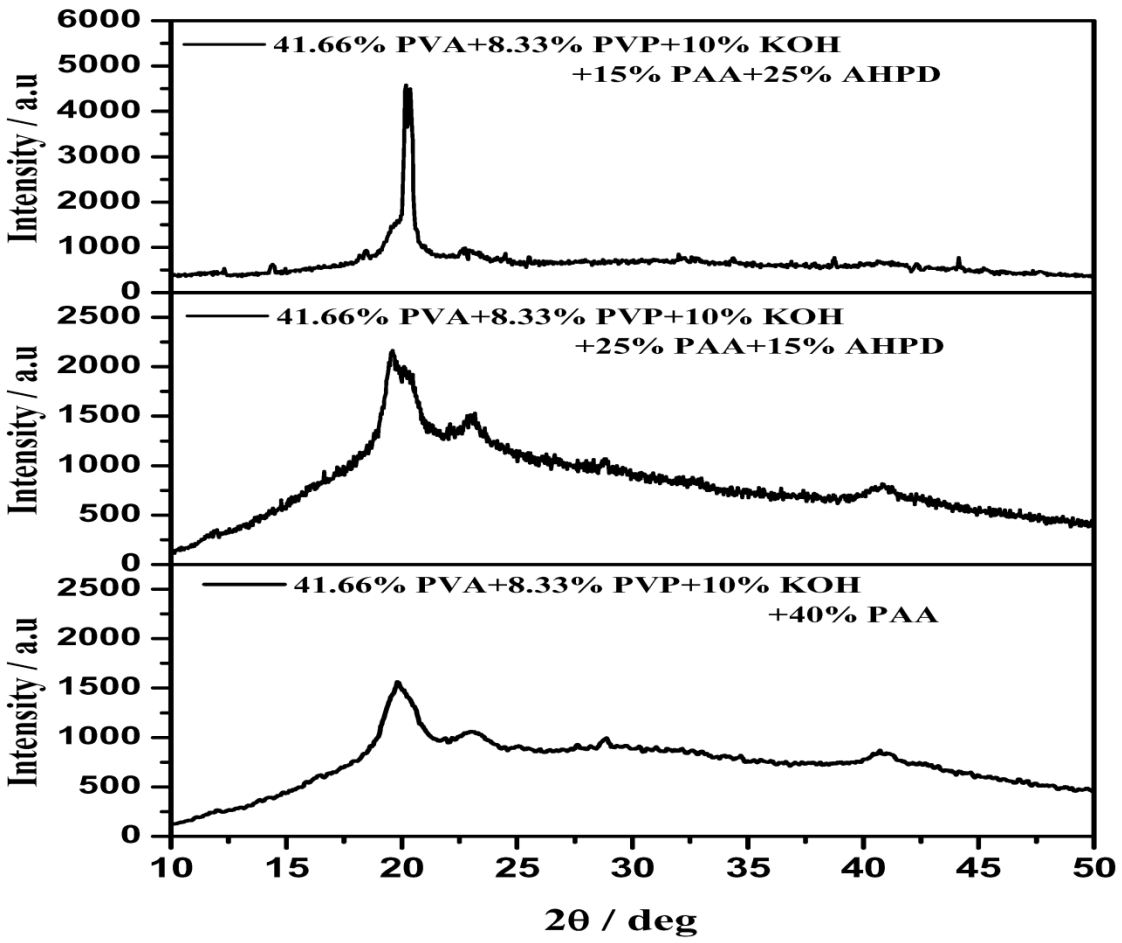

Figure 3.31 XRD spectra of crosslinked-PVA-PVP membrane containing single (PAA) and blended (PAA and AHPD) amines. 60 mole% degree of crosslinking of PVA with HCHO

3.5 SUMMARY

This work reports synthesis and characterization of PVA based thin-film membranes. PVA was crosslinked with HCHO at different degree of crosslinking and blended with PVP to improve the thermal stability of the membrane. The optimum degree of crosslinking of PVA with HCHO was 60 mole%. The PVA/PVP ratio of 1:0.2 was

chosen for the further study. Different combinations of amine carrier were incorporated into the crosslinked-PVA-PVP hydrogel to improve the CO_2 transport property through the membrane. Four sets of different amine based membranes were prepared. Those are crosslinked-PVA-PVP membranes containing PEI, PAA, PEI + TEPA, PEI + PEHA, PAA + PEHA and PAA + AHPD.

Each TGA curve showed three main steps of weight loss. The first weight loss was due to the evaporation of absorbed moisture from the atmosphere. The second weight loss was due to removal of hydroxyl groups or amine. The third weight loss was due to decomposition of the polymer backbones. T_g and T_m were improved after crosslinking and polymer blending. But after addition of the amine to the polymer hydrogel the T_g was slightly reduced. The band frequencies observed from FTIR analysis for all the membranes at 3267, 2912, 1650, 1580, 1419 and 1141 cm^{-1} are the stretching vibrations of the hydroxyl (-OH) groups, symmetric vibrations of alkyl groups (C–H), (C=C) stretching vibrations, combination of (O-H) and (C-H) bending, CH_2 bending, combination of (–C–O–C–) and (C–O) bond, respectively. The other bending vibrations less than 888 cm^{-1} are the fingerprint zone. The X-ray diffraction pattern for all the amine doped membranes obtained by XRD analysis displayed a semi-crystalline structure with peaks at 2Ɵ angles of 20^o.

REFERENCES

[1]. J. M. G. Cowie, in Encyclopedia of Polymer Science and Engineering, 2nd edn, Supplement, ed. H. F. Mark, N. M. Bikales, C. G. Overberge, G. Menges and J. I. Kroschwits, John Wiley & Sons, New York, 1988, p. 455.

[2]. H. Feng, Z. Feng and L. Shen, A high resolution solid-state n.m.r. and d.s.c. study of miscibility and crystallization behaviour of poly(vinyl alcohol)poly(N-vinyl-2-pyrrolidone) blends, Polymer. 34 (1993) 2516-2519.

[3]. X. Zhang, K. Takegoshi and K. Hikichi, High-resolution solid-state ^{13}C nuclear magnetic resonance study on poly(vinyl alcohol)/poly(vinylpyrrolidone) blends, Polymer. 33 (1992) 712-717.

[4]. K. J. Zhu, W. Liqun, W. Ji and Y. Shilin, Study of the miscibility of poly(N-vinyl-2-pyrrolidone) with poly[styrene-co-(4-hydroxystyrene)], Macromol. Chem. Phys. 195 (1994) 1965-1972.

[5]. F. L. Marten, in Encyclopedia of Polymer Science and Engineering, Vol. 17, 2nd edn, ed. H. F. Mark, N. M. Bikales, C. G. Overberge, G. Menges and J. I. Kroschwitz, John Wiley & Sons, New York, 1988, p. 167.

[6]. Y. Nishio, H. Suzuki and K. Sato, Molecular orientation and optical anisotropy induced by the stretching of poly(vinyl alcohol)poly(N-vinyl pyrrolidone) blends, Polymer. 35 (1994) 1452-1461.

[7]. H. Zhang and J. Yin, Small-angle X-ray scattering studies on poly(vinyl alcohol)/poly(N-vinyl-2-pyrrolidone) blends, Macromol. Chem. Phys. 191 (1990) 375-380.

[8]. J. I. Eguiazabal, H. Calahorra, M. Cortfizar and G. M. Guzman, Miscibility of mixtures from partially hydrolyzed poly(vinyl acetate) and poly(N-vinyl-2-pyrrolidone), Macromol. Chem. Phys. 187 (1986) 2439-2444.

[9]. Z. Ping, Q. T. Nguyen and J. Neel, Investigation of poly(vinyl alcohol)/poly(N-vinyl-2-pyrrolidone) blends, 3. Permeation properties of polymer blend membranes, Macromol. Chem. Phys. 195 (1994) 2107-2116.

[10]. Y. Nishio, T. Haratani and T. Takahashi, Miscibility and orientation behavior of poly(vinyl alcohol) / poly(vinyl pyrrolidone) blends, J. Polym. Sci. Part B Polym. Phys. 28 (1990) 355-376.

[11]. Y. Cai, Z. Wang, C. Yi, Y. Bai, J. Wang and S. Wang, Gas transport property of polyallylamine–poly(vinyl alcohol)/polysulfone composite membranes, J. Membr. Sci. 310 (2008) 184-196.

[12]. L. Deng, T. J. Kim and M. B. Hagg, Facilitated transport of CO_2 in novel PVAm/PVA blend membrane, J. Membr. Sci. 340 (2009) 154-163.

[13]. L. Deng, T. J. Kim, M. Sandru and M. B. Hagg, PVA/PVAm blend FSC membrane for natural gas sweetening, Proceedings of the 1st Annual Gas Processing Symposium, Elsevier, Norway, 2009.

[14]. G. J. Francisco, A. Chakma and X. Feng, Membranes comprising of alkanolamines incorporated into poly(vinyl alcohol) matrix for CO_2/N_2 separation, J. Membr. Sci. 303 (2007) 54-63.

[15]. M. J. Kim, Y. I. Park, K. H. O. Youm and K. H. O. Lee, Facilitated transport of CO_2 through ethylenediamine-fixed cation-exchange polysaccharide membranes, J. Membr. Sci. 245 (2004) 79-86.

[16]. H. Matsuyama, A. Terada, T. Nakagawara, Y. Kitamura and M. Teramoto, Facilitated transport of CO_2 through polyethylenimine/poly(vinyl alcohol) blend membrane, J. Membr. Sci. 163 (1999) 221-227.

[17]. J. Shen, J. Qiu, L. Wu and C. Gao, Facilitated transport of carbon dioxide through poly (2-N,N-dimethyl aminoethyl methacrylate-co-acrylic acid sodium) membrane, Sep. Purif. Technol. 51 (2006) 345-351.

[18]. J. Shen, L. Wu, D. Wang and C. Gao, Sorption behavior and separation performance of novel facilitated transport membranes for CO_2/CH_4 mixtures, Desalination. 223 (2008) 425-437.

[19]. W. J. Ward, W. R. Browal and R. M. Salemme, Ultrathin silicone/polycarbonate membranes for gas separation processes, J. Membr. Sci. 1 (1976) 99-108.

[20]. G. M. Wu, S. J. Lin and C. C. Yang, Preparation and characterization of PVA/PAA membranes for solid polymer electrolytes, J. Membr. Sci. 275 (2006) 127-133.

[21]. R. Xing and W. S. W. Ho, Synthesis and characterization of crosslinked polyvinylalcohol/polyethyleneglycol blend membranes for CO_2/CH_4 separation, J. Taiw. Inst. Che. Eng. 40 (2009) 654-662.

[22]. R. Yegani, H. Hirozawa, M. Teramoto, H. Himei, O. Okada, T. Takigawa, N. Ohmura, N. Matsumiya and H. Matsuyama, Selective separation of CO_2 by using novel facilitated transport membrane at elevated temperatures and pressures, J. Membr. Sci. 291 (2007) 157-164.

[23]. J. Zou and W. S. W. Ho, CO_2-selective polymeric membranes containing amines in crosslinked poly(vinyl alcohol), J. Membr. Sci. 286 (2006) 310-321.

[24]. B. Mandal and W. S. W. Ho, Gas purification by polymeric membranes containing fixed and mobile carriers, Int. J. Chem. Sci. 5(4) (2007) 1938-1946.

[25]. A. Mondal and B. Mandal, Synthesis and characterization of crosslinked poly(vinyl alcohol)/poly(allylamine)/2-amino-2-hydroxymethyl-1,3-propanediol/polysulfone composite membrane for CO_2/N_2 separation, J. Membr. Sci. 446 (2013) 383-394.

[26]. A. Lucke, J. Teβmar, E. Schnell, G. Schmeer and A. Gopferich, Biodegradable poly(D,L-lactic acid)-poly(ethylene glycol)-monomethyl ether diblock copolymers: structures and surface properties relevant to their use as biomaterials, Biomaterials. 21 (2000) 2361-2370.

[27]. G. Zhou and C. Xiao, Synthesis and properties of degradable poly(vinyl alcohol) hydrogel, Polym. Deg. Stab. 81 (2003) 297-301.

[28]. G. M. Wu, S. J. Lin and C. C. Yang, Preparation and characterization of PVA/PAA membranes for solid polymer electrolytes, J. Membr. Sci. 275 (2006) 127-133.

[29]. H. S. Mansur, C. M. Sadahira, A. N Souza and A. A. P. Mansur, FTIR spectroscopy characterization of poly (vinyl alcohol) hydrogel with different hydrolysis degree and chemically crosslinked with glutaraldehyde, Mat. Sci. Eng. C. 28 (2008) 539-548.

[30]. E. M. Abdelrazek, I. S. Elashmawi and S. Labeeb, Chitosan filler effects on the experimental characterization, spectroscopic investigation and thermal studies of PVA/PVP blend films, Physica B. 405 (2010) 2021-2027.

[31]. L. Deng, T. J. Kim and M. B. Hagg, Facilitated transport of CO_2 in novel PVAm/PVA blend membrane, J. Membr. Sci. 340 (2009) 154–163.

[32]. S. K. Mallapragada and N. A. Peppas, Dissolution mechanism of semicrystalline poly(vinyl alcohol) in water, J. Polym. Sci. Part B: Polym. Phy. 34 (1996) 1339-1346.

Chapter 4

CO_2 SEPARATION FROM MIXED GAS BY POLYMER MEMBRANES CONTAINING AMINE CARRIERS

This chapter presents the permeation study of novel CO_2-selective membranes containing different amines and their blends. The effect of operating conditions on transport properties (CO_2 flux, CO_2 permeability, CO_2/N_2 selectivity) is investigated. Membrane compositions are also optimized.

4.1 INTRODUCTION

Production of high purity gases, barrier materials for food packaging and beverage industry are few of the most important industrial applications for polymer membrane based separation. There are many novel polymer materials available which gives much more versatility and simplicity in customized system designs. Due to numerous practical benefits, several investigations are underway to understand the gas transport phenomena and synthesis procedure of novel polymers with better separation properties. Although interest in polymers has been around for a century, last three decades were the successful period for the major development in the field of polymer science [1]. Applications of

synthetic polymers boost the sudden advances in the field of separation process. These polymers have better thermal stability and mechanical properties than natural polymers and also applicable in the field of wide range of gas transport and separation. Polymer membrane based separation may become a potential method to capture CO_2 with less energy consumption due to light weight and space efficiency as well as compact modular design. Also, it does not require a separating agent and hence no regeneration is required [2, 3]. While researchers were focusing to develop new polymeric membranes, the study of the involved transport phenomena was limited by instrumentation. Simple experimental techniques are still subject of interest to study the gas transport phenomena. Primarily, gas separation properties are estimated using single gas permeation experiment through the membrane. It was only in the last decade that mixed gas permeation experiments were carried out to understand the true separation behavior of the membrane [4]. Proper understanding of the mixed gas transport phenomena is still hampered by the lack of mixed gas permeation data. Hence, an effort is necessary to design an experimental technique, which would help simultaneous observation of the gas transport behavior under mixed gas conditions. The aim of this thesis is to develop an experimental technique which would help in our understanding of the involved transport phenomena under real conditions.

The material like crosslinked PVA hydrogels containing amine carrier are one of the interesting research topic today for gas separation application because of their high permeability as well as high thermal stability [5-13]. In this research, novel crosslinked-PVA-PVP membranes containing single as well as blended amines have been synthesized. To enhance the CO_2 transport property through the membrane, it is very

essential to introduce suitable carrier into the polymer backbone which should have higher CO_2-carrier reaction rate along with high CO_2 loading capacity. Different primary sterically hindered, primary sterically unhindered amines and their blends have been used as carriers. These amines are polyethyleneimine (PEI), tetraethylenepentamine (TEPA), pentaethylenehexamine (PEHA), polyallylamine (PAA) and 2-amino-2-hydroxymethyl-1,3-propanediol (AHPD). The effects of membrane thickness as well as membrane compositions on the CO_2 and N_2 transport properties were studied to obtain the optimum membrane composition. The CO_2 gas transport properties (CO_2 flux, CO_2 permeability, CO_2/N_2 selectivity) were obtained by using the best membrane of each set at different physical conditions; i.e. pressure, temperature and moisture content.

4.2 GAS PERMEATION MEASUREMENTS

4.2.1 Experimental Instrumentation

The gas permeation tests were carried out by using a stainless steel counter-current permeation module. The schematic and real permeation measurement set-up is shown in Figures 4.1 and 4.2, respectively. The full set-up is categorized in five major sections which is interconnected to each other and performs different functions at various stages of an experimental run, such as, mass flow controller, temperature controlled hot-air oven, HPLC-pump, back-pressure regulator and gas chromatograph (GC). The present set-up employs in-line gas sampling technique for automated sample injection into a gas chromatograph time to time. The set-up is constructed with 316 stainless steel tubing and fittings for high pressure permeation studies (0 to 50 atm).

The feed gas mixture containing 20% CO_2 and 80% N_2 on dry basis was used. Pure argon was used as a permeate side carrier gas. Two mass flow controllers (AALBORG, USA) were used; one for feed side and another for permeate side to control the accurate gas flow rate. Both the feed and permeate side gas flow rates were kept nearly constant at 30 cm^3/min. The module was kept inside the temperature controlled hot-air oven (Reico Pvt. Ltd, India) to maintain the accurate temperature. Appropriate amount of water was pumped in two different humidifiers using two Varian Prostar 210 HPLC-pumps (Varian Inc., Palo Alto, CA) where the feed and carrier gas saturated with moisture, respectively, before they entered the permeation cell. The pressure at feed side and permeate side of the membrane module was maintained by two different back-pressure regulators. The absolute feed pressure was varied from 1.7 to 6.2 atm and the absolute permeate pressure was maintained close to atmospheric pressure. Both the retentate and permeate streams leaving from the permeation cell was collected in two different water knockout vessels which was kept at ambient temperature. Most of the water vapor becomes condensed inside the water knockout and partially moisture free gas from water knockouts were entered to the gas chromatograph (GC) for composition analysis through two different moisture trappers.

The compositions of both the retentate and permeate gas were then analyzed sequentially using a Varian 450 gas chromatograph (Varian Inc., Palo Alto, CA) with one thermal conductivity detector (TCD). Helium was used as the GC carrier gas for TCD detector. The GC columns were used as CP7430 capillary columns (Agilent Technologies, Palo Alto, CA) which were the combination of two different capillary columns, one was CP-Molsieve 5A and the other was CP-PoraBOND Q.

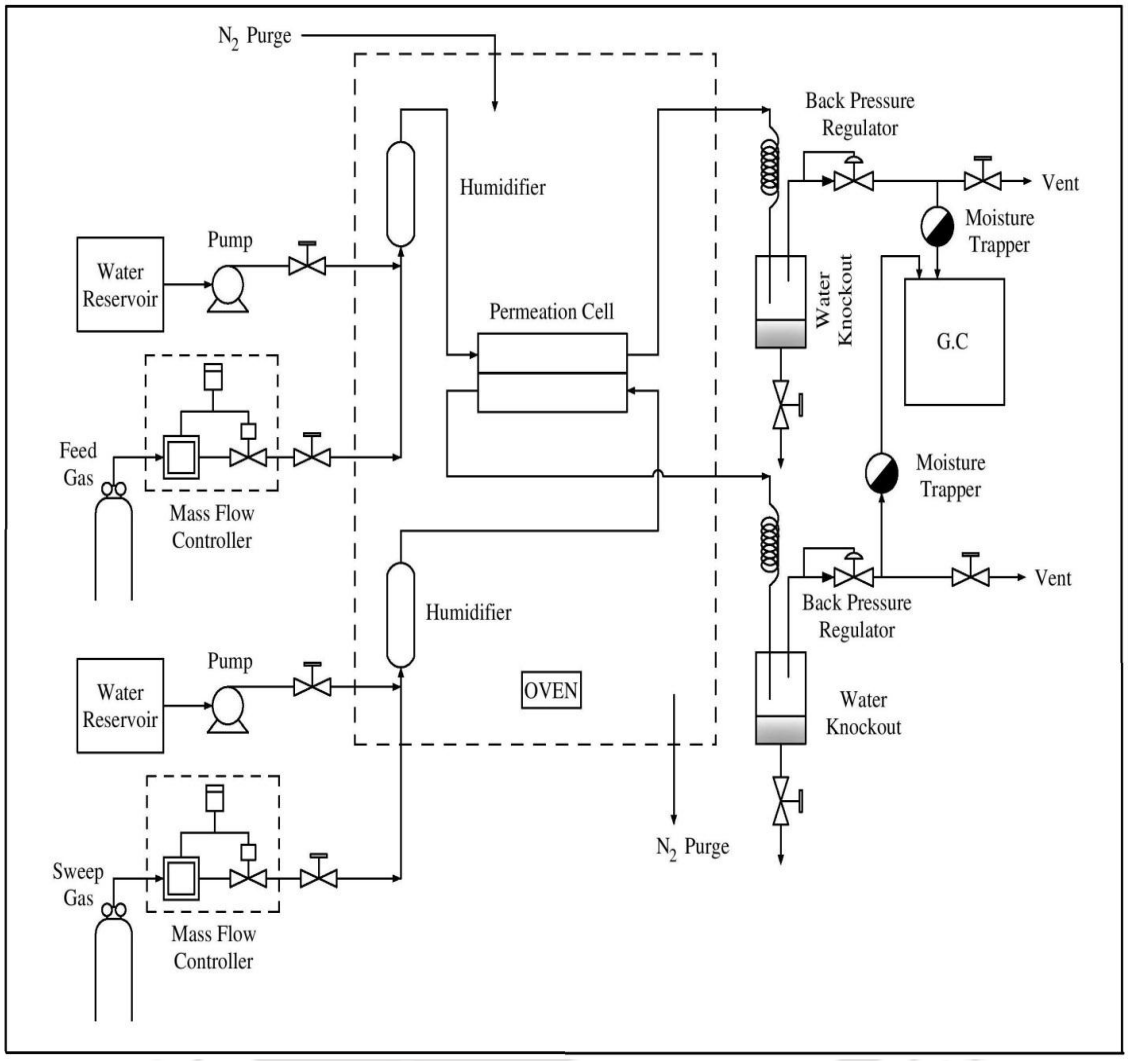

Figure 4.1 Schematic representation of gas permeation apparatus

Figure 4.2 Gas permeation experimental set up

Transport properties of synthesized crosslinked thin film composite membranes with an active membrane area of 51.5 cm^2 were measured against temperature, feed absolute pressure and sweep side moisture content. Each of the membrane permeation measurements was carried out for at least 10 hours at a specific temperature, pressure and water flow rate, which allowed for the steady state permeation. All the gas permeation data presented were the average of three replicate measurements. The detailed calculations of CO_2 flux, N_2 flux, CO_2 permeability, N_2 permeability and CO_2/N_2 selectivity were given in Appendix A2.1.

4.2.1.1 Feed Gas Control and Regulatory System

The feed section supplies mixed gas (20% CO_2 and 80% N_2) to the feed side of the membrane module. Two stage pressure regulators were used to control the cylinder outlet pressure (1-25 bar) which was connected to the mass flow controller (MFC) at feed side. The outlet connection of the MFC (flow range: 0-250 ml/min, maximum pressure limit: 1000 psi) was connected to the feed side of the membrane module through the humidifier. On-off valve was used to depressurizing the system. Outlet of the feed side membrane module was connected to the back pressure regulator (0-20 bar) through the water knockout to maintain pressure at feed side of the membrane module. Finally the outlet of the back pressure regulator was connected to the G.C for composition analysis.

4.2.1.2 Permeate Gas Control and Regulatory System

The permeate section supplies pure argon (Ar) gas as a carrier to the permeate side of the membrane module. Other connections of the permeate side were similar to the feed side with separate MFC (flow range: 0-250 ml/min, maximum pressure limit: 1000 psi),

humidifier, back pressure regulator (0-5 bar) and water knockout, as mentioned before in section 4.2.1.1.

4.2.1.3 Membrane Cell

The round shape membrane module shown in Figure 3.1, was the custom made design made by stainless steel 316. The module is divided in two part, upper section is called feed side and the lower section is called permeate side. A porous stainless steel membrane was used as a support for polymer composite membrane (shown in Figure 3.1). The porous stainless steel support was kept at the permeate side of the membrane module. Then the polymer composite membrane was placed carefully on the top of the metal support. Finally both parts of the module were sealed by two silicones O-rings with the help of six allen key socket head screw.

4.2.1.4 HPLC Pump

Two HPLC pumps were connected with the two humidifiers (Figure 4.2). Automated program controller helps to maintain very low water flow rate (0.01-0.1 ml/min) against pressure to moist feed and carrier gases.

4.2.1.5 Temperature Controlled Hot-Air Oven

The membrane module and two humidifiers (Figure 4.2) were kept inside the oven to maintain the appropriate temperature of the membrane and moist both the feed and carrier gas, respectively, before they entered the permeation cell. Automated program controller was used to control temperature along with heating rate. Also it had been observed that the temperature fluctuation against set temperature was around ± 1^{o}C.

4.2.1.6 Gas Chromatograph with Gas Sampling Valve (GSV)

During the permeation experiment, gas sampling valve was used for automatic sample gas injection with 100 micro liter sample loop. Initially the G.C was calibrated with five known concentration of CO_2 and N_2 gas mixture. (4% CO_2 + 4% N_2, balance Argon), (8% CO_2 + 8% N_2, balance Argon), (12% CO_2 + 12% N_2, balance Argon), (20% CO_2, balance N_2) and (40% CO_2, balance N_2) were used as calibration gas. Calibration results, G.C operating protocol and calibration gas purity list are shown in Appendix A2.2 (Figure A2.1, Figure A2.2 and Table A2.1)). The chromatograph was equipped with Thermal Conductivity Detector (TCD) and CP7430 capillary column (Agilent Technologies, Palo Alto, CA) which was the combination of two different capillary columns, one being the CP-Molsieve 5A and the other CP-PoraBOND Q. CP-PoraBOND Q (length = 25 m, I.D = 0.32 mm and df = 7 micron) is highly sensitive and accurate for the measurement of CO_2 concentration and CP-Molsieve 5A (length = 50 m, I.D = 0.53 mm and df = 50 micron) is capable for the separation of N_2 and Ar (argon). He (helium) was used for the G.C carrier gas.

4.2.2 Permeation Set-Up Operational Protocols

4.2.2.1 Inherent Leak Testing

The leak rate of the feed and permeate section observed by using transparent cellophane paper as a membrane and pressurizing the entire set-up for one day. The pressure increment in the two sections was then monitored for a day. Finally, the experiment was repeated with another cellophane paper to confirm the leak rate and the proper sealing of the membrane cell.

4.2.2.2 Operational Protocols

The proper placement of the polymer composite membrane in the module is important to prevent membrane damage and accurately define the surface area of the membrane available for permeation. The module was carefully installed in the oven with the help of stainless steel gasket at room temperature (25^{o}C).

After the membrane installation, test was conducted to check for any membrane defects, such as stress fracture or pin-holes. For that reason, pressure at feed side was increased at a certain set point and kept for some time to observe the gas flow rate at permeate side. Then the temperature was slowly increased and also observed the gas flow rate at permeate side to check the membrane damage against temperature. The carrier gas (Ar) was injected at the permeate side of the module and the HPLC pump was then switched-on for both sides with particular water flow rates.

4.3 EFFECT OF PARAMETERS ON CO_2 SEPARATION BY PVA-PVP MEMBRANES CONTAINING PEI, TEPA AND THEIR BLENDS

Two different amines such as polyethyleneimine (PEI), tetraethylenepentamine (TEPA) and their blends were chosen as carriers. The structures of these amines are shown in Figure 2.7. Membranes with three different compositions were synthesized as mentioned in Chapter 3 (Section 3.3.1.3).

4.3.1 Effect of Membrane Thickness and Composition Optimization

The effects of active layer thickness on CO_2 flux, N_2 flux, CO_2 permeance, N_2 permeance, CO_2 permeability, N_2 permeability and CO_2/N_2 selectivity were studied using

crosslinked-PVA-PVP membrane containing single as well as blended amines. Three different compositions of amine were chosen to find out the best separation performance. These are crosslinked-PVA-PVP membranes containing (40 wt% PEI), (30 wt% PEI + 10 wt% TEPA) and (15 wt% PEI + 25 wt% TEPA), respectively. It is very difficult to maintain exactly same active layer thickness of the membrane for all three different amine compositions by manual solution casting technique. To find out optimum composition it is necessary to compare CO_2 flux, N_2 flux, CO_2 permeance, N_2 permeance, CO_2 permeability, N_2 permeability and CO_2/N_2 selectivity at a fixed thickness for different compositions. Feed side and sweep side absolute pressures were maintained constant at around 2.8 and 1.15 atm, respectively. Temperature was kept constant at 95^oC along with constant water flow rate at both sides (feed/sweep = 0.03/0.04 cm^3/min). Both feed gas (20% CO_2 balance N_2 on dry basis) and carrier gas (Ar) flow rates were maintained at 30 cm^3/min throughout the experiment. Seven different crosslinked-PVA-PVP membranes with different active layer thickness containing single as well as blended amines along with separation performance are given in Table 4.1 and also shown in Figures 4.3**(a-b)** and 4.4**(a-b)**.

The effect of thickness on CO_2 flux as well as N_2 flux is shown in Figure 4.3**(a)**. The CO_2 and N_2 fluxes are decreased by about 1.8 times when the thickness is increased from 34 to 87 microns at a particular composition. With increase in active layer thickness, the total mass transfer resistance increases and hence the CO_2 flux decreases [14-16]. At constant active layer thickness of 69 micron for crosslinked-PVA-PVP containing (40 wt% PEI), (30 wt% PEI + 10 wt% TEPA) and (15 wt% PEI + 25 wt% TEPA)

membranes, the CO_2 flux was 295 × 10^{-6} cm^3 (STP)/cm^2sec, 344 × 10^{-6} cm^3 (STP)/cm^2sec and 370 × 10^{-6} cm^3 (STP)/cm^2sec, respectively (Table. 4.2).

The CO_2 permeance decreases with increasing active layer thickness at a particular composition (Figure 4.3**(b)**). This trend is possibly because the mass flux through the membrane is inversely proportional to the membrane thickness.

The CO_2 permeability and CO_2/N_2 selectivity are also increased with increase in active layer thicknesses at a particular composition. The CO_2 permeability is directly proportional to the membrane thickness [17]. The N_2 permeability is essentially constant with the increase in the membrane thickness whereas CO_2 permeability increases as the thickness is increased and hence CO_2/N_2 selectivity goes up [15-17]. At constant active layer thickness of 69 micron for crosslinked-PVA-PVP containing (40 wt% PEI), (30 wt% PEI + 10 wt% TEPA) and (15 wt% PEI + 25 wt% TEPA) membranes, the CO_2 permeability was 1200 Barrer, 1359 Barrer, 1485 Barrer, respectively and CO_2/N_2 selectivity was 202, 230 and 267, respectively (Figure 4.4**(a-b)** and Table. 4.2).

As observed, 41.66 wt% PVA + 8.33 wt% PVP + 10 wt% KOH + 15 wt% PEI + 25 wt% TEPA with 60 mol% degree of crosslinking by HCHO membrane showed best separation performances among others. Hence, this membrane composition has been chosen for the detailed performance study (effect of pressure, temperature and sweep side water flow rate) via permeation measurement.

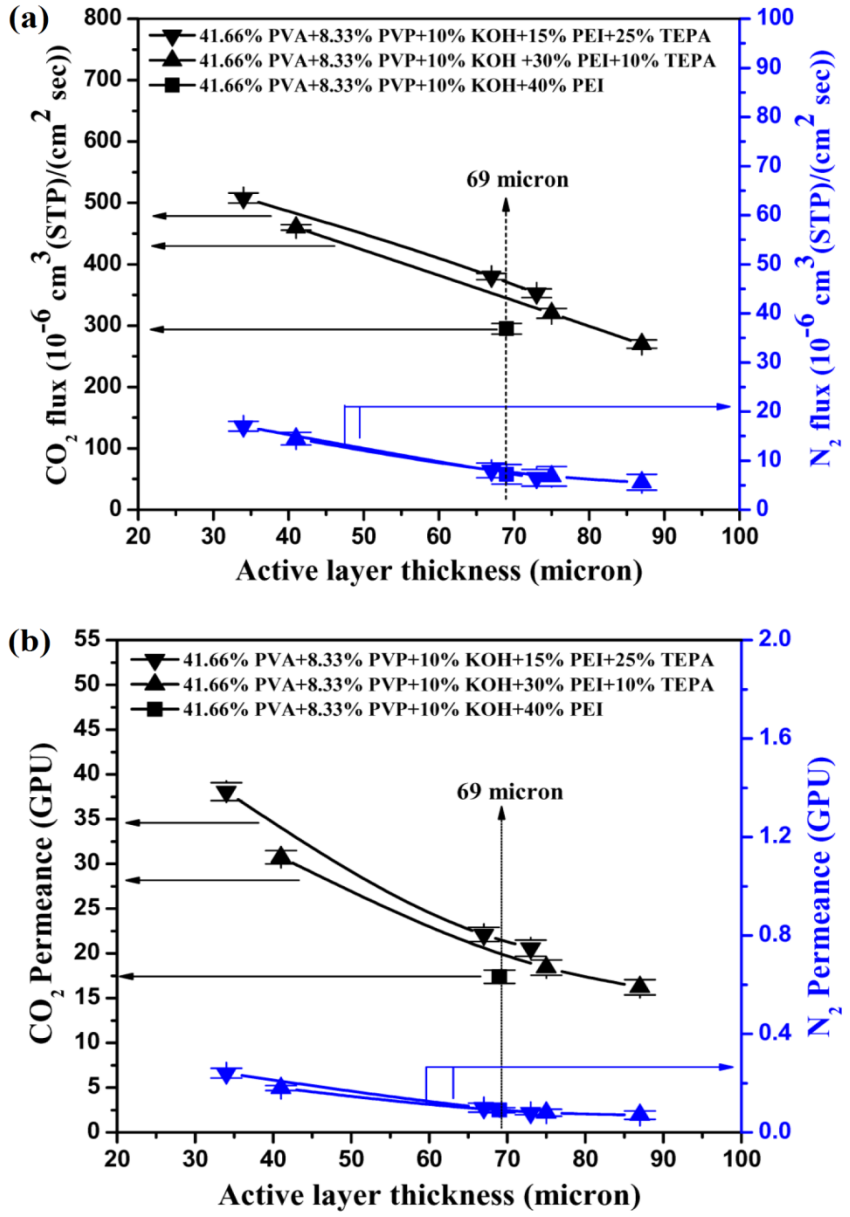

Figure 4.3 Effect of active layer thickness on **(a)** CO_2 and N_2 flux. (▼) (15 wt% PEI + 25 wt% TEPA); (▲) (30 wt% PEI + 10 wt% TEPA); (■) (40 wt% PEI0), **(b)** CO_2 and N_2 permeance (GPU). (▼) (15 wt% PEI + 25 wt% TEPA); (▲) (30 wt% PEI + 10 wt% TEPA); (■) (40 wt% PEI), at Temperature = 95 ^oC, Feed absolute pressure = 2.8 atm, sweep absolute pressure = 1.15 atm, sweep/feed water flow rate = 0.05/0.03 ml/min

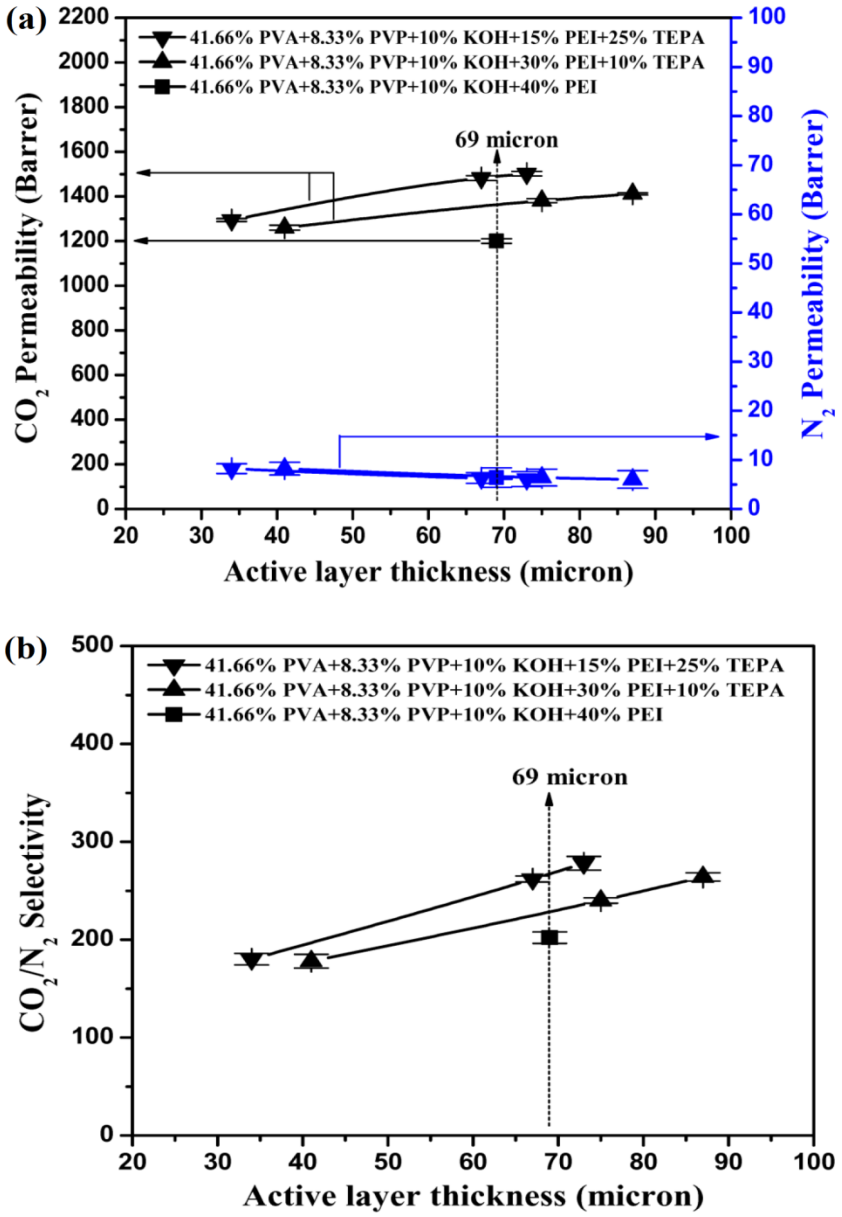

Figure 4.4 Effect of active layer thickness on **(a)** CO_2 and N_2 permeability (Barrer). (▼) (15 wt% PEI + 25 wt% TEPA); (▲) (30 wt% PEI + 10 wt% TEPA); (■) (40 wt% PEI) and **(b)** CO_2 and N_2 selectivity. (▼) (15 wt% PEI + 25 wt% TEPA); (▲) (30 wt% PEI + 10 wt% TEPA); (■) (40 wt% PEI), at Temperature = 95 ^oC, Feed absolute pressure = 2.8 atm, sweep absolute pressure = 1.15 atm, sweep/feed water flow rate = 0.05/0.03 ml/min

Table 4.1 CO_2 transport property of different active layer thickness membranes of different compositions containing PEI and TEPA at constant physical condition (Temperature = 95 ^oC, Feed absolute pressure = 2.8 atm, sweep absolute pressure = 1.15 atm, sweep/feed water flow rate = 0.05/0.03 ml/min.)

Active layer composition (wt%)	Active layer Thickness (micron)	CO_2 flux 10^{-6} $cm^3(STP)/cm^2$ sec	CO_2 Permeability (Barrer)	CO_2 Permeance (GPU)	CO_2/N_2 Selectivity
M1	34	508	1294	38	180
	67	380	1482	22.1	262
	73	353	1502	20.5	278
M2	41	460	1260	30.7	178
	75	320	1381	18.4	240
	87	270	1411	16.2	264
M3	69	295	1200	17.3	202

M1 : 41.66% PVA+8.33% PVP+10% KOH+15% PEI+25% TEPA

M2 : 41.66% PVA+8.33% PVP+10% KOH+30% PEI+10% TEPA

M3 : 41.66% PVA+8.33% PVP+10% KOH+40% PEI

Table 4.2 CO_2 transport property of constant active layer thickness, around 69 micron membranes of different compositions containing PEI and TEPA at constant physical condition (Temperature = 95 ^oC, Feed absolute pressure = 2.8 atm, sweep absolute pressure = 1.15 atm, sweep/feed water flow rate = 0.05/0.03 ml/min.)

Active layer Thickness (micron)	Active layer composition (wt%)	CO_2 flux 10^{-6} $cm^3(STP)/cm^2$ sec	CO_2 Permeability (Barrer)	CO_2 Permeance (GPU)	CO_2/N_2 Selectivity
69	M1	370	1485	21.5	267
69	M2	344	1359	19.6	230
69	M3	295	1200	17.3	202

M1 : 41.66% PVA+8.33% PVP+10% KOH+15% PEI+25% TEPA

M2 : 41.66% PVA+8.33% PVP+10% KOH+30% PEI+10% TEPA

M3 : 41.66% PVA+8.33% PVP+10% KOH+40% PEI

4.3.2 Effects of Feed Pressure

The effect of feed pressure on CO_2 and N_2 fluxes, CO_2 and N_2 permeabilities as well as CO_2/N_2 selectivity are shown in Figures 4.5**(a-c)**, respectively. The feed side absolute pressure was varied from 1.7 to 6.2 atm, while sweep side absolute pressure was maintained constant at around 1.15 atm. Both the feed gas (20% CO_2 balance N_2 on dry basis) and carrier gas (Ar) flow rates were maintained at 30 cm^3/min throughout the experiment. Feed side and sweep side water flow rates were kept constant at 0.03 and 0.04 cm^3/min, respectively. The effect of feed pressure was studied at 100^oC using

crosslinked thin-film composite membrane containing blended amines (15 wt% PEI + 25 wt% TEPA). The dense selective layer thickness on porous polysulfone membrane was 45 micron.

As shown in Figures 4.5**(a-c)**, N_2 flux is increased linearly with increase in feed pressure in accordance with the solution-diffusion mechanism. On the other hand, the CO_2 flux is increased rapidly in the low pressure region and then remained almost constant at higher pressure. This might be due to the fact that with increase in feed pressure more amount of CO_2 is dissolved in the membrane through the formation of CO_2-amine complex and hence the driving force for CO_2 transport is enhanced. At a certain CO_2 partial pressure when the carrier is saturated with CO_2, further enhancement of CO_2 transport ceases and CO_2 flux reaches a constant value [18]. With increase in absolute pressure from 1.7 to 6.2 atm, the CO_2 flux increases from 330 × 10^{-6} cm^3 (STP)/cm^2sec to 486 × 10^{-6} cm^3 (STP)/cm^2sec (Figure 4.5**(a)**). Similar observation for CO_2 flux through a membrane containing other amine carriers have also been reported in the literature [19-22].

The CO_2 permeability and CO_2/N_2 selectivity were also decreased with increase in feed pressure (Figures 4.5**(b-c)**). At low feed gas pressure, the CO_2 permeability is high due to contribution of CO_2-amine reactions in presence of the abundance of free amine groups. At higher pressure, the availability of free amine groups becomes less and the CO_2 transport is dominated by solution-diffusion mechanism and hence permeation decreases with increase in feed pressure [19]. However, with increase in the feed pressure N_2 permeability mostly does not change throughout the membrane and hence the CO_2/N_2 selectivity drops. Permeation results are given in Appendix A2.3 (Table A2.2).

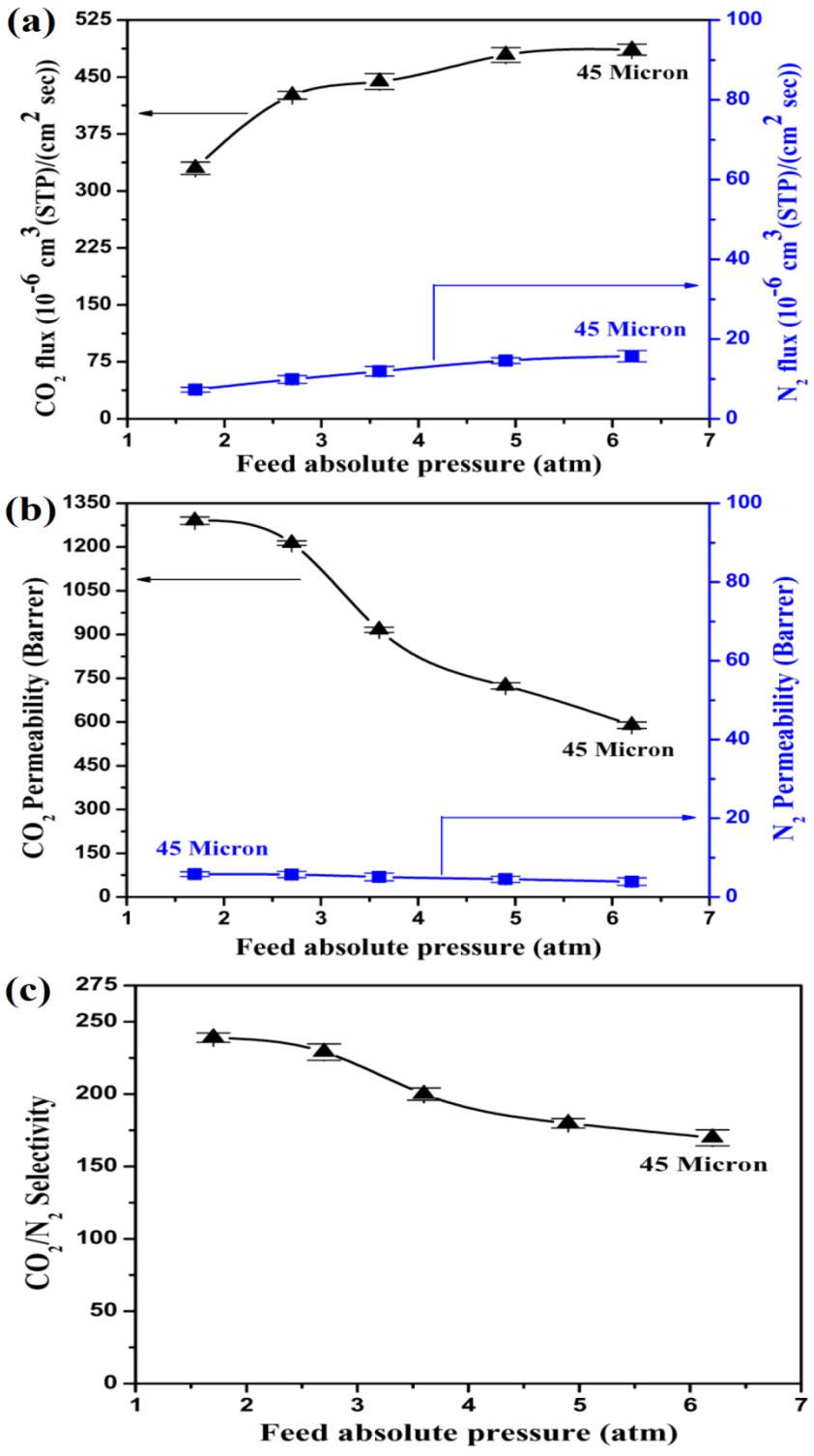

Figure 4.5 Effect of feed pressure on **(a)** CO_2 and N_2 flux. (▲) CO_2 flux; (■) N_2 flux, **(b)** CO_2 and N_2 permeability. (▲) CO_2 permeability (Barrer); (■) N_2 permeability (Barrer) and **(c)** CO_2/N_2 selectivity. (▲) CO_2/N_2 selectivity; at 100 °C with water rates = 0.03/0.04 ml/min (feed/sweep) for crosslinked-PVA-PVP membrane with (15 wt% PEI + 25 wt% TEPA)

4.3.3 Effects of Sweep Side Water Flow Rate

The effects of sweep side water flow rate (cm^3/min) on CO_2 flux, N_2 flux, CO_2 permeability, N_2 permeability and CO_2/N_2 selectivity were studied at 90°C using crosslinked thin film composite membrane containing blended amines (15 wt% PEI + 25 wt% TEPA). Sweep side water flow rate was varied from 0.02 to 0.075 cm^3/min and feed side water flow rate was maintained constant throughout this experiment at 0.03 cm^3/min. Feed and sweep side absolute pressure was kept constant at 2.7 and 1.15 atm, respectively. Both feed gas (20% CO_2 balance N_2) and carrier gas (Ar) flow rates were kept constant at 30 cm^3/min throughout the experiment. Figures 4.6**(a-c)** depicts the effect of sweep side water content on CO_2 and N_2 permeabilities, CO_2 and N_2 fluxes as well as CO_2/N_2 selectivity for the membrane, respectively.

It has been observed that with increase in the water flow rate at sweep side, the CO_2 flux, CO_2 permeability and CO_2/N_2 selectivity initially increased rapidly and then became constant. This increase might be due to the increase in mobility of the CO_2-carriers complex occurring through the CO_2-carrier reactions in the presence of water vapor [13, 17 and 18]. However, N_2 flux and permeability remains almost constant with increase in sweep side water flow rate. When the sweep side water flow rate is increased from 0.02 to 0.075 cm^3/min, CO_2 permeability is increased from 261 to as high as 1250 Barrer (Figure 4.6**(a)**). At 0.075 cm^3/min sweep side water flow rate, the CO_2 and N_2 flux as well as CO_2/N_2 selectivity reached 417×10^{-6} cm^3 (STP)/cm^2sec, 8×10^{-6} cm^3 (STP)/cm^2sec and 270, respectively (Figure 4.6**(b-c)**). Permeation results are given in Appendix A2.3 (Table A2.3).

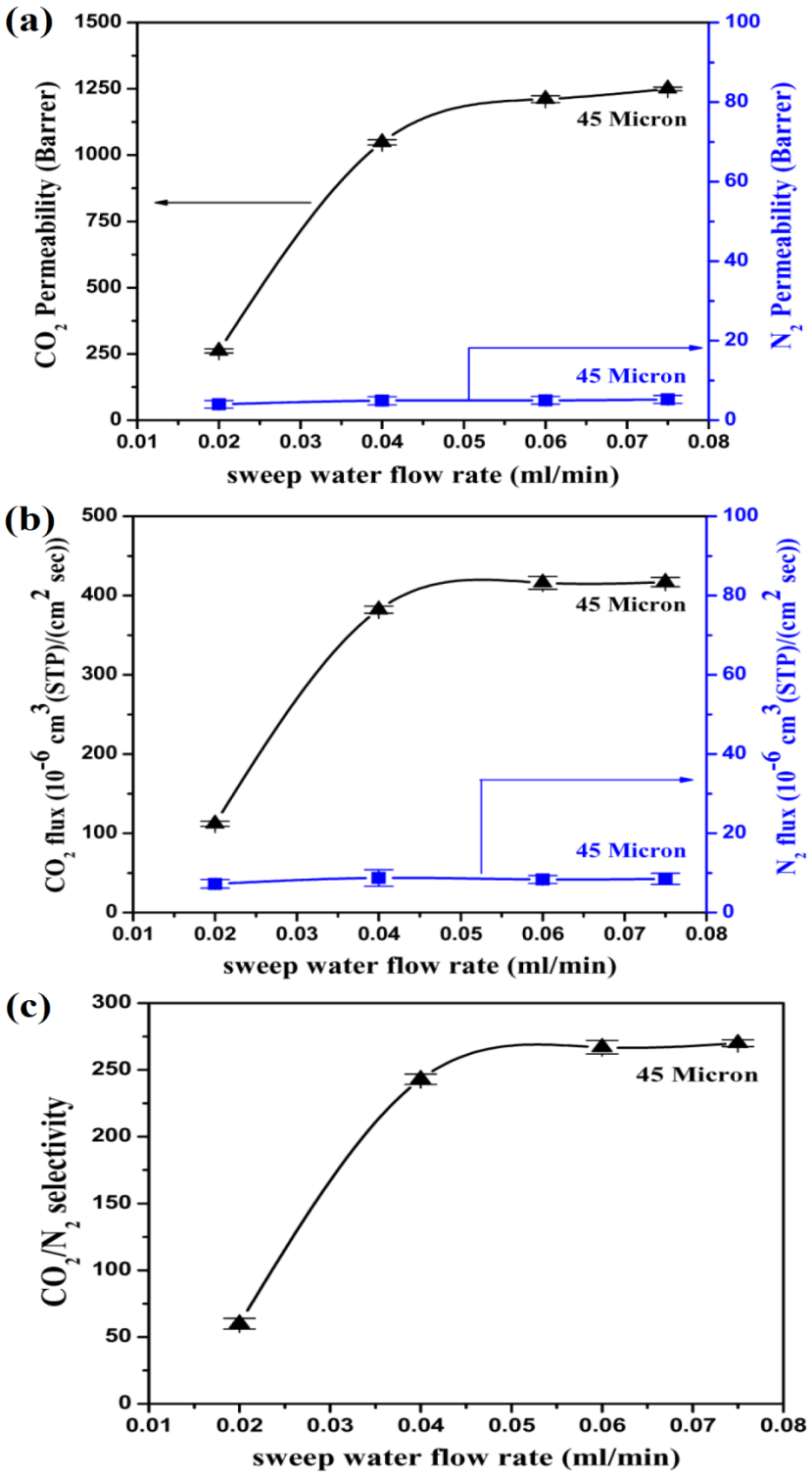

Figure 4.6 Effect of sweep side water flow rate on **(a)** CO_2 and N_2 permeability. (▲) CO_2 permeability (Barrer); (■) N_2 permeability (Barrer), **(b)** CO_2 and N_2 flux. (▲) CO_2 flux; (■) N_2 flux and **(c)** CO_2/N_2 selectivity. (▲) CO_2/N_2 selectivity; at 90 °C with feed absolute pressure = 2.7 atm, feed water flow rate = 0.03 ml/min for crosslinked-PVA-PVP membrane with (15 wt% PEI + 25 wt% TEPA)

4.3.4 Effects of Temperature

The effects of temperature on CO_2 flux, N_2 flux, CO_2 permeability, N_2 permeability and CO_2/N_2 selectivity were investigated. The temperature was varied from 90^oC to 125^oC. Feed and sweep side absolute pressure was maintained constant at 2.7 and 1.15 atm, respectively. Also the feed and sweep side water flow rate were kept constant at 0.03 and 0.04 cm^3/min, respectively. Both the feed gas and carrier gas flow rates were maintained at 30 cm^3/min.

The effect of temperature on CO_2 and N_2 permeabilities, CO_2 and N_2 fluxes as well as CO_2/N_2 selectivity is shown in Figures 4.7**(a-c)**, respectively. It has been observed that with increase in the temperature, the CO_2 permeability, CO_2 flux and CO_2/N_2 selectivity were decreased whereas N_2 flux remains almost constant. When the temperature was 125^oC, the CO_2 permeability, CO_2 and N_2 flux as well as CO_2/N_2 selectivity reached 393 Barrer, 162×10^{-6} cm^3 (STP)/cm^2sec, 9×10^{-6} cm^3 (STP)/cm^2sec and 73, respectively (Figures 4.7**(a-c)**). This might be due to the fact that with increase in temperature at a constant water flow rate, the water retention throughout the membrane is reduced. This in turn affects the mobility and reaction rate of CO_2 with carriers resulting in the decrease in permeability. Permeation results are given in Appendix A2.3 (Table A2.4).

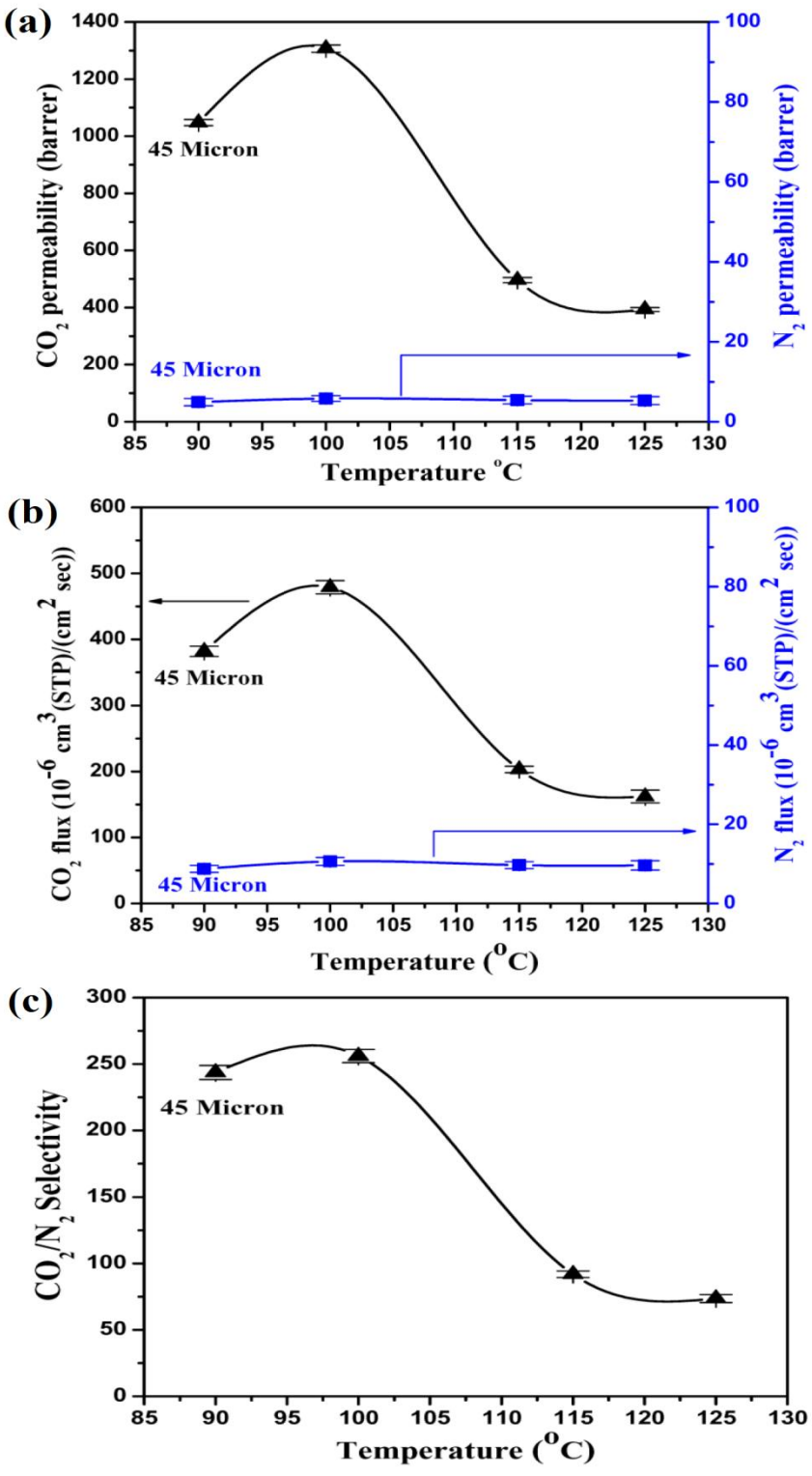

Figure 4.7 Effect of temperature on **(a)** CO_2 and N_2 permeability. (▲) CO_2 permeability (Barrer); (■) N_2 permeability (Barrer), **(b)** CO_2 and N_2 flux. (▲) CO_2 flux; (■) N_2 flux and **(c)** CO_2/N_2 selectivity. (▲) CO_2/N_2 selectivity; at 2.7 atm feed absolute pressure with water rates = 0.03/0.04 ml/min (feed/sweep) for crosslinked-PVA-PVP membrane with (15 wt% PEI + 25 wt% TEPA)

4.4 EFFECT OF PARAMETERS ON CO_2 SEPARATION BY PVA-PVP MEMBRANES CONTAINING PEI, TEPA, PEHA AND THEIR BLENDS

Three different compositions of amine among PEI and TEPA were chosen to find out the best separation performance, shown in previous section (Section 4.3.1). Among them, the crosslinked-PVA-PVP membrane containing blended amines (15 wt% PEI + 25 wt% TEPA) showed best performance at constant operating conditions. A new amine such as pentaethylenehexamine (PEHA) was introduced in place of tetraethylenepentamine (TEPA) keeping the composition of the amines constant. One mole of PEHA contain one extra (-NH) group (Figure 2.7) which may enhance the CO_2 transport through the membrane via series of reversible reaction between amine and CO_2 in presence of moisture [17]. The structures of these amines are shown in Figure 2.7. The performance of synthesized crosslinked-PVA-PVP membrane containing 15 wt% PEI and 25 wt% PEHA was compared with crosslinked-PVA-PVP membrane containing 15 wt% PEI and 25 wt% TEPA. The detailed membrane compositions are mentioned in Chapter 3 (Section 3.3.1.3).

4.4.1 Effect of Membrane Thickness and Composition Optimization

The effects of active layer thickness on CO_2 flux, N_2 flux, CO_2 permeance, N_2 permeance, CO_2 permeability, N_2 permeability and CO_2/N_2 selectivity were studied using crosslinked-PVA-PVP membrane containing blended amines. Feed side and sweep side absolute pressures were maintained constant at around 2.8 and 1.15 atm, respectively. Temperature was kept constant at 95^oC along with constant water flow rate at both sides (feed/sweep = 0.03/0.04 cm^3/min). Both feed gas (20% CO_2 balance N_2 on dry basis) and

carrier gas (Ar) flow rates were maintained at 30 cm^3/min throughout the experiment.

Three different crosslinked-PVA-PVP membranes with different active layer thickness containing blended amines (15 wt% PEI + 25 wt% PEHA) along with separation performance are given in Table 4.3 and also shown in Figures 4.8**(a-b)** and Figures 4.9**(a-b).** This result also compared with three different crosslinked-PVA-PVP membranes with different active layer thickness containing blended amines (15 wt% PEI + 25 wt% TEPA)**.**

The effect of thickness on CO_2 flux and N_2 flux are shown in Figure 4.8**(a)**. The CO_2 and N_2 fluxes are decreased by about 1.5 times when the thickness is increased from 34 to 75 microns at a particular composition. At constant active layer thickness of 55 micron for crosslinked-PVA-PVP membranes containing (15 wt% PEI + 25 wt% PEHA) and (15 wt% PEI + 25 wt% TEPA), the CO_2 flux was 483 × 10^{-6} cm^3 (STP)/cm^2sec and 430 × 10^{-6} cm^3 (STP)/cm^2sec, respectively (Table 4.4).

The CO_2 permeance decreases with increasing active layer thicknesses at a particular composition (Figure 4.8**(b)**). At constant active layer thickness of 55 micron for crosslinked-PVA-PVP membranes containing (15 wt% PEI + 25 wt% PEHA) and (15 wt% PEI + 25 wt% TEPA), the CO_2 permeance was 28 GPU and 25.8 GPU, respectively (Table 4.4). This trend is possibly because the mass flux through the membrane is inversely proportional to the membrane thickness.

The CO_2 permeability and CO_2/N_2 selectivity is also increased with increase in active layer thicknesses at a particular composition. At constant active layer thickness of 55 micron for crosslinked-PVA-PVP membranes containing (15 wt% PEI + 25 wt% PEHA)

and (15 wt% PEI + 25 wt% TEPA), the CO_2 permeability was 1535 Barrer and 1421 Barrer, respectively and CO_2/N_2 selectivity was 354 and 230, respectively (Figures 4.9**(a-b)** and Table 4.4).

It can be observed from Figure 4.8**(a-b)** and Figure 4.9**(a-b)** that at constant active layer thickness, the CO_2 flux, CO_2 permeance, CO_2 permeability and CO_2/N_2 selectivity increased for membrane containing 15 wt% PEI and 25 wt% PEHA compared to membrane containing 15 wt% PEI and 25 wt% TEPA at a constant physical condition mentioned above (Table 4.4). Hence, the membrane with 15 wt% PEI and 25 wt% PEHA has been chosen for the detailed performance study (effect of pressure, temperature and sweep side water flow rate) via permeation measurement and compared with the values obtained by the membrane containing 15 wt% PEI and 25 wt% TEPA.

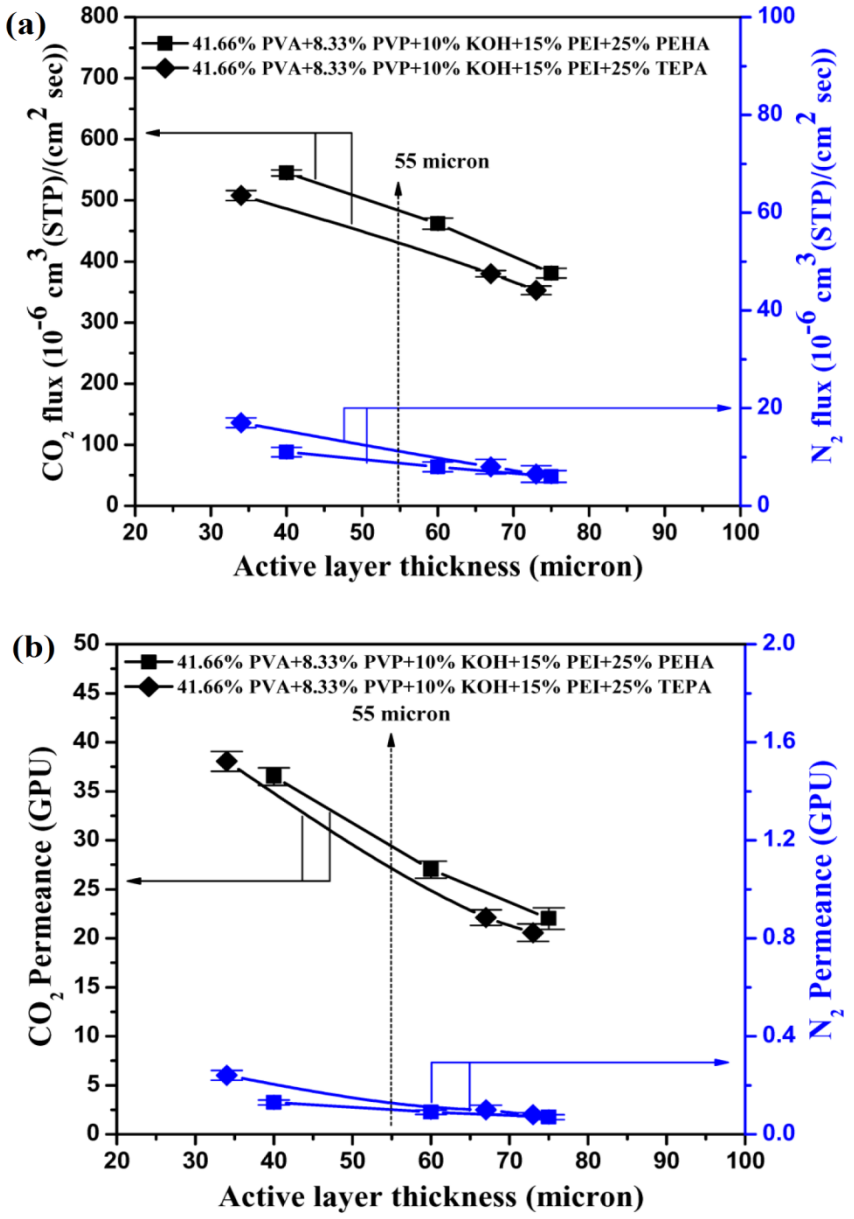

Figure 4.8 Effect of active layer thickness on **(a)** CO_2 and N_2 flux. (■) (15 wt% PEI + 25 wt% PEHA); (♦) (15 wt% PEI + 25 wt% TEPA), **(b)** CO_2 and N_2 permeance (GPU). (■) (15 wt% PEI + 25 wt% PEHA); (♦) (15 wt% PEI + 25 wt% TEPA), at Temperature = 95 ^{o}C, Feed absolute pressure = 2.8 atm, sweep absolute pressure = 1.15 atm, sweep/feed water flow rate = 0.05/0.03 ml/min

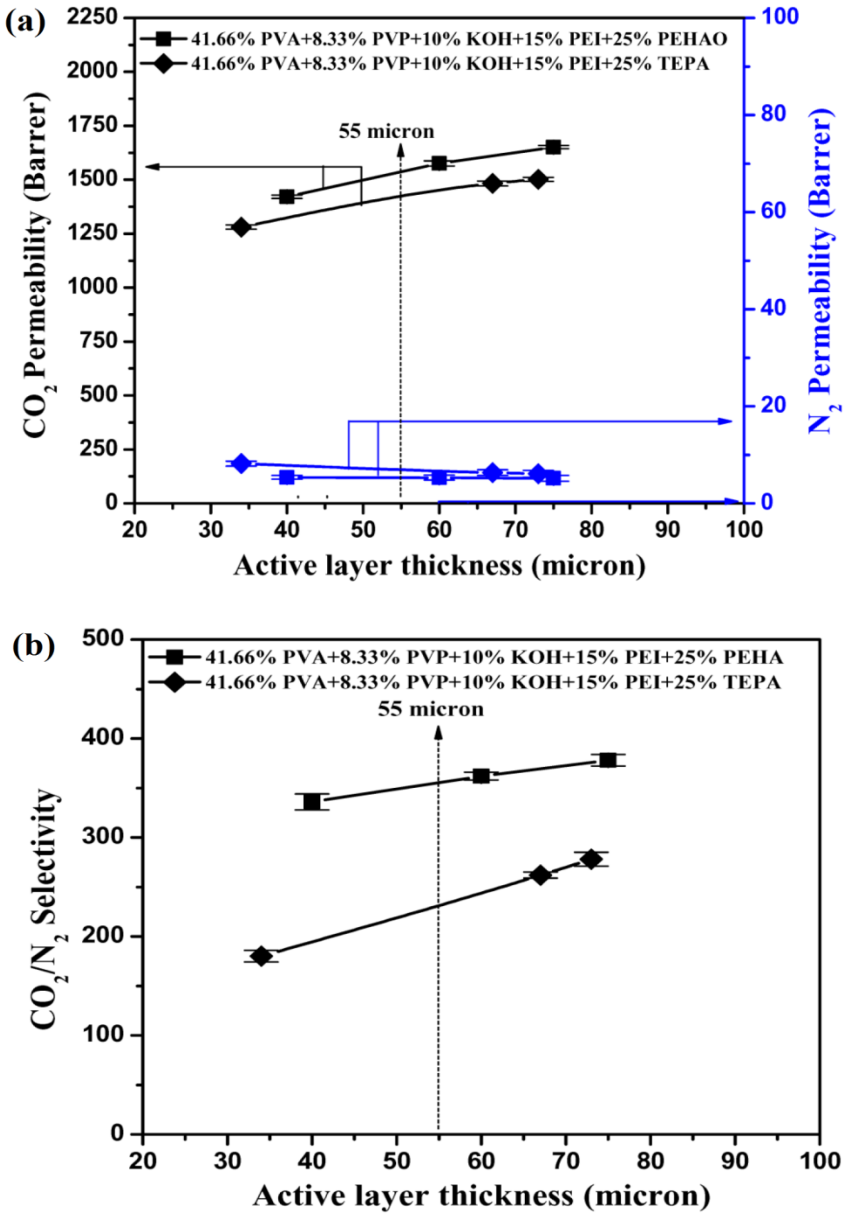

Figure 4.9 Effect of active layer thickness on **(a)** CO_2 and N_2 permeability (Barrer). (■) (15 wt% PEI + 25 wt% PEHA); (♦) (15 wt% PEI + 25 wt% TEPA) and **(b)** CO_2 and N_2 selectivity. (■) (15 wt% PEI + 25 wt% PEHA); (♦) (15 wt% PEI + 25 wt% TEPA), at Temperature = 95 ^oC, Feed absolute pressure = 2.8 atm, sweep absolute pressure = 1.15 atm, sweep/feed water flow rate = 0.05/0.03 ml/min

Table 4.3 CO_2 transport property of different active layer thickness membranes of different compositions containing PEI, TEPA and PEHA at constant physical condition (Temperature = 95 ^oC, Feed absolute pressure = 2.8 atm, sweep absolute pressure = 1.15 atm, sweep/feed water flow rate = 0.05/0.03 ml/min.)

Active layer composition (wt%)	Active layer Thickness (micron)	CO_2 flux 10^{-6} $cm^3(STP)/cm^2$ sec	CO_2 Permeability (Barrer)	CO_2 Permeance (GPU)	CO_2/N_2 Selectivity
M1	34	508	1294	38	180
	67	380	1482	22.1	262
	73	353	1502	20.5	278
M4	40	545	1420	35.5	336
	60	462	1575	26.2	362
	75	381	1651	22	378

M1 : 41.66% PVA+8.33% PVP+10% KOH+15% PEI+25% TEPA

M4: 41.66% PVA+8.33% PVP+10% KOH+15% PEI+25% PEHA

Table 4.4 CO_2 transport property of constant active layer thickness, around 55 micron membranes of different compositions containing PEI, TEPA and PEHA at constant physical condition (Temperature = 95 ^oC, Feed absolute pressure = 2.8 atm, sweep absolute pressure = 1.15 atm, sweep/feed water flow rate = 0.05/0.03 ml/min.)

Active layer Thickness (micron)	Active layer composition (wt%)	CO_2 flux 10^{-6} $cm^3(STP)/cm^2$ sec	CO_2 Permeability (Barrer)	CO_2 Permeance (GPU)	CO_2/N_2 Selectivity
55	M4	483	1535	28	354
55	M1	430	1421	25.8	230

M1 : 41.66% PVA+8.33% PVP+10% KOH+15% PEI+25% TEPA

M4: 41.66% PVA+8.33% PVP+10% KOH+15% PEI+25% PEHA

4.4.2 Effects of Feed Pressure

The effect of feed pressure on CO_2 and N_2 fluxes, CO_2 and N_2 permeabilities as well as CO_2/N_2 selectivity for the composite membrane containing blended amines (15 wt% PEI + 25 wt% PEHA) and (15 wt% PEI + 25 wt% TEPA) are shown in Figures 4.10**(a-c)**, respectively. The feed side absolute pressure was varied from 1.7 to 6.2 atm, while sweep side absolute pressure was maintained constant at around 1.15 atm for both the membrane. Both the feed gas (20% CO_2 balance N_2 on dry basis) and carrier gas (Ar) flow rates were maintained at 30 cm^3/min throughout the experiment. Feed side and sweep side water flow rates were kept constant at 0.03 and 0.04 cm^3/min, respectively for both the membrane. The effects of feed pressure on CO_2 flux, N_2 flux, CO_2 permeability,

N_2 permeability and CO_2/N_2 selectivity were studied at 100°C using crosslinked thin-film composite membrane containing blended amines (15 wt% PEI + 25 wt% PEHA) and compared with the membrane containing 15 wt% PEI and 25 wt% TEPA. The thickness of the dense selective layer on porous polysulfone for the membrane containing blended amines (15 wt% PEI + 25 wt% PEHA) was 40 micron whereas the membrane containing 15 wt% PEI and 25 wt% TEPA was 45 micron.

As shown in Figures 4.10**(a-c)**, N_2 flux is increased linearly with increase in feed pressure in accordance with the solution-diffusion mechanism. On the other hand, the CO_2 flux is increased rapidly in the low pressure region and then remained almost constant at higher pressure for both the membrane. At 100°C temperature when feed side absolute pressure increased from 1.7 to 6.2 atm along with constant water flow rate at both side (feed/sweep = 0.03/0.04 cm^3/min), the CO_2 flux increased from 408 × 10^{-6} cm^3 (STP)/cm^2sec to 689 × 10^{-6} cm^3 (STP)/cm^2sec for membrane containing 15 wt% PEI and 25 wt% PEHA and increased from 330 × 10^{-6} cm^3 (STP)/cm^2sec to 486 × 10^{-6} cm^3 (STP)/cm^2sec for membrane containing 15 wt% PEI and 25 wt% TEPA (Figure 4.10**(a)**). Similar observation for CO_2 flux through a membrane containing other amine carriers have also been reported in the literature [19-22].

The CO_2 permeability and CO_2/N_2 selectivity were also decreased with increase in feed pressure for both the membrane (Figures 4.10**(b-c)**). At low feed gas pressure, the CO_2 permeability is high due to contribution of CO_2-amine reactions in presence of the abundance of free amine groups. At higher pressure, the availability of free amine groups becomes less and the CO_2 transport is dominated by solution-diffusion mechanism and

hence permeation decreases with increase in feed pressure [20]. However, with increase in the feed pressure N_2 permeability mostly does not change throughout the membrane and hence the CO_2/N_2 selectivity dropped for both the membrane. Permeation results are given in Table A2.5 (Appendix A2.4).

4.4.3 Effects of Sweep Side Water Flow Rate

The effects of sweep side water flow rate (cm^3/min) on CO_2 flux, N_2 flux, CO_2 permeability, N_2 permeability and CO_2/N_2 selectivity were studied at 90^oC using crosslinked thin-film composite membrane containing blended amines (15 wt% PEI + 25 wt% PEHA) and compared with membranes containing 15 wt% PEI and 25 wt% TEPA. Sweep side water flow rate was varied from 0.02 to 0.075 cm^3/min and feed side water flow rate was maintained constant throughout this experiment at 0.03 cm^3/min for both the membrane. Feed and sweep side absolute pressure was kept constant at 2.7 and 1.15 atm, respectively. Both feed gas (20% CO_2 balance N_2) and carrier gas (Ar) flow rates were kept constant at 30 cm^3/min, throughout the experiment. Figures 4.11**(a-c)** depicts the effect of sweep side water content on CO_2 and N_2 permeabilities, CO_2 and N_2 fluxes as well as CO_2/N_2 selectivity for the composite membrane containing blended amines (15 wt% PEI + 25 wt% PEHA) and (15 wt% PEI + 25 wt% TEPA), respectively. It has been observed that with increase in the water flow rate at sweep side, the CO_2 flux, CO_2 permeability and CO_2/N_2 selectivity initially increased rapidly and then became constant for both the membrane. This increase might be due to the increase in mobility of the CO_2-carriers complex occurring through the CO_2-carrier reactions in the presence of water vapor [13, 17, and 18]. However, N_2 flux and permeability remains almost constant with

increase in sweep side water flow rate for both the membrane. When the sweep side water flow rate is increased from 0.02 to 0.075 cm^3/min, CO_2 permeability is increased from 545 to as high as 1474 Barrer for blended amines of (15 wt% PEI + 25 wt% PEHA) composite membrane and increased from 261 to as high as 1250 Barrer for blended amines of (15 wt% PEI + 25 wt% TEPA) composite membrane, respectively (Figure 4.11**(a)**). At 0.075 cm^3/min sweep side water flow rate, the CO_2 and N_2 flux as well as CO_2/N_2 selectivity reached 543×10^{-6} cm^3 (STP)/cm^2sec, 9×10^{-6} cm^3 (STP)/cm^2sec and 409, respectively for blended amines of (15 wt% PEI + 25 wt% PEHA) composite membrane, whereas the CO_2 and N_2 flux as well as CO_2/N_2 selectivity reached 417×10^{-6} cm^3 (STP)/cm^2sec, 8×10^{-6} cm^3 (STP)/cm^2sec and 270, respectively for blended amines of (15 wt% PEI + 25 wt% TEPA) composite membrane (Figures 4.11**(b-c)**). Permeation results of sweep side water flow rate are given in Table A2.6 (Appendix A2.4).

4.4.4 Effects of Temperature

The effects of temperature on CO_2 flux, N_2 flux, CO_2 permeability, N_2 permeability and CO_2/N_2 selectivity were investigated. The temperature was varied from 90^{o}C to 125^{o}C. Feed and sweep side absolute pressure was maintained constant at 2.7 and 1.15 atm, respectively. Also the feed and sweep side water flow rate were kept constant at 0.03 and 0.04 cm^3/min, respectively. Both the feed gas and carrier gas flow rates were maintained at 30 cm^3/min.

The effect of temperature on CO_2 and N_2 permeabilities, CO_2 and N_2 fluxes as well as CO_2/N_2 selectivity is shown in Figures 4.12**(a-c)** for the composite membrane containing blended amines (15 wt% PEI + 25 wt% PEHA) and compared with blended amines (15

wt% PEI + 25 wt% TEPA), respectively. It has been observed that with increase in the temperature, the CO_2 permeability, CO_2 flux and CO_2/N_2 selectivity were decreased whereas N_2 flux remains almost constant for both the membrane. When the temperature was 125^oC, the CO_2 permeability, CO_2 and N_2 flux as well as CO_2/N_2 selectivity reached 400 Barrer, 186×10^{-6} cm^3 (STP)/cm^2sec, 9×10^{-6} cm^3 (STP)/cm^2sec and 94, respectively for blended amines of (15 wt% PEI + 25 wt% PEHA) composite membrane, whereas the CO_2 permeability, CO_2 and N_2 flux as well as CO_2/N_2 selectivity reached 393 Barrer, 162×10^{-6} cm^3 (STP)/cm^2sec, 9×10^{-6} cm^3 (STP)/cm^2sec and 73, respectively for blended amines of (15 wt% PEI + 25 wt% TEPA) composite membrane (Figures 4.12**(a-c)**). This might be due to the fact that with increase in temperature at a constant water flow rate, the water retention throughout the membrane is reduced. This in turn affects the mobility and reaction rate of CO_2 with carriers resulting in the decrease in permeability for both the membrane. Permeation results are given in Table A2.7 (Appendix A2.4).

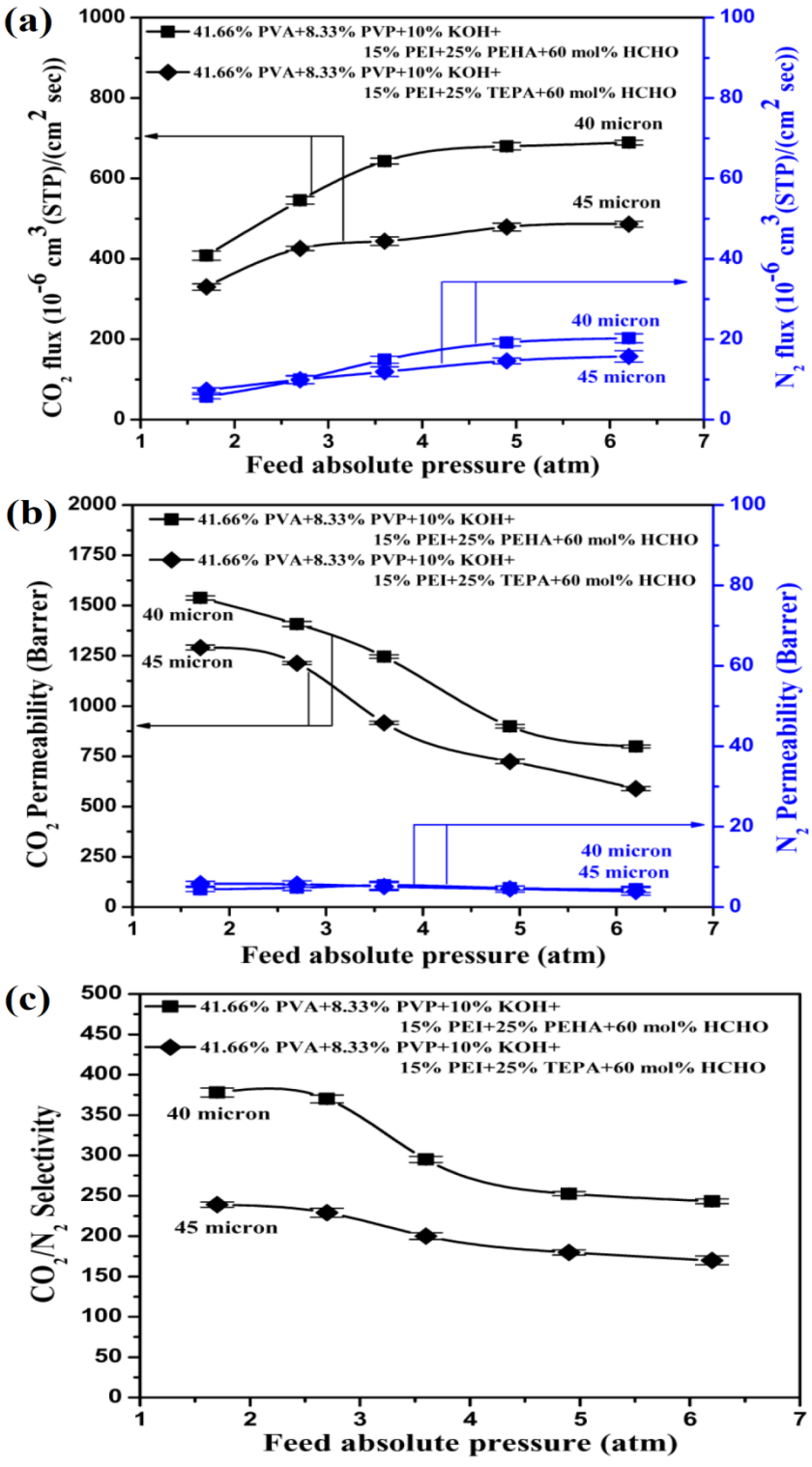

Figure 4.10 Effect of feed pressure on **(a)** CO_2 and N_2 flux. (■) (15 wt% PEI + 25 wt% PEHA); (♦) (15 wt% PEI + 25 wt% TEPA), **(b)** CO_2 and N_2 permeability (Barrer). (■) (15 wt% PEI + 25 wt% PEHA); (♦) (15 wt% PEI + 25 wt% TEPA) and **(c)** CO_2/N_2 selectivity. (■) (15 wt% PEI + 25 wt% PEHA); (♦) (15 wt% PEI + 25 wt% TEPA); at 100 ^{o}C with water rates = 0.03/0.04 ml/min (feed/sweep)

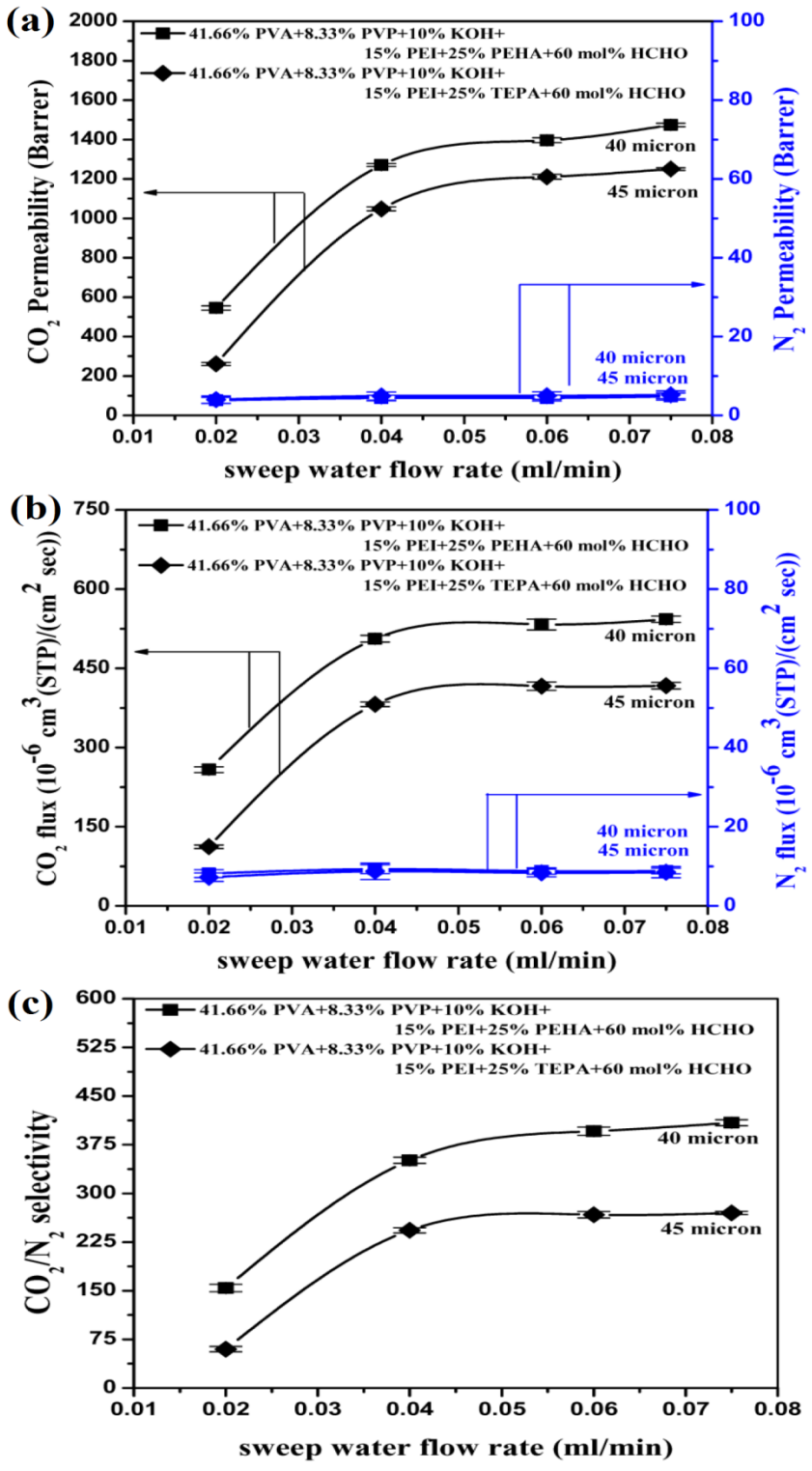

Figure 4.11 Effect of sweep side water flow rate on **(a)** CO_2 and N_2 permeability (Barrer). (■) (15 wt% PEI + 25 wt% PEHA); (♦) (15 wt% PEI + 25 wt% TEPA), **(b)** CO_2 and N_2 flux. (■) (15 wt% PEI + 25 wt% PEHA); (♦) (15 wt% PEI + 25 wt% TEPA) and **(c)** CO_2/N_2 selectivity. (■) (15 wt% PEI + 25 wt% PEHA); (♦) (15 wt% PEI + 25 wt% TEPA); at 90 °C with feed absolute pressure = 2.7 atm, feed water flow rate = 0.03 ml/min

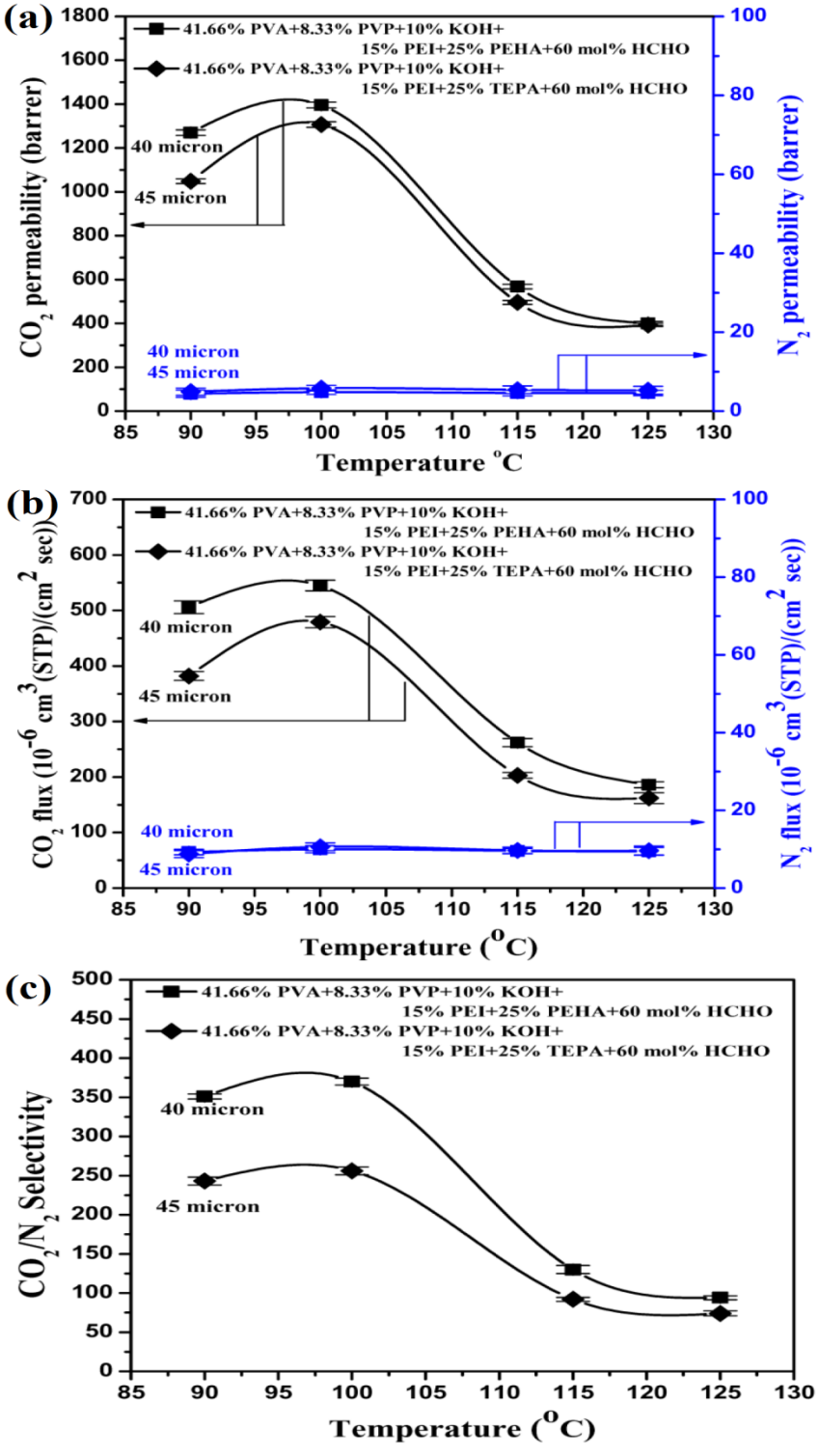

Figure 4.12 Effect of temperature on **(a)** CO_2 and N_2 permeability (Barrer). (■) (15 wt% PEI + 25 wt% PEHA); (♦) (15 wt% PEI + 25 wt% TEPA), **(b)** CO_2 and N_2 flux. (■) (15 wt% PEI + 25 wt% PEHA); (♦) (15 wt% PEI + 25 wt% TEPA) and **(c)** CO_2/N_2 selectivity. (■) (15 wt% PEI + 25 wt% PEHA); (♦) (15 wt% PEI + 25 wt% TEPA); at 2.7 atm feed absolute pressure with water rates = 0.03/0.04 ml/min (feed/sweep)

4.5 EFFECT OF PARAMETERS ON CO_2 SEPARATION BY PVA-PVP MEMBRANES CONTAINING PAA, PEHA AND THEIR BLENDS

It has been observed from the previous study that PEHA gave better separation performance compared to TEPA (Section 4.4.1). In this study, another amine such as poly(allylamine) (PAA) and blends of PAA and PEHA were chosen as carriers. The structures of these amines are shown in Figure 2.7. Membranes with three different compositions were synthesized as mentioned in Chapter 3 (Section 3.3.1.3).

4.5.1 Effect of Membrane Thickness and Composition Optimization

The effects of active layer thickness on CO_2 flux, N_2 flux, CO_2 permeance, N_2 permeance, CO_2 permeability, N_2 permeability and CO_2/N_2 selectivity were studied using crosslinked-PVA-PVP membrane containing single as well as blended amines. Three different compositions of amine among PAA and PEHA were chosen to find out the best separation performance. These are crosslinked-PVA-PVP membranes containing (40 wt% PAA), (15 wt% PAA + 25 wt% PEHA) and (25 wt% PAA + 15 wt% PEHA), respectively. For the permeation experiment, feed side and sweep side absolute pressure was maintained constant at around 2.8 and 1.15 atm, respectively. Temperature was kept constant at 95^oC along with constant water flow rate at both sides (feed/sweep = 0.03/0.05 cm^3/min). Both feed gas (20% CO_2 balance N_2 on dry basis) and carrier gas (Ar) flow rates were maintained at 30 cm^3/min throughout the experiment. Seven different crosslinked-PVA-PVP membranes with different active layer thickness containing single or blended amines along with separation performance are given in Table 4.5 and also shown in Figure 4.13**(a-b)** and Figure 4.14**(a-b)**.

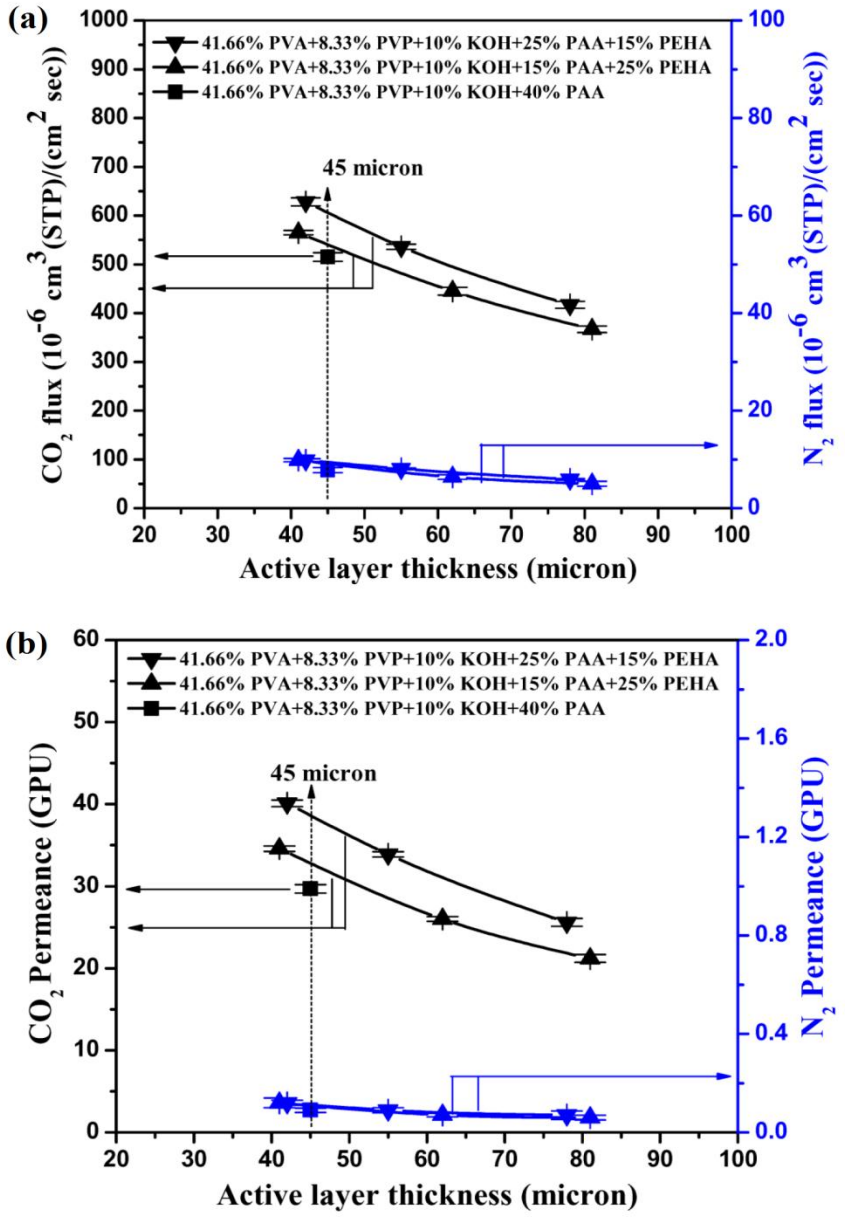

Figure 4.13 Effect of active layer thickness on **(a)** CO_2 and N_2 flux. (▼) (25 wt% PAA + 15 wt% PEHA); (▲) (15 wt% PAA + 25 wt% PEHA); (■) (40 wt% PAA), **(b)** CO_2 and N_2 permeance (GPU). (▼) (25 wt% PAA + 15 wt% PEHA); (▲) (15 wt% PAA + 25 wt% PEHA); (■) (40 wt% PAA), at Temperature = 95 ^oC, Feed absolute pressure = 2.8 atm, sweep absolute pressure = 1.15 atm, sweep/feed water flow rate = 0.05/0.03 ml/min

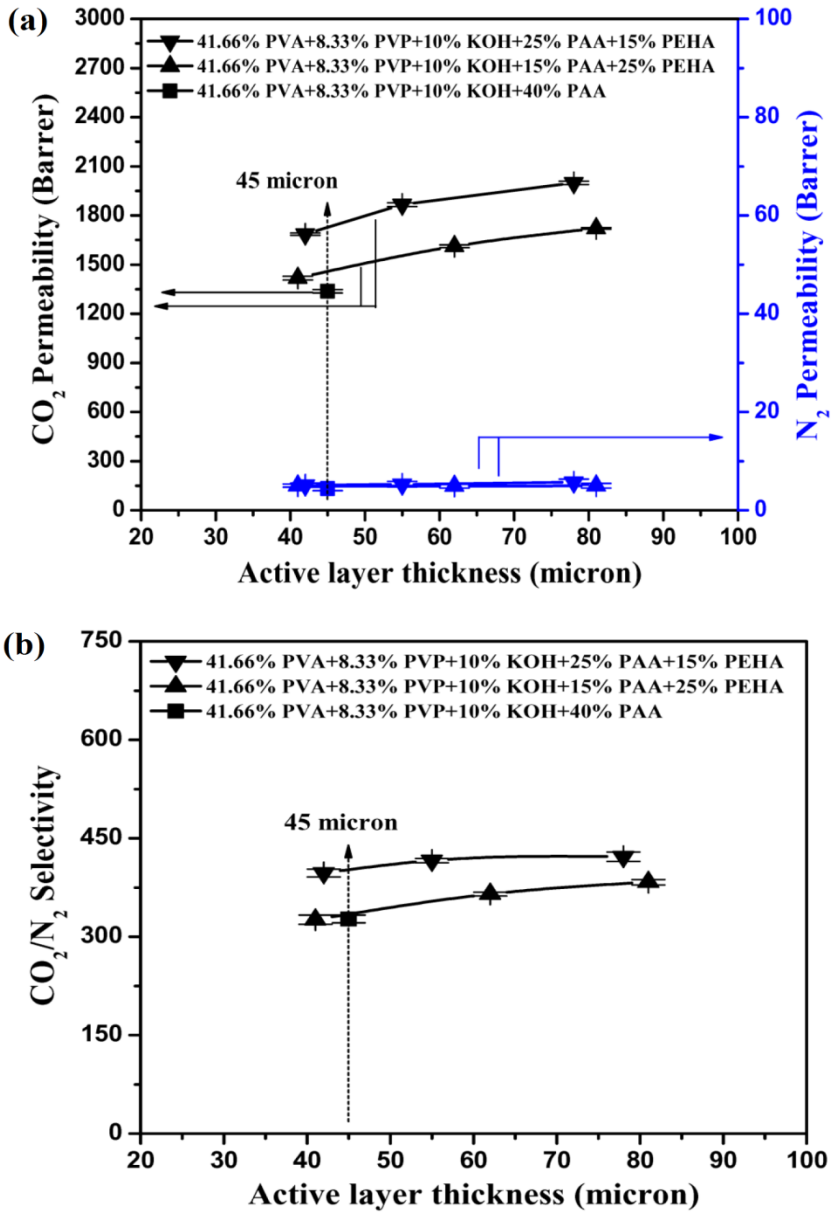

Figure 4.14 Effect of active layer thickness on **(a)** CO_2 and N_2 permeability (Barrer). (▼) (25 wt% PAA + 15 wt% PEHA); (▲) (15 wt% PAA + 25 wt% PEHA); (■) (40 wt% PAA) and **(b)** CO_2 and N_2 selectivity. (▼) (25 wt% PAA + 15 wt% PEHA); (▲) (15 wt% PAA + 25 wt% PEHA); (■) (40 wt% PAA), at Temperature = 95 ^oC, Feed absolute pressure = 2.8 atm, sweep absolute pressure = 1.15 atm, sweep/feed water flow rate = 0.05/0.03 ml/min

Table 4.5 CO_2 transport property of different active layer thickness membranes of different compositions containing PAA and PEHA at constant physical condition (Temperature = 95 ^oC, Feed absolute pressure = 2.8 atm, sweep absolute pressure = 1.15 atm, sweep/feed water flow rate = 0.05/0.03 ml/min.)

Active layer composition (wt%)	Active layer Thickness (micron)	CO_2 flux 10^{-6} $cm^3(STP)/cm^2$ sec	CO_2 Permeability (Barrer)	CO_2 Permeance (GPU)	CO_2/N_2 Selectivity
M5	42	628	1685	40.1	397
	55	536	1865	33.9	416
	78	417	1999	25.6	422
M6	41	565	1418	34.5	326
	62	445	1612	26	365
	81	367	1721	21.2	383
M7	45	515	1336	29.6	327

M5 : 41.66% PVA+8.33% PVP+10% KOH+25% PAA+15% PEHA

M6 : 41.66% PVA+8.33% PVP+10% KOH+15% PAA+25% PEHA

M7 : 41.66% PVA+8.33% PVP+10% KOH+40% PAA

The effect of thickness on CO_2 flux and N_2 flux are shown in Figure 4.13**(a)**. The CO_2 and N_2 fluxes are decreased by about 1.5 times when the thickness is increased from 42 to 81 microns at a particular composition. At constant active layer thickness of 45 micron for crosslinked-PVA-PVP membranes containing (40 wt% PAA), (15 wt% PAA + 25

wt% PEHA) and (25 wt% PAA + 15 wt% PEHA), the CO_2 flux was 515 × 10^{-6} cm^3 (STP)/cm^2sec, 542 × 10^{-6} cm^3 (STP)/cm^2sec and 605 × 10^{-6} cm^3 (STP)/cm^2sec, respectively. The detailed results are given in Table 4.6.

The CO_2 permeance decreases with increasing active layer thicknesses at a particular composition (Figure 4.13**(b)**). This trend is possibly because the mass flux through the membrane is inversely proportional to the membrane thickness. At constant active layer thickness of 45 micron for crosslinked-PVA-PVP membranes containing (40 wt% PAA), (15 wt% PAA + 25 wt% PEHA) and (25 wt% PAA + 15 wt% PEHA), the permeance was 29.7 GPU, 32.4 GPU and 38.5 GPU, respectively. The detailed results are included in Table 4.6.

The CO_2 permeability and CO_2/N_2 selectivity is also increased with increase in active layer thicknesses at a particular composition (Figures 4.14**(a-b)**). At constant active layer thickness of 45 micron for crosslinked-PVA-PVP membranes containing (40 wt% PAA), (15 wt% PAA + 25 wt% PEHA) and (25 wt% PAA + 15 wt% PEHA), the CO_2 permeability was 1337 Barrer, 1460 Barrer, 1734 Barrer, respectively and CO_2/N_2 selectivity was 327, 335 and 403, respectively, (Figures 4.14**(a-b)** and Table 4.6).

As observed, 41.66 wt% PVA + 8.33 wt% PVP + 10 wt% KOH + 25 wt% PAA + 15 wt% PEHA with 60 mol% degree of crosslinking by HCHO membrane showed best separation performances among others. Hence, this membrane composition has been chosen for the detailed performance study (effect of pressure, temperature and sweep side water flow rate) via permeation measurement.

Table 4.6 CO_2 transport property of constant active layer thickness, around 45 micron membranes of different compositions containing PAA and PEHA at constant physical condition (Temperature = 95 ^oC, Feed absolute pressure = 2.8 atm, sweep absolute pressure = 1.15 atm, sweep/feed water flow rate = 0.05/0.03 ml/min.)

Active layer Thickness (micron)	Active layer composition (wt%)	CO_2 flux 10^{-6} $cm^3(STP)/cm^2$ sec	CO_2 Permeability (Barrer)	CO_2 Permeance (GPU)	CO_2/N_2 Selectivity
45	M5	605	1734	38.5	403
45	M6	542	1460	32.4	335
45	M7	515	1337	29.7	327

M5 : 41.66% PVA+8.33% PVP+10% KOH+25% PAA+15% PEHA

M6 : 41.66% PVA+8.33% PVP+10% KOH+15% PAA+25% PEHA

M7 : 41.66% PVA+8.33% PVP+10% KOH+40% PAA

4.5.2 Effects of Feed Pressure

The effect of feed pressure on CO_2 and N_2 fluxes, CO_2 and N_2 permeabilities as well as CO_2/N_2 selectivity are shown in Figures 4.15**(a-c)**, respectively. The feed side absolute pressure was varied from 1.7 to 6.2 atm, while sweep side absolute pressure was maintained constant at around 1.15 atm. Both the feed gas (20% CO_2 balance N_2 on dry basis) and carrier gas (Ar) flow rates were maintained at 30 cm^3/min throughout the experiment. Feed side and sweep side water flow rates were kept constant at 0.03 and 0.04 cm^3/min, respectively. The effects of feed pressure were studied at 100^oC using

crosslinked thin-film composite membrane containing blended amines (25 wt% PAA + 15 wt% PEHA). The dense selective layer thickness on porous polysulfone membrane was 42 micron.

As shown in Figures 4.15**(a-c)**, N_2 flux is increased linearly with increase in feed pressure in accordance with the solution-diffusion mechanism. On the other hand, the CO_2 flux is increased rapidly in the low pressure region and then remained almost constant at higher pressure. At 100^oC temperature when feed side absolute pressure increased from 1.7 to 6.2 atm along with constant water flow rate at both side (feed/sweep = 0.03/0.04 cm^3/min), the CO_2 flux increased from 411 × 10^{-6} cm^3 (STP)/cm^2sec to 678 × 10^{-6} cm^3 (STP)/cm^2sec (Figure 4.15**(a)**). Similar observation for CO_2 flux through a membrane containing other amine carriers have also been reported in the literature [19-22].

The CO_2 permeability and CO_2/N_2 selectivity were also decreased with increase in feed pressure (Figures 4.15**(b-c)**). At low feed gas pressure, the CO_2 permeability is high due to contribution of CO_2-amine reactions in presence of the abundance of free amine groups. At higher pressure, the availability of free amine groups becomes less and the CO_2 transport is dominated by solution-diffusion mechanism and hence permeation decreases with increase in feed pressure [20]. However, with increase in the feed pressure N_2 permeability mostly does not change throughout the membrane and hence the CO_2/N_2 selectivity drops for both the membrane. Permeation results are presented in Table A2.8 (Appendix A2.5).

4.5.3 Effects of Sweep Side Water Flow Rate

The effects of sweep side water flow rate (cm^3/min) on CO_2 flux, N_2 flux, CO_2 permeability, N_2 permeability and CO_2/N_2 selectivity were studied at 90°C using crosslinked thin film composite membrane containing blended amines (25 wt% PAA + 15 wt% PEHA). Sweep side water flow rate was varied from 0.02 to 0.075 cm^3/min and feed side water flow rate was maintained constant throughout this experiment at 0.03 cm^3/min. Feed and sweep side absolute pressure was kept constant at 2.7 and 1.15 atm, respectively. Both feed gas (20% CO_2 balance N_2) and carrier gas (Ar) flow rates were kept constant at 30 cm^3/min, throughout the experiment. Figures 4.16**(a-c)** depicts the effect of sweep side water content on CO_2 and N_2 permeabilities, CO_2 and N_2 fluxes as well as CO_2/N_2 selectivity for the composite membrane, respectively. When the sweep side water flow rate is increased from 0.02 to 0.075 cm^3/min, CO_2 permeability is increased from 716 to as high as 1613 Barrer (Figure 4.16**(a)**). At 0.075 cm^3/min sweep side water flow rate, the CO_2 and N_2 flux as well as CO_2/N_2 selectivity reached 584×10^{-6} cm^3 (STP)/cm^2sec, 8×10^{-6} cm^3 (STP)/cm^2sec and 411, respectively (Figures 4.16**(b-c)**). Permeation results are included in Table A2.9 (Appendix A2.5).

4.5.4 Effects of Temperature

The effect of temperature on CO_2 and N_2 permeabilities, CO_2 and N_2 fluxes as well as CO_2/N_2 selectivity is shown in Figure 4.17**(a-c)**, respectively. The temperature was varied from 90°C to 125°C. Feed and sweep side absolute pressure was maintained constant at 2.7 and 1.15 atm, respectively. Also the feed and sweep side water flow rate were kept constant at 0.03 and 0.04 cm^3/min, respectively. Both the feed gas and carrier gas flow

rates were maintained at 30 cm^3/min. It has been observed that with increase in the temperature, the CO_2 permeability, CO_2 flux and CO_2/N_2 selectivity were decreased whereas N_2 flux remains almost constant. When the temperature was 125^oC, the CO_2 permeability, CO_2 and N_2 flux as well as CO_2/N_2 selectivity reached 512 Barrer, 226×10^{-6} cm^3 (STP)/cm^2sec, 10×10^{-6} cm^3 (STP)/cm^2sec and 117, respectively (Figure 4.17**(a-c)**). This might be due to the fact that with increase in temperature at a constant water flow rate, the water retention throughout the membrane is reduced. This in turn affects the mobility and reaction rate of CO_2 with carriers resulting in the decrease in permeability. Permeation results are given in Table A2.10 (Appendix A2.5).

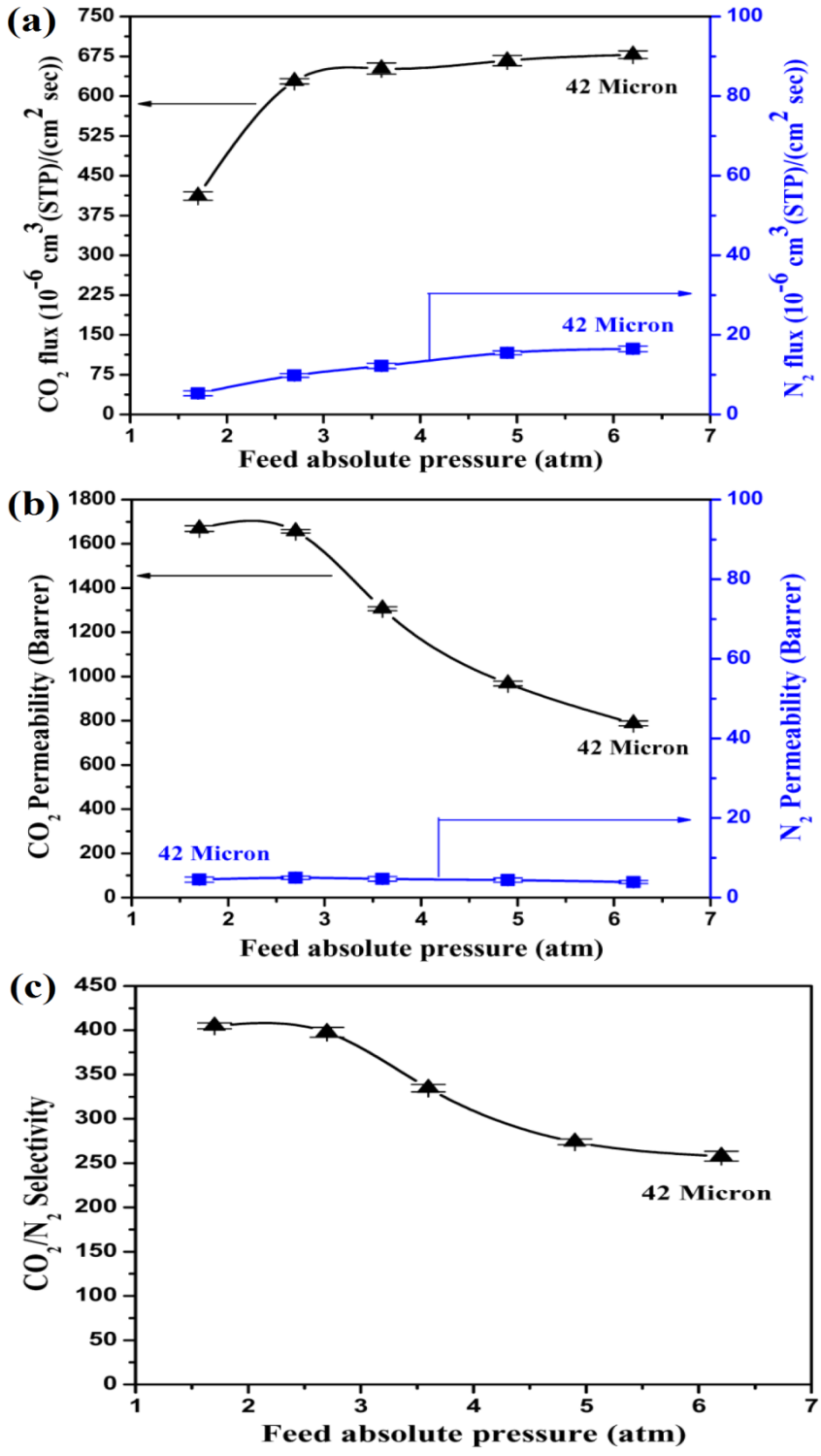

Figure 4.15 Effect of feed pressure on **(a)** CO_2 and N_2 flux. (▲) CO_2 flux; (■) N_2 flux, **(b)** CO_2 and N_2 permeability. (▲) CO_2 permeability (Barrer); (■) N_2 permeability (Barrer) and **(c)** CO_2/N_2 selectivity. (▲) CO_2/N_2 selectivity, at 100 ^oC with water rates = 0.03/0.04 ml/min (feed/sweep) for crosslinked-PVA-PVP membrane with (25 wt% PAA + 15 wt% PEHA)

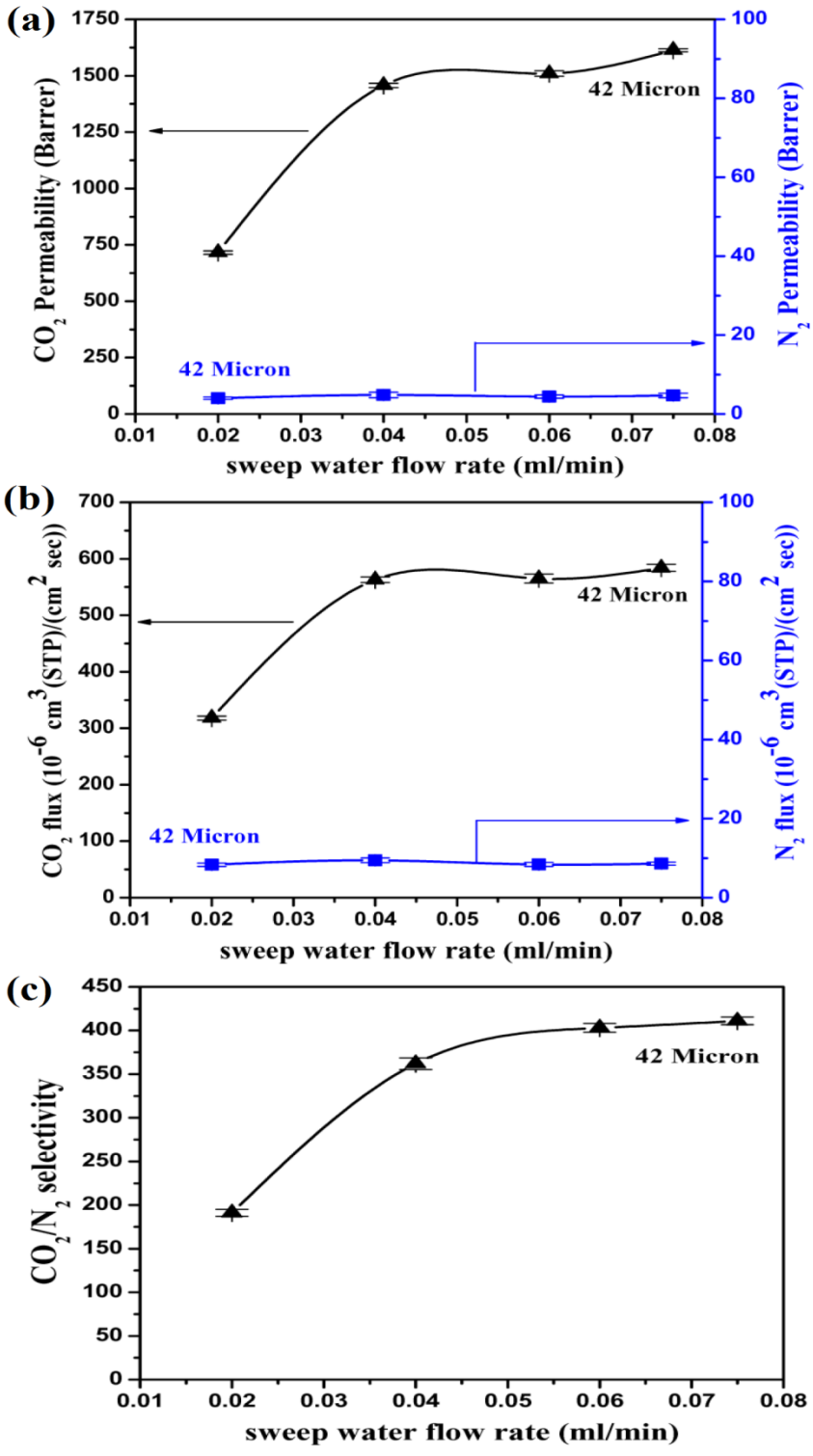

Figure 4.16 Effect of sweep side water flow rate on **(a)** CO_2 and N_2 permeability. (▲) CO_2 permeability (Barrer); (■) N_2 permeability (Barrer), **(b)** CO_2 and N_2 flux. (▲) CO_2 flux; (■) N_2 flux and **(c)** CO_2/N_2 selectivity. (▲) CO_2/N_2 selectivity, at 90 ^oC with feed absolute pressure = 2.7 atm, feed water flow rate = 0.03 ml/min for crosslinked-PVA-PVP membrane with (25 wt% PAA + 15 wt% PEHA)

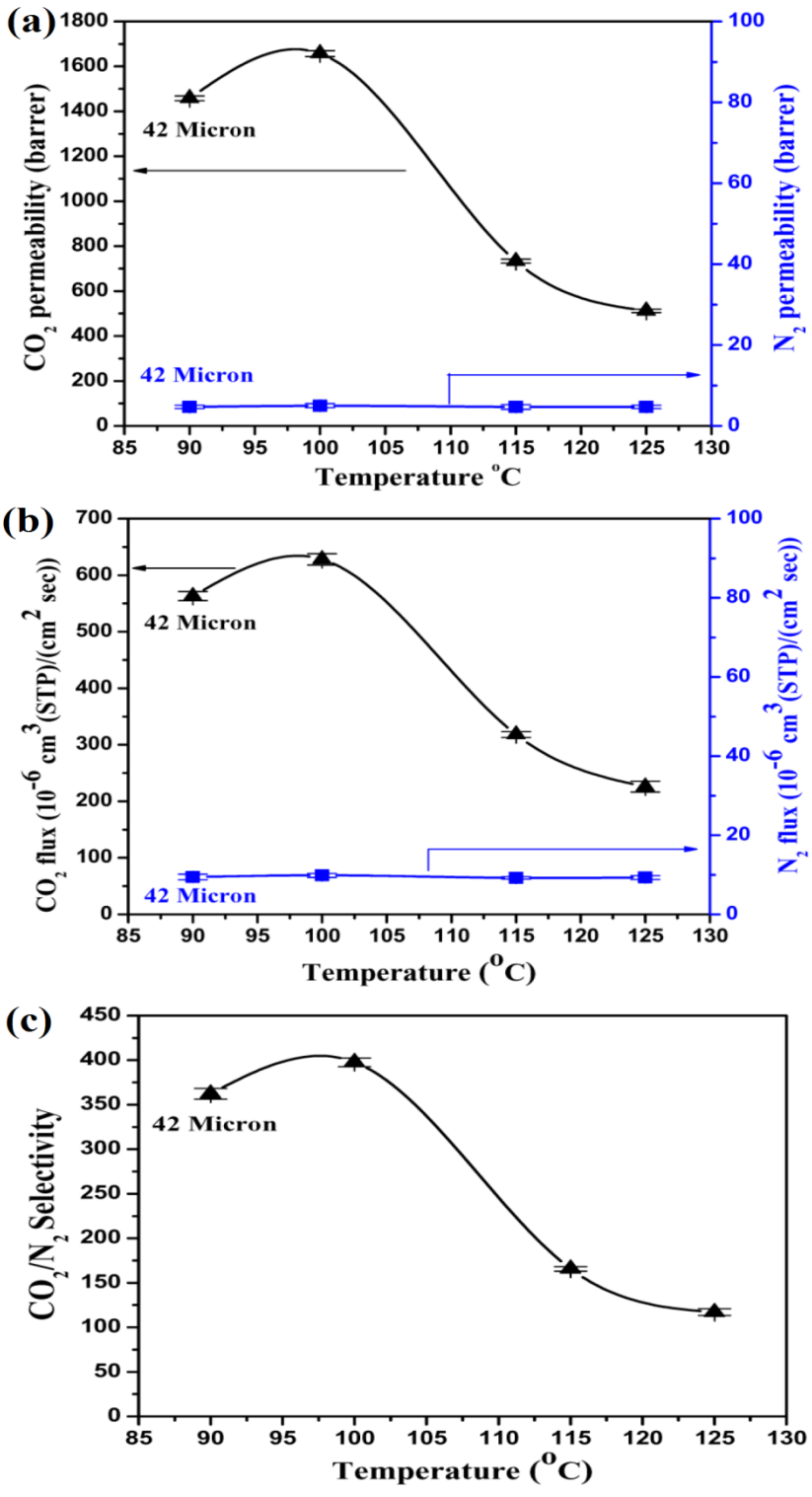

Figure 4.17 Effect of temperature on **(a)** CO_2 and N_2 permeability. (▲) CO_2 permeability (Barrer); (■) N_2 permeability (Barrer), **(b)** CO_2 and N_2 flux. (▲) CO_2 flux; (■) N_2 flux and **(c)** CO_2/N_2 selectivity. (▲) CO_2/N_2 selectivity, at 2.7 atm feed absolute pressure with water rates = 0.03/0.04 ml/min (feed/sweep) for crosslinked-PVA-PVP membrane with (25 wt% PAA + 15 wt% PEHA)

4.6 EFFECT OF PARAMETERS ON CO_2 SEPARATION BY PVA-PVP MEMBRANES CONTAINING PAA, AHPD AND THEIR BLENDS

Poly(allylamine) (PAA) was found to performed better than PEHA (Section 4.5.1). In this study, a new sterically hindered primary amine i.e. 2-amino-2-hydroxymethyl-1,3-propanediol (AHPD) and blends of AHPD and PAA were chosen as carriers. The structures of these amines are shown in Figure 2.2 and Figure 2.7. Membranes with three different compositions were synthesized as mentioned in Chapter 3 (Section 3.3.1.3).

4.6.1 Effect of Membrane Thickness and Composition Optimization

The effects of active layer thickness on CO_2 flux, N_2 flux, CO_2 permeance, N_2 permeance, CO_2 permeability, N_2 permeability and CO_2/N_2 selectivity were studied using crosslinked-PVA-PVP membrane containing single or blended amines. Three different compositions of amine among PAA and AHPD were chosen to find out the best separation performance. These are crosslinked-PVA-PVP membranes containing (40 wt% PAA), (15 wt% PAA + 25 wt% AHPD) and (25 wt% PAA + 15 wt% AHPD), respectively. Seven different crosslinked-PVA-PVP membranes with different active layer thickness containing single or blended amines along with separation performance are given in Table 4.7 and also shown in Figure 4.18**(a-b)** and Figure 4.19**(a-b)**. Feed side and sweep side absolute pressure was maintained constant at around 2.8 and 1.15 atm, respectively. Temperature was kept constant at 95^{o}C along with constant water flow rate at both sides (feed/sweep = 0.03/0.05 cm^3/min). Both feed gas (20% CO_2 balance N_2 on dry basis) and carrier gas (Ar) flow rates were maintained at 30 cm^3/min throughout the experiment.

It can be seen from Figure 4.18**(a)** that with increase in active layer thickness the CO_2 flux is decreased rapidly with a particular composition. As expected, with increase in active layer thickness, the total mass transfer resistance increases and hence the CO_2 flux decreases [14-16]. At constant active layer thickness of 45 micron for crosslinked-PVA-PVP membranes containing (40 wt% PAA), (15 wt% PAA + 25 wt% PEHA) and (25 wt% PAA + 15 wt% PEHA), the CO_2 flux was 515×10^{-6} cm^3 (STP)/cm^2sec, 560×10^{-6} cm^3 (STP)/cm^2sec and 651×10^{-6} cm^3 (STP)/cm^2sec, respectively. The detailed results are given in Table 4.8.

The CO_2 permeance decreases with increasing active layer thicknesses at a particular composition (Figure 4.18**(b)**). This trend is possibly because the mass flux through the membrane is inversely proportional to the membrane thickness. At constant active layer thickness of 45 micron for crosslinked-PVA-PVP membranes containing (40 wt% PAA), (15 wt% PAA + 25 wt% PEHA) and (25 wt% PAA + 15 wt% PEHA), the CO_2 permeance was 29.7 GPU, 36.4 GPU and 42 GPU, respectively. The detailed results are given in Table 4.8.

The CO_2 permeability and CO_2/N_2 selectivity is also increased with increase in active layer thicknesses at a particular composition (Figures 4.19**(a-b)**). At constant active layer thickness of 45 micron for crosslinked-PVA-PVP membranes containing (40 wt% PAA), (15 wt% PAA + 25 wt% PEHA) and (25 wt% PAA + 15 wt% PEHA), the CO_2 permeability was 1337 Barrer, 1640 Barrer, 1890 Barrer, respectively and CO_2/N_2 selectivity was 327, 360 and 437, respectively, (Figures 4.19**(a-b)** and Table 4.8).

As observed, 41.66 wt% PVA + 8.33 wt% PVP + 10 wt% KOH + 25 wt% PAA + 15 wt% AHPD with 60 mol% degree of crosslinking by HCHO membrane showed best separation performances among others. Hence, this membrane composition has been chosen for the detailed performance study (effect of pressure, temperature and sweep side water flow rate) via permeation measurement.

4.6.2 Effects of Feed Pressure

The effect of feed pressure on CO_2 and N_2 fluxes, CO_2 and N_2 permeabilities as well as CO_2/N_2 selectivity are shown in Figures 4.20**(a-c)**, respectively. The effects of feed pressure were studied at 100^oC using crosslinked thin-film composite membrane containing blended amines (25 wt% PAA + 15 wt% AHPD). The dense selective layer thickness of 44 micron on porous polysulfone membrane was used. Feed side absolute pressure was varied from 1.7 to 6.2 atm, while sweep side absolute pressure was maintained constant at around 1.15 atm. Both the feed gas (20% CO_2 balance N_2 on dry basis) and carrier gas (Ar) flow rates were maintained at 30 cm^3/min throughout the experiment. Feed side and sweep side water flow rates were kept constant at 0.03 and 0.04 cm^3/min, respectively.

As shown in Figures 4.20**(a-c)**, N_2 flux is increased linearly with increase in feed pressure in accordance with the solution-diffusion mechanism. On the other hand, the CO_2 flux is increased rapidly in the low pressure region and then remained almost constant at higher pressure. At 100^oC temperature when feed side absolute pressure increased from 1.7 to 6.2 atm along with constant water flow rate at both side (feed/sweep = 0.03/0.04

cm^3/min), the CO_2 flux increased from 431 × 10^{-6} cm^3 (STP)/cm^2sec to 682 × 10^{-6} cm^3 (STP)/cm^2sec (Figure 4.20**(a)**).

The CO_2 permeability and CO_2/N_2 selectivity were also decreased with increase in feed pressure (Figures 4.20**(b-c)**). As discussed before, the CO_2 permeability is high at low CO_2 partial pressure due to contribution of CO_2-amine reactions in presence of the abundance of free amine groups. At higher pressure, the availability of free amine groups becomes less and the CO_2 transport is dominated by solution-diffusion mechanism and hence permeation decreases with increase in feed pressure. However, with increase in the feed pressure N_2 permeability mostly does not change throughout the membrane and hence the CO_2/N_2 selectivity drops for both the membrane. Permeation results are given in Table A2.11 (Appendix A2.6).

4.6.3 Effects of Sweep Side Water Flow Rate

The effects of sweep side water flow rate (cm^3/min) on CO_2 flux, N_2 flux, CO_2 permeability, N_2 permeability and CO_2/N_2 selectivity were studied at 90^oC using crosslinked thin film composite membrane containing blended amines (25 wt% PAA + 15 wt% AHPD). Sweep side water flow rate was varied from 0.02 to 0.075 cm^3/min and feed side water flow rate was maintained constant throughout this experiment at 0.03 cm^3/min. Feed and sweep side absolute pressure was kept constant at 2.7 and 1.15 atm, respectively. Both feed gas (20% CO_2 balance N_2) and carrier gas (Ar) flow rates were kept constant at 30 cm^3/min, throughout the experiment. Figures 4.21**(a-c)** depicts the effect of sweep side water content on CO_2 and N_2 permeabilities, CO_2 and N_2 fluxes as well as CO_2/N_2 selectivity for the composite membrane, respectively. When the sweep

side water flow rate is increased from 0.02 to 0.075 cm^3/min, CO_2 permeability is increased from 950 to as high as 1896 Barrer (Figure 4.21**(a)**). At 0.075 cm^3/min sweep side water flow rate, the CO_2 and N_2 flux as well as CO_2/N_2 selectivity reached 645×10^{-6} cm^3 (STP)/cm^2sec, 8×10^{-6} cm^3 (STP)/cm^2sec and 477, respectively (Figures 4.21**(b-c)**). Permeation results are given in Table A2.12 (Appendix A2.6).

4.6.4 Effects of Temperature

The effects of temperature on CO_2 flux, N_2 flux, CO_2 permeability, N_2 permeability and CO_2/N_2 selectivity were investigated. The temperature was varied from 90°C to 125°C. Feed and sweep side absolute pressure was maintained constant at 2.7 and 1.15 atm, respectively. Also the feed and sweep side water flow rate were kept constant at 0.03 and 0.04 cm^3/min, respectively. Both the feed gas and carrier gas flow rates were maintained at 30 cm^3/min. The effect of temperature on CO_2 and N_2 permeabilities, CO_2 and N_2 fluxes as well as CO_2/N_2 selectivity is shown in Figure 4.22**(a-c)**, respectively. It has been observed that with increase in the temperature, the CO_2 permeability, CO_2 flux and CO_2/N_2 selectivity were decreased whereas N_2 flux remains almost constant. When the temperature was 125°C, the CO_2 permeability, CO_2 and N_2 flux as well as CO_2/N_2 selectivity reached 560 Barrer, 238×10^{-6} cm^3 (STP)/cm^2sec, 9×10^{-6} cm^3 (STP)/cm^2sec and 122, respectively (Figure 4.22**(a-c)**). Permeation results are given in Table A2.13 (Appendix A2.6).

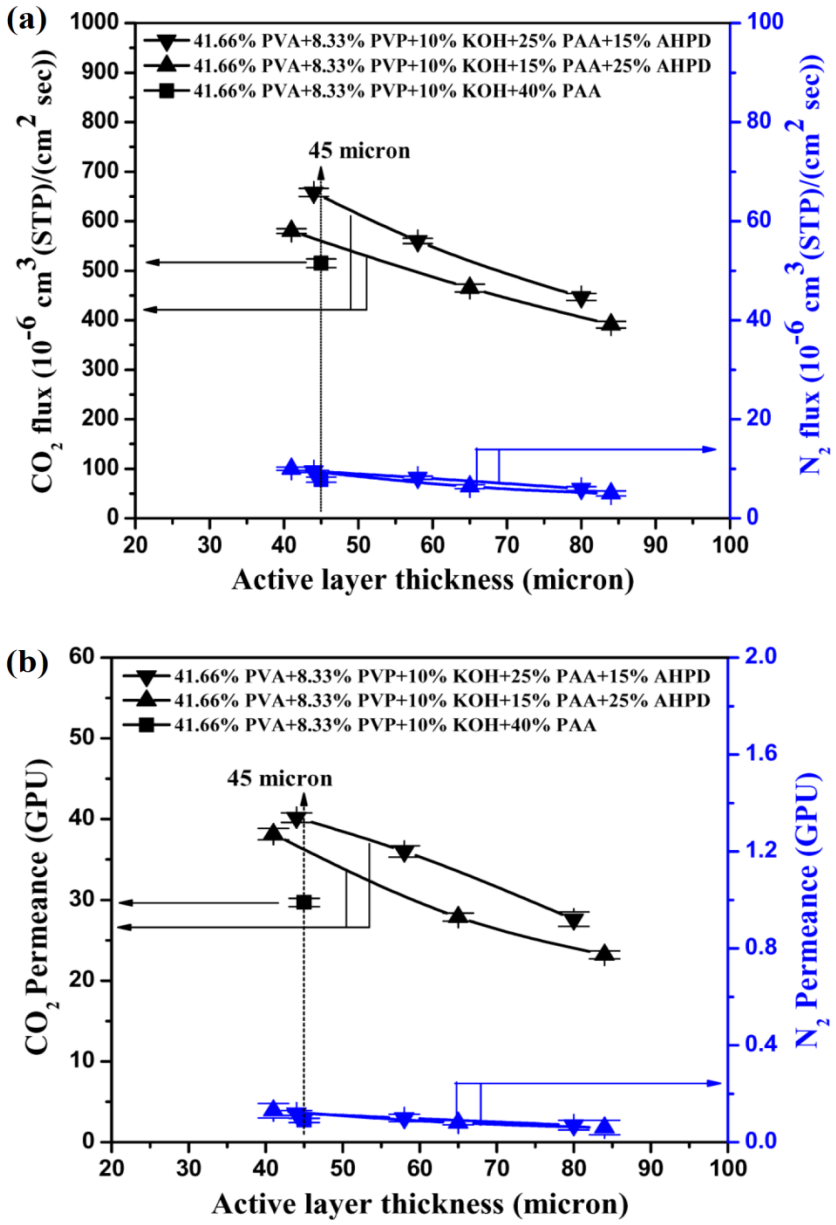

Figure 4.18 Effect of active layer thickness on **(a)** CO_2 and N_2 flux. (▼) (25 wt% PAA + 15 wt% AHPD); (▲) (15 wt% PAA + 25 wt% AHPD); (■) (40 wt% PAA), **(b)** CO_2 and N_2 permeance (GPU). (▼) (25 wt% PAA + 15 wt% AHPD); (▲) (15 wt% PAA + 25 wt% AHPD); (■) (40 wt% PAA)**,** at Temperature = 95 ^oC, Feed absolute pressure = 2.8 atm, sweep absolute pressure = 1.15 atm, sweep/feed water flow rate = 0.05/0.03 ml/min

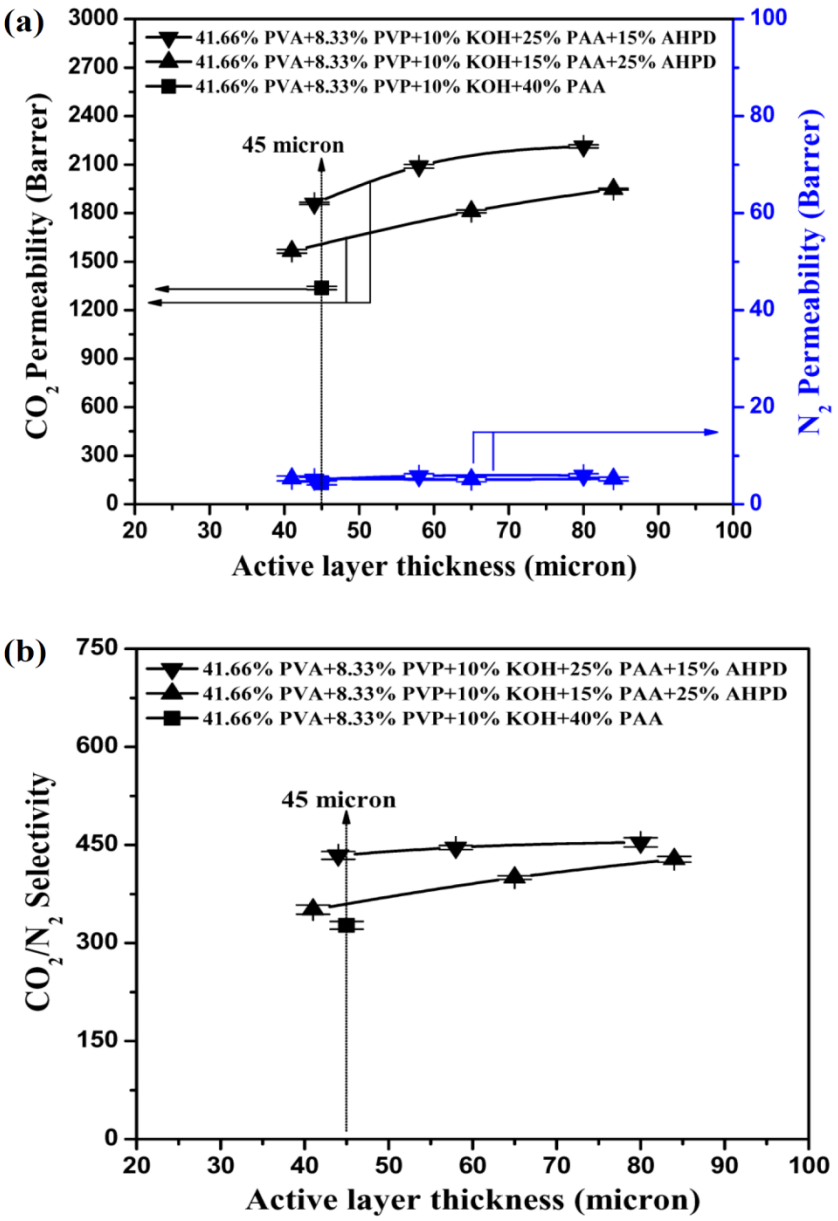

Figure 4.19 Effect of active layer thickness on **(a)** CO_2 and N_2 permeability (Barrer). (▼) (25 wt% PAA + 15 wt% AHPD); (▲) (15 wt% PAA + 25 wt% AHPD); (■) (40 wt% PAA) and **(b)** CO_2 and N_2 selectivity. (▼) (25 wt% PAA + 15 wt% AHPD); (▲) (15 wt% PAA + 25 wt% AHPD); (■) (40 wt% PAA), at Temperature = 95 ^oC, Feed absolute pressure = 2.8 atm, sweep absolute pressure = 1.15 atm, sweep/feed water flow rate = 0.05/0.03 ml/min

Table 4.7 CO_2 transport property of different active layer thickness membranes of different compositions containing PAA and AHPD at constant physical condition (Temperature = 95 ^oC, Feed absolute pressure = 2.8 atm, sweep absolute pressure = 1.15 atm, sweep/feed water flow rate = 0.05/0.03 ml/min.)

Active layer composition (wt%)	Active layer Thickness (micron)	CO_2 flux 10^{-6} $cm^3(STP)/cm^2$ sec	CO_2 Permeability (Barrer)	CO_2 Permeance (GPU)	CO_2/N_2 Selectivity
M8	44	658	1860	42.2	434
	58	560	2090	36	446
	80	447	2213	27.6	454
M9	43	579	1564	36.3	351
	65	465	1811	27.8	400
	84	391	1948	23.1	428
M7	45	515	1336	29.6	327

M8 : 41.66% PVA+8.33% PVP+10% KOH+25% PAA+15% AHPD

M9 : 41.66% PVA+8.33% PVP+10% KOH+15% PAA+25% AHPD

M7 : 41.66% PVA+8.33% PVP+10% KOH+40% PAA

Table 4.8 CO_2 transport property of constant active layer thickness, around 45 micron membranes of different compositions containing PAA and AHPD at constant physical condition (Temperature = 95 ^oC, Feed absolute pressure = 2.8 atm, sweep absolute pressure = 1.15 atm, sweep/feed water flow rate = 0.05/0.03 ml/min.)

Active layer Thickness (micron)	Active layer composition (wt%)	CO_2 flux 10^{-6} $cm^3(STP)/cm^2$ sec	CO_2 Permeability (Barrer)	CO_2 Permeance (GPU)	CO_2/N_2 Selectivity
45	M8	651	1890	42	437
45	M9	560	1640	36.4	360
45	M7	515	1337	29.7	327

M8 : 41.66% PVA+8.33% PVP+10% KOH+25% PAA+15% AHPD

M9 : 41.66% PVA+8.33% PVP+10% KOH+15% PAA+25% AHPD

M7 : 41.66% PVA+8.33% PVP+10% KOH+40% PAA

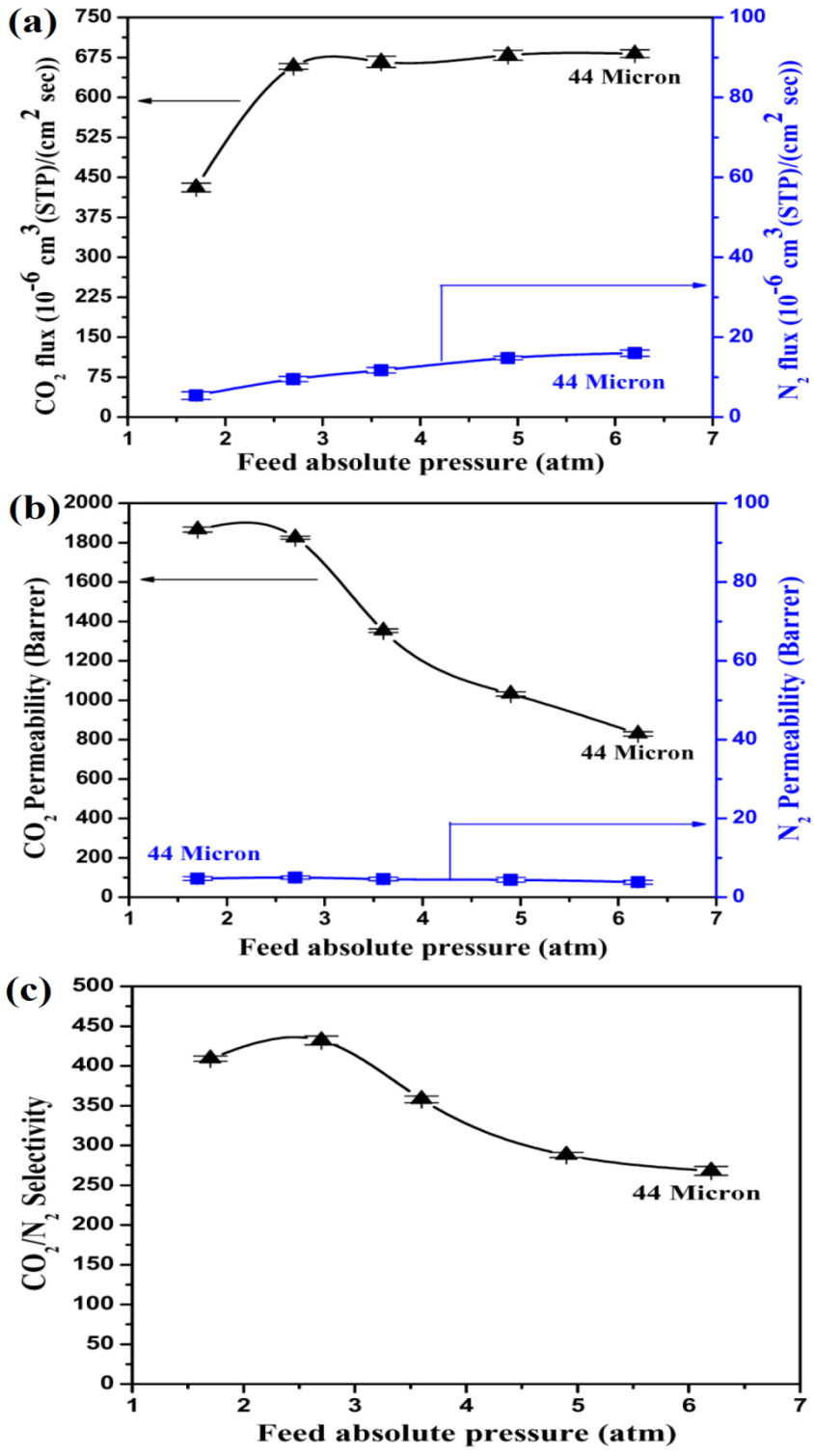

Figure 4.20 Effect of feed pressure on **(a)** CO_2 and N_2 flux. (▲) CO_2 flux; (■) N_2 flux, **(b)** CO_2 and N_2 permeability. (▲) CO_2 permeability (Barrer); (■) N_2 permeability (Barrer) and **(c)** CO_2/N_2 selectivity. (▲) CO_2/N_2 selectivity, at 100 ^oC with water rates = 0.03/0.04 ml/min (feed/sweep) for crosslinked-PVA-PVP membrane with (25 wt% PAA + 15 wt% AHPD)

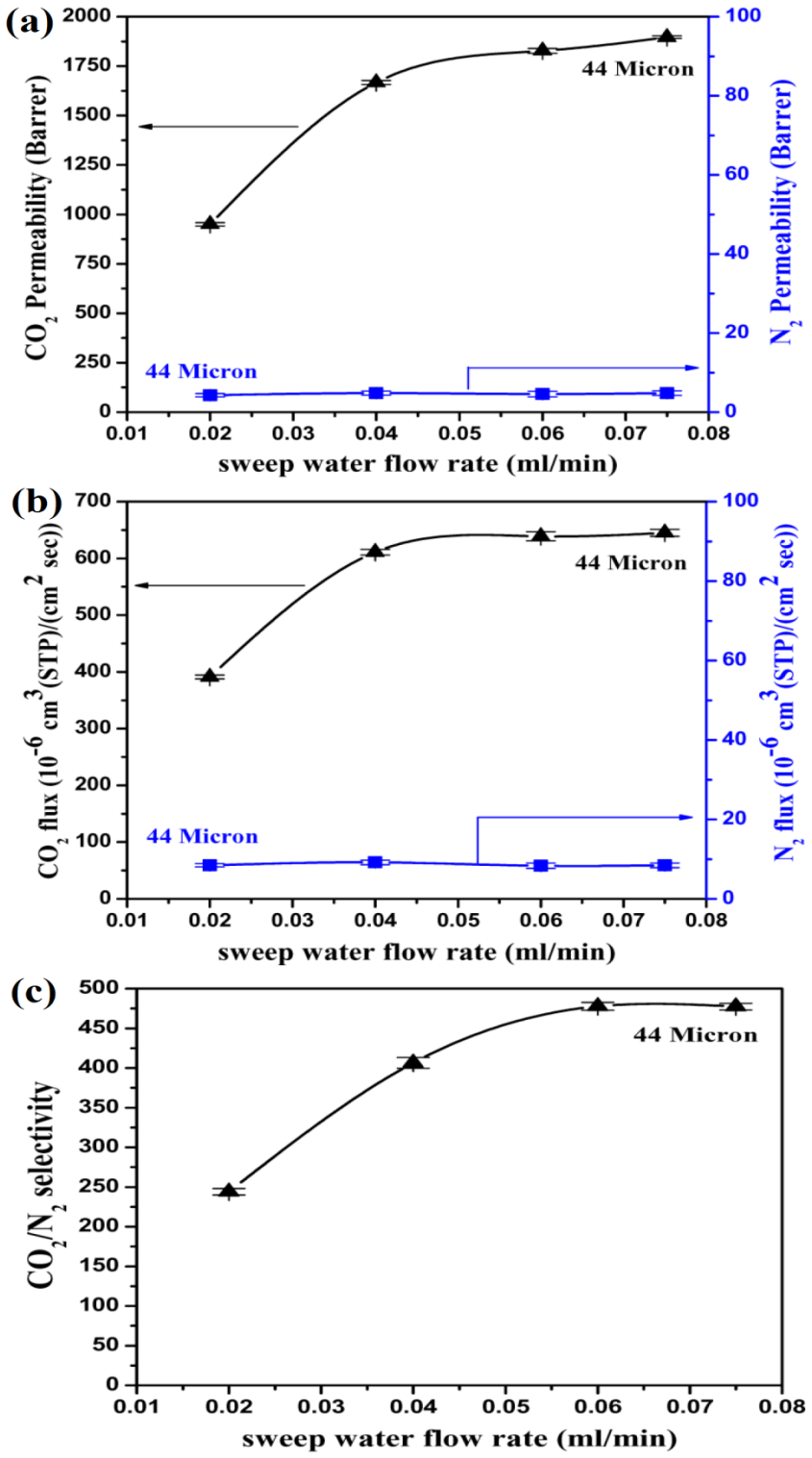

Figure 4.21 Effect of sweep side water flow rate on **(a)** CO_2 and N_2 permeability. (▲) CO_2 permeability (Barrer); (■) N_2 permeability (Barrer), **(b)** CO_2 and N_2 flux. (▲) CO_2 flux; (■) N_2 flux and **(c)** CO_2/N_2 selectivity. (▲) CO_2/N_2 selectivity, at 90 °C with feed absolute pressure = 2.7 atm, feed water flow rate = 0.03 ml/min for crosslinked-PVA-PVP membrane with (25 wt% PAA + 15 wt% AHPD)

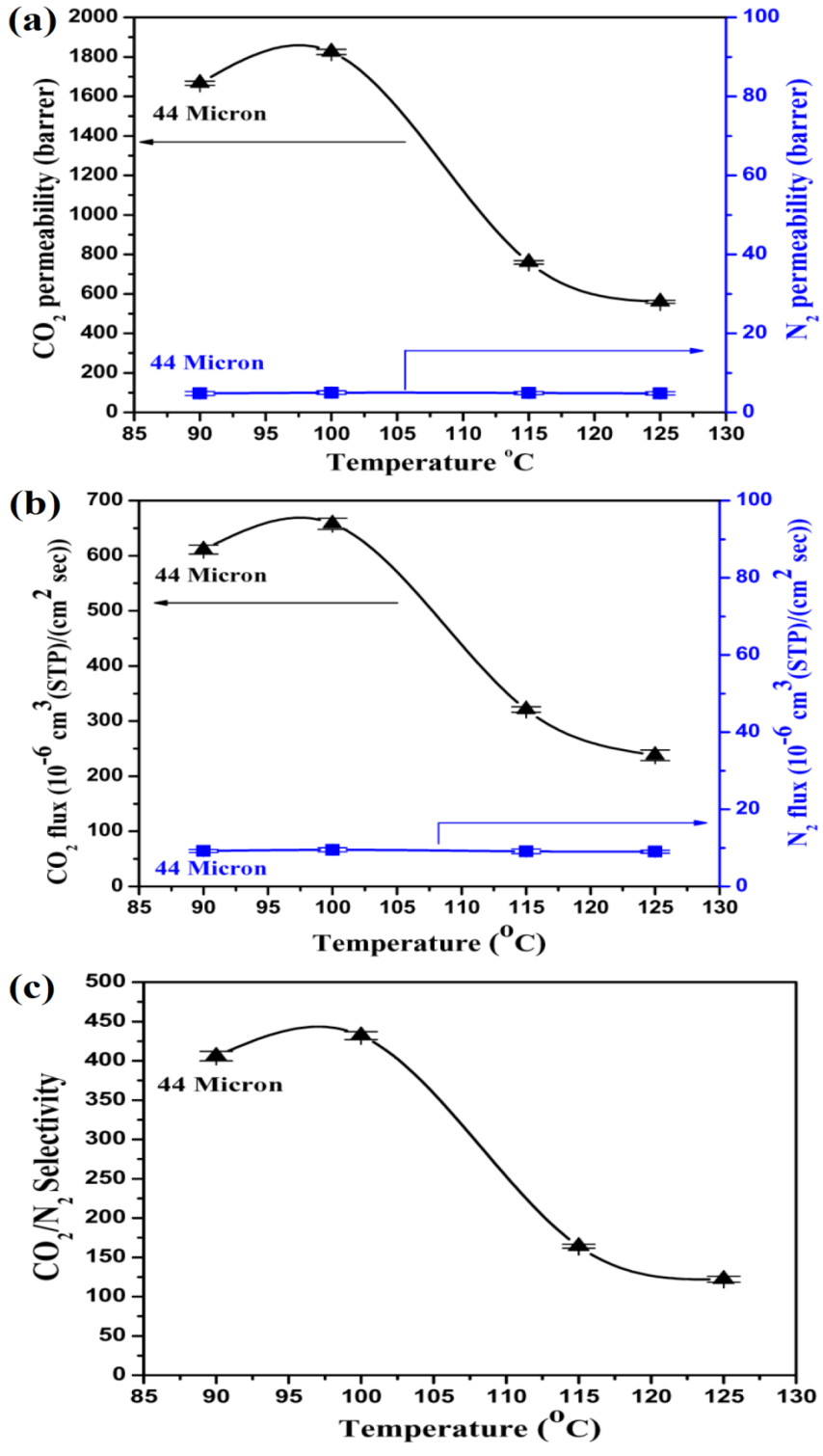

Figure 4.22 Effect of temperature on **(a)** CO_2 and N_2 permeability. (▲) CO_2 permeability (Barrer); (■) N_2 permeability (Barrer), **(b)** CO_2 and N_2 flux. (▲) CO_2 flux; (■) N_2 flux and **(c)** CO_2/N_2 selectivity. (▲) CO_2/N_2 selectivity, at 2.7 atm feed absolute pressure with water rates = 0.03/0.04 ml/min (feed/sweep) for crosslinked-PVA-PVP membrane with (25 wt% PAA + 15 wt% AHPD)

To find out the best composition among all the different blended amines compositions discussed above, we took the best composition of each set of combinations and compared among them. Five different amines and their blends were used as carriers. The compositions of all sets of membranes are mentioned in Chapter 3 (Table 3.1) and also the performance of those membranes are discussed above. It has been observed that crosslinked-PVA-PVP with (15 wt% PEI + 25 wt% TEPA), crosslinked-PVA-PVP with (15 wt% PEI + 25 wt% PEHA), crosslinked-PVA-PVP with (25 wt% PAA + 15 wt% PEHA) and crosslinked-PVA-PVP with (25 wt% PAA + 15 wt% AHPD) were the best compositions of set-1, set-2, set-3 and set-4, respectively.

The constant active layer thicknesses for each composition along with separation performance are given in Table 4.9 and also shown in Figure 4.23**(a-b)** and Figure 4.24**(a-b)**. At constant active layer thickness of 50 micron for crosslinked-PVA-PVP doped with (25 wt% PAA + 15 wt% AHPD), (25 wt% PAA + 15 wt% PEHA), (15 wt% PEI + 25 wt% PEHA) and (15 wt% PEI + 25 wt% TEPA) membranes, the CO_2 flux was 618×10^{-6} cm^3 (STP)/cm^2sec, 573×10^{-6} cm^3 (STP)/cm^2sec, 508×10^{-6} cm^3 (STP)/cm^2sec and 450×10^{-6} cm^3 (STP)/cm^2sec, respectively, (Table 4.9).

At constant active layer thickness of 50 micron for crosslinked-PVA-PVP doped with (25 wt% PAA + 15 wt% AHPD), (25 wt% PAA + 15 wt% PEHA), (15 wt% PEI + 25 wt% PEHA) and (15 wt% PEI + 25 wt% TEPA) membranes, the CO_2 permeability was 1971 Barrer, 1803 Barrer, 1506 Barrer and 1391 Barrer, respectively and CO_2/N_2 selectivity was 439, 410, 349 and 218, respectively, (Figures 4.24**(a-b)** and Table 4.9).

As observed, 41.66 wt% PVA + 8.33 wt% PVP + 10 wt% KOH + 25 wt% PAA + 15 wt% AHPD with 60 mol% degree of crosslinking by HCHO membrane showed best separation performances among others. Hence, this membrane has been chosen for the comparison with the crosslinked-PVA without carrier membrane. The detailed Gas Chromatography results of all membranes at different conditions are shown in Figure A2.3 to Figure A2.78 (Appendix A2.7 to A2.14).

4.7 COMPARISON BETWEEN CROSSLINKED PVA MEMBRANE WITH AND WITHOUT CARRIERS

Figures 4.25**(a-c)** shows the comparison of transport property between crosslinked-PVA-PVP membranes containing 25 wt% PAA and 15 wt% AHPD and crosslinked-PVA membrane without carrier against feed pressure. It has been clearly observed from the figure that with increase in the feed pressure, CO_2 flux is linearly increased for crosslinked-PVA without carrier membrane which attributed to the solution-diffusion mechanism. The CO_2 flux increased about 13 times due to addition of the amine carrier into the membrane compared to the crosslinked-PVA membrane without carrier. The CO_2 permeability and CO_2/N_2 selectivity at different feed pressures were changed marginally for the membrane without carrier (Figures 4.25**(b-c)**).

Figures 4.26**(a-c)** shows the comparison of transport properties through crosslinked-PVA-PVP membrane blended with 25 wt% PAA and 15 wt% AHPD and crosslinked-PVA membrane without carrier against sweep water flow rate. It has been illustrated from the figure that the transport properties of membrane without carrier remains almost

constant with increasing in the sweep water flow rate whereas these properties were much higher in case of blended amines membrane due to presence of carrier.

Figures 4.27**(a-c)** shows the comparison of transport properties between crosslinked-PVA-PVP membrane blended with 25 wt% PAA and 15 wt% AHPD and crosslinked-PVA membrane without carrier against temperature. As expected, the transport properties of blended amines membrane are significantly higher compared to membrane without carrier.

Permeation experimental data was compared with other polymeric membranes by famous upper bound relationship proposed by Robeson [23]. The data of CO_2 permeability (Barrer) and CO_2/N_2 selectivity was calculated at a temperature of around 100^oC against 2.7 atm feed absolute pressure with 0.03/0.04 ml/min feed/sweep side water flow rate. CO_2 permeability and CO_2/N_2 selectivity data of the other polymers were taken from Robeson's work [17, 23 and 24] and the upper bound relationship shown in Figure 4.28 and Table 4.10. The crosslinked PVA with blended amines (15 wt% PEI + 25 wt% AHPD) composite membrane was found to have the highest CO_2 permeability along with highest CO_2/N_2 selectivity which is higher than the upper bound (Figure 4.28).

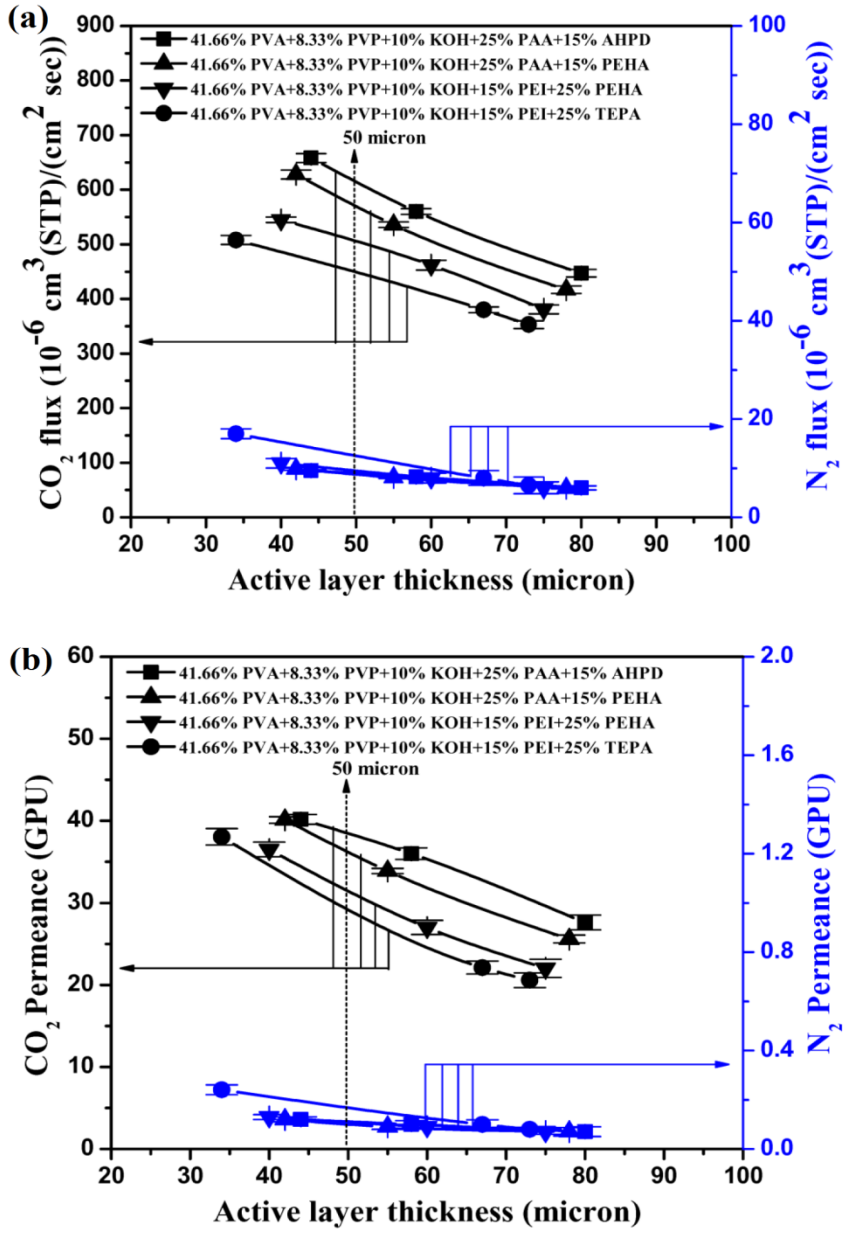

Figure 4.23 Effect of active layer thickness on **(a)** CO_2 and N_2 flux. (■) (25 wt% PAA + 15 wt% AHPD); (▲) (25 wt% PAA + 15 wt% PEHA); (▼) (15 wt% PEI + 25 wt% PEHA); (●) (15 wt% PEI + 25 wt% TEPA), **(b)** CO_2 and N_2 permeance (GPU). (■) (25 wt% PAA + 15 wt% AHPD); (▲) (25 wt% PAA + 15 wt% PEHA); (▼) (15 wt% PEI + 25 wt% PEHA); (●) (15 wt% PEI + 25 wt% TEPA), at Temperature = 95 ^{o}C, Feed absolute pressure = 2.8 atm, sweep absolute pressure = 1.15 atm, sweep/feed water flow rate = 0.05/0.03 ml/min

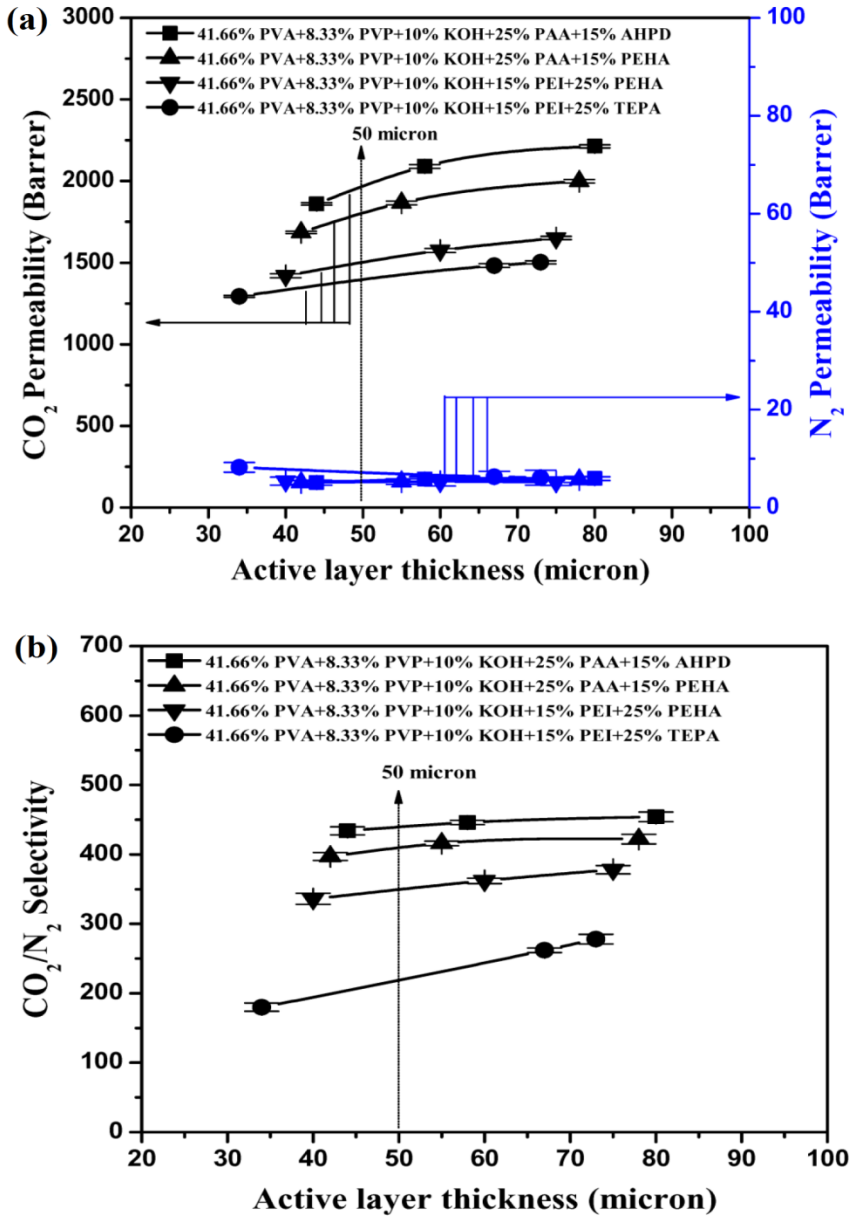

Figure 4.24 Effect of active layer thickness on **(a)** CO_2 and N_2 permeability (Barrer). (■) (25 wt% PAA + 15 wt% AHPD); (▲) (25 wt% PAA + 15 wt% PEHA); (▼) (15 wt% PEI + 25 wt% PEHA); (●) (15 wt% PEI + 25 wt% TEPA) and **(b)** CO_2/N_2 selectivity. (■) (25 wt% PAA + 15 wt% AHPD); (▲) (25 wt% PAA + 15 wt% PEHA); (▼) (15 wt% PEI + 25 wt% PEHA); (●) (15 wt% PEI + 25 wt% TEPA), at Temperature = 95 ^{o}C, Feed absolute pressure = 2.8 atm, sweep absolute pressure = 1.15 atm, sweep/feed water flow rate = 0.05/0.03 ml/min

Table 4.9 CO_2 transport property of constant active layer thickness, around 50 micron membranes of different compositions containing PEI, TEPA, PEHA, PAA and AHPD at constant physical condition (Temperature = 95 ^oC, Feed absolute pressure = 2.8 atm, sweep absolute pressure = 1.15 atm, sweep/feed water flow rate = 0.05/0.03 ml/min.)

Active layer Thickness (micron)	Active layer composition (wt%)	CO_2 flux 10^{-6} $cm^3(STP)/cm^2$ sec	CO_2 Permeability (Barrer)	CO_2 Permeance (GPU)	CO_2/N_2 Selectivity
50	M8	618	1971	39.4	439
50	M5	573	1803	36	410
50	M4	508	1506	30	349
50	M1	450	1391	27.8	218

M8 : 41.66% PVA+8.33% PVP+10% KOH+25% PAA+15% AHPD

M5 : 41.66% PVA+8.33% PVP+10% KOH+25% PAA+15% PEHA

M4 : 41.66% PVA+8.33% PVP+10% KOH+15% PEI+25% PEHA

M1 : 41.66% PVA+8.33% PVP+10% KOH+15% PEI+25% TEPA

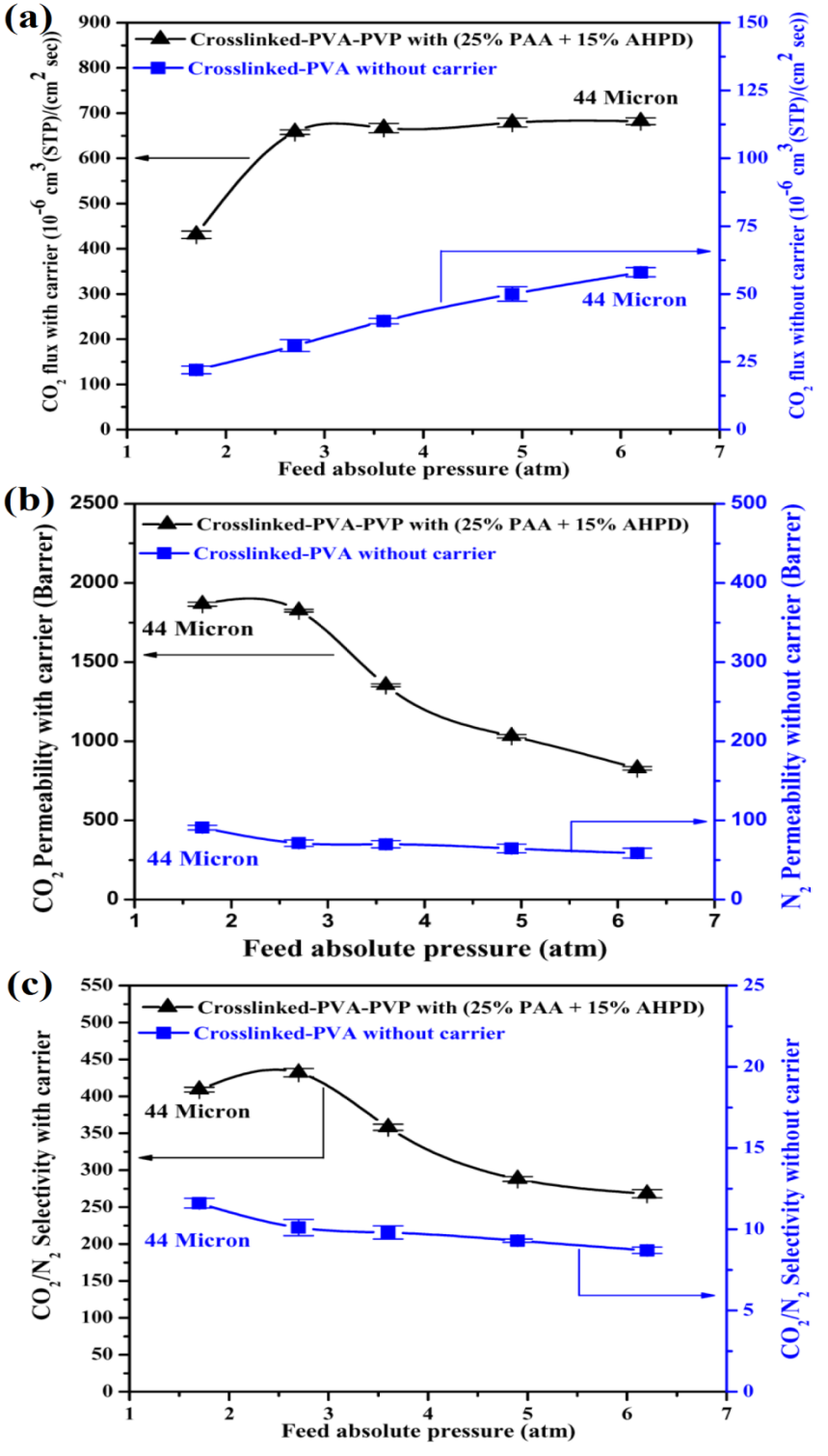

Figure 4.25 Effect of feed pressure on **(a)** CO_2 flux. (▲) crosslinked-PVA-PVP with (25% PAA + 15% AHPD); (■) crosslinked-PVA without carrier membrane, **(b)** CO_2 permeability (Barrer). (▲) crosslinked-PVA-PVP with (25% PAA + 15% AHPD); (■) crosslinked-PVA without carrier membrane and **(c)** CO_2/N_2 selectivity. (▲) crosslinked-PVA-PVP with (25% PAA + 15% AHPD); (■) crosslinked-PVA without carrier membrane, at 100 °C with water rates = 0.03/0.04 ml/min (feed/sweep)

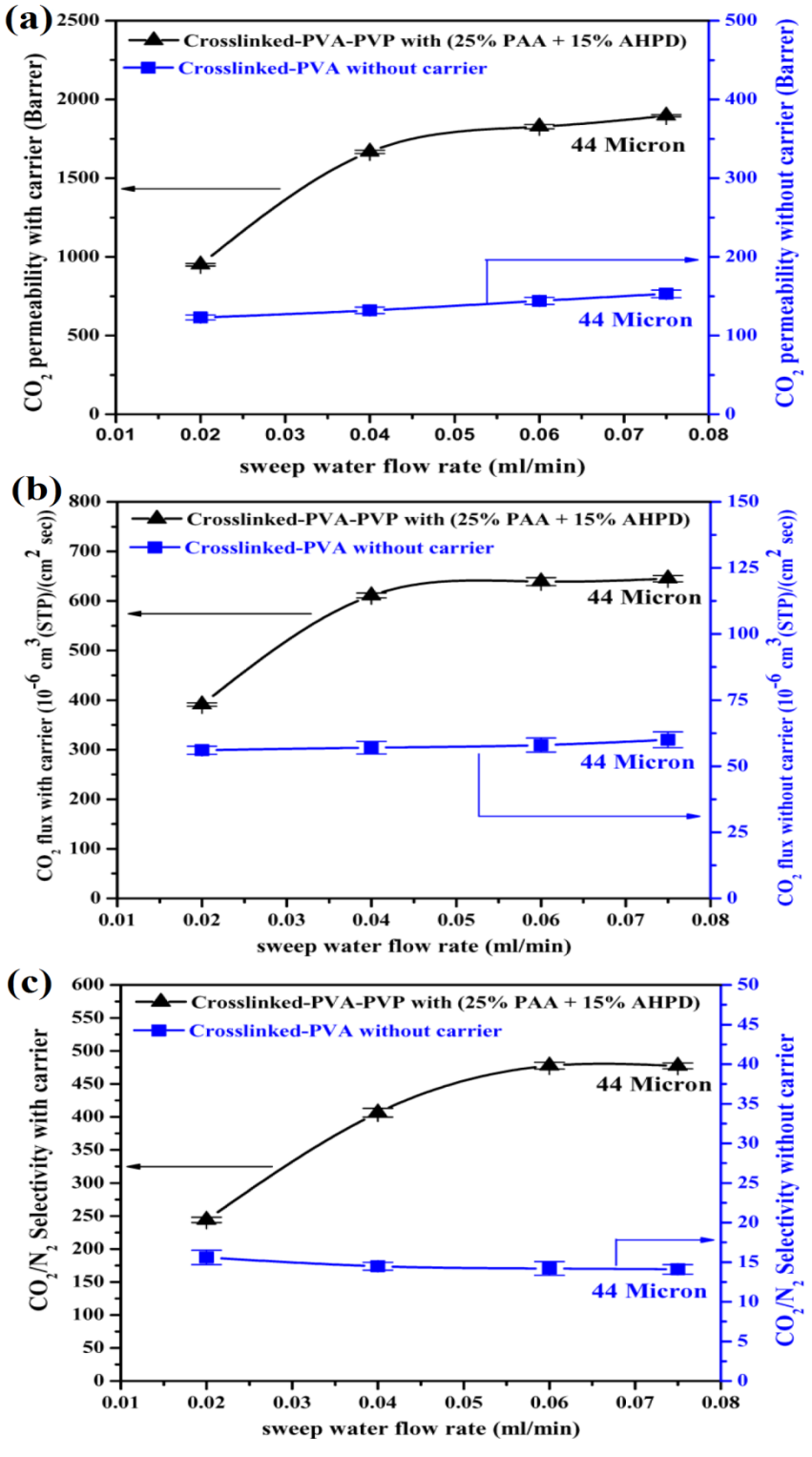

Figure 4.26 Effect of sweep side water flow rate on **(a)** CO_2 permeability (Barrer). (▲) crosslinked-PVA-PVP with (25% PAA + 15% AHPD); (■) crosslinked-PVA without carrier membrane, **(b)** CO_2 flux. (▲) crosslinked-PVA-PVP with (25% PAA + 15% AHPD); (■) crosslinked-PVA without carrier membrane and **(c)** CO_2/N_2 selectivity. (▲) crosslinked-PVA-PVP with (25% PAA + 15% AHPD); (■) crosslinked-PVA without carrier membrane, at 90 °C temperature with feed absolute pressure = 2.7 atm, feed water flow rate = 0.03 ml/min

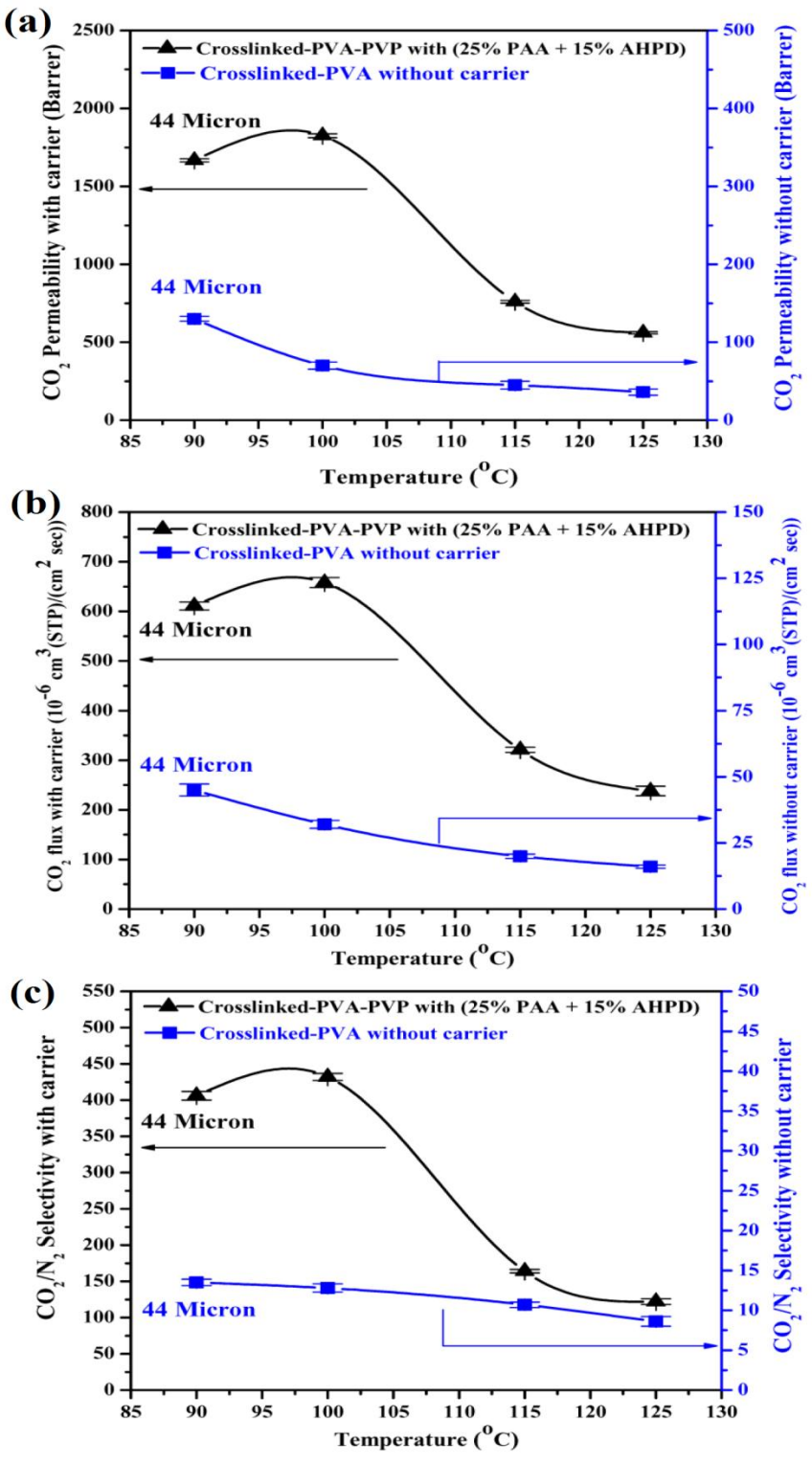

Figure 4.27 Effect of temperature on **(a)** CO_2 permeability (Barrer). (▲) crosslinked-PVA-PVP with (25% PAA + 15% AHPD); (■) crosslinked-PVA without carrier membrane, **(b)** CO_2 flux. (▲) crosslinked-PVA-PVP with (25% PAA + 15% AHPD); (■) crosslinked-PVA without carrier membrane and **(c)** CO_2/N_2 selectivity. (▲) crosslinked-PVA-PVP with (25% PAA + 15% AHPD); (■) crosslinked-PVA without carrier membrane, at 2.7 atm feed absolute pressure with water rates = 0.03/0.04 ml/min (feed/sweep)

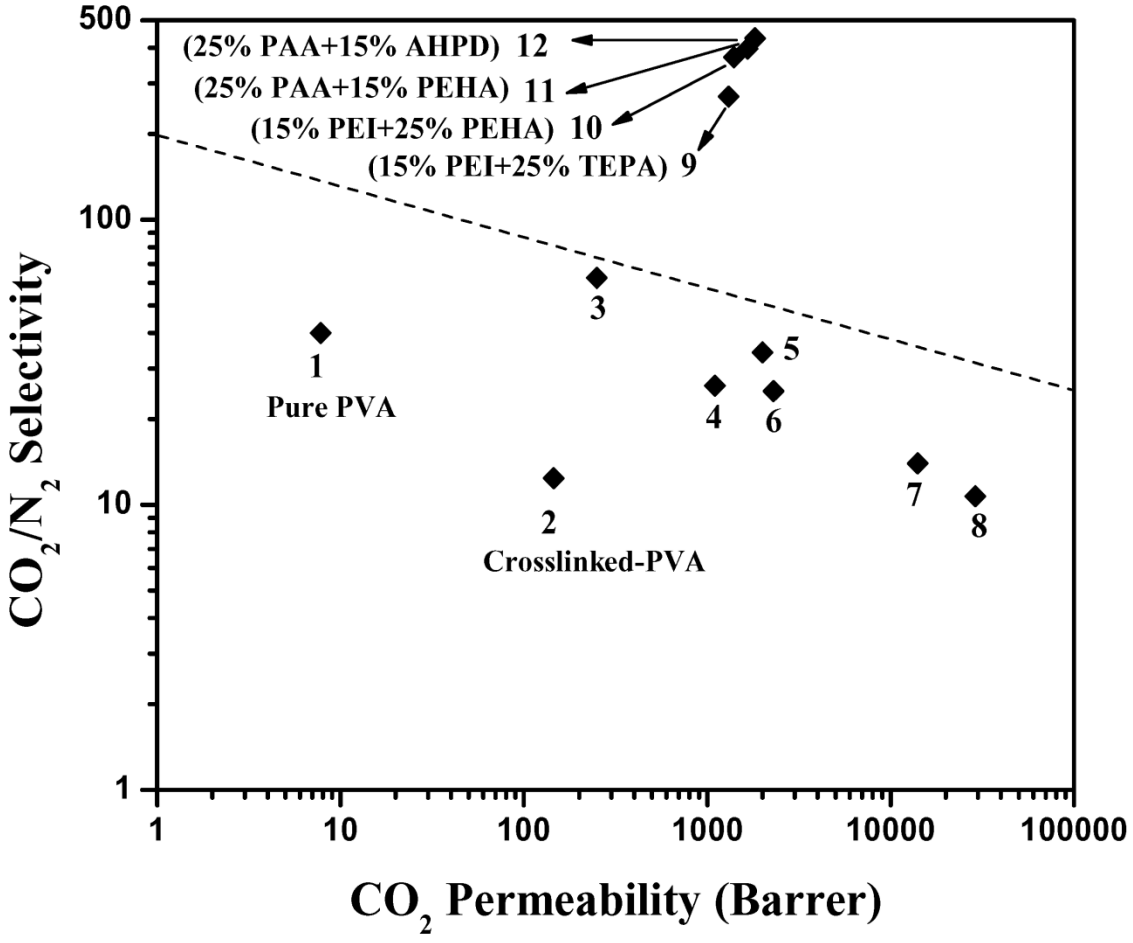

Figure 4.28 The upper bound relationship of CO_2 permeability and CO_2/N_2 selectivity of different polymeric membranes

Table 4.10 CO_2 permeability and CO_2/N_2 selectivity of different polymers

Compositions in Figure 4.28	Polymer	CO_2 Permeability (Barrer)	CO_2/N_2 selectivity	Reference
1	Pure PVA without carrier	7.8	40	[24]
2	Crosslinked-PVA without carrier	145	12.4	
3	Poly[bis(2-(2-methoxyethoxy)ethoxy) phosphazene]	250	62.5	[23]
4	PIM-7	1100	26.2	[23]
5	Modified poly(dimethylsiloxane)	2000	34.2	[23]
6	PIM-1	2300	25	[23]
7	Poly(trimethylgermylpropyne)	14000	14	[23]
8	Poly(trimethylsilylpropyne)	29000	10.7	[23]
9	41.66% PVA+8.33% PVP+10% KOH+15% PEI+25% TEPA+60 mol% HCHO	1307	270	
10	41.66% PVA+8.33% PVP+10% KOH+15% PEI+25% PEHA+60 mol% HCHO	1400	371	
11	41.66% PVA+8.33% PVP+10% KOH+25% PAA+15% PEHA+60 mol% HCHO	1657	398	
12	41.66% PVA+8.33% PVP+10% KOH+25% PAA+15% AHPD+60 mol% HCHO	1826	432	

4.8 SUMMARY

Separation of CO_2 through novel crosslinked-PVA-PVP based membranes containing different amine and their blends has been presented in this research. There are four sets of different amine based membranes have been synthesized. These are discussed in Chapter 3 (Section 3.3.1.3). It has been observed from the experiment that composition of the membrane plays a significant role in gas permeation. Along with change in amine composition and operating conditions the CO_2 separation performance changes. Membranes containing blended amines showed better performances compered to single amine. Crosslinked-PVA-PVP membrane containing 25 wt% PAA and 15 wt% AHPD showed best separation performances over others. The highest CO_2/N_2 selectivity and CO_2 permeability were obtained at 1.3 atm absolute pressure difference (ΔP), 100^oC temperature and 0.03/0.04 ml/min feed/sweep water flow rate.

The effects of active layer thickness, feed pressure, sweep side water flow rate and temperature were studied and also compared with crosslinked-PVA membrane without carrier. Drastic improvement was observed in case of amine carrier doped membrane compared to non-carrier membrane. The significant increase of the CO_2 flux was observed with increase in the feed pressure at low pressure region. With increase in sweep side water flow rate the permeability as well as CO_2/N_2 selectivity increased significantly. This suggests that water played an important role in the facilitated transport of CO_2. As the temperature was increased from 90^oC to 100^oC, the CO_2 flux, CO_2 permeability and CO_2/N_2 selectivity were increased. However beyond 100^oC, all the CO_2

transport properties were decreased, which was presumably due to the reduction of water retention in the membrane as the temperature is increased.

REFERENCES

[1]. V. Stannett, The transport of gases in synthetic polymeric membranes-an historic perspective, J. Membr. Sci. 3 (1978) 97.

[2]. T. C. Merkel, H. Lin, X. Wei and R. Baker, Power plant post-combustion carbon dioxide capture: An opportunity for membranes, J. Membr. Sci. 359 (2010) 126-139.

[3]. Y. Zhao and W. S. W. Ho, Steric hindrance effect on amine demonstrated in solid polymer membranes for CO_2 transport, J. Membr. Sci. Volumes 415-416 (2012) 132-138.

[4]. W. J. Koros and R. T. Chern, Separation of gaseous mixtures using polymer membranes, Handbook of Separation Process Technology, edit. R. W. Rousseau, (1987).

[5]. G. J. Francisco, A. Chakma and X. Feng, Membranes comprising of alkanolamines incorporated into poly(vinyl alcohol) matrix for CO_2/N_2 separation, J. Membr. Sci. 303 (2007) 54-63.

[6]. M. J. Kim, Y. I. Park, K. H. O. Youm and K. H. O. Lee, Facilitated transport of CO_2 through ethylenediamine-fixed cation-exchange polysaccharide membranes, J. Membr. Sci. 245 (2004) 79-86.

[7]. H. Matsuyama, A. Terada, T. Nakagawara, Y. Kitamura and M. Teramoto, Facilitated transport of CO_2 through polyethylenimine/poly(vinyl alcohol) blend membrane, J. Membr. Sci. 163 (1999) 221-227.

[8]. J. Shen, J. Qiu, L. Wu and C. Gao, Facilitated transport of carbon dioxide through poly (2-N,N-dimethyl aminoethyl methacrylate-co-acrylic acid sodium) membrane, Sep. Purif. Technol. 51 (2006) 345-351.

[9]. J. Shen, L. Wu, D. Wang and C. Gao, Sorption behavior and separation performance of novel facilitated transport membranes for CO_2/CH_4 mixtures, Desalination. 223 (2008) 425-437.

[10]. W. J. Ward, W. R. Browal and R. M. Salemme, Ultrathin silicone/polycarbonate membranes for gas separation processes, J. Membr. Sci. 1 (1976) 99-108.

[11]. G. M. Wu, S. J. Lin and C. C. Yang, Preparation and characterization of PVA/PAA membranes for solid polymer electrolytes, J. Membr. Sci. 275 (2006) 127-133.

[12]. R. Xing and W. S. W. Ho, Synthesis and characterization of crosslinked polyvinylalcohol/polyethyleneglycol blend membranes for CO_2/CH_4 separation, J. Taiw. Inst. Che. Eng. 40 (2009) 654-662.

[13]. R. Yegani, H. Hirozawa, M. Teramoto, H. Himei, O. Okada, T. Takigawa, N. Ohmura, N. Matsumiya and H. Matsuyama, Selective separation of CO_2 by using novel facilitated transport membrane at elevated temperatures and pressures, J. Membr. Sci. 291 (2007) 157-164.

[14]. W. S. Ho and D. C. Dalrymple, Facilitated transport of olefins in Ag^+ -containing polymer membranes, J. Membr. Sci. 91 (1994) 13-25.

[15]. H. Matsuyama, K. Matsui, Y. Kitamura, T. Maki and M. Teramoto, Effects of membrane thickness and membrane preparation condition on facilitated transport of CO_2 through ionomer membrane, Sep. Purif. Technol. 17 (1999) 235-241.

[16]. J. H. Kim, S. M. Park, J. Won and Y. S. Kang, Dependence of facilitated olefin transport on the thickness of silver polymer electrolyte membranes, J. Membr. Sci. 236 (2004) 209-212.

[17]. A. Mondal and B. Mandal, Synthesis and characterization of crosslinked poly(vinyl alcohol)/poly(allylamine)/2-amino-2-hydroxymethyl-1,3-propanediol/polysulfone composite membrane for CO_2/N_2 separation, J. Membr. Sci. 446 (2013) 383-394.

[18]. J. Zou and W. S. W. Ho, CO_2-selective polymeric membranes containing amines in crosslinked poly(vinyl alcohol), J. Membr. Sci. 286 (2006) 310-321.

[19]. S. B. Hamouda, Q.T. Nguyen, D. Langevin and S. Roudesli, Poly(vinylalcohol) / poly(ethyleneglycol) / poly(ethyleneimine) blend membranes - structure and CO_2 facilitated transport, C. R. Chimie. 13 (2010) 372-379.

[20]. S. B. Hamouda and S. Roudesli, Transport properties of PVA/PEI/PEG composite membranes: sorption and permeation characterizations, Cent. Eur. J. Chem. 6 (2008) 634-640.

[21]. C. Yi, Z. Wang, M. Li, J. Wang and S. Wang, Facilitated transport of CO_2 through polyvinylamine/polyethlene glycol blend membranes, Desalination. 193 (2006) 90-96.

[22]. G. J. Francisco, A. Chakma and X. Feng, Separation of carbon dioxide from nitrogen using diethanolamine-impregnated poly(vinyl alcohol) membranes, Sep. Purif. Technol. 71 (2010) 205-213.

[23]. L. M. Robeson, The upper bound revisited, J. Membr. Sci. 320 (2008) 390-400.

[24]. Y. Cai, Z. Wang, C. Yi, Y. Bai, J. Wang and S. Wang, Gas transport property of polyallylamine-poly(vinyl alcohol)/polysulfone composite membranes, J. Membr. Sci. 310 (2008) 184-196.

Chapter 5

CONCLUSIONS AND RECOMMENDATION FOR FUTURE WORK

In this chapter the salient accomplishments and major conclusions of this work are summarized and recommendations on future directions in the subject are made.

5.1 CONCLUSIONS

The main objective of this work was to systematically investigate the binary gas (20% CO_2 balance N_2) separation characteristics of synthesized novel polymer composite membrane at elevated temperature (> 100^oC). Poly (vinyl alcohol) (PVA) was judicially chosen for the base polymer in this research due to ease of its preparation as well as its excellent physical properties and film-forming ability, good compatibility with amine, hydrophilic in nature, semi crystalline polymer consists of crystalline domain and amorphous domain and moderate thermal stability. This complete research work was broadly divided into two parts. In the first part, thermal stability of the PVA membrane was improved by changing degree of crosslinking with formaldehyde (HCHO) and then by polymer blending with more thermally stable polyvinylpyrrolidone (PVP). In the

second part of the work, different new amine carriers (polyethyleneimine, tetraethylenepentamine, pentaethylenehexamine, polyallylamine, 2-amino-2-hydroxymethyl-1,3-propanediol and their blends) were introduced into the crosslinked-PVA-PVP membrane to increase the CO_2 flux, CO_2 permeability and CO_2/N_2 selectivity. The salient accomplishments and major conclusions from this work are summarized in the following sections.

5.1.1 Synthesis and Characterization of the Membranes

All the membranes were prepared by solution casting technique onto porous polysulfone support for permeation or onto glass plate for characterization. The optimum degree of crosslinking of PVA with HCHO was obtained as 60 mole%. The PVA/PVP ratio of 1: 0.2 was considered. Four sets of different amine based membranes have been prepared. Those are crosslinked-PVA-PVP membrane containing single amines (PEI and PAA), blends of PEI with TEPA, PEI with PEHA, PAA with PEHA and PAA with AHPD.

Three main steps of weight loss had been observed from each TGA curve. The first weight loss was due to evaporation of absorbed moisture from the atmosphere. The second weight loss was due to removal of hydroxyl groups or amine and the final weight loss was due to decomposition of the polymer backbones. It was illustrated from the TGA curve that the weight loss of pure PVA at 200-340^oC was largely reduced (around 55%) after crosslinking and polymer blending. The melting temperature (T_m) and glass transition temperature (T_g) of pure PVA were satisfactorily increased around 24^oC and 17^oC, respectively after crosslinking and polymer blending. But after addition of the

amine carrier to the polymer hydrogel, the T_g was slightly reduced. The band frequencies observed from FTIR analysis for all the membranes at 3267, 2912, 1650, 1580, 1419 and 1141 cm^{-1} are the stretching vibrations of the hydroxyl (-OH) groups, symmetric vibrations of alkyl groups (C–H), (C=C) stretching vibrations, combination of (O-H) and (C-H) bending, CH_2 bending, combination of (–C–O–C–) and (C–O) bond, respectively. The other bending vibrations less than 888 cm^{-1} are the fingerprint zone. It had been observed from the FTIR analysis that along with increasing the degree of crosslinking (10-80 mole %) the peak intensity at 1141 cm^{-1} was marginally increased due to the formation of (-C-O-C-) linkage. The X-ray diffraction pattern for all the amine doped membranes obtained by XRD analysis displayed a semi-crystalline structure with peaks at 2Θ angles of 20^o.

5.1.2 Binary Gas Permeation Experiment

In line with the earlier characterizations works, separation of CO_2 using novel crosslinked-PVA-PVP based membranes containing different amine carriers and their blends had been analyzed. It was observed from the experiment that along with change in amine composition and operating conditions the CO_2 separation performance changes. Crosslinked-PVA-PVP membrane containing blends of 25 wt% PAA and 15 wt% AHPD showed best separation performances over others. The highest CO_2/N_2 selectivity of 432, CO_2 permeability of 1825 Barrer and CO_2 flux of 658 × 10^{-6} $cm^3(STP)/cm^2s$ were obtained at 1.3 atm absolute pressure difference (ΔP), 100^oC temperature and 0.03/0.04 ml/min feed/sweep water flow rate. The effects of active layer thickness, feed pressure, sweep side water flow rate and temperature had been studied and also compared with

crosslinked-PVA membrane without amine carrier. The significant increase of the CO_2 flux was observed with increase in the feed pressure at low pressure region. With increase in sweep side water flow rate, the permeability as well as CO_2/N_2 selectivity increased significantly. This suggests that water played an important role in the facilitated transport of CO_2. As the temperature was increased from 90^oC to 100^oC, the CO_2 flux, CO_2 permeability and CO_2/N_2 selectivity were increased but beyond 100^oC, all the CO_2 transport properties tend to decrease. This was presumably due to the reduction of water retention in the membrane as the temperature is increased.

This work has been studied systematically to understand the gas transport behavior and applicability of CO_2-selective membrane. The experimental results would provide a good data base for rational design of membrane process. The results obtained in this work suggest that CO_2-selective polymer membranes have a very good potential for CO_2 separation from flue gas.

5.2 RECOMMENDATIONS ON FUTURE DIRECTIONS

This work presents a systematic and detailed investigation to understand the reactive membrane based separation characteristics with different amine carriers. There are certainly several areas which merit further research attention.

- In this work, the thermal stability of PVA has been improved by using crosslinking agent (HCHO) and blending with PVP polymer. Further studies using more thermally stable polymers like chitosan, polybenzimidazole etc. is recommended for high temperature application.

- PVA based membranes have been synthesized with different amine carriers such as Polyethyleneimine (PEI), Tetraethylenepentamine (TEPA), Pentaethylenehexamine (PEHA), Polyallylamine (PAA) and 2-amino-2-hydroxymethyl-1,3-propanediol (AHPD). Further studies using some other new amine carriers are necessary to see the behavior of CO_2 transport property through the membrane.

- The stability of the membranes has been tested for 250-300 hours. The membranes may be tested for longer period.

- The effect of impurities such as SOx and NOx present in the power plant flue gas on the performance and stability of the membrane can be studied.

- Rigorous model may be developed for the successful design of a membrane transport process.

APPENDIX 1

GENERALIZED CALCULATION OF DRY MEMBRANE COMPOSITIONS

A1.1 General Calculation Procedure

The materials considered for the calculation of membrane composition are PVA, PVP, KOH and different amines (PEI, TEPA, PEHA, PAA and AHPD). HCHO is used as a crosslinking agent.

The generalized composition of the membrane can be written as (X) wt. % PVA + (Y) wt. % PVP + (Z) wt. % KOH + (M) wt. % amine with (N) mole % degree of crosslinking with HCHO. The total dry weight of the membrane is 100 wt%.

Amount of PVA taken as a Basis = 2 gm.

$$\text{mole of PVA taken} = \frac{2}{44} = 0.045 \text{ mole}$$

[Molecular weight of one repeating unit of PVA = 44 gm. / mole]

$$\text{Amount of (OH) groups of PVA reacting} = 0.045 \times \text{wt\% of PVA} \times \text{mole\% of degree of crosslinking}$$

$$= 0.045 \times \frac{X}{100} \times \frac{N}{100} \text{ mole}$$

$$= 0.0000045 \times X \times N \text{ mole}$$

$$\text{Amount of HCHO required} = (0.0000045 \times X \times N) \times (\frac{30.03}{0.37}) \text{ gm}$$

[Molecular weight of HCHO = 30.03 gm. / mole and HCHO solution concentration = 37 wt. %]

$$\text{Weight of PVA increased after reaction} = 0.045 \times \frac{N}{100} \times \frac{X}{100} \times (30.03 - 18) \text{ gm}$$

[Molecular weight of H_2O = 18 gm. / mole]

$$\text{Membrane weight after reaction} = [0.045 \times \frac{N}{100} \times \frac{X}{100} \times (30.03 - 18)] + 2 \text{ gm}$$

$$\text{Total membrane weight increased after reaction} = [(0.045 \times \frac{N}{100} \times \frac{X}{100} \times (30.03 - 18)) + 2] \times \frac{100}{X} \text{ gm}$$

$$\text{Total membrane weight increased after reaction} = [(0.045 \times \frac{N}{100} \times \frac{X}{100} \times (30.03 - 18)) + 2] \times \frac{100}{X} \text{ gm}$$

Now,

$$\text{Amount of KOH is required} = \{[(0.045 \times \frac{N}{100} \times \frac{X}{100} \times (30.03 - 18)) + 2] \times \frac{100}{X}\} \times (\frac{Z}{100}) \text{ gm}$$

Amount of amine is required = $\{[(0.045\times\frac{N}{100}\times\frac{X}{100}\times(30.03-18))+2]\times\frac{100}{X}\}\times(\frac{M}{100})$ gm

Amount of PVP is required = $\{[(0.045\times\frac{N}{100}\times\frac{X}{100}\times(30.03-18))+2]\times\frac{100}{X}\}\times(\frac{Y}{100})$ gm

A1.2 Membrane composition of 90wt% PVA + 10 wt% KOH, with 60 mole% degree of crosslinking by HCHO

The total dry weight of the membrane is 100 wt%.

Amount of PVA taken as a Basis = 2 gm.

Mole of PVA taken = 2/44 = 0.045 mole.

Amount of (OH) groups of PVA reacting = 0.045 × 0.9 × 0.6 = 0.0243 mole.

Amount of HCHO required = 0.0243 × (30.03/0.37) = 1.97 gm.

Weight of PVA increased after reaction = 0.045 × 0.6 × 0.9 × (30.03 - 18) gm.

= 0.292 gm.

Membrane weight after reaction = 2 + 0.292 gm. = 2.292 gm.

Total membrane weight increased after reaction = 2.292 × (100/90) = 2.547 gm.

Now,

Amount of KOH is required = 2.547 × 0.1 = 0.25 gm.

A1.3 Membrane composition of 72 wt% PVA + 18 wt% PVP + 10 wt% KOH, with 60 mole% degree of crosslinking by HCHO

The total dry weight of the membrane is 100 wt%.

Amount of PVA taken as a Basis = 2 gm.

Mole of PVA taken = 2/44 = 0.045 mole.

Amount of (OH) groups of PVA reacting = 0.045 × 0.72 × 0.6 = 0.01944 mole.

Amount of HCHO required = 0.01944 × (30.03/0.37) = 1.57 gm.

Weight of PVA increased after reaction = 0.045 × 0.6 × 0.72 × (30.03 - 18) gm.

= 0.233 gm.

Membrane weight after reaction = 2 + 0.233 gm. = 2.233 gm.

Total membrane weight increased after reaction = 2.233 × (100/72) = 3.102 gm.

Now,

Amount of KOH is required = 3.102 × 0.1 = 0.31 gm.

Amount of PVP is required = 3.102 × 0.18 = 0.55 gm.

A1.4 Membrane composition of 41.66 wt% PVA + 8.33 wt% PVP + 10 wt% KOH + 15 wt% PEI + 25 wt% TEPA, with 60 mole% degree of crosslinking by HCHO

The total dry weight of the membrane is 100 wt%.

Amount of PVA taken as a Basis = 2 gm.

Mole of PVA taken = 2/44 = 0.045 mole.

Amount of (OH) groups of PVA reacting = 0.045 × 0.4166 × 0.6 = 0.0112 mole.

Amount of HCHO required = 0.0112 × (30.03/0.37) = 0.91 gm.

Weight of PVA increased after reaction = 0.045 × 0.6 × 0.0.4166 × (30.03 - 18) gm.

= 0.135 gm.

Membrane weight after reaction = 2 + 0.135 gm. = 2.135 gm.

Total membrane weight increased after reaction = 2.135 × (100/41.66) = 5.12 gm.

Now,

Amount of KOH is required = 5.12 × 0.1 = 0.51 gm.

Amount of PVP is required = 5.12 × 0.0833 = 0.42 gm.

Amount of PEI is required = 5.12 × 0.15 = 0.768 gm.

Amount of TEPA is required = 5.12 × 0.25 = 1.28 gm.

A1.5 Membrane composition of 41.66 wt% PVA + 8.33 wt% PVP + 10 wt% KOH + 15 wt% PEI + 25 wt% PEHA, with 60 mole% degree of crosslinking by HCHO

The total dry weight of the membrane is 100 wt%.

Amount of PVA taken as a Basis = 2 gm.

Mole of PVA taken = 2/44 = 0.045 mole.

Amount of (OH) groups of PVA reacting = 0.045 × 0.4166 × 0.6 = 0.0112 mole.

Amount of HCHO required = 0.0112 × (30.03/0.37) = 0.91 gm.

Weight of PVA increased after reaction = 0.045 × 0.6 × 0.0.4166 × (30.03 - 18) gm.

= 0.135 gm.

Membrane weight after reaction = 2 + 0.135 gm. = 2.135 gm.

Total membrane weight increased after reaction = 2.135 × (100/41.66) = 5.12 gm.

Now,

Amount of KOH is required = 5.12 × 0.1 = 0.51 gm.

Amount of PVP is required = 5.12 × 0.0833 = 0.42 gm.

Amount of PEI is required = 5.12 × 0.15 = 0.768 gm.

Amount of PEHA is required = 5.12 × 0.25 = 1.28 gm.

A1.6 Membrane composition of 41.66 wt% PVA + 8.33 wt% PVP + 10 wt% KOH + 25 wt% PAA + 15 wt% PEHA, with 60 mole% degree of crosslinking by HCHO

The total dry weight of the membrane is 100 wt%.

Amount of PVA taken as a Basis = 2 gm.

Mole of PVA taken = 2/44 = 0.045 mole.

Amount of (OH) groups of PVA reacting = 0.045 × 0.4166 × 0.6 = 0.0112 mole.

Amount of HCHO required = 0.0112 × (30.03/0.37) = 0.91 gm.

Weight of PVA increased after reaction = 0.045 × 0.6 × 0.0.4166 × (30.03 - 18) gm.

= 0.135 gm.

Membrane weight after reaction = 2 + 0.135 gm. = 2.135 gm.

Total membrane weight increased after reaction = 2.135 × (100/41.66) = 5.12 gm.

Now,

Amount of KOH is required = 5.12 × 0.1 = 0.51 gm.

Amount of PVP is required = 5.12 × 0.0833 = 0.42 gm.

Amount of PEHA is required = 5.12 × 0.15 = 0.768 gm.

Amount of PAA is required = 5.12 × 0.25 = 1.28 gm.

A1.7 Membrane composition of 41.66 wt% PVA + 8.33 wt% PVP + 10 wt% KOH + 25 wt% PAA + 15 wt% AHPD, with 60 mole% degree of crosslinking by HCHO

The total dry weight of the membrane is 100 wt%.

Amount of PVA taken as a Basis = 2 gm.

Mole of PVA taken = 2/44 = 0.045 mole.

Amount of (OH) groups of PVA reacting = 0.045 × 0.4166 × 0.6 = 0.0112 mole.

Amount of HCHO required = 0.0112 × (30.03/0.37) = 0.91 gm.

Weight of PVA increased after reaction = 0.045 × 0.6 × 0.0.4166 × (30.03 - 18) gm.

= 0.135 gm.

Membrane weight after reaction = 2 + 0.135 gm. = 2.135 gm.

Total membrane weight increased after reaction = 2.135 × (100/41.66) = 5.12 gm.

Now,

Amount of KOH is required = 5.12 × 0.1 = 0.51 gm.

Amount of PVP is required = 5.12 × 0.0833 = 0.42 gm.

Amount of AHPD is required = 5.12 × 0.15 = 0.768 gm.

Amount of PAA is required = 5.12 × 0.25 = 1.28 gm.

APPENDIX 2

GAS TRANSPORT PARAMETERS CALCULATION AND GAS CHROMATOGRAPHY DATA

A2.1 Gas Transport Parameters (CO_2 and N_2 fluxes, CO_2 and N_2 permeability, CO_2/N_2 selectivity) Calculation

η_R (Mole/min) = retentate molar flux per unit area = $\frac{PV}{RT}$ (1)

where

P (atmospheric pressure at which the retentate gas is emitting) = 1 atm.

V (volumetric flow rate of mixed gas at retentate side) = 30 cc/min = 30×10^{-06} m^3/min.

T (room temperature at ^oK) = 298.15 ^oK.

R (universal gas constant) = 8.205746×10^{-5} m^3 atm / ^oK mol.

η_R **(Mole/min) =** $\frac{1 \times 30 \times 10^{-06}}{8.205746 \times 10^{-05} \times 298.15}$ **= 1.22 × 10 $^{-03}$ mole/min.**

η_{Ar} (Mole/min) = argon (carrier gas) molar flux per unit area = $\frac{PV}{RT}$ (2)

where

P (atmospheric pressure at which the carrier gas is emitting) = 1 atm.

V (volumetric flow rate of carrier gas at permeate side) = 27 cc/min = 27×10^{-06} m^3/min.

T (room temperature at ^{o}K) = 298.15 ^{o}K.

R (universal gas constant) = 8.205746 × 10^{-5} m^3 atm / ^{o}K mol.

η_{Ar} **(Mole/min) =** $\dfrac{1\times 27\times 10^{-06}}{8.205746\times 10^{-05}\times 298.15}$ **= 1.08 × 10^{-03} mole/min.**

η_P (Mole/min) = permeate molar flux per unit area =

$$[(CO_2\ mole\ fraction\times\frac{CO_2(P)_{G.C}}{CO_2(F)_{G.C}})+(N_2\ mole\ fraction\times\frac{N_2(P)_{G.C}}{N_2(F)_{G.C}})]\times\frac{Ar\ molar\ flux(mol/\min)}{[1-(CO_2\ mole\ fraction\times\frac{CO_2(P)_{G.C}}{CO_2(F)_{G.C}})-(N_2\ mole\ fraction\times\frac{N_2(P)_{G.C}}{N_2(F)_{G.C}})]} \quad (3)$$

where

$CO_2(P)_{G.C}$ = CO_2 concentration at permeate side from G.C analysis = 0.057 **(Figure A2.20)**

$CO_2(F)_{G.C}$ = CO_2 concentration at feed side from G.C analysis = 0.1997 **(Figure A2.20)**

$N_2(P)_{G.C}$ = N_2 concentration at permeate side from G.C analysis = 0.0012 **(Figure A2.20)**

$N_2(F)_{G.C}$ = N_2 concentration at feed side from G.C analysis = 0.799 **(Figure A2.20)**

CO_2 mole fraction = 0.2

N_2 mole fraction = 0.8

Ar molar flux = 1.08 × 10^{-03} mole/min

η_P **(Mole/min) = permeate molar flux per unit area = 6.74 × 10^{-05} mole/min**

$p_{CO_2}(R, psi)$ = CO_2 partial pressure at retentate side =

$$[BP_F + P_{ambient} \times \frac{14.7}{101.325}] \times \frac{[\eta_R - 0.5 \times \eta_P] \times CO_2\ mole\ fraction \times [0.5 + 0.5 \times \frac{CO_2(R)_{G.C}}{CO_2(F)_{G.C}}]}{[\eta_R - 0.5 \times \eta_P] + \frac{[0.5 \times H_2O_F] + [0.5 \times H_2O_{distribution} \times (H_2O_F + H_2O_S)]}{18}} \quad (4)$$

where

BP_F = Back pressure (psig) at feed side of the membrane module = 25 psig

$P_{ambient}$ = Ambient pressure (kPa) = 101.6 kPa

$CO_2(R)_{G.C}$ = CO_2 concentration at retentate side from G.C analysis = 0.1486 **(Figure A2.20)**

$CO_2(F)_{G.C}$ = CO_2 concentration at feed side from G.C analysis = 0.1997 **(Figure A2.20)**

H_2O_F = Feed side water flow rate (ml/min) = 0.03 ml/min **(Appendix A2.8, effect of temperature)**

H_2O_S = Sweep side water flow rate (ml/min) = 0.04 ml/min **(Appendix A2.8, effect of temperature)**

$H_2O_{distribution}$ = Total water distribution (ml/min) = 0.22 ml/min

$\eta_R = 1.22 \times 10^{-03}$ mole/min

$\eta_P = 6.74 \times 10^{-05}$ mole/min

CO_2 mole fraction = 0.2

$p_{CO_2}(R, psi)$ = CO_2 partial pressure at retentate side = 3.35 psi

$p_{CO_2}(P, psi)$ = CO_2 partial pressure at permeate side =

$$[BP_S + P_{ambient} \times \frac{14.7}{101.325}] \times \frac{[(\eta_{Ar} + 0.5 \times \eta_P) \times CO_2\ mole\ fraction \times 0.5 \times \frac{CO_2(P)_{G.C}}{CO_2(F)_{G.C}}]}{[\eta_{Ar} + 0.5 \times \eta_P] + \frac{[0.5 \times H_2O_S] + [0.5 \times (1 - H_2O\ distribution) \times (H_2O_F + H_2O_S)]}{18}} \quad (5)$$

where

BP_S = Back pressure (psig) at sweep side of the membrane module = 3.5 psig

$P_{ambient}$ = Ambient pressure (kPa) = 101.6 kPa

$CO_2(P)_{G.C}$ = CO_2 concentration at permeate side from G.C analysis = 0.057 **(Figure A2.20)**

$CO_2(F)_{G.C}$ = CO_2 concentration at feed side from G.C analysis = 0.1997 **(Figure A2.20)**

H_2O_F = Feed side water flow rate (ml/min) = 0.03 ml/min **(Appendix A2.8, effect of temperature)**

H_2O_S = Sweep side water flow rate (ml/min) = 0.04 ml/min **(Appendix A2.8, effect of temperature)**

$H_2O_{distribution}$ = Total water distribution (ml/min) = 0.22 ml/min

η_{Ar} = 1.08×10^{-03} mole/min

η_P = 6.74×10^{-05} mole/min

CO_2 mole fraction = 0.2

$p_{CO_2}(P, psi)$ = CO_2 partial pressure at permeate side = 0.16 psi

$p_{N_2}(R, psi)$ = N_2 partial pressure at retentate side =

$$[BP_F + P_{ambient} \times \frac{14.7}{101.325}] \times \frac{[\eta_R - 0.5 \times \eta_P] \times N_2\ mole\ fraction \times [0.5 + 0.5 \times \frac{N_2(R)_{G.C}}{N_2(F)_{G.C}}]}{[\eta_R - 0.5 \times \eta_P] + \frac{[0.5 \times H_2O_F] + [0.5 \times H_2O\ distribution \times (H_2O_F + H_2O_S)]}{18}} \quad (6)$$

where

BP_F = Back pressure (psig) at feed side of the membrane module = 25 psig

$P_{ambient}$ = Ambient pressure (kPa) = 101.6 kPa

$N_2(R)_{G.C}$ = N_2 concentration at retentate side from G.C analysis = 0.851 **(Figure A2.20)**

$N_2(F)_{G.C}$ = N_2 concentration at feed side from G.C analysis = 0.799 **(Figure A2.20)**

H_2O_F = Feed side water flow rate (ml/min) = 0.03 ml/min **(Appendix A2.8, effect of temperature)**

H_2O_S = Sweep side water flow rate (ml/min) = 0.04 ml/min **(Appendix A2.8, effect of temperature)**

$H_2O_{distribution}$ = Total water distribution (ml/min) = 0.22 ml/min

$\eta_R = 1.22 \times 10^{-03}$ mole/min

$\eta_P = 6.74 \times 10^{-05}$ mole/min

N_2 mole fraction = 0.8

$p_{N_2}(R, psi)$ **= N_2 partial pressure at retentate side = 15.84 psi**

$p_{N_2}(P, psi)$ = N_2 partial pressure at permeate side =

$$[BP_S + P_{ambient} \times \frac{14.7}{101.325}] \times \frac{[(\eta_{Ar} + 0.5 \times \eta_P) \times N_2\ mole\ fraction \times 0.5 \times \frac{N_2(P)_{G.C}}{N_2(F)_{G.C}}]}{[\eta_{Ar} + 0.5 \times \eta_P] + \frac{[0.5 \times H_2O_S] + [0.5 \times (1 - H_2O\ distribution) \times (H_2O_F + H_2O_S)]}{18}} \quad (7)$$

where

BP_S = Back pressure (psig) at sweep side of the membrane module = 3.5 psig

$P_{ambient}$ = Ambient pressure (kPa) = 101.6 kPa

$N_2(P)_{G.C}$ = N_2 concentration at permeate side from G.C analysis = 0.0012 **(Figure A2.20)**

$N_2(F)_{G.C}$ = N_2 concentration at feed side from G.C analysis = 0.799 **(Figure A2.20)**

H_2O_F = Feed side water flow rate (ml/min) = 0.03 ml/min **(Appendix A2.8, effect of temperature)**

H_2O_S = Sweep side water flow rate (ml/min) = 0.04 ml/min **(Appendix A2.8, effect of temperature)**

$H_2O_{distribution}$ = Total water distribution (ml/min) = 0.22 ml/min

$\eta_{Ar} = 1.08 \times 10^{-03}$ mole/min

$\eta_P = 6.74 \times 10^{-05}$ mole/min

N_2 mole fraction = 0.8

$p_{N_2}(P, psi)$ = N_2 partial pressure at permeate side = 0.0034 psi

V_{CO2} (cm^3/sec) = permeate volumetric gas flow rate of CO_2 =

$$\frac{\eta_{Ar} \times CO_2(P)_{G.C} \times CO_2 \ mole\ fraction \times 8.314 \times 273.15 \times 1000000}{CO_2(F)_{G.C} \times 101325 \times 60 \times [1-(CO_2\ mol\ fraction \times \frac{CO_2(P)_{G.C}}{CO_2(F)_{G.C}})-(N_2\ mol\ fraction \times \frac{N_2(P)_{G.C}}{N_2(F)_{G.C}})]} \quad (8)$$

V_{CO2} (cm^3/sec) = permeate volumetric gas flow rate of CO_2 = 2.47 × 10^{-02} cm^3/sec

V_{N2} (cm^3/sec) = permeate volumetric gas flow rate of N_2 =

$$\frac{\eta_{Ar} \times N_2(P)_{G.C} \times N_2 \ mole\ fraction \times 8.314 \times 273.15 \times 1000000}{N_2(F)_{G.C} \times 101325 \times 60 \times [1-(CO_2\ mol\ fraction \times \frac{CO_2(P)_{G.C}}{CO_2(F)_{G.C}})-(N_2\ mol\ fraction \times \frac{N_2(P)_{G.C}}{N_2(F)_{G.C}})]} \quad (9)$$

V_{N2} (cm^3/sec) = permeate volumetric gas flow rate of N_2 = 5.45 × 10^{-04} cm^3/sec

CO_2 Flux ($10^{-6}cm^3$(STP)/cm^2sec), CO_2 Permeability (Barrer), CO_2 Permeance (GPU) and CO_2/N_2 Selectivity

$(\Delta p)_{CO_2}\ at\ psi$ = partial pressure difference at psi = $p_{CO_2}(R, psi) - p_{CO_2}(P, psi)$

$(\Delta p)_{CO_2}\ at\ psi = 3.19\ psi$

$(\Delta p)_{CO_2}\ at\ cmHg$ = partial pressure difference at cmHg = $\dfrac{(\Delta p)_{CO_2}\ at\ psi}{14.7} \times 76$

$(\Delta p)_{CO_2}\ at\ cmHg = 16.49\ cmHg$

$$CO_2 \text{flux} = \frac{V_{CO_2}(cm^3/\sec)}{area\ of\ membrane\left(cm^2\right)}$$

where,

V_{CO2} (cm^3/sec) = 2.47 × 10^{-02} cm^3/sec

Area of membrane = 51.5 cm^2

CO_2 flux = 479 × 10^{-6} cm^3 (STP) / cm^2s (Table A2.4)

$$CO_2 \text{ permeability} = \frac{V_{CO_2}(cm^3/\sec) \times thickness\left(cm\right)}{area\ of\ membrane\left(cm^2\right) \times (\Delta p)_{CO_2}\ at\ cmHg}$$

where,

V_{CO2} (cm^3/sec) = 2.47 × 10^{-02} cm^3/sec

Area of membrane = 51.5 cm^2

Thickness = 0.0045 cm = 45 micron (Appendix A2.8)

$(\Delta p)_{CO_2}\ at\ cmHg = 16.49\ cmHg$

CO_2 permeability = 1307 × 10^{-10} cm^3 (STP) cm / cm^2 s cmHg = 1307 Barrer (Table A2.4)

$$CO_2 \text{ permeance} = \frac{CO_2 \text{ permeability}}{\text{thickness}} = \frac{1307\ (Barrer)}{45} = 29\ GPU$$

1 GPU = 10^{-6} cm^3 (STP) / cm^2 s cmHg

$$\frac{CO_2}{N_2}\ Selectivity = \frac{\frac{CO_2(P)_{G.C}}{N_2(P)_{G.C}}}{\frac{CO_2(R)_{G.C}}{N_2(R)_{G.C}}} = \frac{\frac{0.057}{0.00126}}{\frac{0.1486}{0.851}} = 259$$

N_2 Flux ($10^{-6}$$cm^3$(STP)/$cm^2$sec), N_2 Permeability (Barrer), N_2 Permeance (GPU) and CO_2/N_2 Selectivity

$(\Delta p)_{N_2}\ at\ psi$ = partial pressure difference at psi = $p_{N_2}(R, psi) - p_{N_2}(P, psi)$

$(\Delta p)_{N_2}\ at\ psi = 15.84\ psi$

$$(\Delta p)_{N_2}\ at\ cmHg = \text{partial pressure difference at cmHg} = \frac{(\Delta p)_{N_2}\ at\ psi}{14.7} \times 76$$

$(\Delta p)_{N_2}\ at\ cmHg = 81.89\ cmHg$

$$N_2 \text{flux} = \frac{V_{N_2}(cm^3/\text{sec})}{area\ of\ membrane\left(cm^2\right)}$$

where,

V_{N2} (cm^3/sec) = 5.45 × 10^{-04} cm^3/sec

Area of membrane = 51.5 cm^2

N_2 flux = 10 × 10^{-6} cm^3 (STP) / cm^2s (Table A2.4)

$$N_2 \text{ permeability} = \frac{V_{N_2}(cm^3/\text{sec}) \times thickness\left(cm\right)}{area\ of\ membrane\left(cm^2\right) \times (\Delta p)_{N_2}\ at\ cmHg}$$

where,

V_{N2} (cm^3/sec) = 5.45 × 10^{-04} cm^3/sec

Area of membrane = 51.5 cm^2

Thickness = 0.0045 cm = 45 micron (Appendix A2.8)

$(\Delta p)_{N_2}\ at\ cmHg = 81.89\ cmHg$

N_2 permeability = 5.8 × 10^{-10} cm^3 (STP) cm / cm^2 s cmHg = 5.8 Barrer (Table A2.4)

$$N_2 \text{ permeance} = \frac{N_2 \text{ permeability}}{\text{thickness}} = \frac{5.8}{45} = 0.12\ GPU$$

1 GPU = 10^{-6} cm^3 (STP) / cm^2 s cmHg

A2.2 Gas Chromatography Data of Calibration Gases and G.C Operating Protocol

A2.2.1 Calibration Gases for G.C

Five known concentration of CO_2 and N_2 gas mixture were used as calibration gas. This was (4% CO_2 + 4% N_2, balance Argon), (8% CO_2 + 8% N_2, balance Argon), (12% CO_2 + 12% N_2, balance Argon), (20% CO_2, balance N_2) and (40% CO_2, balance N_2).

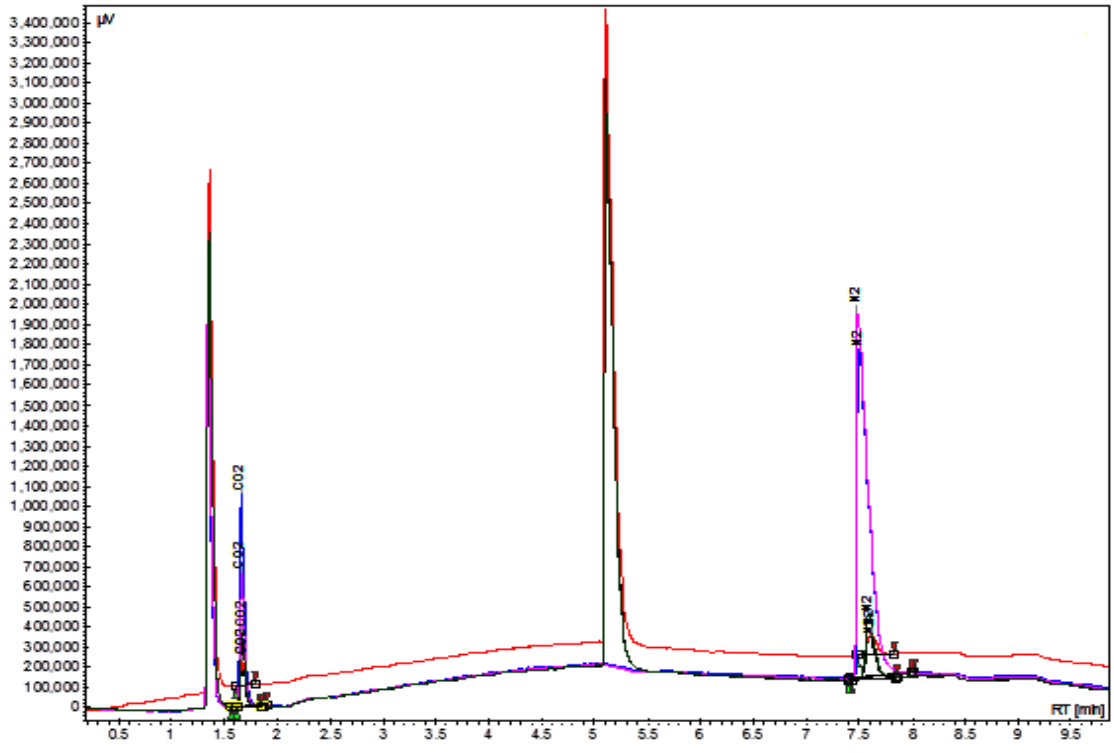

Figure A2.1 Peak intensity and position of all five CO_2 and N_2 calibration gases

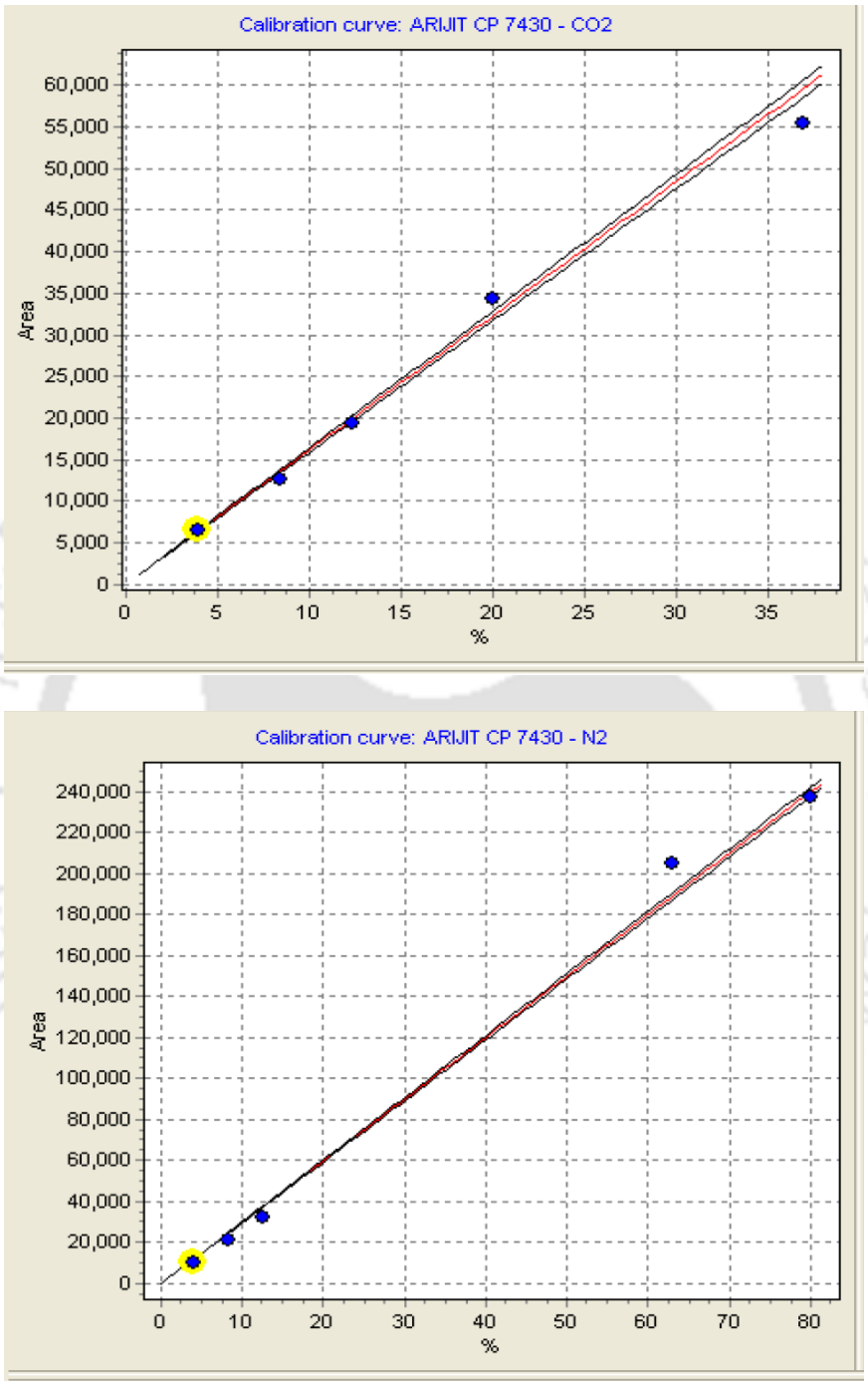

Figure A2.2 Plot of all five CO_2 and N_2 calibration gases

A2.2.2 G.C operating protocol

Here, we have used Varian-450 G.C for all the permeation experiments. The detail G.C operating protocols are mentioned below:

Injector programing: Heater (ON) at 120^{o}C

Tine (min)	**Split state**	**Split ratio**
Initial	ON	1
0.00	ON	1
1.00	ON	1

Oven programing:

Column oven (ON) and Rear oven (ON) at 100^{o}C

Rate (^{o}C/min)	**Temperature (^{o}C)**	**Time (min)**	**Total time (min)**
initial	40	2.00	2.00
10	70	5.00	10.00
			Total time 10.00

Column pneumatics: (pressure program)

Rate (psi/min)	**Pressure (psi)**	**Time (min)**	**Total time (min)**
Initial	15	10.00	10.00
			Total time 10.00

Detector (TCD) programing:

Heater (ON) at 95^{o}C

Electronics (ON)

Filament temperature at 235^{o}C

Filament temperature limit at 390^{o}C

TCD event table

Time (min)	Range	Auto zero	Polarity
Initial	0.05	YES	Negative

Gas sampling valve (GSV) programing:

Time (min)	Gas sampling valve
Initial	Fill
0.02	Inject

A2.2.3 Detail Purity of all Calibration gases

Table A2.1 Detail purity percentage of all calibration gases

Name	Purity compositions
4% CO_2 + 4% N_2, balance Argon	CO_2 (99.999%), N_2 (99.999%), Ar (99.999%), H_2O (< 2 ppm) and CO (< 0.5 ppm)
8% CO_2 + 8% N_2, balance Argon	CO_2 (99.999%), N_2 (99.999%), Ar (99.999%), H_2O (< 2 ppm) and CO (< 0.5 ppm)
12% CO_2 + 12% N_2, balance Argon	CO_2 (99.999%), N_2 (99.999%), Ar (99.999%), H_2O (< 2 ppm) and CO (< 0.5 ppm)
20% CO_2, balance N_2	CO_2 (99.999%), N_2 (99.999%), H_2O (< 2 ppm) and CO (< 0.5 ppm)
40% CO_2, balance N_2	CO_2 (99.999%), N_2 (99.999%), H_2O (< 2 ppm) and CO (< 0.5 ppm)

A2.3 Permeation Results of Crosslinked-PVA-PVP Membrane Containing 15wt% PEI and 25wt% TEPA with Active Layer Thickness of 45 Micron

Table A2.2 Effect of feed pressure on separation performances at constant feed/sweep water flow rate = 0.03/0.04 (ml/min), constant temperature = 100°C and constant sweep pressure = 3.5 psig

Feed Pressure (atm)	CO_2/N_2 Selectivity	CO_2 Permeability (Barrer)	N_2 Permeability (Barrer)	CO_2 Flux 10^{-6} $cm^3(STP)/cm^2s$	N_2 Flux 10^{-6} $cm^3(STP)/cm^2s$
1.7	239	1290	5.8	330	7
2.7	229	1213	5.7	426	10
3.6	200	916	5.1	444	12
4.9	179	724	4.5	479	14
6.2	169	589	3.9	486	16

Table A2.3 Effect of sweep water flow rate on separation performances at constant feed/sweep pressure = 25/3.5 (psig), constant temperature = 90°C and constant feed water flow rate = 0.03 (ml/min)

Sweep water flow rate (ml/min)	CO_2/N_2 Selectivity	CO_2 Permeability (Barrer)	N_2 Permeability (Barrer)	CO_2 Flux 10^{-6} $cm^3(STP)/cm^2s$	N_2 Flux 10^{-6} $cm^3(STP)/cm^2s$
0.02	60	261	4	112	8
0.04	243	1048	4.9	382	8
0.06	267	1211	5	416	8
0.075	270	1250	5.2	417	8

Table A2.4 Effect of temperature on separation performances at constant feed/sweep pressure = 25/3.5 (psig) and constant feed/sweep water flow rate = 0.03/0.04 (ml/min)

Temperature (^oC)	CO_2/N_2 Selectivity	CO_2 Permeability (Barrer)	N_2 Permeability (Barrer)	CO_2 Flux 10^{-6} $cm^3(STP)/cm^2s$	N_2 Flux 10^{-6} $cm^3(STP)/cm^2s$
90	243	1048	4.9	382	9
100	259	1307	5.8	479	10
115	91	496	5.4	203	9
125	73	393	5.3	162	9

A2.4 Permeation Results of Crosslinked-PVA-PVP Membrane Containing 15wt% PEI and 25wt% PEHA with Active Layer Thickness of 40 Micron

Table A2.5 Effect of feed pressure on separation performances at constant feed/sweep water flow rate = 0.03/0.04 (ml/min), constant temperature = 100^{o}C and constant sweep pressure = 3.5 psig

Feed Pressure (atm)	CO_2/N_2 Selectivity	CO_2 Permeability (Barrer)	N_2 Permeability (Barrer)	CO_2 Flux 10^{-6} $cm^3(STP)/cm^2s$	N_2 Flux 10^{-6} $cm^3(STP)/cm^2s$
1.7	378	1538	4.4	408	5
2.7	370	1408	4.8	545	10
3.6	295	1246	5.4	643	15
4.9	252	899	4.7	680	19
6.2	243	799	4.4	689	20

Table A2.6 Effect of sweep water flow rate on separation performances at constant feed/sweep pressure = 25/3.5 (psig), constant temperature = 90°C and constant feed water flow rate = 0.03 (ml/min)

Sweep water flow rate (ml/min)	CO_2/N_2 Selectivity	CO_2 Permeability (Barrer)	N_2 Permeability (Barrer)	CO_2 Flux 10^{-6} $cm^3(STP)/cm^2s$	N_2 Flux 10^{-6} $cm^3(STP)/cm^2s$
0.02	154	545	3.8	258	8
0.04	351	1270	4.4	506	8
0.06	396	1396	4.4	533	9
0.075	409	1474	4.8	543	9

Table A2.7 Effect of temperature on separation performances at constant feed/sweep pressure = 25/3.5 (psig) and constant feed/sweep water flow rate = 0.03/0.04 (ml/min)

Temperature (°C)	CO_2/N_2 Selectivity	CO_2 Permeability (Barrer)	N_2 Permeability (Barrer)	CO_2 Flux 10^{-6} $cm^3(STP)/cm^2s$	N_2 Flux 10^{-6} $cm^3(STP)/cm^2s$
90	351	1270	4.4	506	9
100	370	1396	4.8	545	10
115	130	568	4.6	262	9
125	94	400	4.6	186	9

A2.5 Permeation Results of Crosslinked-PVA-PVP Membrane Containing 25wt% PAA and 15wt% PEHA with Active Layer Thickness of 42 Micron

Table A2.8 Effect of feed pressure on separation performances at constant feed/sweep water flow rate = 0.03/0.04 (ml/min), constant temperature = 100°C and constant sweep pressure = 3.5 psig

Feed Pressure (atm)	CO_2/N_2 Selectivity	CO_2 Permeability (Barrer)	N_2 Permeability (Barrer)	CO_2 Flux 10^{-6} $cm^3(STP)/cm^2s$	N_2 Flux 10^{-6} $cm^3(STP)/cm^2s$
1.7	405	1669	4.5	411	5
2.7	397	1656	5	628	10
3.6	334	1306	4.7	652	12
4.9	274	968	4.4	667	15
6.2	257	788	3.9	678	17

Table A2.9 Effect of sweep water flow rate on separation performances at constant feed/sweep pressure = 25/3.5 (psig), constant temperature = 90°C and constant feed water flow rate = 0.03 (ml/min)

Sweep water flow rate (ml/min)	CO_2/N_2 Selectivity	CO_2 Permeability (Barrer)	N_2 Permeability (Barrer)	CO_2 Flux 10^{-6} $cm^3(STP)/cm^2s$	N_2 Flux 10^{-6} $cm^3(STP)/cm^2s$
0.02	191	716	4	318	9
0.04	362	1457	4.8	563	9
0.06	403	1510	4.4	565	8
0.075	411	1613	4.7	584	8

Table A2.10 Effect of temperature on separation performances at constant feed/sweep pressure = 25/3.5 (psig) and constant feed/sweep water flow rate = 0.03/0.04 (ml/min)

Temperature (^oC)	CO_2/N_2 Selectivity	CO_2 Permeability (Barrer)	N_2 Permeability (Barrer)	CO_2 Flux 10^{-6} $cm^3(STP)/cm^2s$	N_2 Flux 10^{-6} $cm^3(STP)/cm^2s$
90	362	1458	4.7	563	9
100	397	1657	5	628	9
115	165	733	4.7	318	10
125	117	512	4.7	226	10

A2.6 Permeation Results of Crosslinked-PVA-PVP Membrane Containing 25wt% PAA and 15wt% AHPD with Active Layer Thickness of 44 Micron

Table A2.11 Effect of feed pressure on separation performances at constant feed/sweep water flow rate = 0.03/0.04 (ml/min), constant temperature = 100^{o}C and constant sweep pressure = 3.5 psig

Feed Pressure (atm)	CO_2/N_2 Selectivity	CO_2 Permeability (Barrer)	N_2 Permeability (Barrer)	CO_2 Flux 10^{-6} $cm^3(STP)/cm^2s$	N_2 Flux 10^{-6} $cm^3(STP)/cm^2s$
1.7	409	1866	4.7	431	5
2.7	432	1825	5	658	9
3.6	358	1353	4.6	667	11
4.9	288	1032	4.4	679	14
6.2	268	829	3.8	682	16

Table A2.12 Effect of sweep water flow rate on separation performances at constant feed/sweep pressure = 25/3.5 (psig), constant temperature = 90°C and constant feed water flow rate = 0.03 (ml/min)

Sweep water flow rate (ml/min)	CO_2/N_2 Selectivity	CO_2 Permeability (Barrer)	N_2 Permeability (Barrer)	CO_2 Flux 10^{-6} $cm^3(STP)/cm^2s$	N_2 Flux 10^{-6} $cm^3(STP)/cm^2s$
0.02	244	950	4.3	391	8
0.04	406	1667	4.8	611	9
0.06	477	1827	4.6	639	8
0.075	477	1896	4.8	645	8

Table A2.13 Effect of temperature on separation performances at constant feed/sweep pressure = 25/3.5 (psig) and constant feed/sweep water flow rate = 0.03/0.04 (ml/min)

Temperature (°C)	CO_2/N_2 Selectivity	CO_2 Permeability (Barrer)	N_2 Permeability (Barrer)	CO_2 Flux 10^{-6} $cm^3(STP)/cm^2s$	N_2 Flux 10^{-6} $cm^3(STP)/cm^2s$
90	406	1667	4.8	611	9
100	432	1825	5	658	9
115	164	760	4.9	321	9
125	122	560	4.8	238	9

A2.7 Gas Chromatography Data of Crosslinked-PVA-PVP Membrane Containing PEI and TEPA (Effect of Thickness)

Three different active layer compositions were prepared as mentioned below:

1. 41.66 wt% PVA + 8.33 wt% PVP + 10 wt% KOH + 15 wt% PEI + 25 wt% TEPA with 60 mol% degree of cross linking by HCHO
2. 41.66 wt% PVA + 8.33 wt% PVP + 10 wt% KOH + 30 wt% PEI + 10 wt% TEPA with 60 mol% degree of cross linking by HCHO
3. 41.66 wt% PVA + 8.33 wt% PVP + 10 wt% KOH + 40 wt% PEI with 60 mol% degree of cross linking by HCHO

Composition one has three different active layer membranes like 34, 67 and 73 micron. Similarly composition two has also three different active layer membranes like 41, 75 and 87 micron. And composition three has only one active layer membrane like 69 micron.

All the permeation experiment was done exactly same operating condition. Feed side and sweep side absolute pressure was maintained constant at around 2.8 and 1.15 atm, respectively. Temperature was kept constant at 95^{o}C along with constant water flow rate at both sides (feed/sweep = 0.03/0.04 cm^3/min). Both feed gas (20% CO_2 balance N_2 on dry basis) and carrier gas (Ar) flow rates were maintained at 30 cm^3/min throughout the experiment.

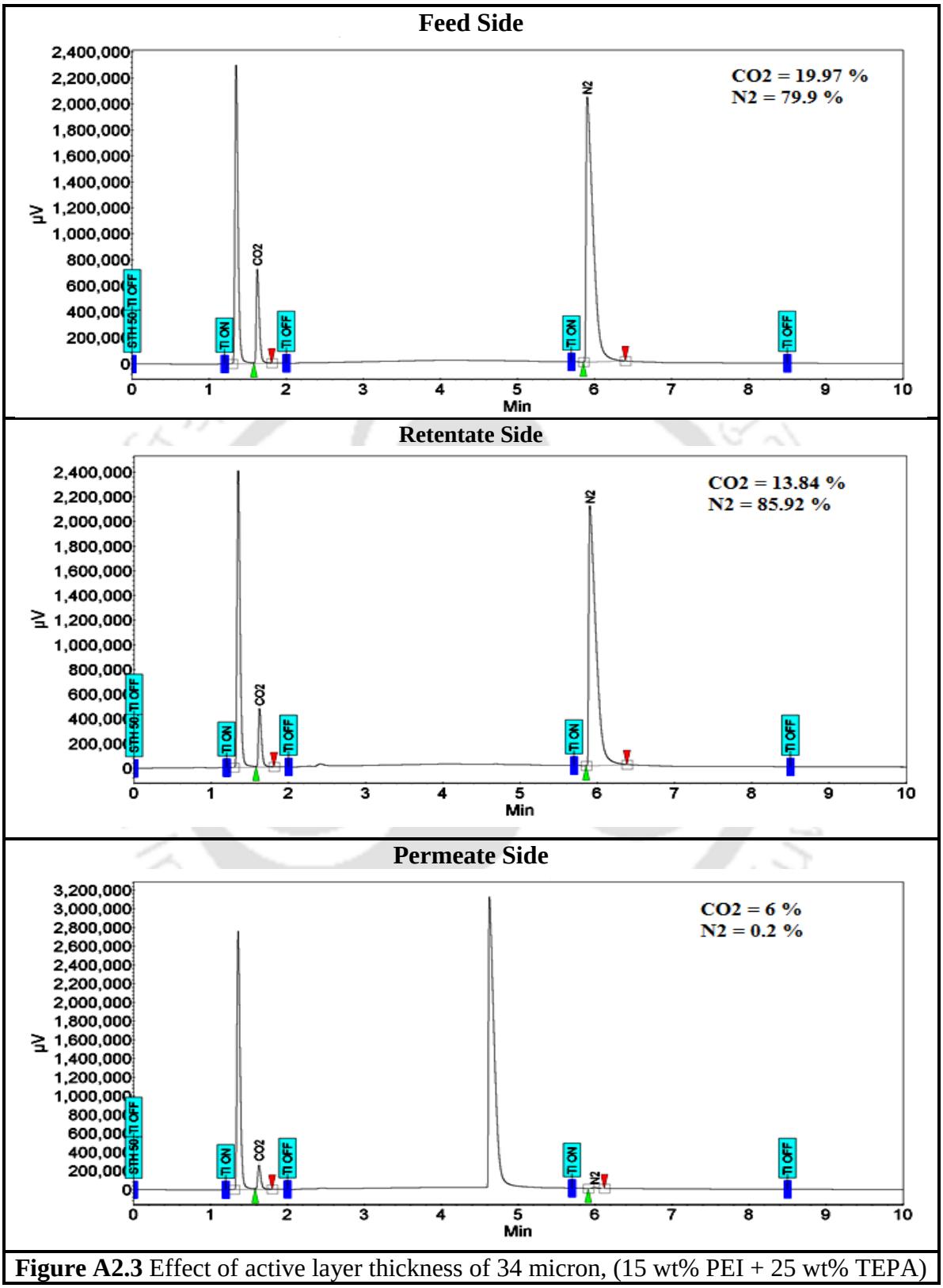

Figure A2.3 Effect of active layer thickness of 34 micron, (15 wt% PEI + 25 wt% TEPA)

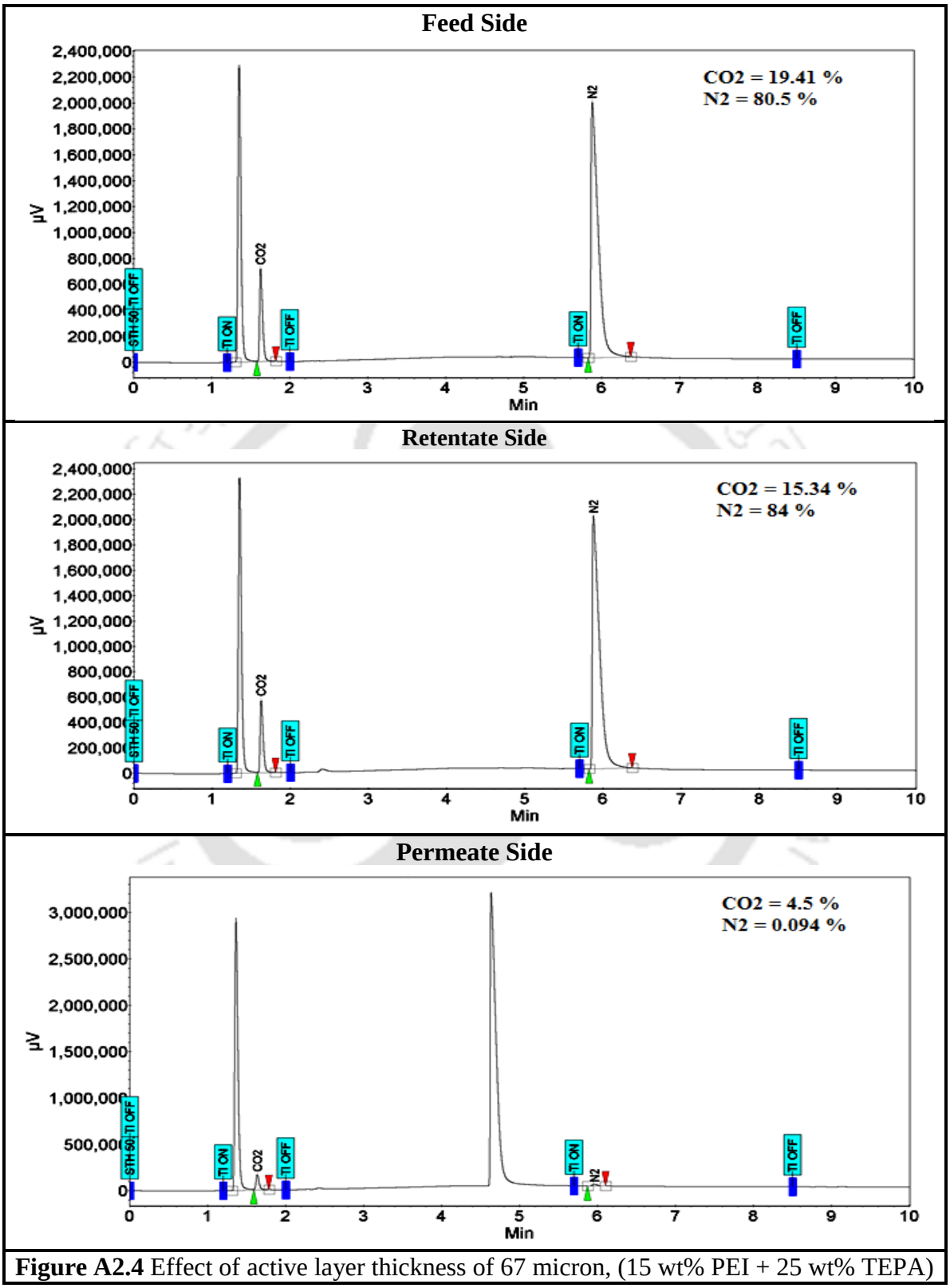

Figure A2.4 Effect of active layer thickness of 67 micron, (15 wt% PEI + 25 wt% TEPA)

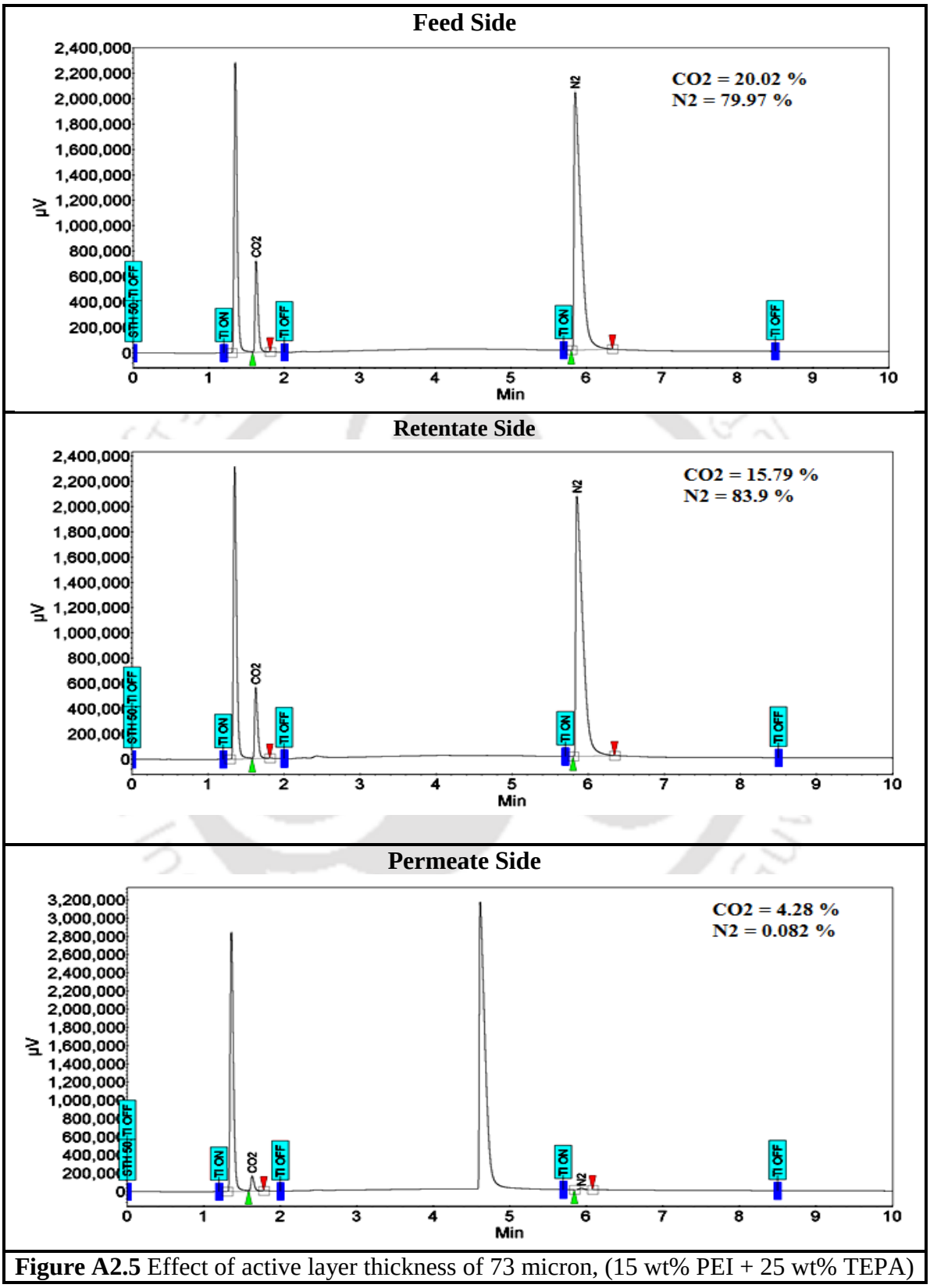

Figure A2.5 Effect of active layer thickness of 73 micron, (15 wt% PEI + 25 wt% TEPA)

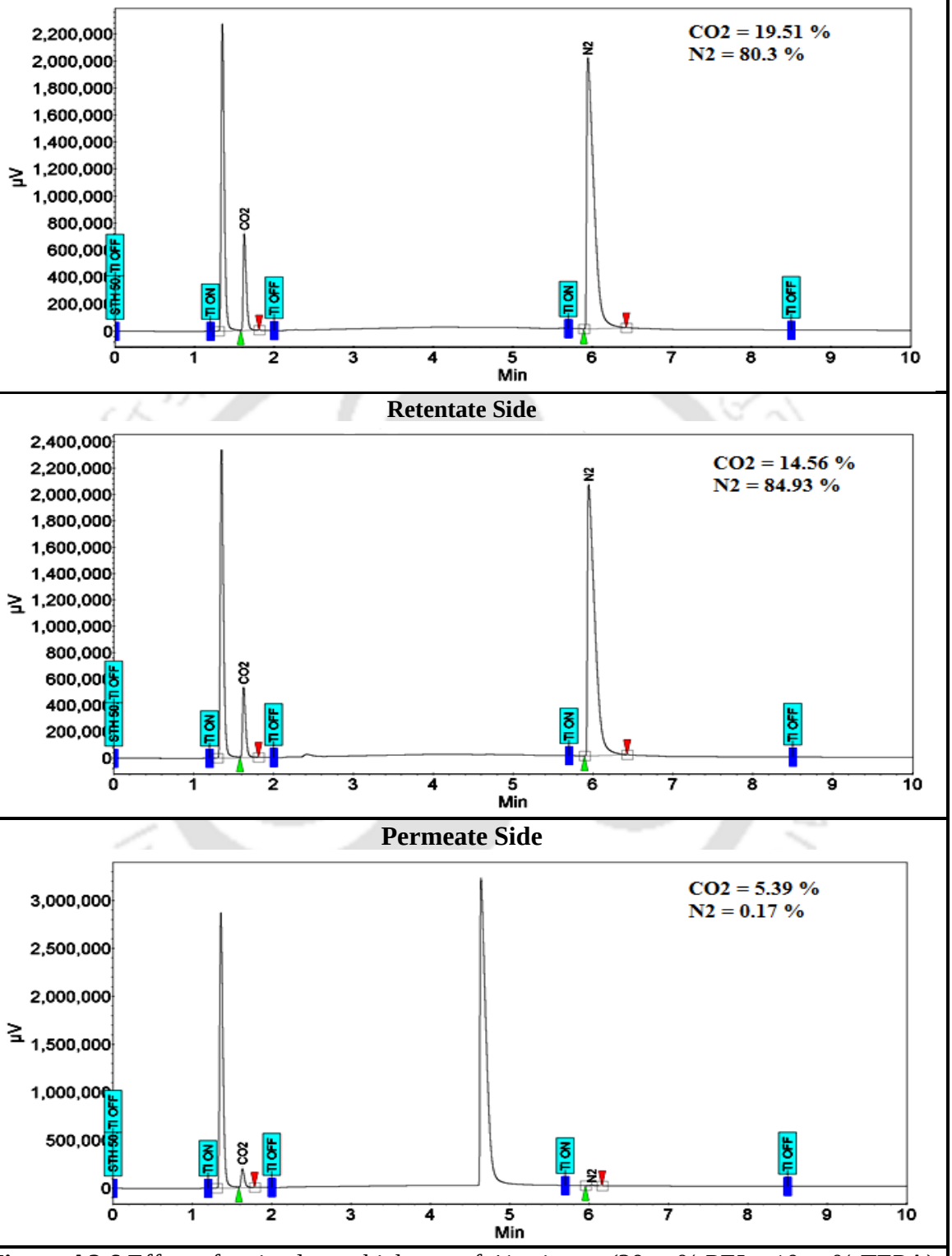

Figure A2.6 Effect of active layer thickness of 41 micron, (30 wt% PEI + 10 wt% TEPA)

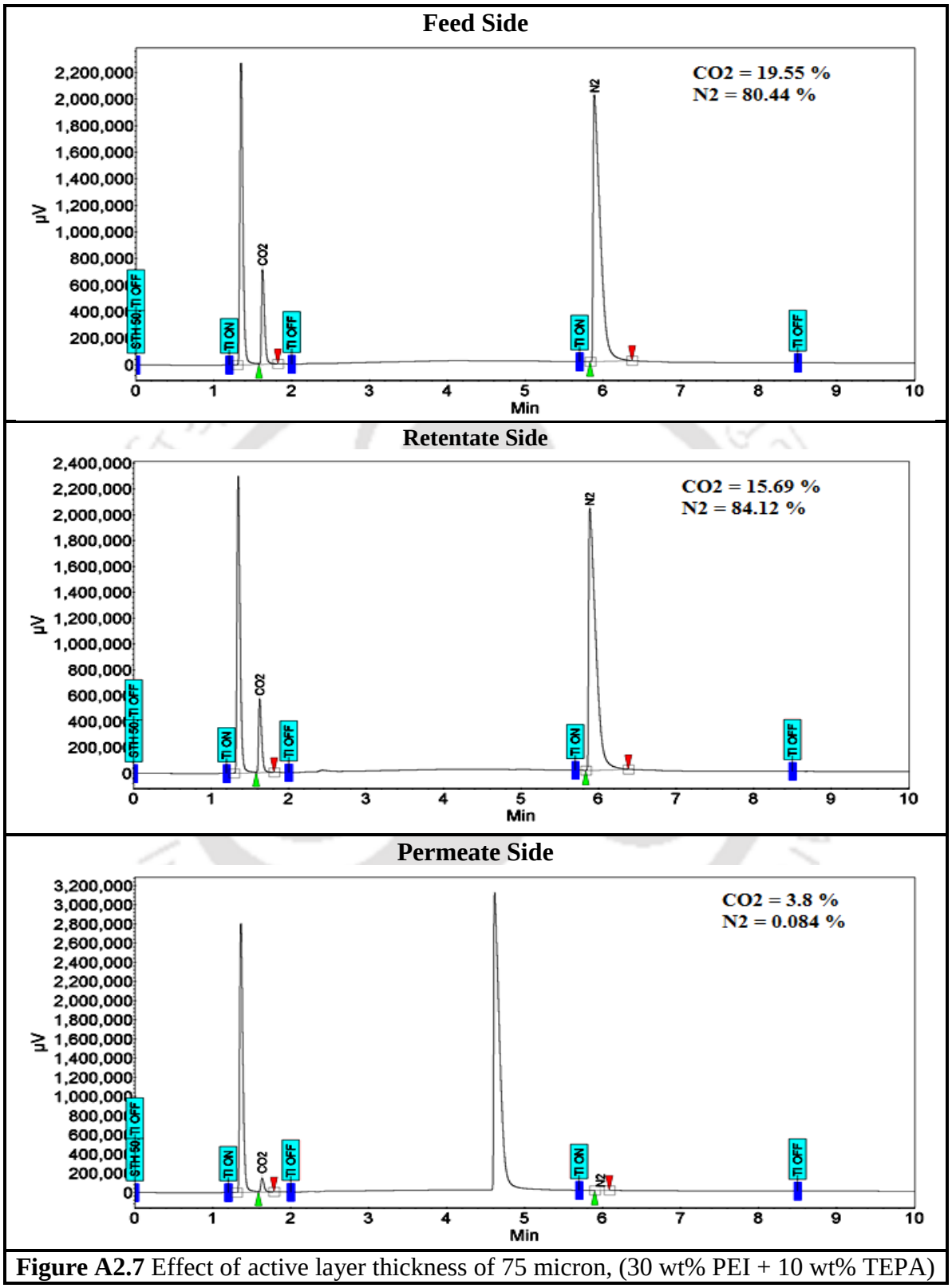

Figure A2.7 Effect of active layer thickness of 75 micron, (30 wt% PEI + 10 wt% TEPA)

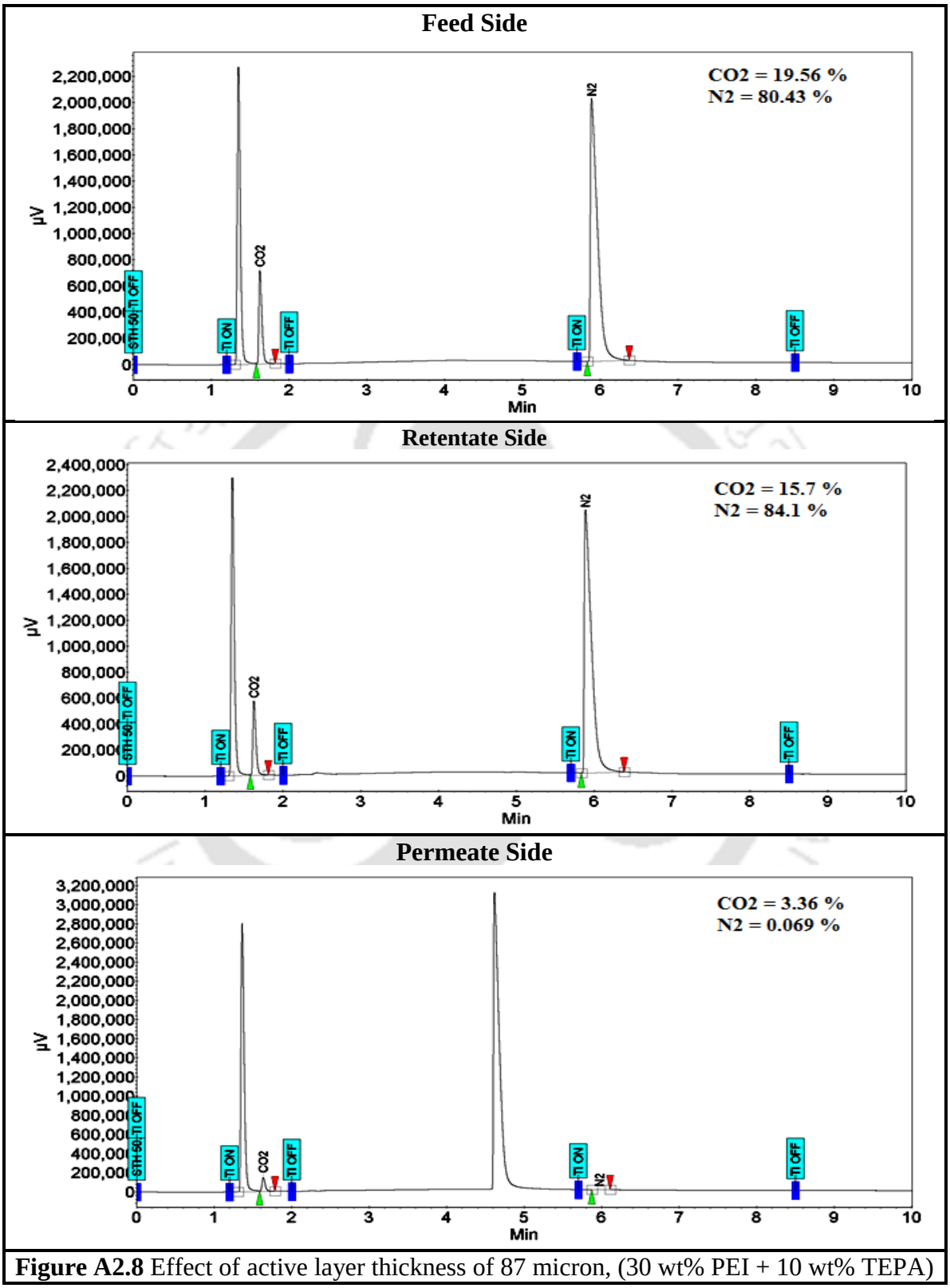

Figure A2.8 Effect of active layer thickness of 87 micron, (30 wt% PEI + 10 wt% TEPA)

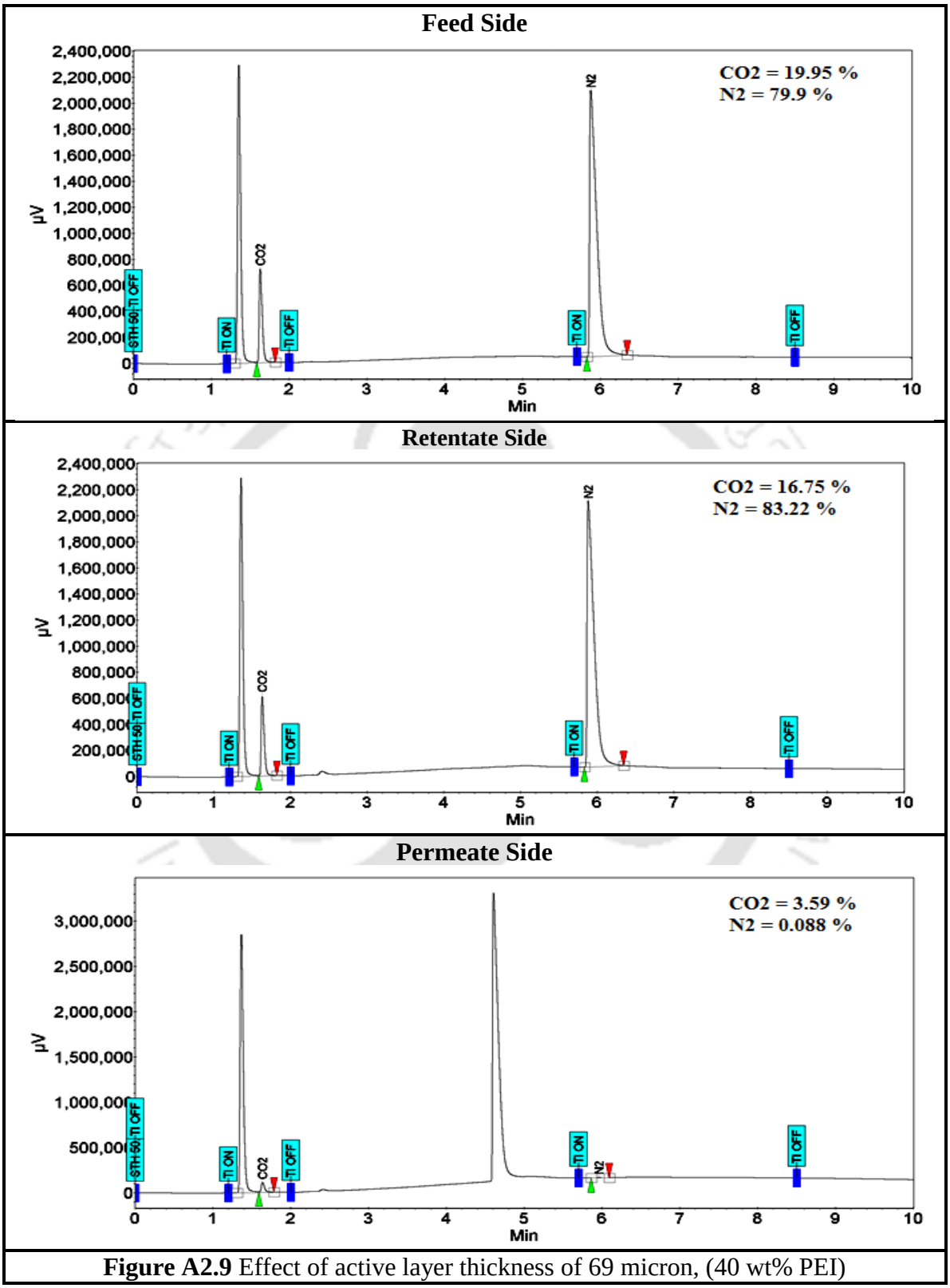

Figure A2.9 Effect of active layer thickness of 69 micron, (40 wt% PEI)

A2.8 Gas Chromatography Data of Crosslinked-PVA-PVP Membrane Containing PEI and TEPA (Permeation Experiment)

Permeation experiment of 41.66 wt% PVA + 8.33 wt% PVP + 10 wt% KOH + 15 wt% PEI + 25 wt% TEPA with 60 mol% degree of cross linking by HCHO membrane with an active layer thickness of 45 micron.

Effects of Feed Pressure on Separation Performance: Feed absolute pressure was varied from 1.7 to 6.2 atm, maintaining other operating conditions constant (temperature = 100^{o}C, sweep side absolute pressure = 1.15 atm and feed side / sweep side water flow rate = 0.03 / 0.04 cm^{3}/min).

Effects of Sweep Side Water Flow Rate on Separation Performance: Sweep side water flow rate was varied from 0.02 to 0.075 cm^{3}/min, maintaining other operating conditions constant (temperature = 90^{o}C, sweep side absolute pressure = 1.15 atm and feed side water flow rates = 0.03 cm^{3}/min).

Effects of Temperature on Separation Performance: Temperature was varied from 90 to 125^{o}C, maintaining other operating conditions constant (feed / sweep side absolute pressure = 2.7 / 1.15 atm and feed / sweep side water flow rate = 0.03 / 0.04 cm^{3}/min).

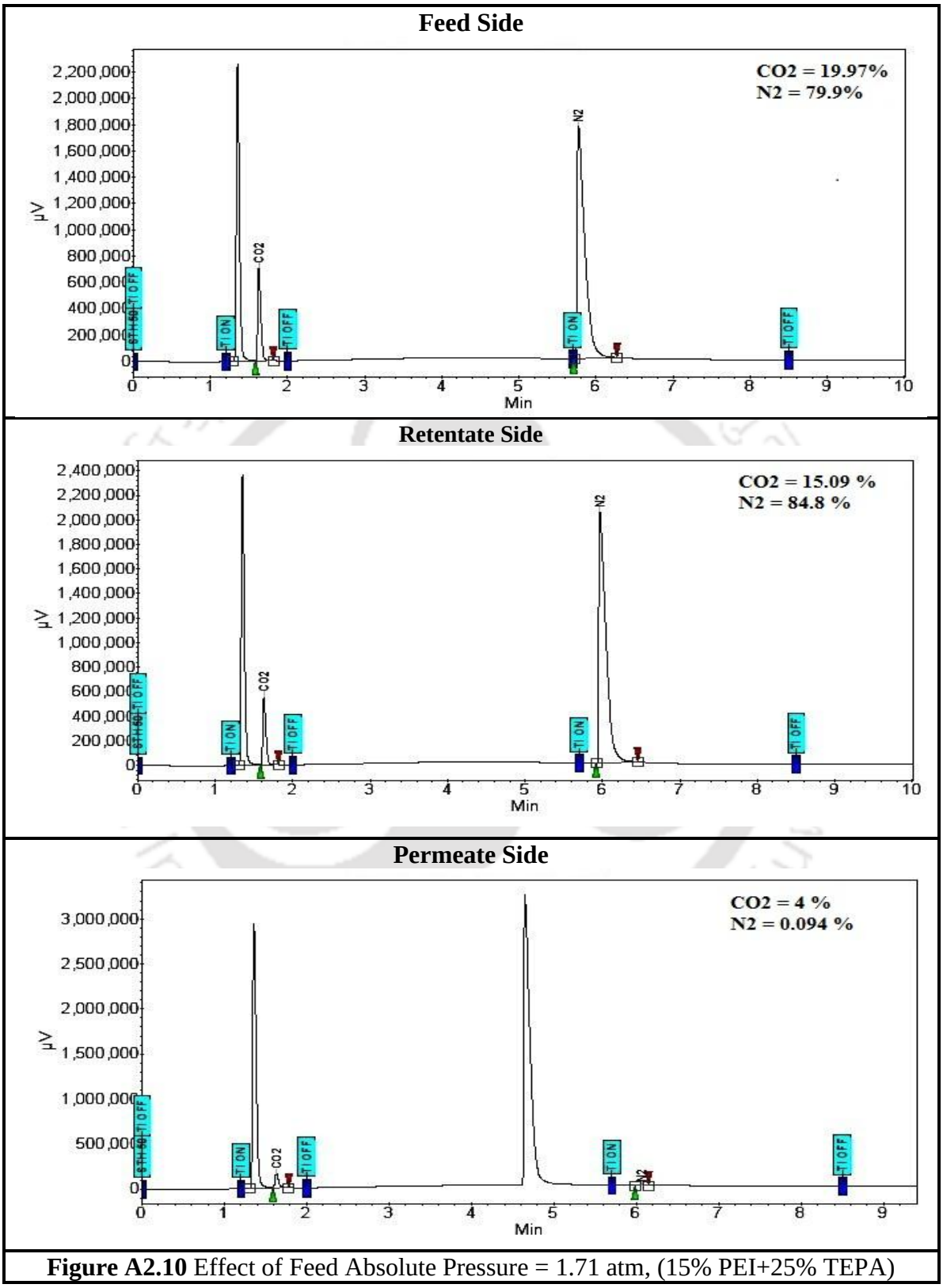

Figure A2.10 Effect of Feed Absolute Pressure = 1.71 atm, (15% PEI+25% TEPA)

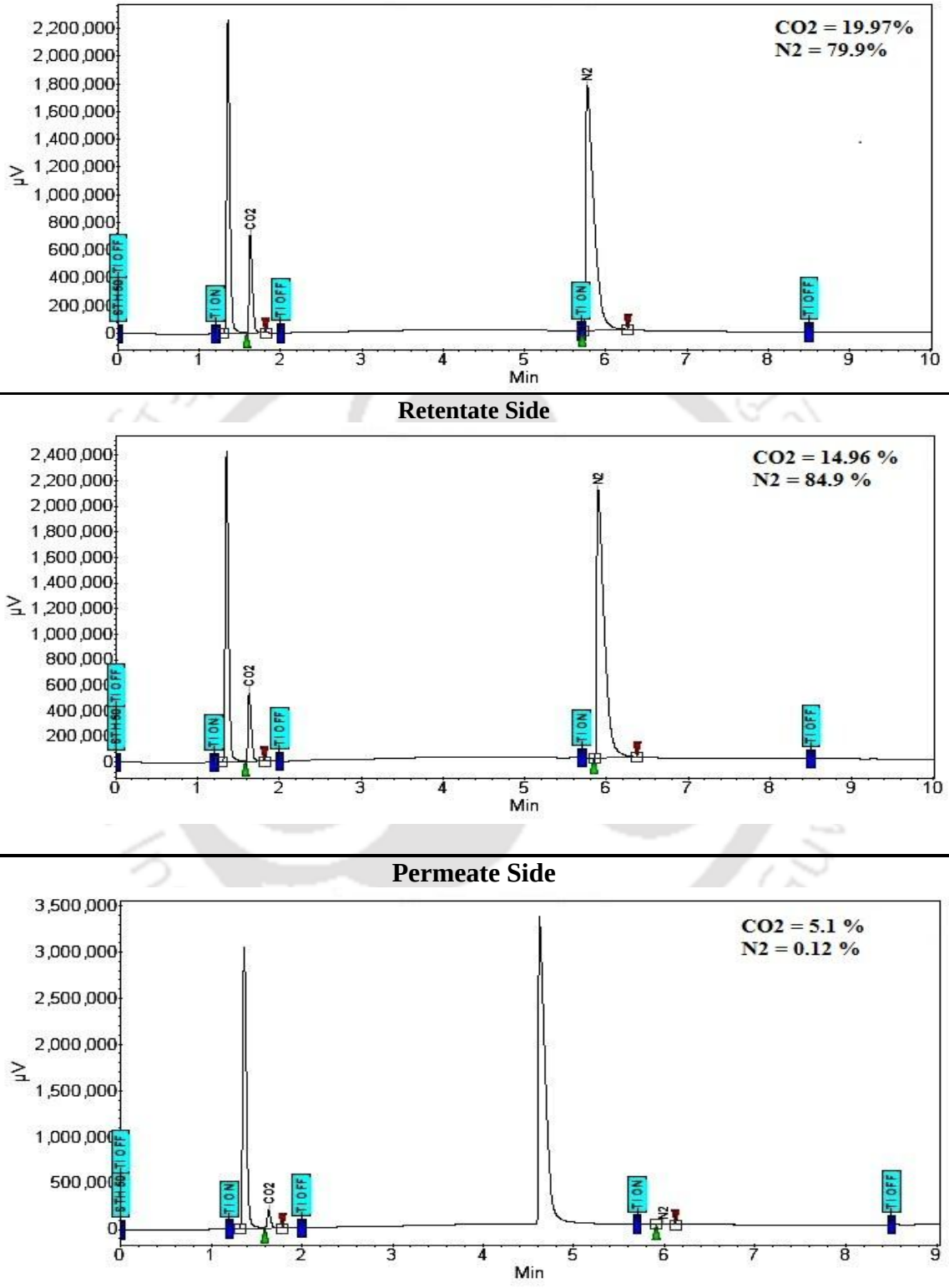

Figure A2.11 Effect of Feed Absolute Pressure = 2.76 atm, (15% PEI+25% TEPA)

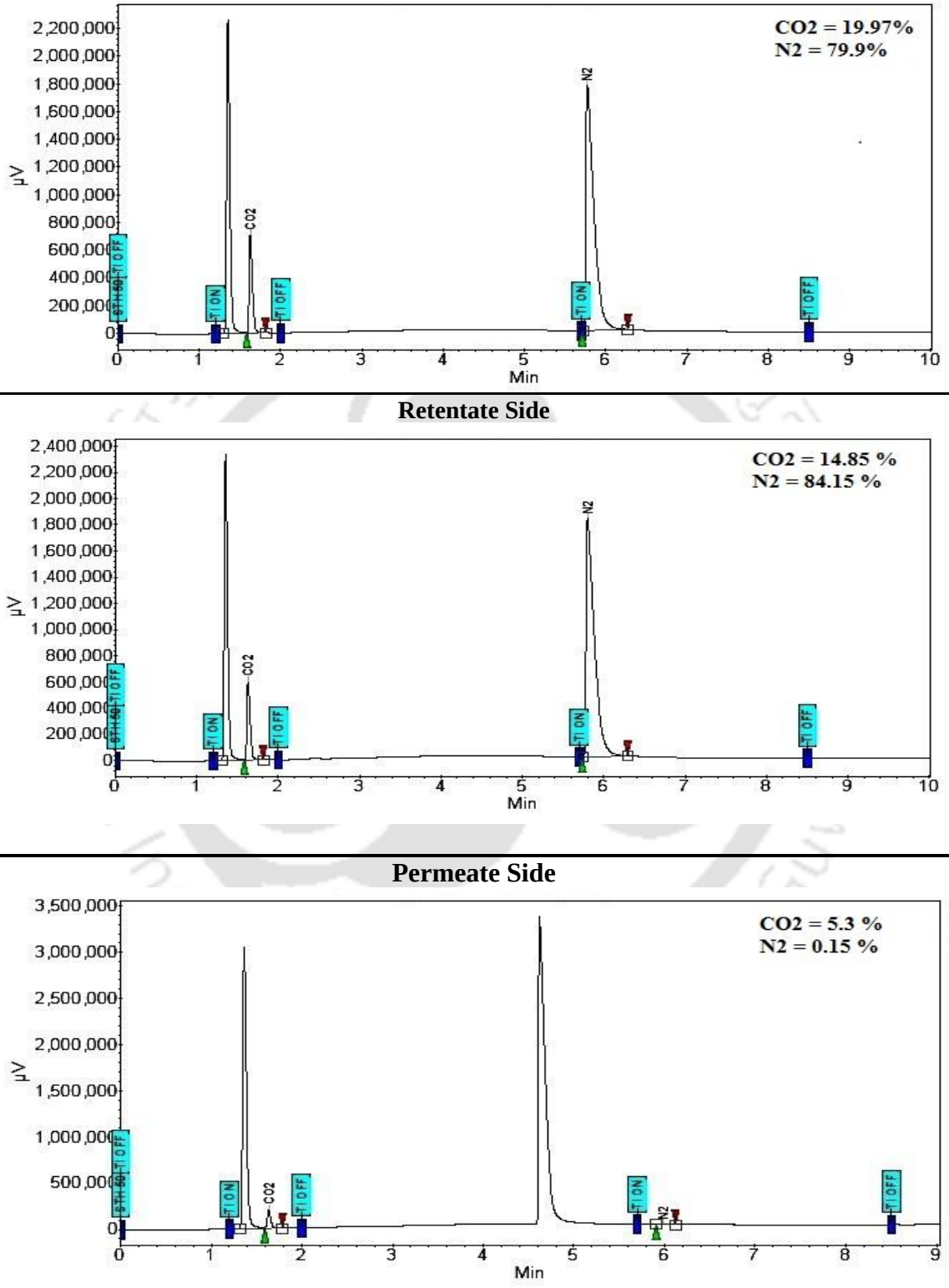

Figure A2.12 Effect of Feed Absolute Pressure = 3.61 atm, (15% PEI+25% TEPA)

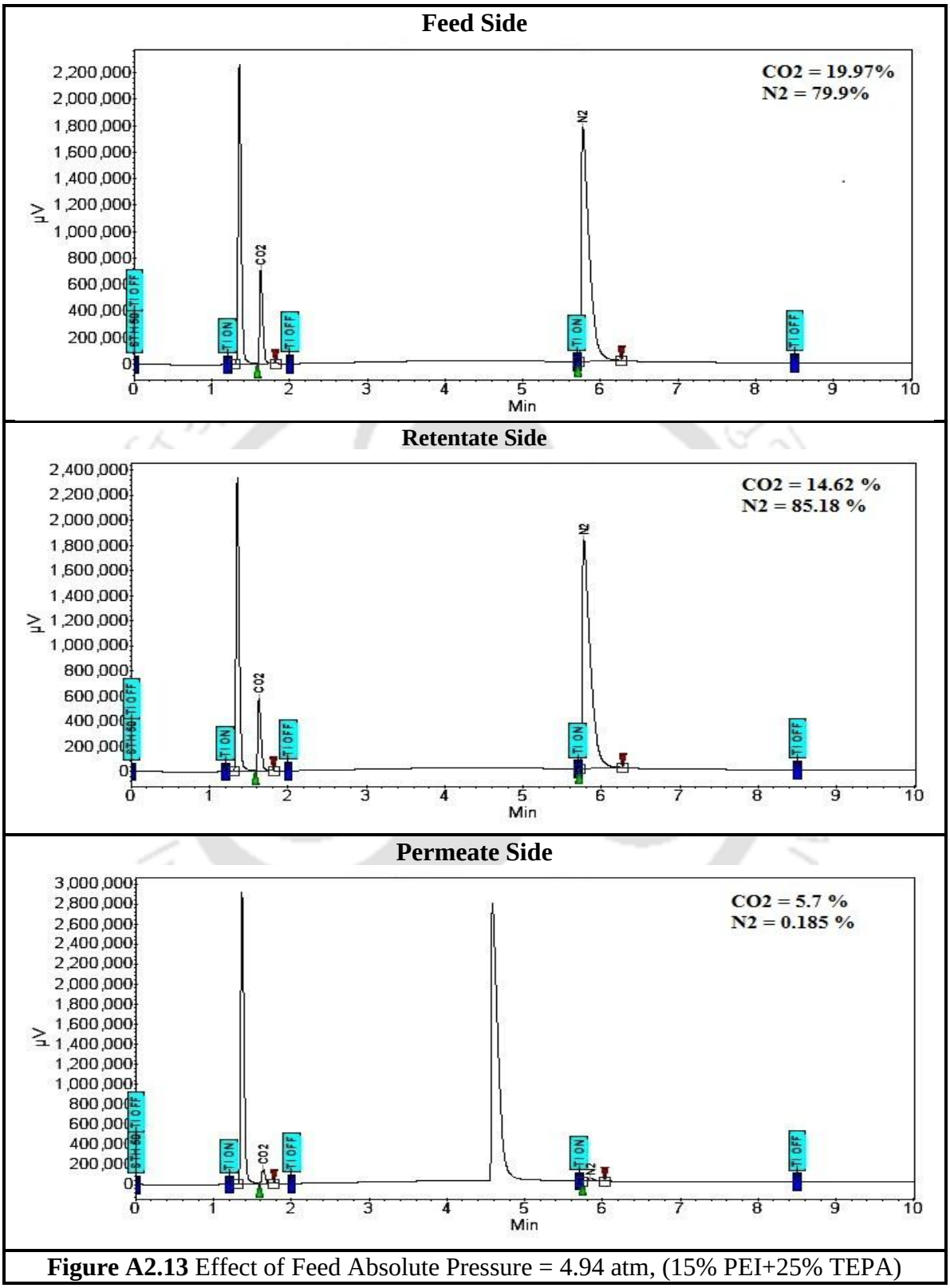

Figure A2.13 Effect of Feed Absolute Pressure = 4.94 atm, (15% PEI+25% TEPA)

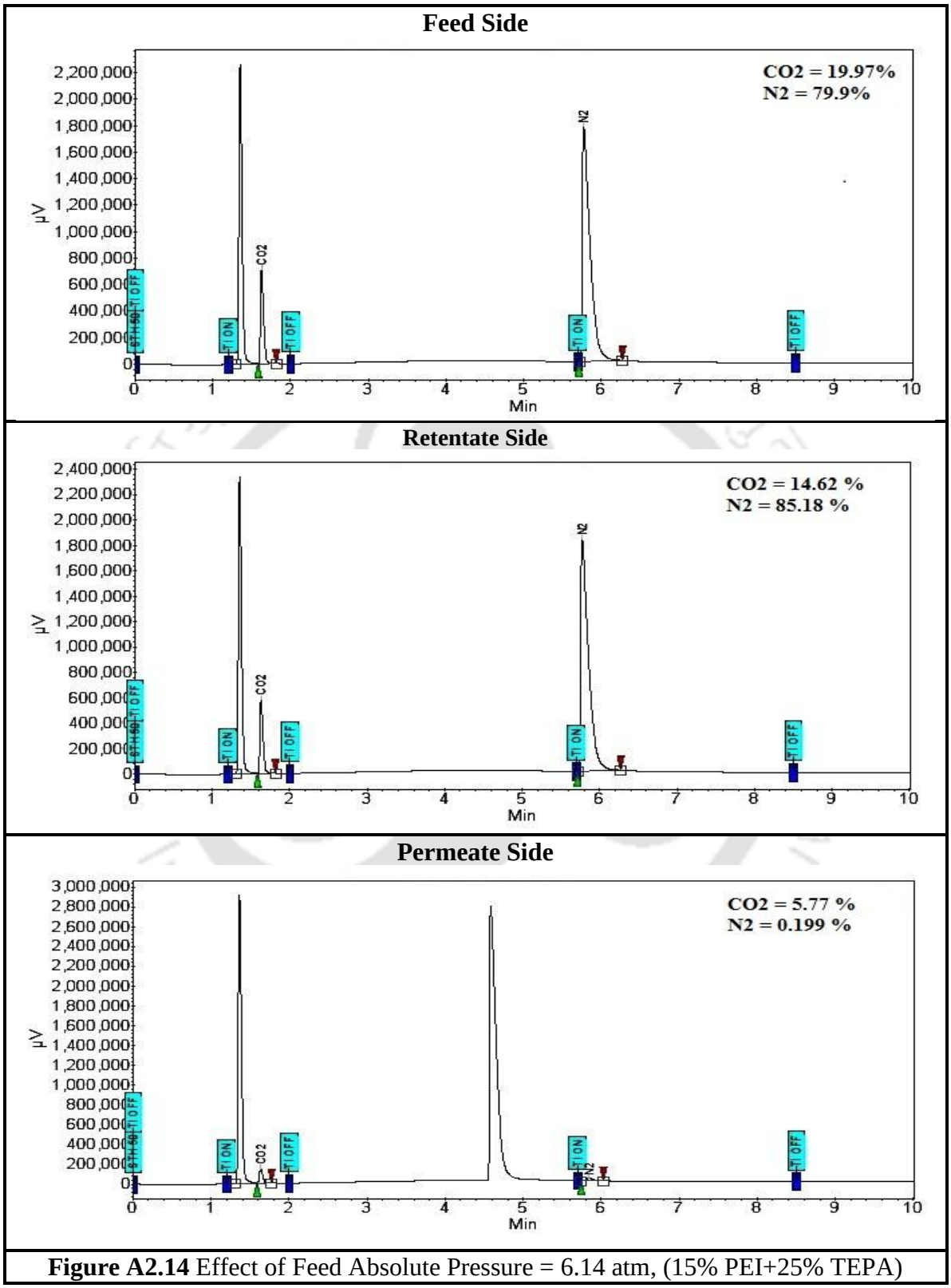

Figure A2.14 Effect of Feed Absolute Pressure = 6.14 atm, (15% PEI+25% TEPA)

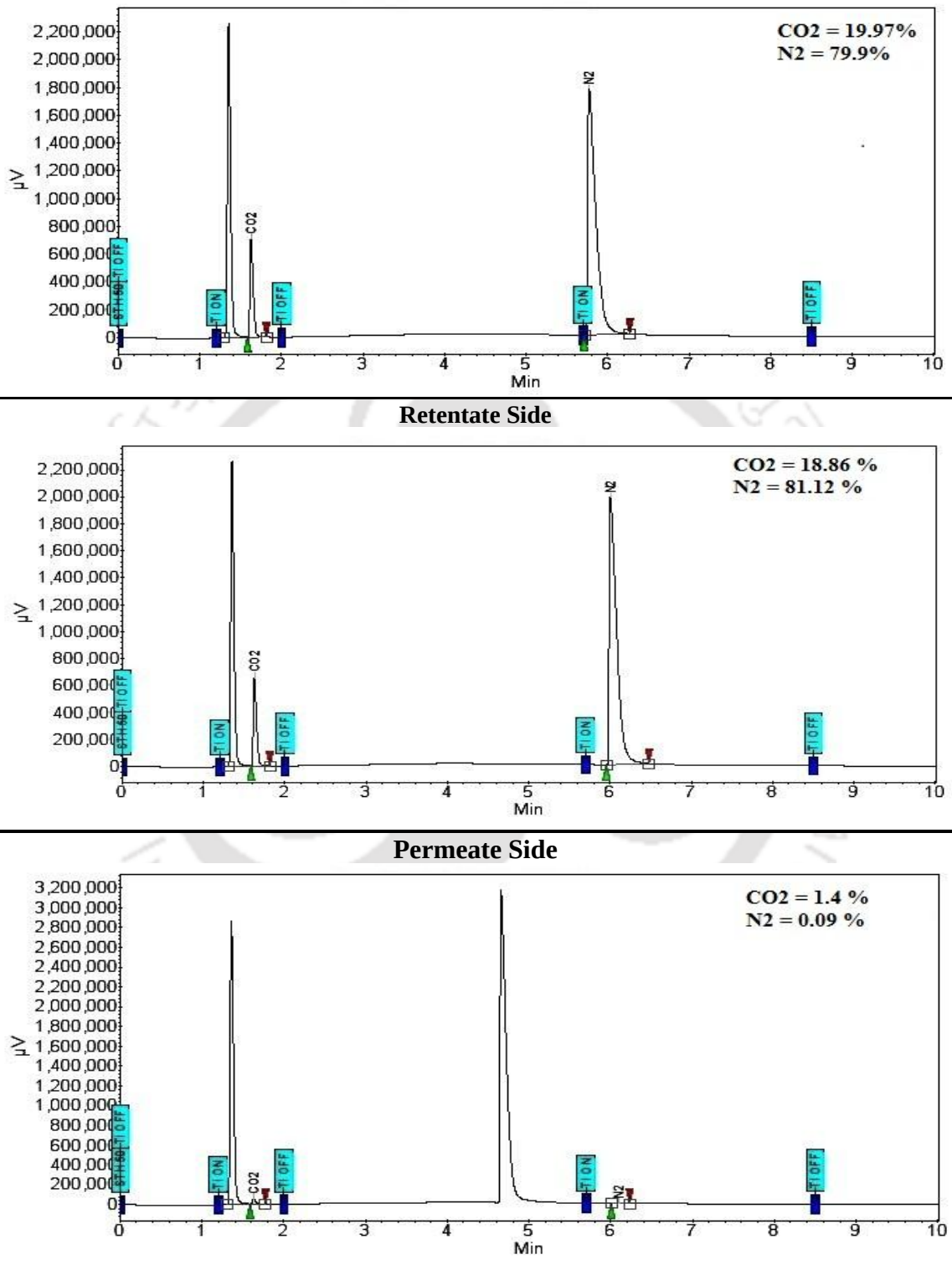

Figure A2.15 Effect of sweep side water flow rate = 0.02 ml/min, (15% PEI+25% TEPA)

Feed Side

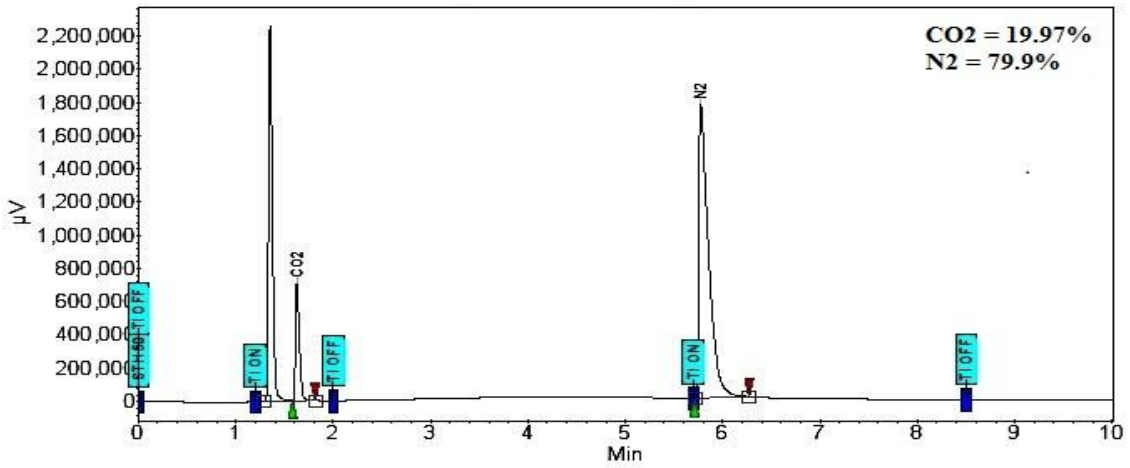

Retentate Side

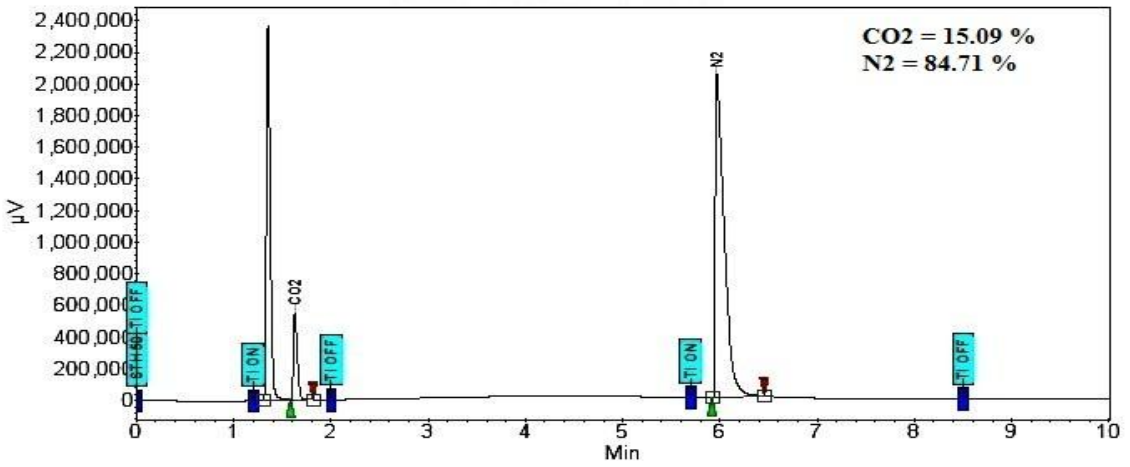

Permeate Side

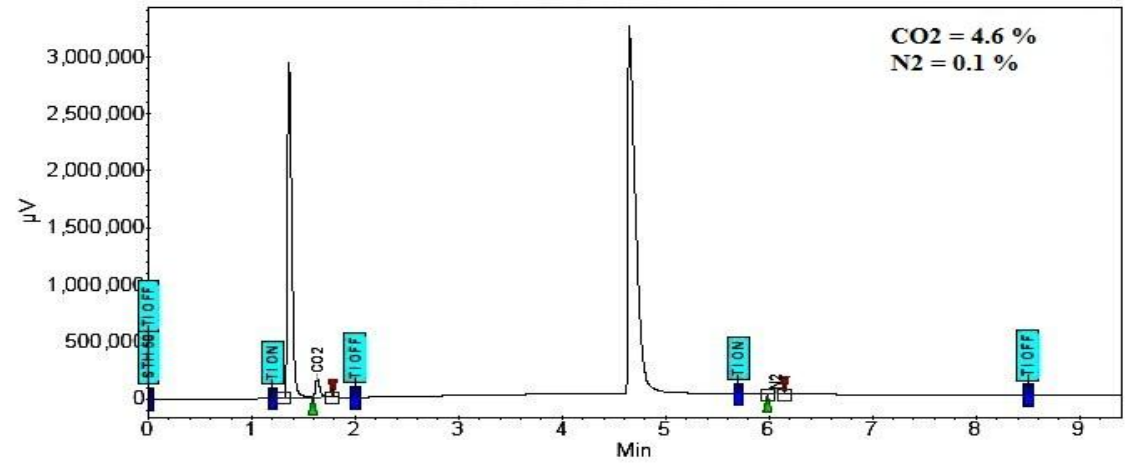

Figure A2.16 Effect of sweep side water flow rate = 0.04 ml/min, (15% PEI+25% TEPA)

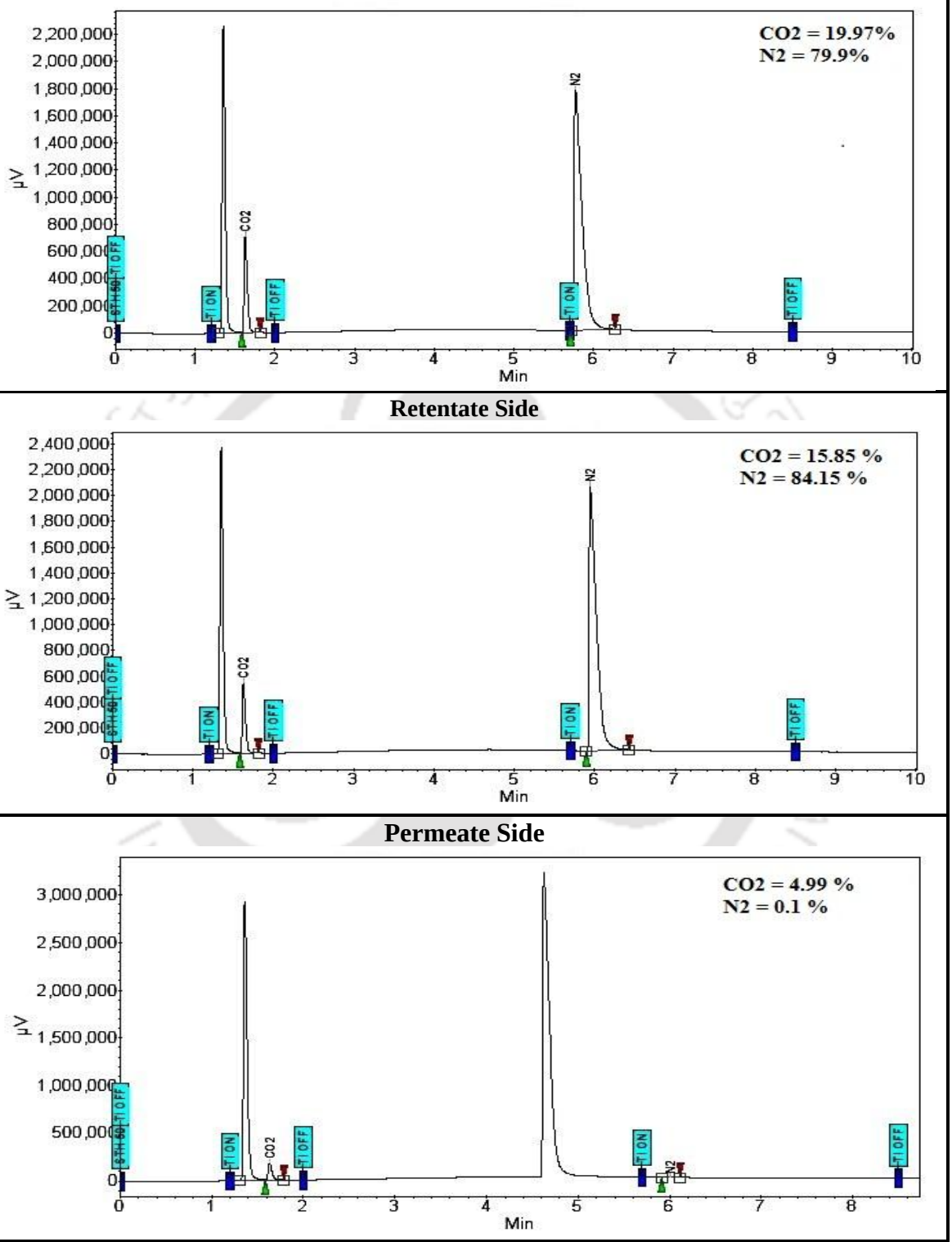

Figure A2.17 Effect of sweep side water flow rate = 0.06 ml/min, (15% PEI+25% TEPA)

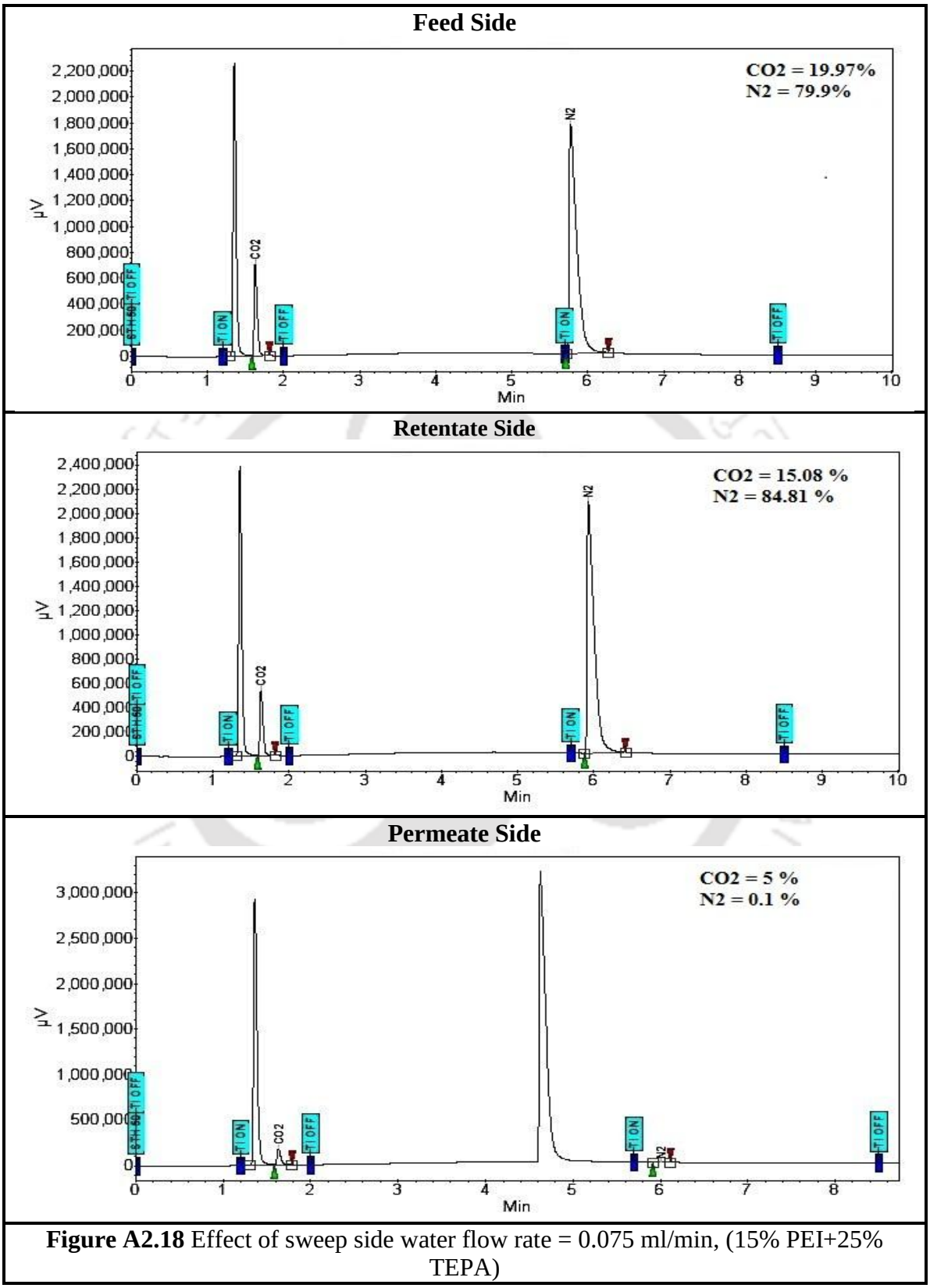

Figure A2.18 Effect of sweep side water flow rate = 0.075 ml/min, (15% PEI+25% TEPA)

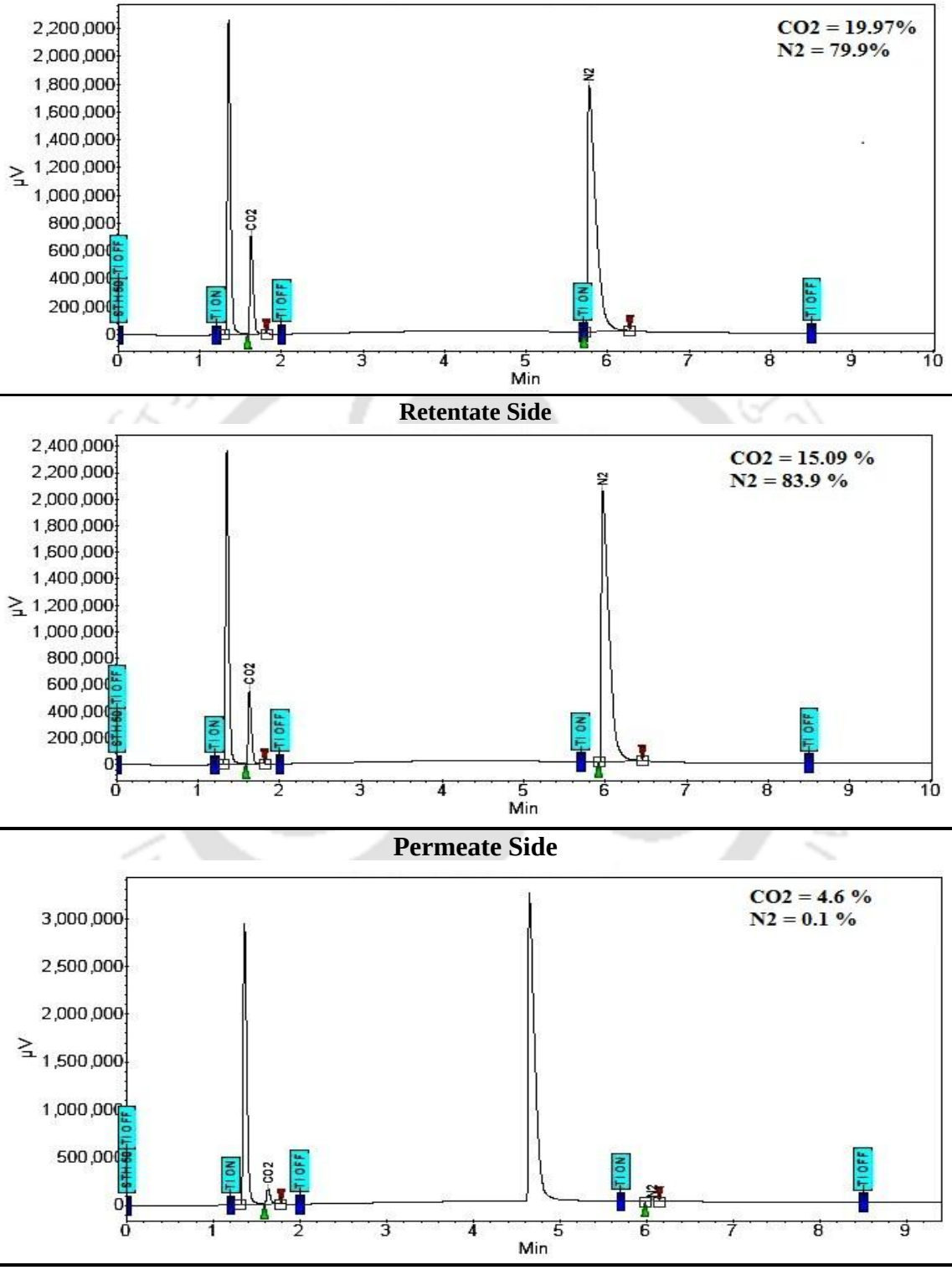

Figure A2.19 Effect of Temperature = 90°C, (15% PEI+25% TEPA)

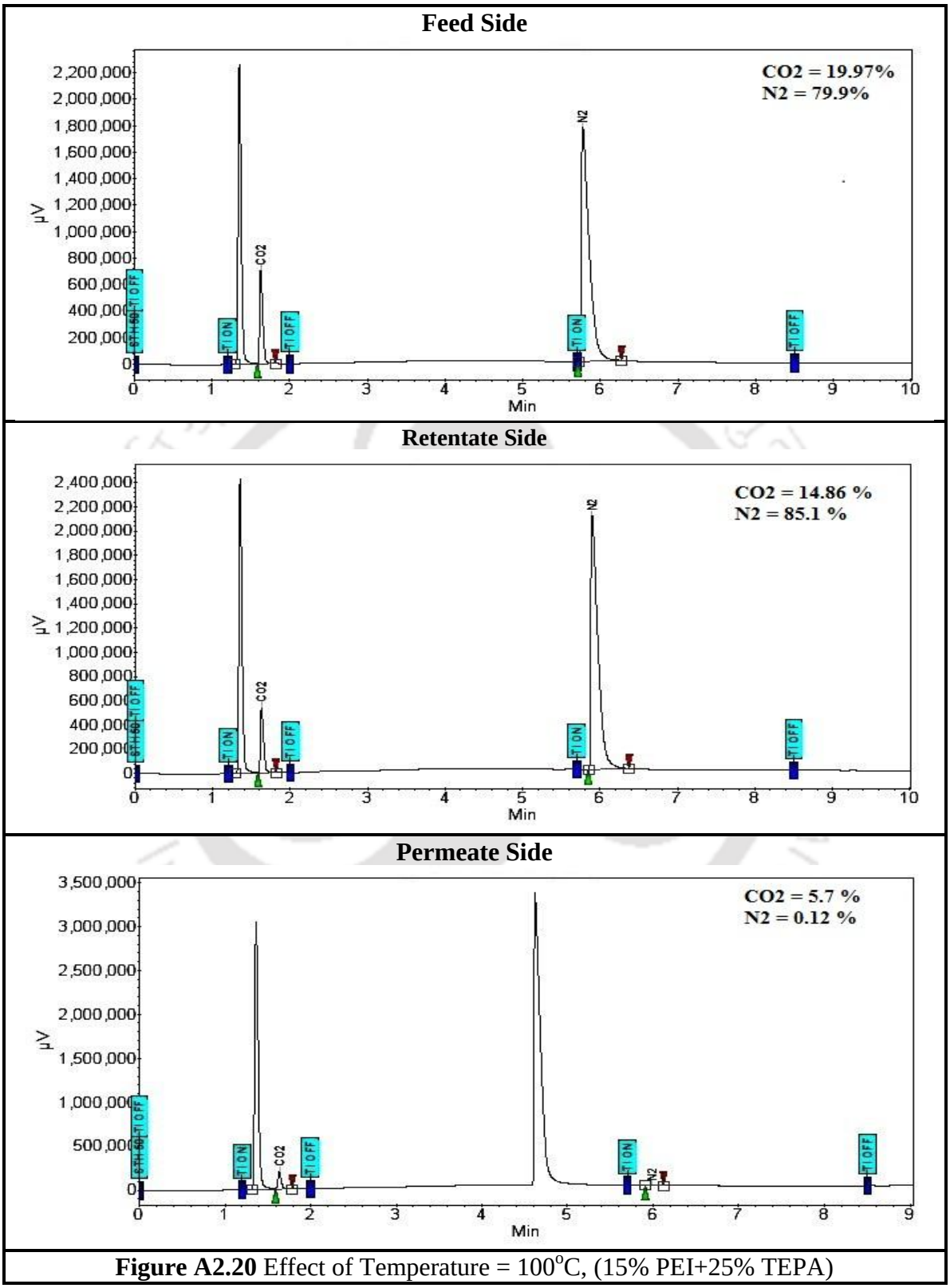

Figure A2.20 Effect of Temperature = 100°C, (15% PEI+25% TEPA)

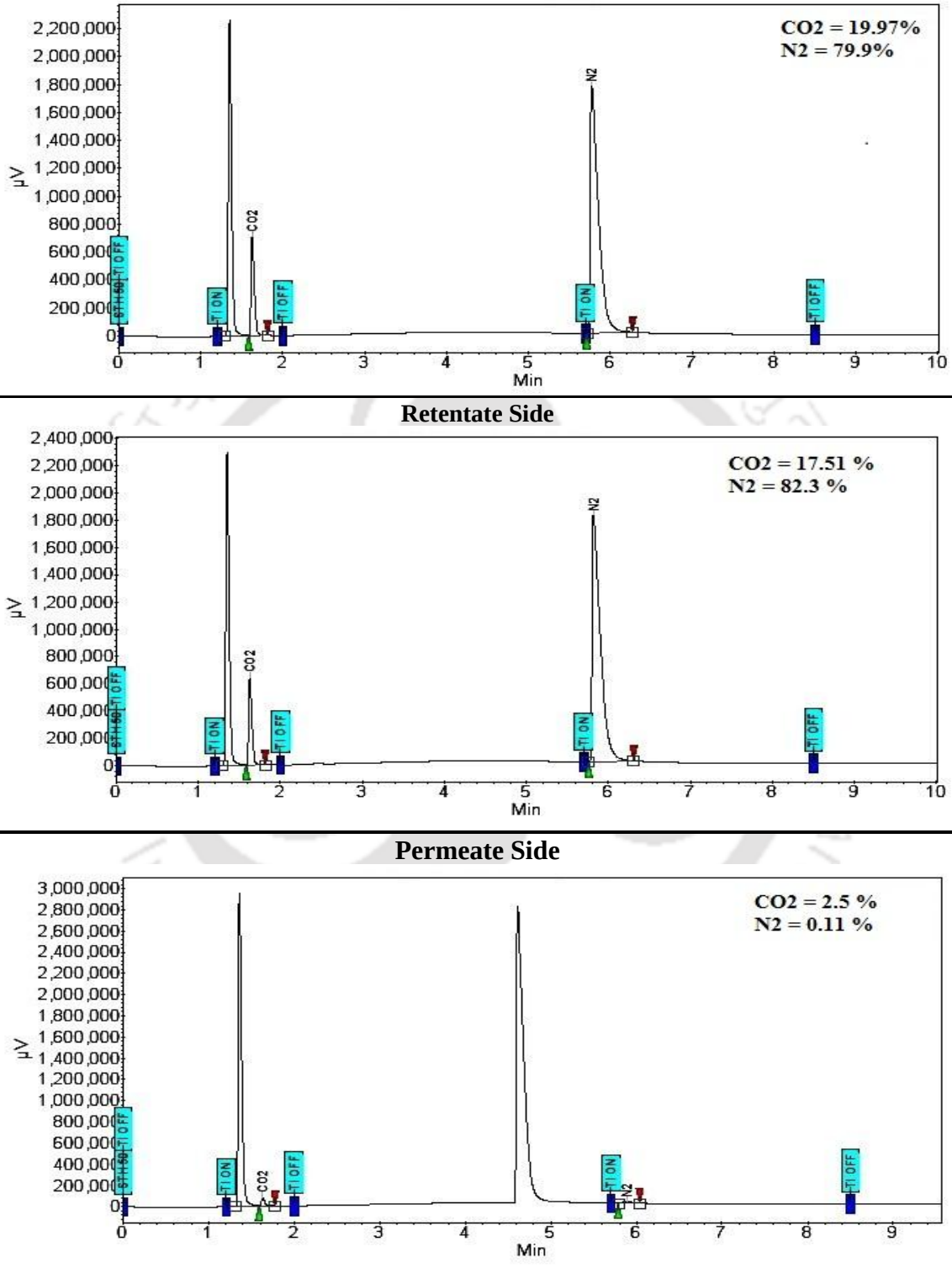

Figure A2.21 Effect of Temperature = 115°C, (15% PEI+25% TEPA)

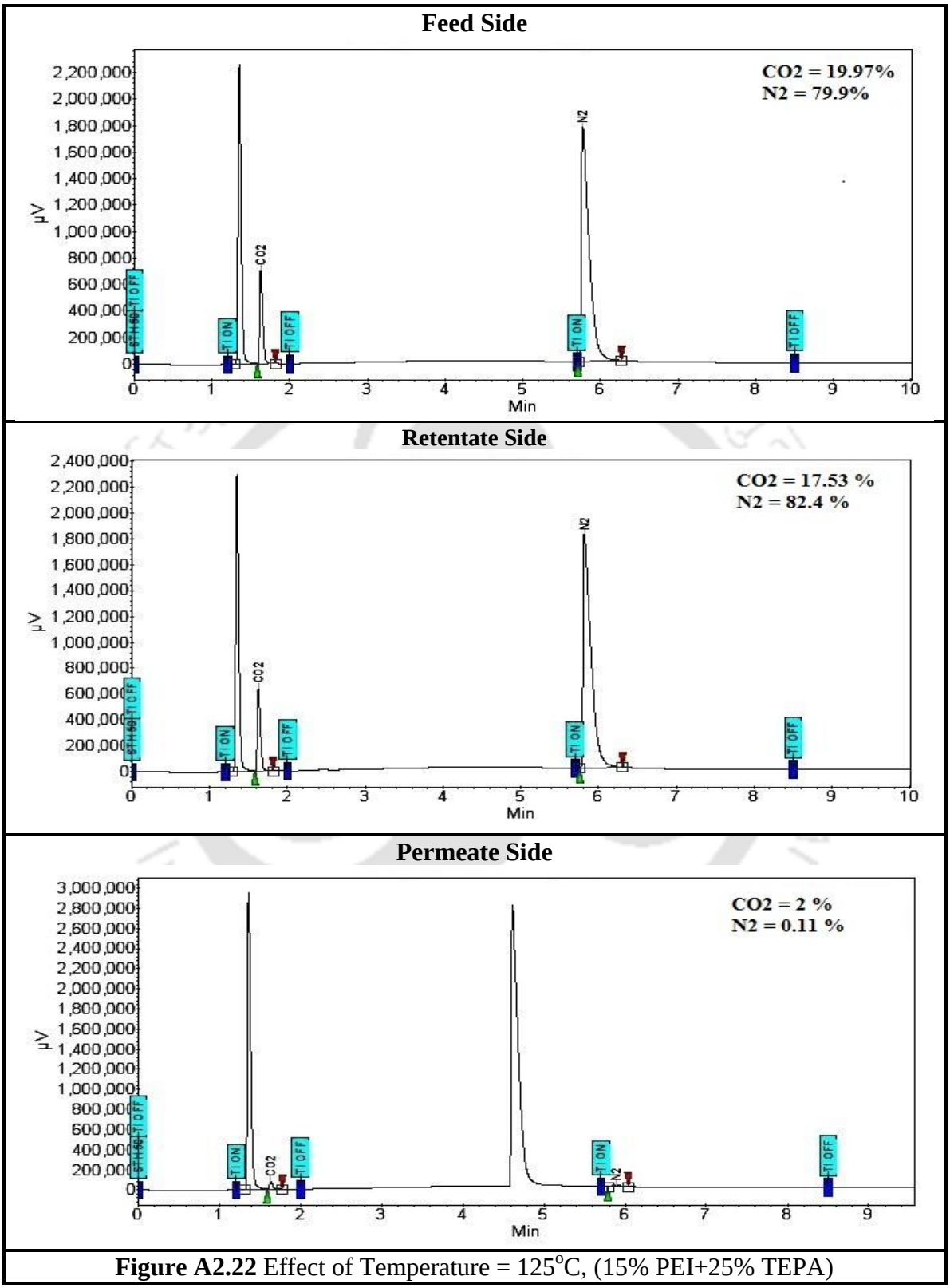

Figure A2.22 Effect of Temperature = 125°C, (15% PEI+25% TEPA)

A2.9 Gas Chromatography Data of Crosslinked-PVA-PVP Membrane Containing PEI and PEHA (Effect of Thickness)

Three different active layer compositions were prepared mention below:

1. 41.66 wt% PVA + 8.33 wt% PVP + 10 wt% KOH + 15 wt% PEI + 25 wt% PEHA with 60 mol% degree of cross linking by HCHO

Composition one has three different active layer membranes like 40, 60 and 75 micron.

All the permeation experiment was done exactly same operating condition. Feed side and sweep side absolute pressure was maintained constant at around 2.8 and 1.15 atm, respectively. Temperature was kept constant at 95^{o}C along with constant water flow rate at both sides (feed/sweep = 0.03/0.04 cm^3/min). Both feed gas (20% CO_2 balance N_2 on dry basis) and carrier gas (Ar) flow rates were maintained at 30 cm^3/min throughout the experiment.

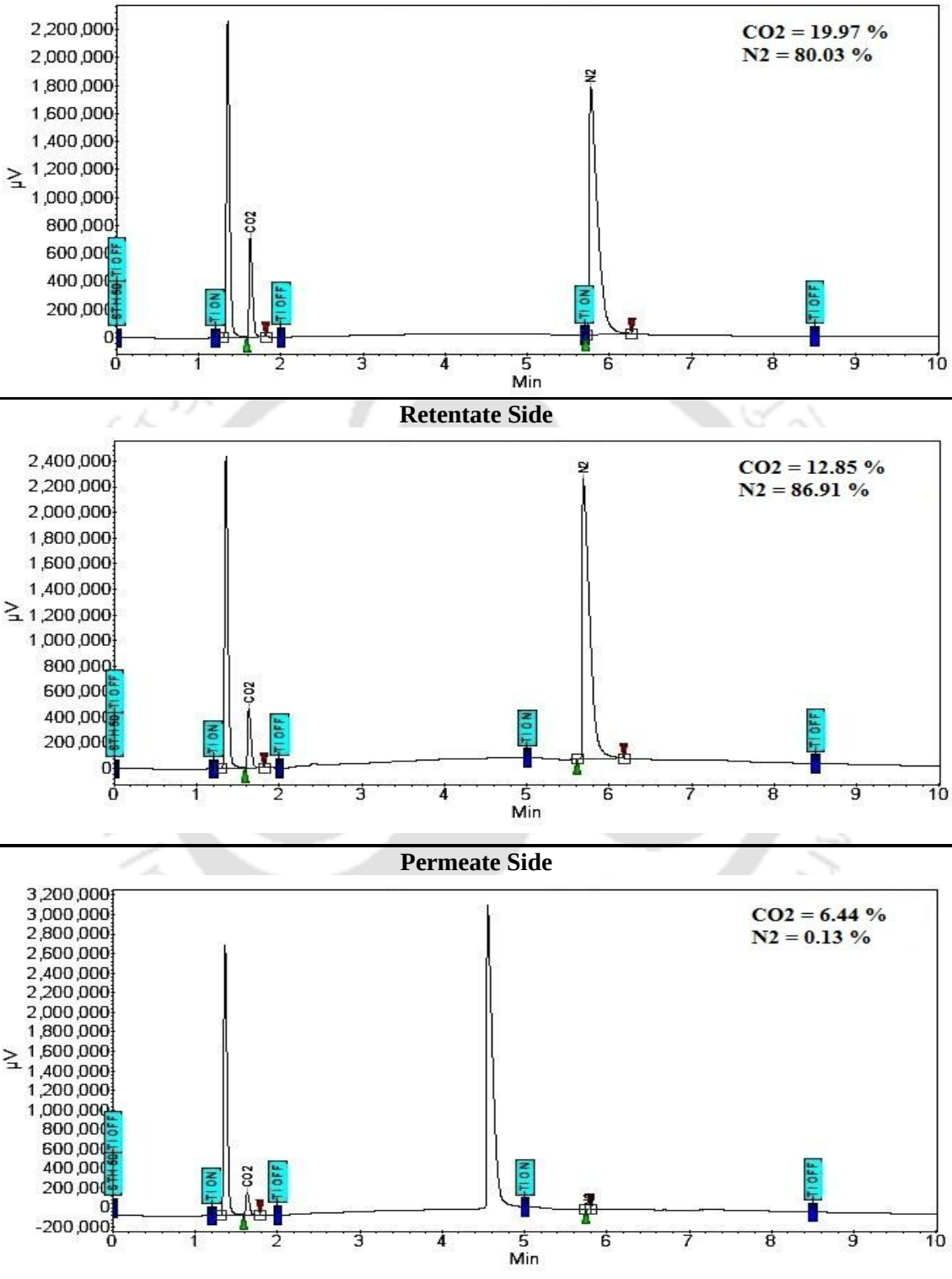

Figure A2.23 Effect of active layer thickness of 40 micron (15 wt% PEI + 25 wt% PEHA)

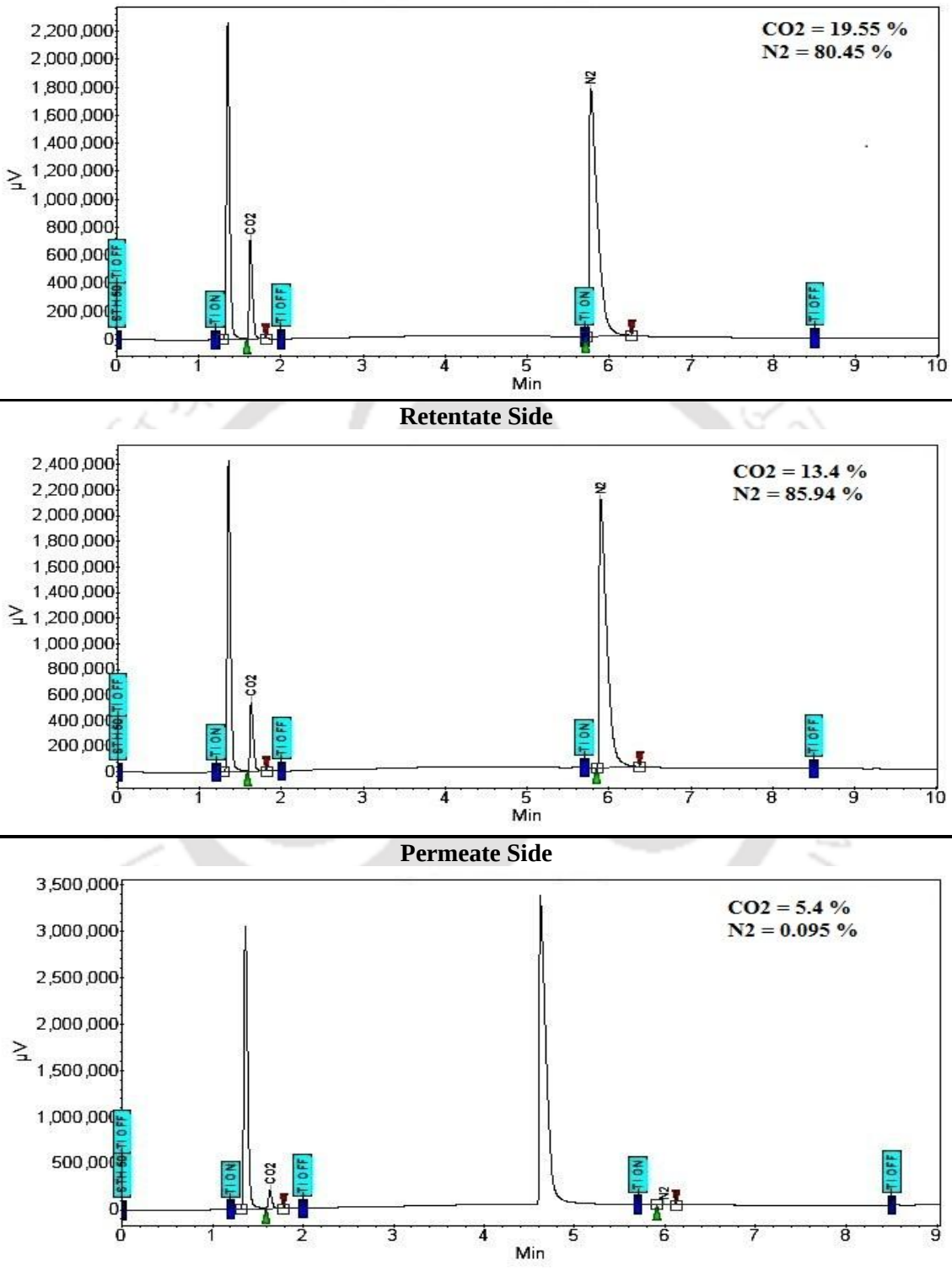

Figure A2.24 Effect of active layer thickness of 60 micron (15 wt% PEI + 25 wt% PEHA)

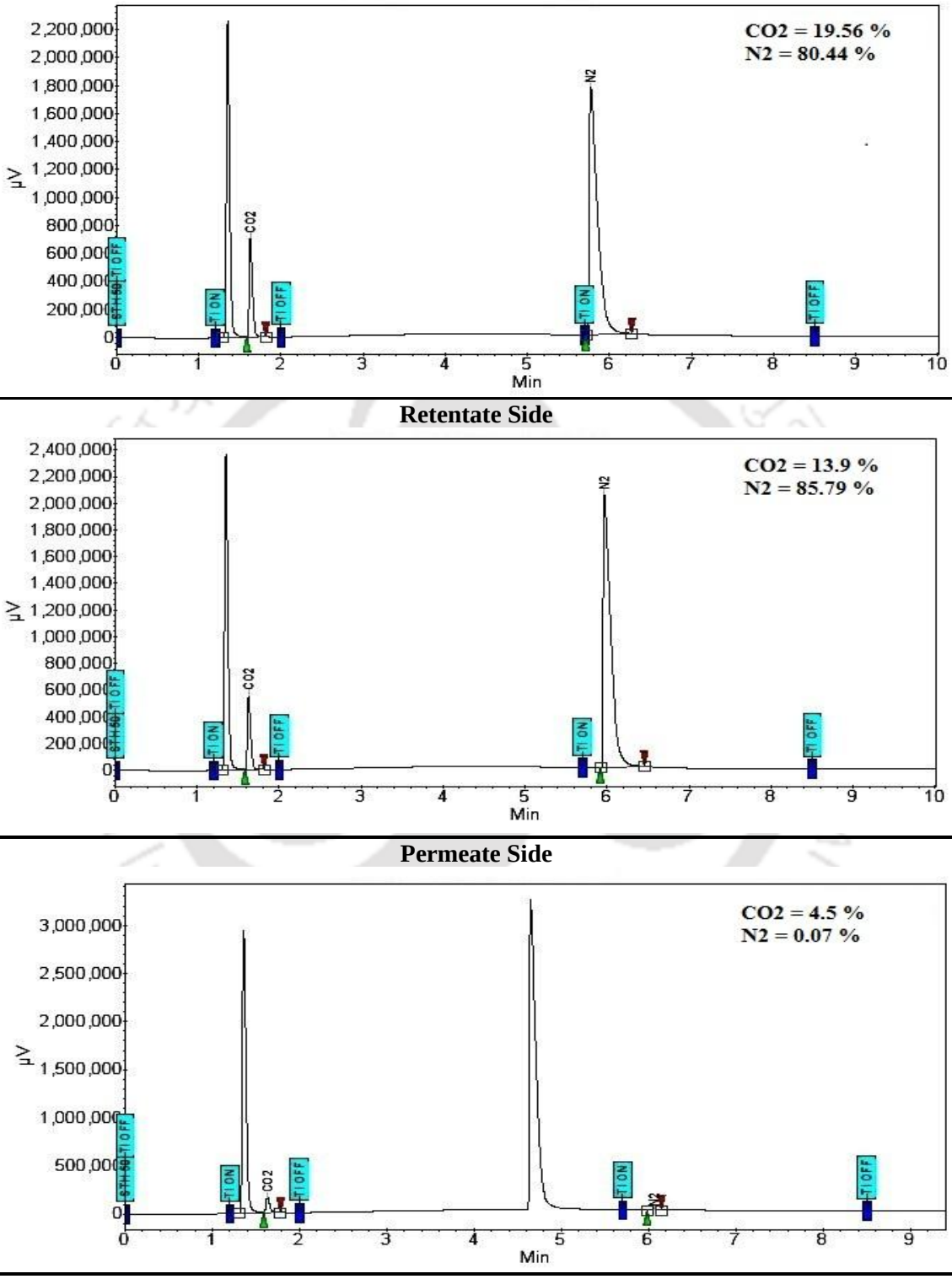

Figure A2.25 Effect of active layer thickness of 75 micron (15 wt% PEI + 25 wt% PEHA)

A2.10 Gas Chromatography Data of Crosslinked-PVA-PVP Membrane Containing PEI and PEHA (Permeation Experiment)

Permeation experiment of 41.66 wt% PVA + 8.33 wt% PVP + 10 wt% KOH + 15 wt% PEI + 25 wt% PEHA with 60 mol% degree of cross linking by HCHO membrane with an active layer thickness of 40 micron.

Effects of Feed Pressure on Separation Performance: Feed absolute pressure was varied from 1.7 to 6.2 atm, maintaining other operating conditions constant (temperature = 100^{o}C, sweep side absolute pressure = 1.15 atm and feed side / sweep side water flow rate = 0.03 / 0.04 cm^{3}/min).

Effects of Sweep Side Water Flow Rate on Separation Performance: Sweep side water flow rate was varied from 0.02 to 0.075 cm^{3}/min, maintaining other operating conditions constant (temperature = 90^{o}C, sweep side absolute pressure = 1.15 atm and feed side water flow rates = 0.03 cm^{3}/min).

Effects of Temperature on Separation Performance: Temperature was varied from 90 to 125^{o}C, maintaining other operating conditions constant (feed / sweep side absolute pressure = 2.7 / 1.15 atm and feed / sweep side water flow rate = 0.03 / 0.04 cm^{3}/min).

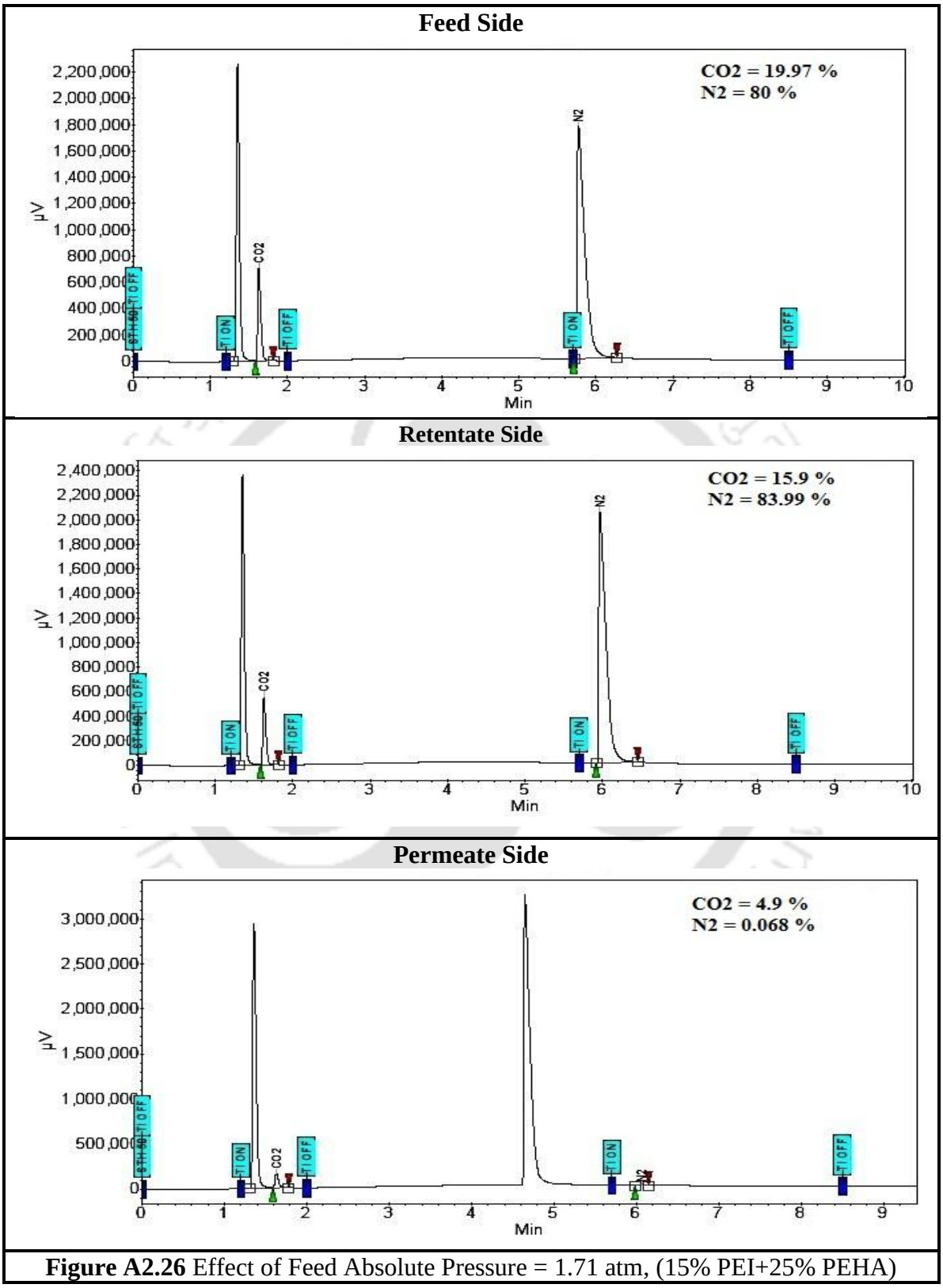

Figure A2.26 Effect of Feed Absolute Pressure = 1.71 atm, (15% PEI+25% PEHA)

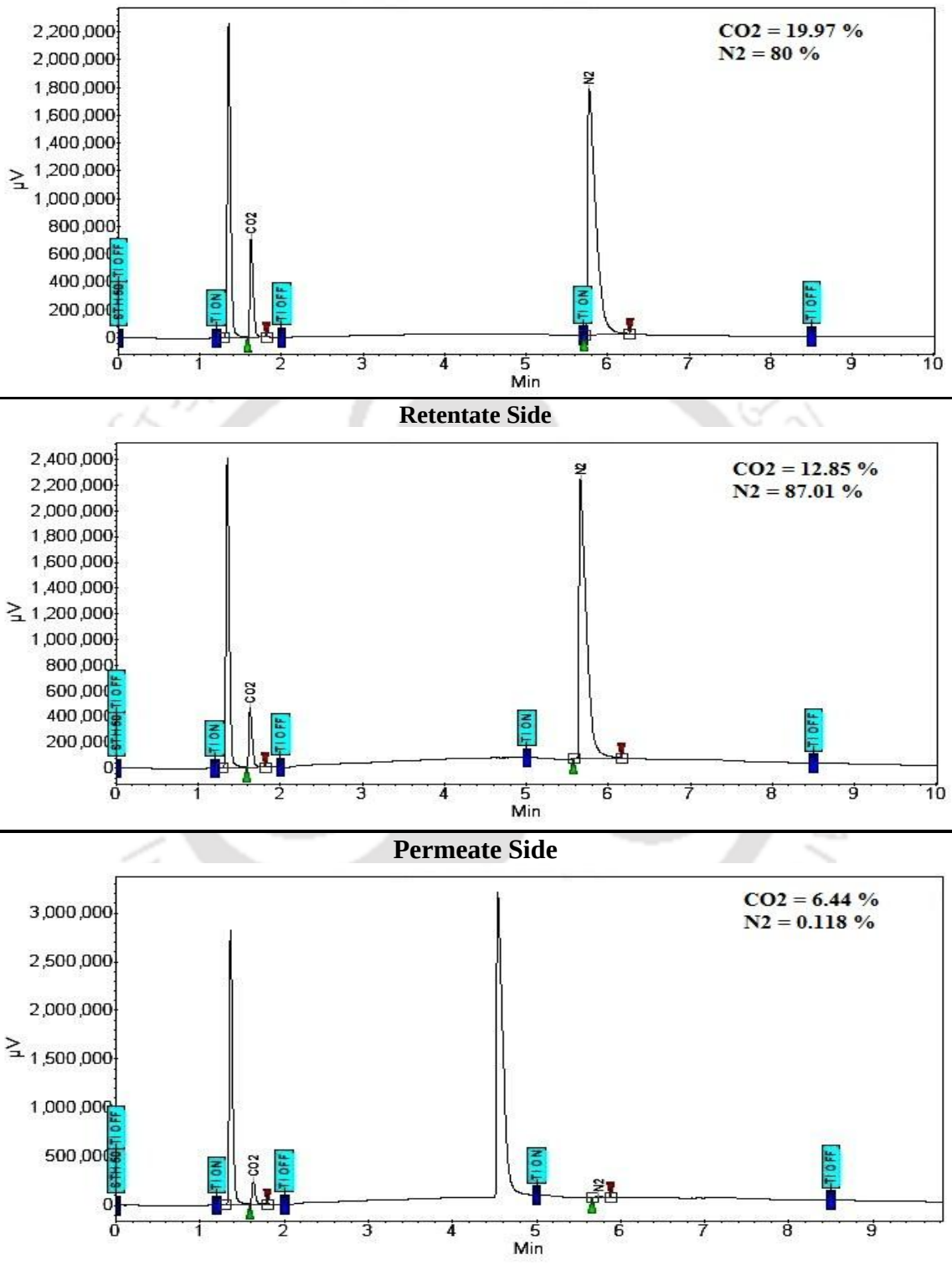

Figure A2.27 Effect of Feed Absolute Pressure = 2.76 atm, (15% PEI+25% PEHA)

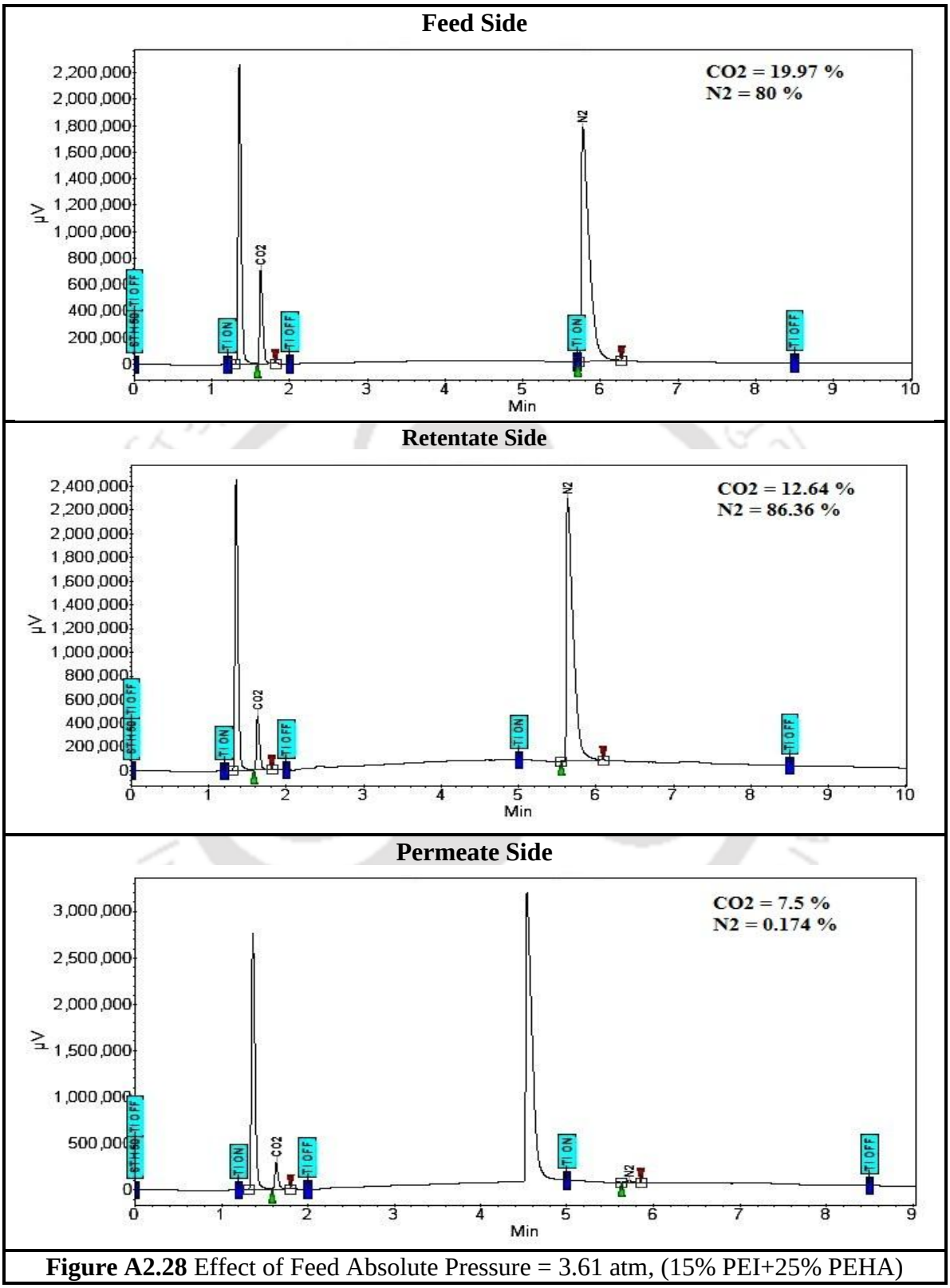

Figure A2.28 Effect of Feed Absolute Pressure = 3.61 atm, (15% PEI+25% PEHA)

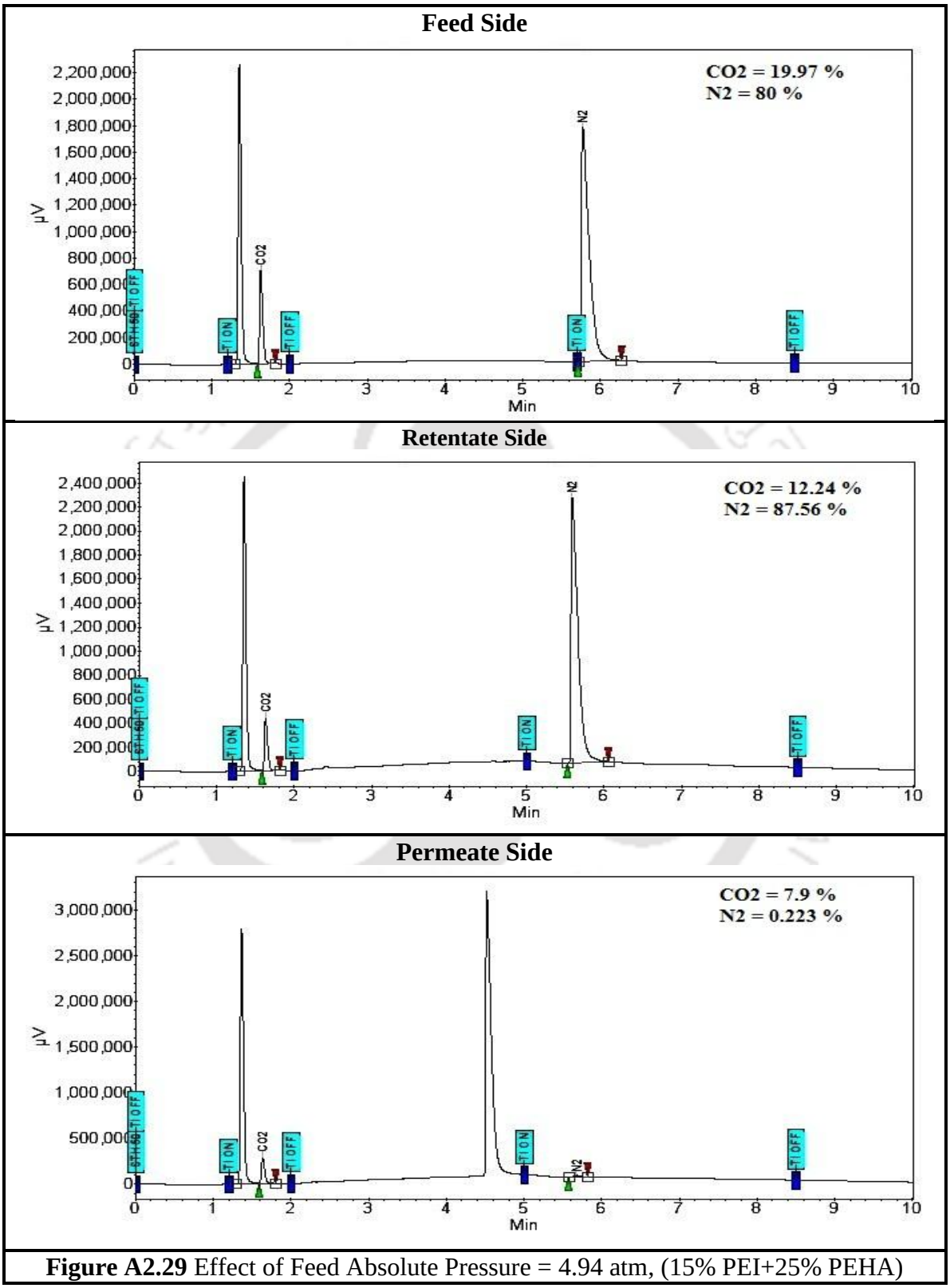

Figure A2.29 Effect of Feed Absolute Pressure = 4.94 atm, (15% PEI+25% PEHA)

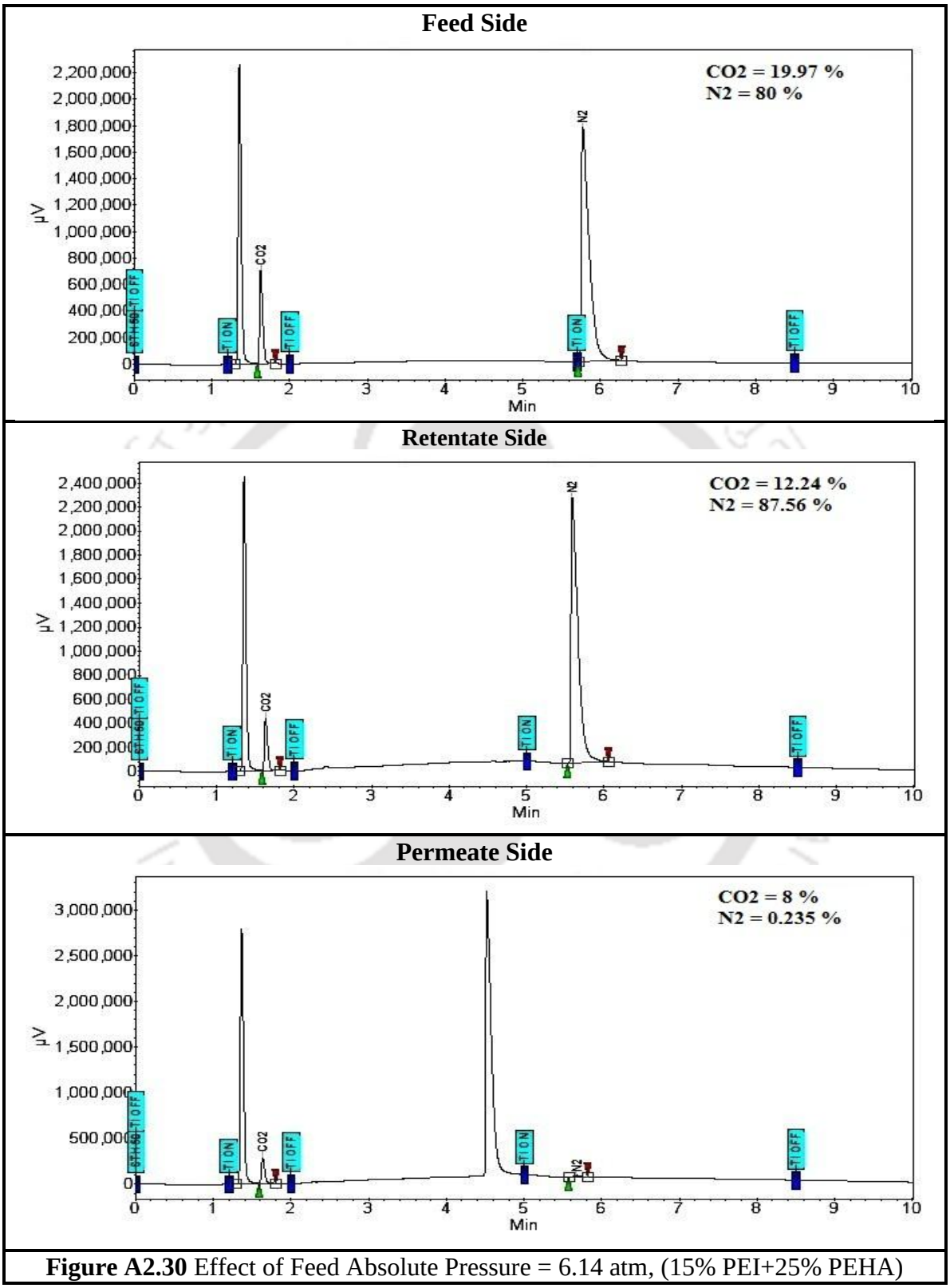

Figure A2.30 Effect of Feed Absolute Pressure = 6.14 atm, (15% PEI+25% PEHA)

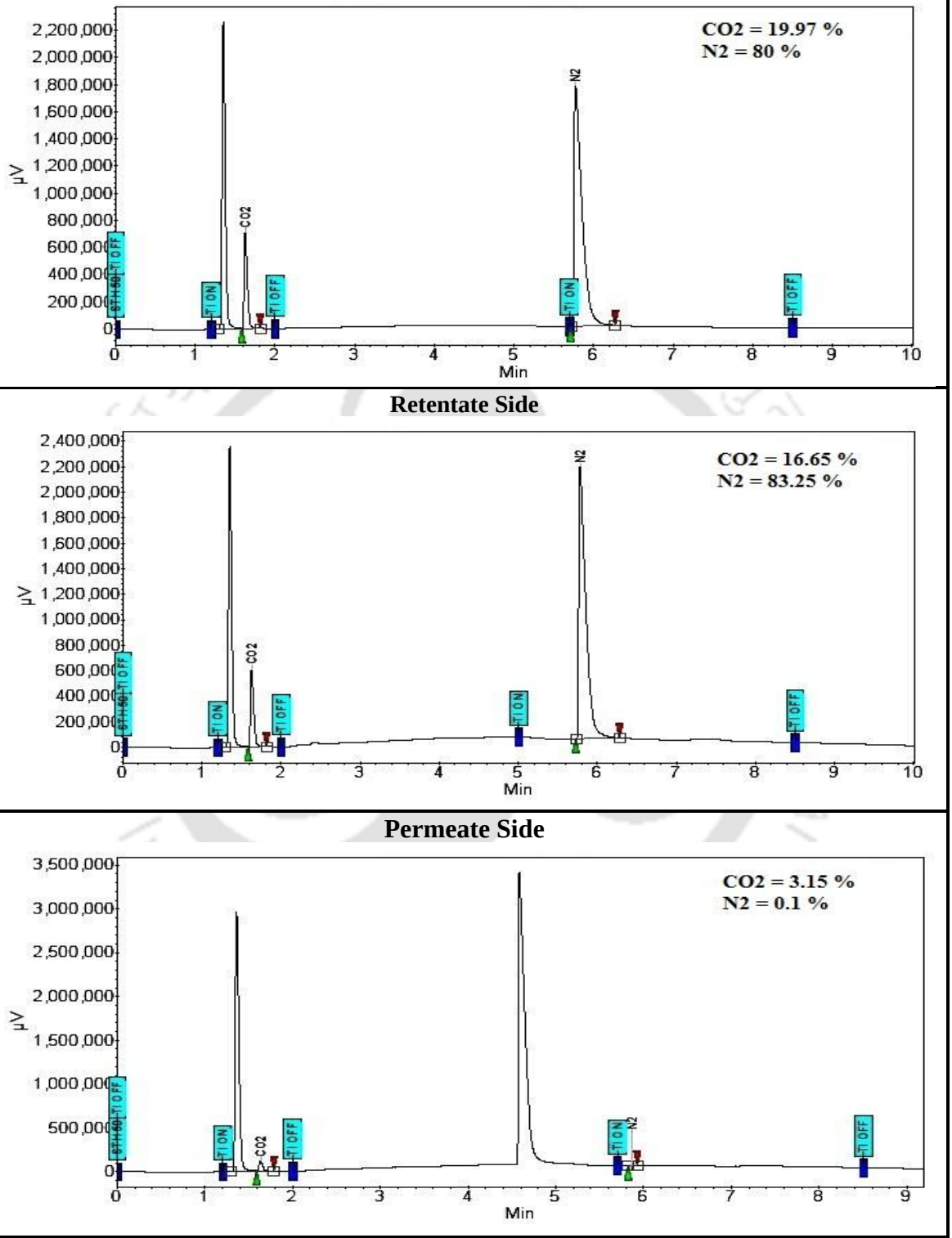

Figure A2.31 Effect of sweep side water flow rate = 0.02 ml/min, (15% PEI+25% PEHA)

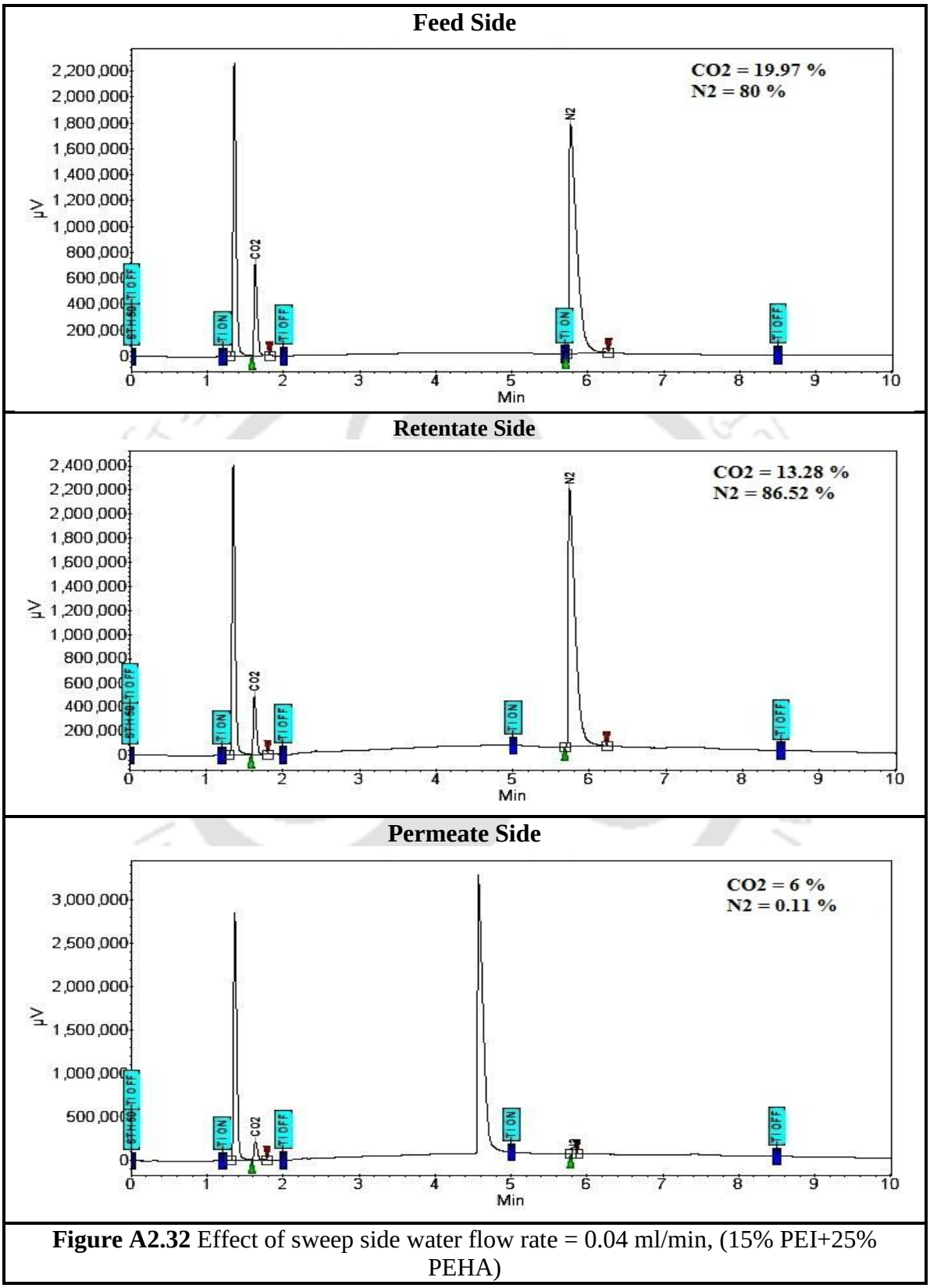

Figure A2.32 Effect of sweep side water flow rate = 0.04 ml/min, (15% PEI+25% PEHA)

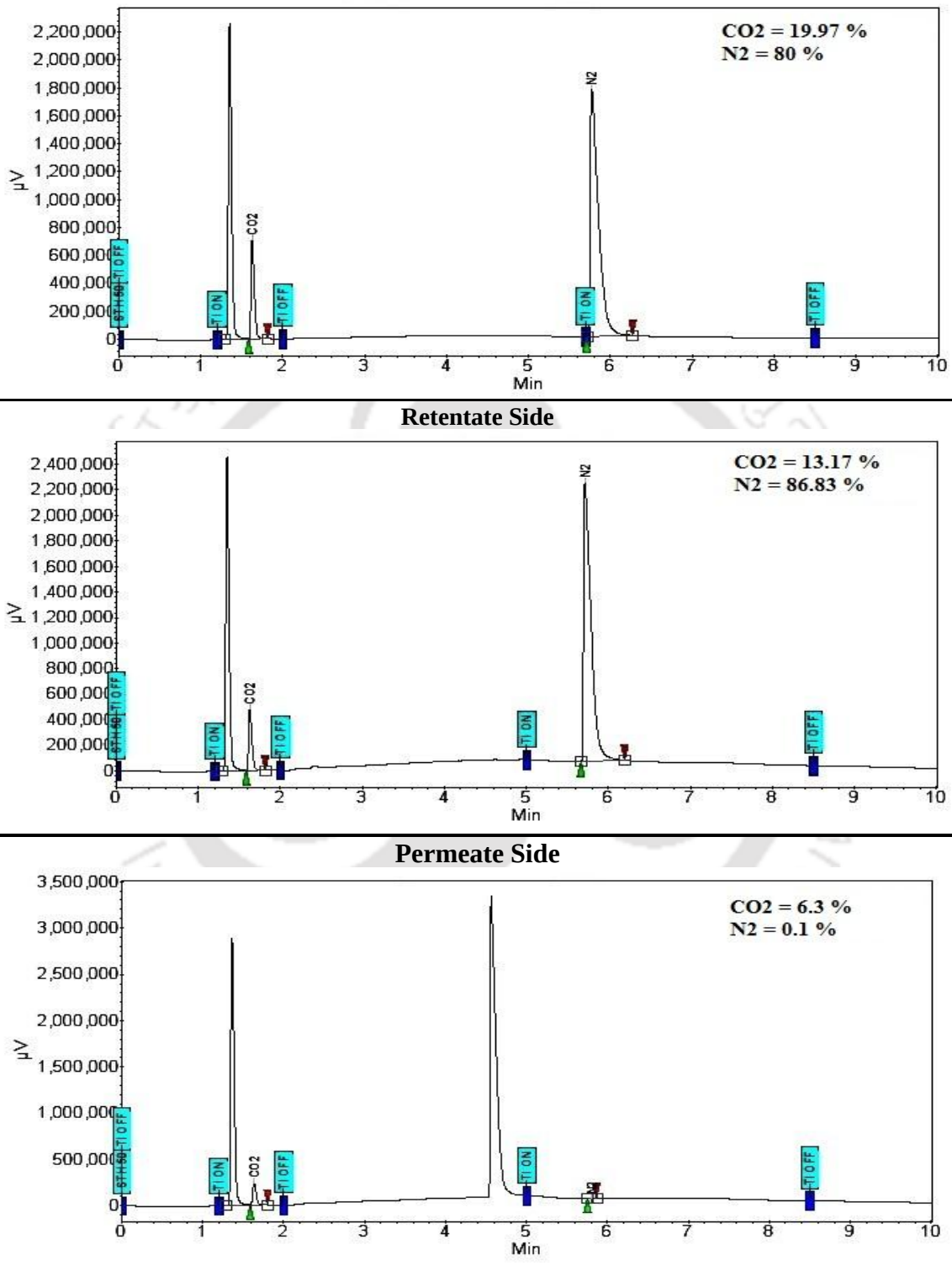

Figure A2.33 Effect of sweep side water flow rate = 0.06 ml/min, (15% PEI+25% PEHA)

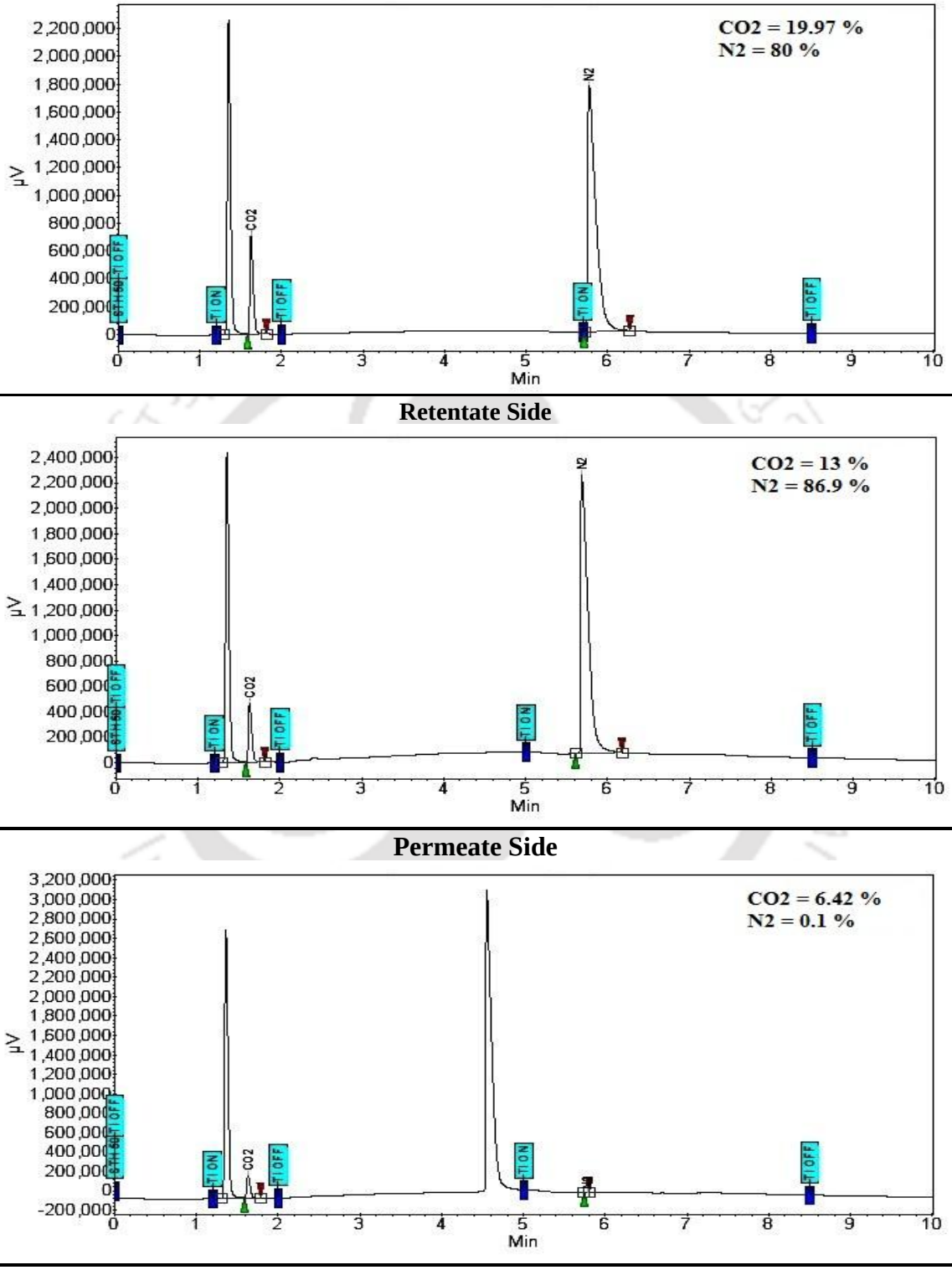

Figure A2.34 Effect of sweep side water flow rate = 0.075 ml/min, (15% PEI+25% PEHA)

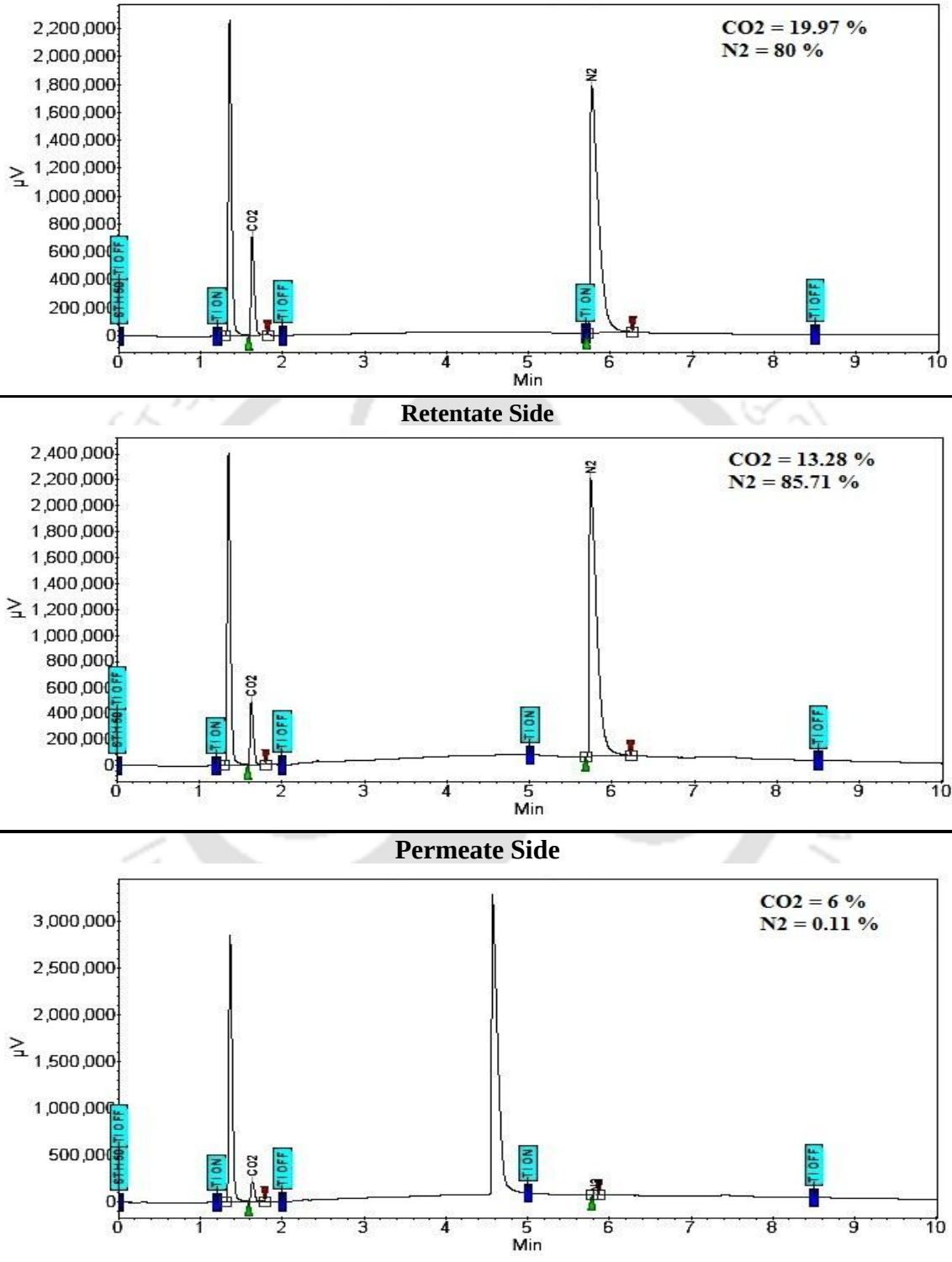

Figure A2.35 Effect of Temperature = 90^{o}C, (15% PEI+25% PEHA)

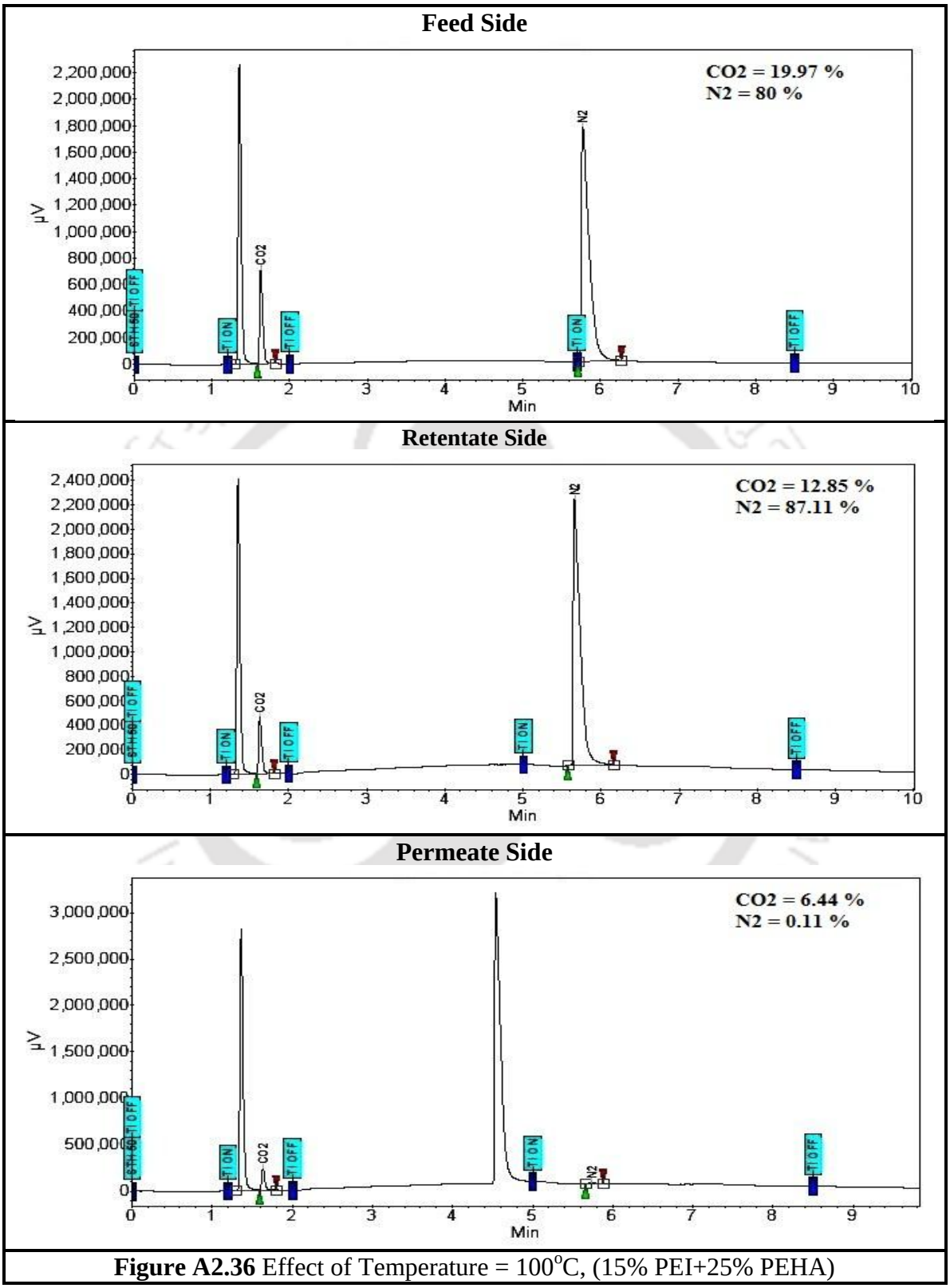

Figure A2.36 Effect of Temperature = 100°C, (15% PEI+25% PEHA)

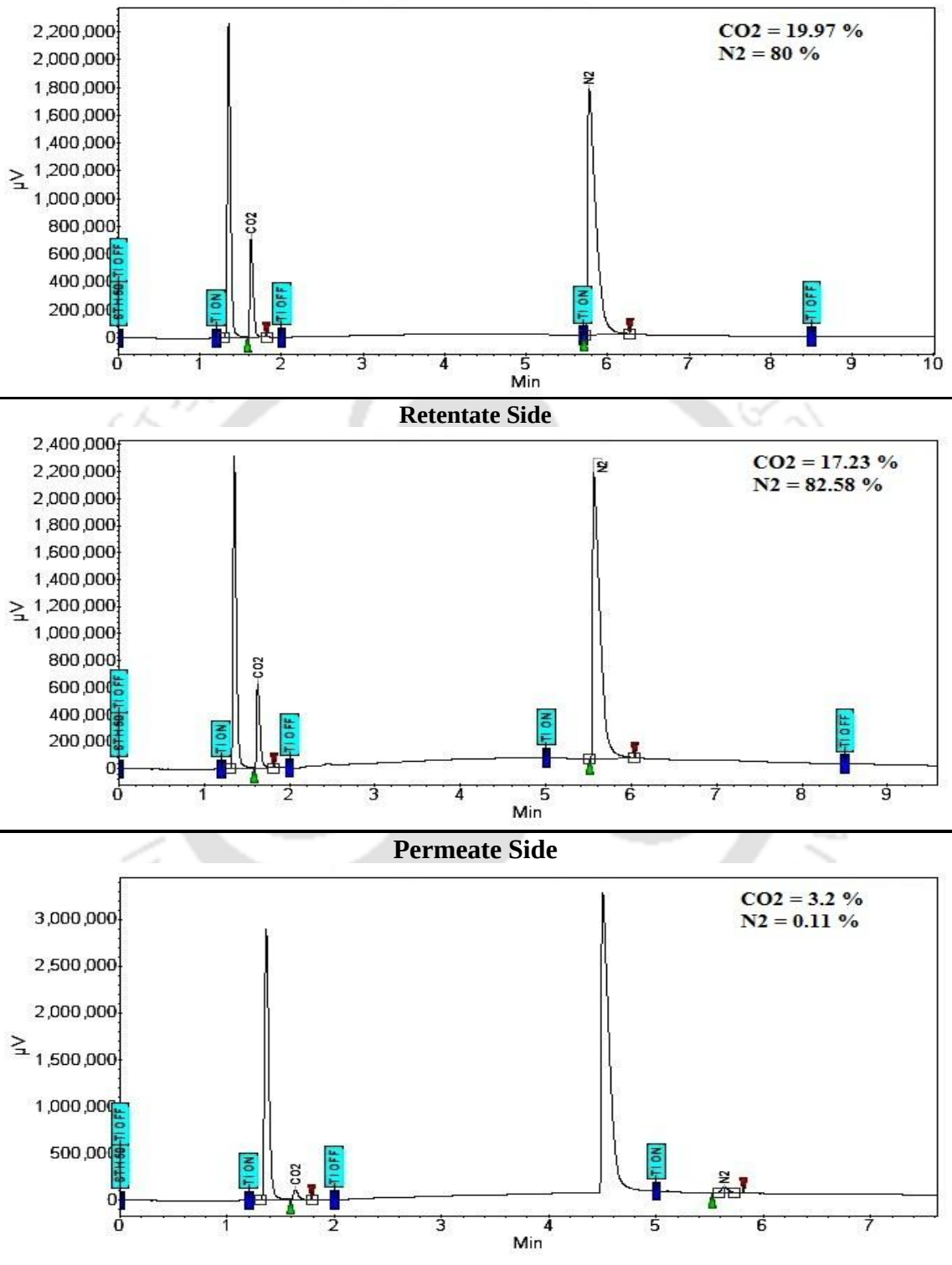

Figure A2.37 Effect of Temperature = 115°C, (15% PEI+25% PEHA)

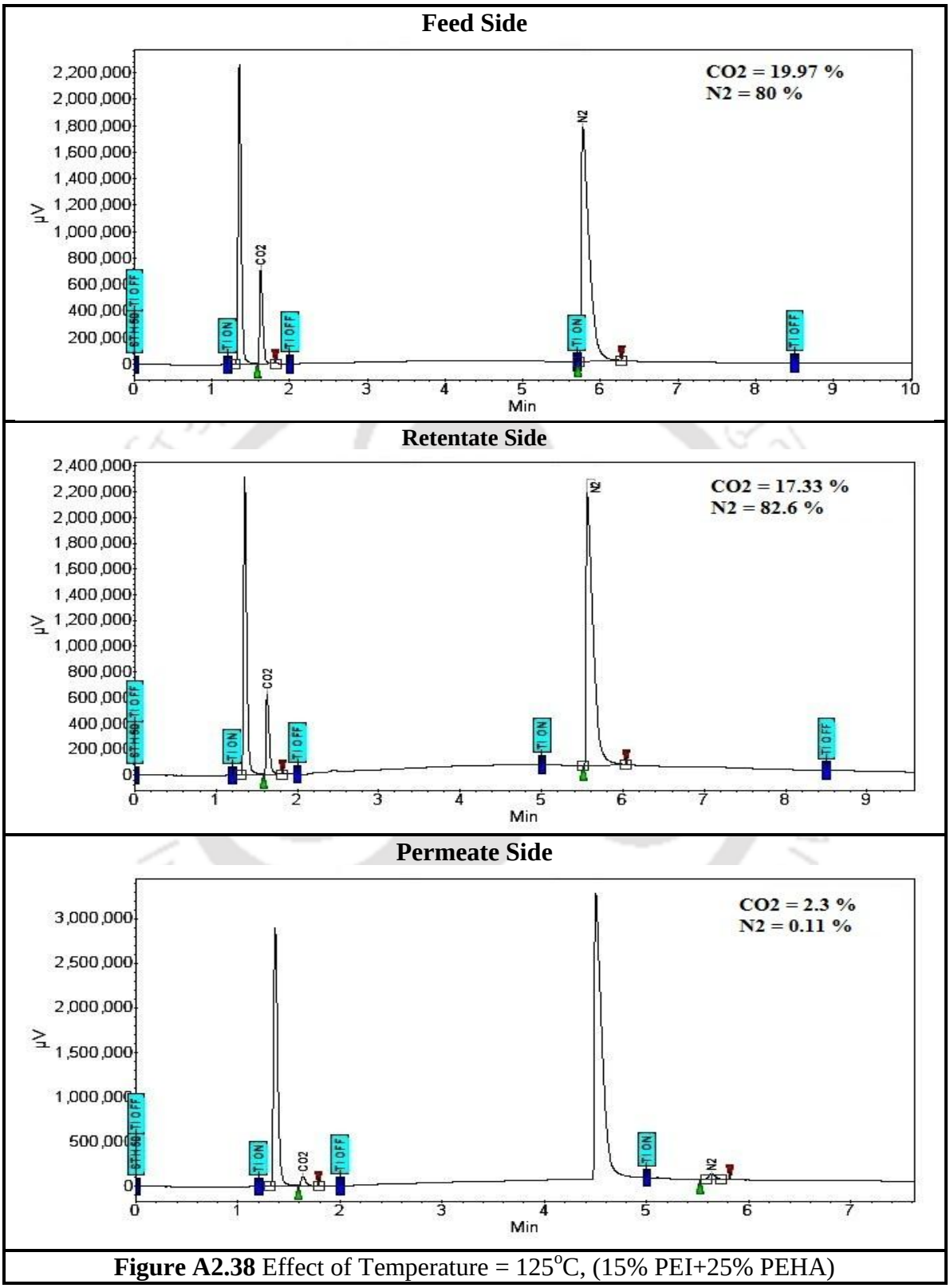

Figure A2.38 Effect of Temperature = 125°C, (15% PEI+25% PEHA)

A2.11 Gas Chromatography Data of Crosslinked-PVA-PVP Membrane Containing PAA and PEHA (Effect of Thickness)

Three different active layer compositions were prepared mention below:

1. 41.66 wt% PVA + 8.33 wt% PVP + 10 wt% KOH + 25 wt% PAA + 15 wt% PEHA with 60 mol% degree of cross linking by HCHO
2. 41.66 wt% PVA + 8.33 wt% PVP + 10 wt% KOH + 15 wt% PAA + 25 wt% PEHA with 60 mol% degree of cross linking by HCHO
3. 41.66 wt% PVA + 8.33 wt% PVP + 10 wt% KOH + 40 wt% PAA with 60 mol% degree of cross linking by HCHO

Composition one has three different active layer membranes like 42, 55 and 78 micron. Similarly composition two has also three different active layer membranes like 41, 62 and 81 micron. And composition three has only one active layer membrane like 45 micron.

All the permeation experiment was done exactly same operating condition. Feed side and sweep side absolute pressure was maintained constant at around 2.8 and 1.15 atm, respectively. Temperature was kept constant at 95^{o}C along with constant water flow rate at both sides (feed/sweep = 0.03/0.04 cm^3/min). Both feed gas (20% CO_2 balance N_2 on dry basis) and carrier gas (Ar) flow rates were maintained at 30 cm^3/min throughout the experiment.

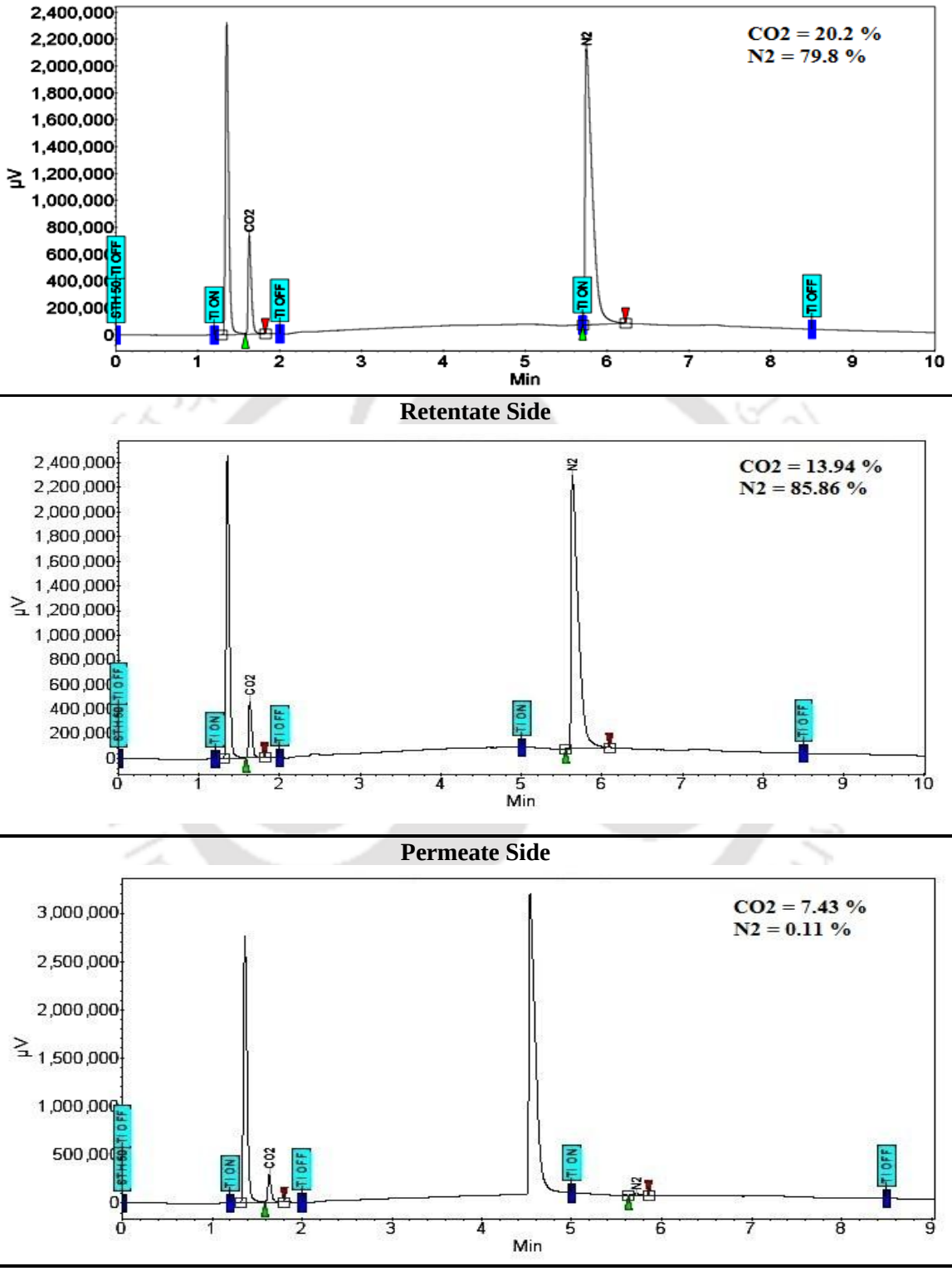

Figure A2.39 Effect of active layer thickness of 42 micron (25 wt% PAA + 15 wt% PEHA)

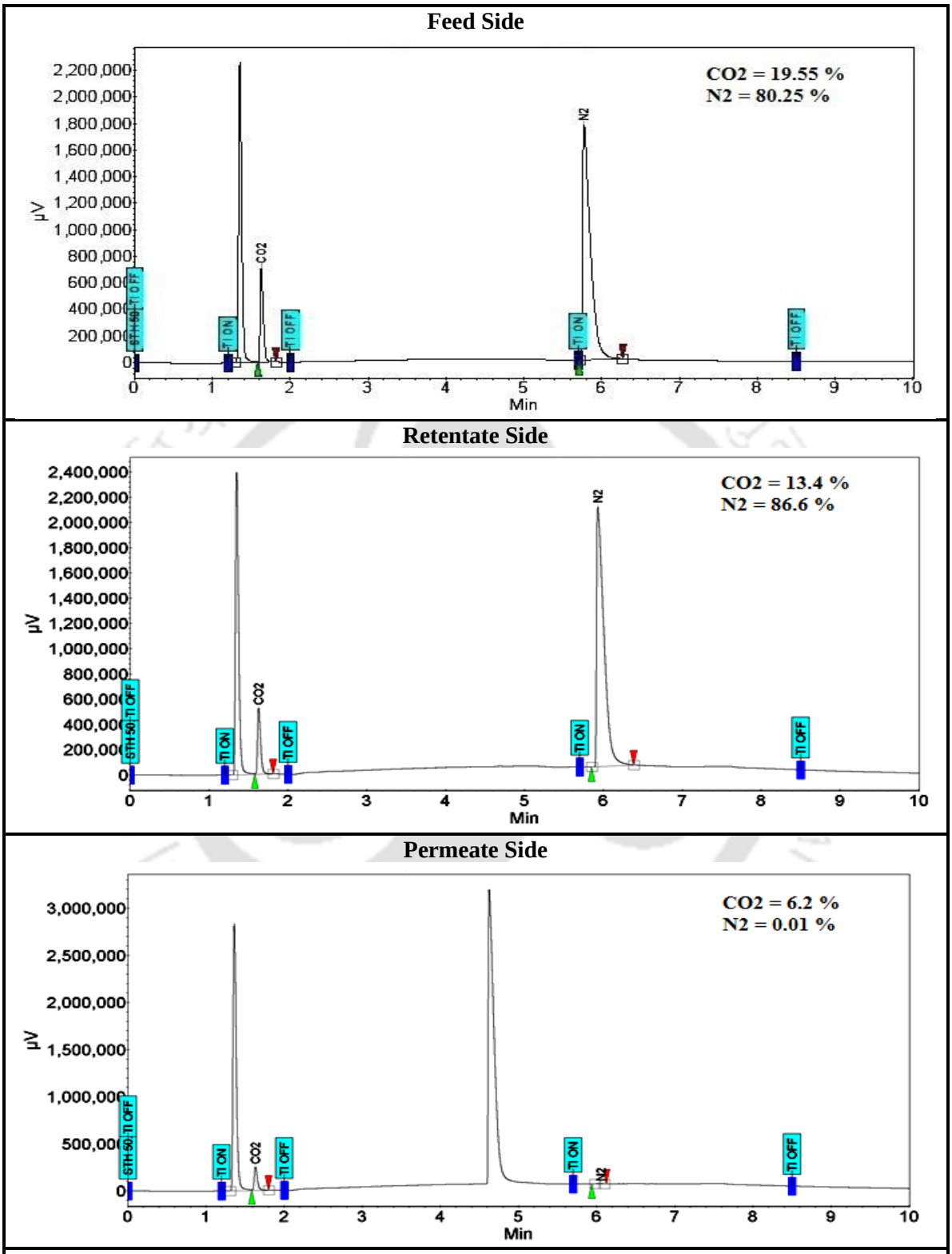

Figure A2.40 Effect of active layer thickness of 55 micron (25 wt% PAA + 15 wt% PEHA)

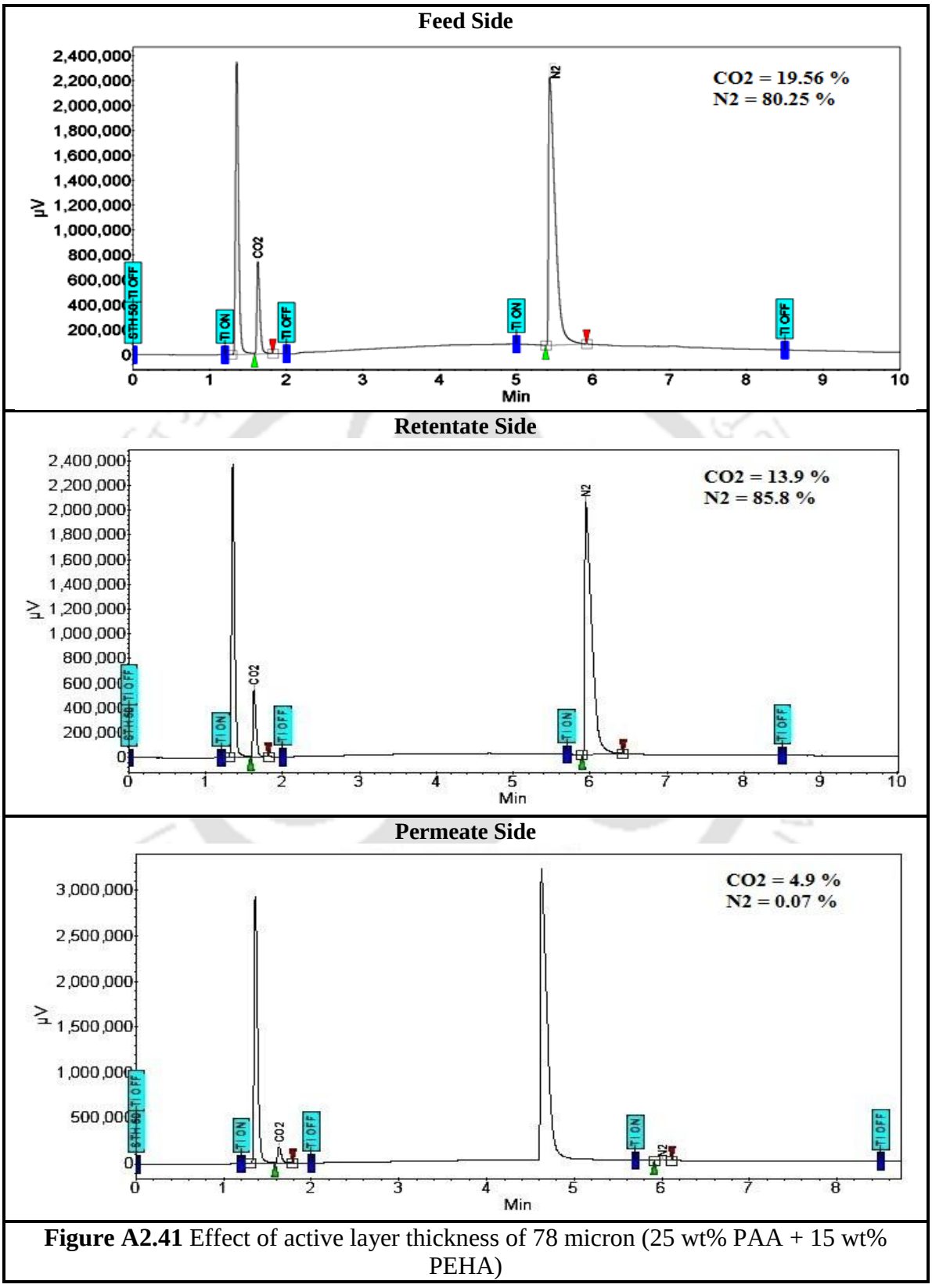

Figure A2.41 Effect of active layer thickness of 78 micron (25 wt% PAA + 15 wt% PEHA)

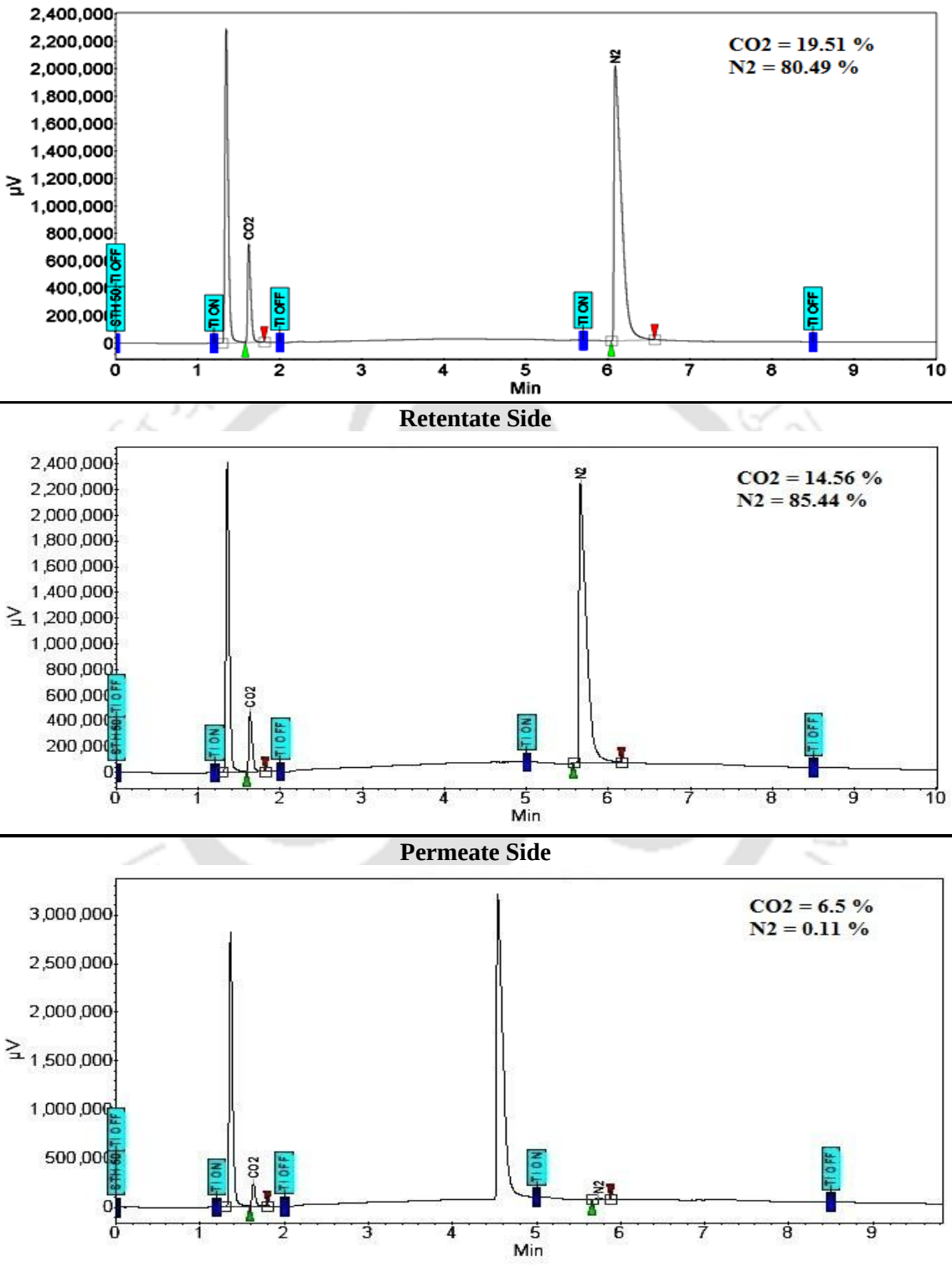

Figure A2.42 Effect of active layer thickness of 41 micron (15 wt% PAA + 25 wt% PEHA)

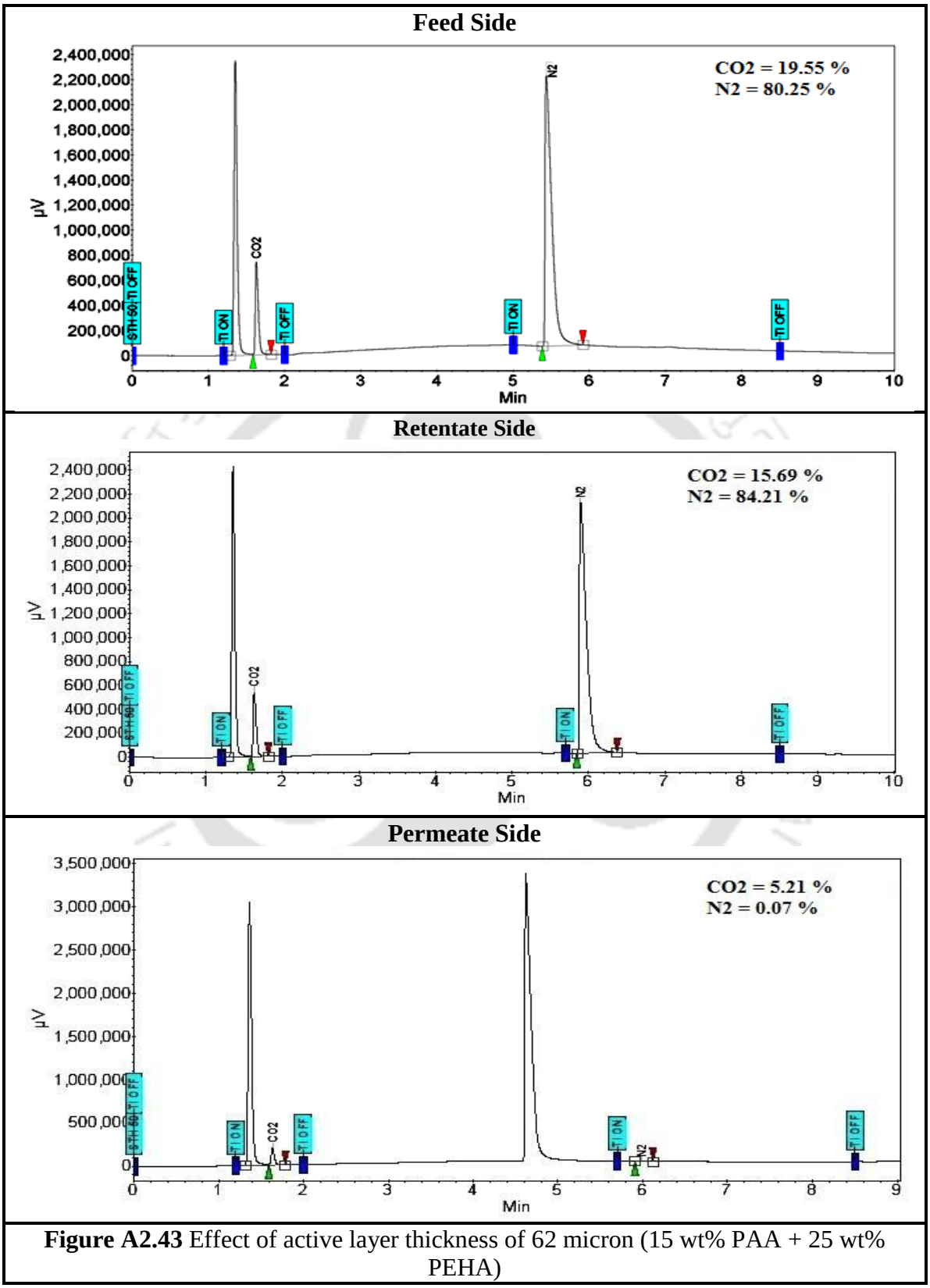

Figure A2.43 Effect of active layer thickness of 62 micron (15 wt% PAA + 25 wt% PEHA)

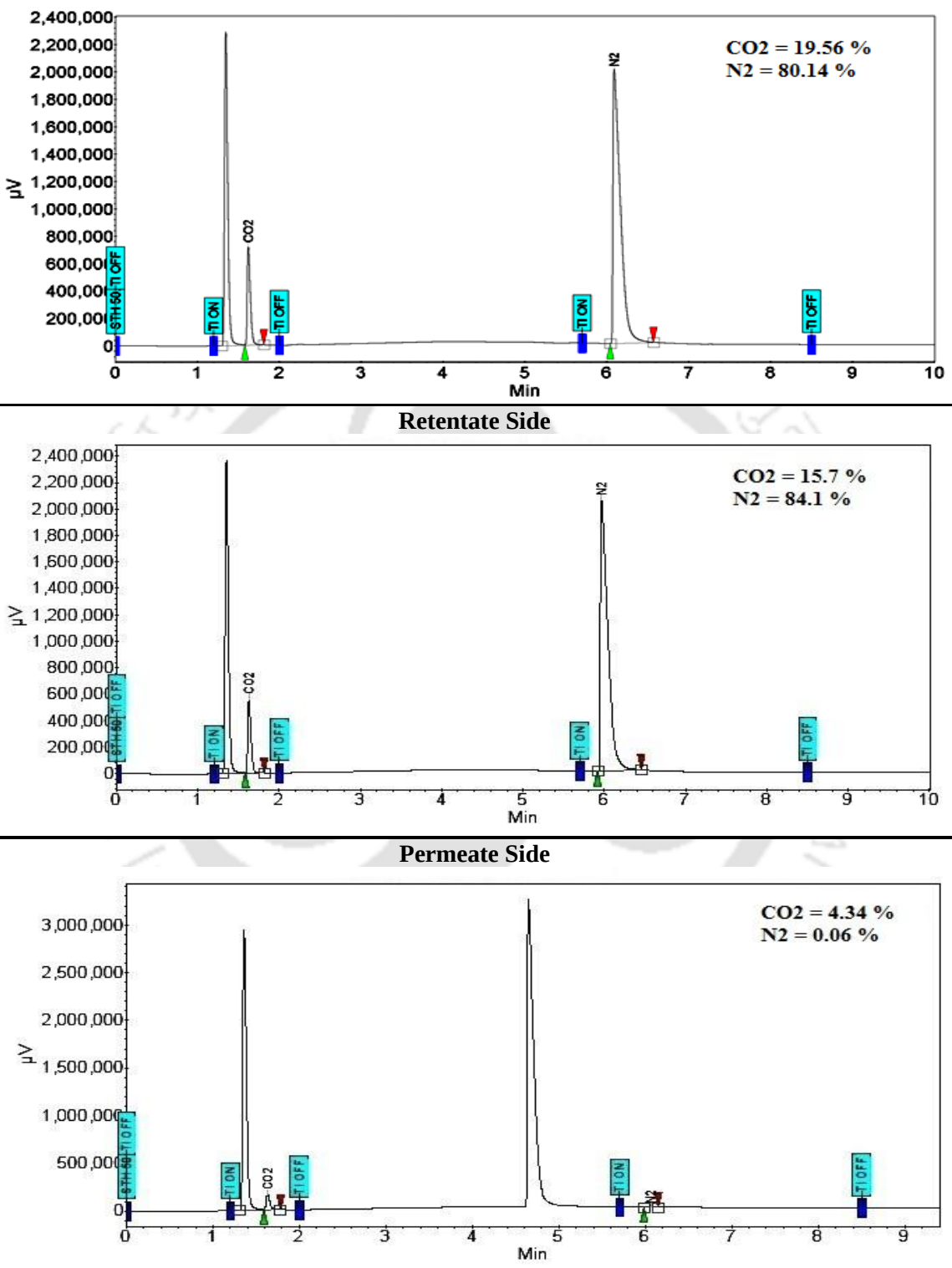

Figure A2.44 Effect of active layer thickness of 81 micron (15 wt% PAA + 25 wt% PEHA)

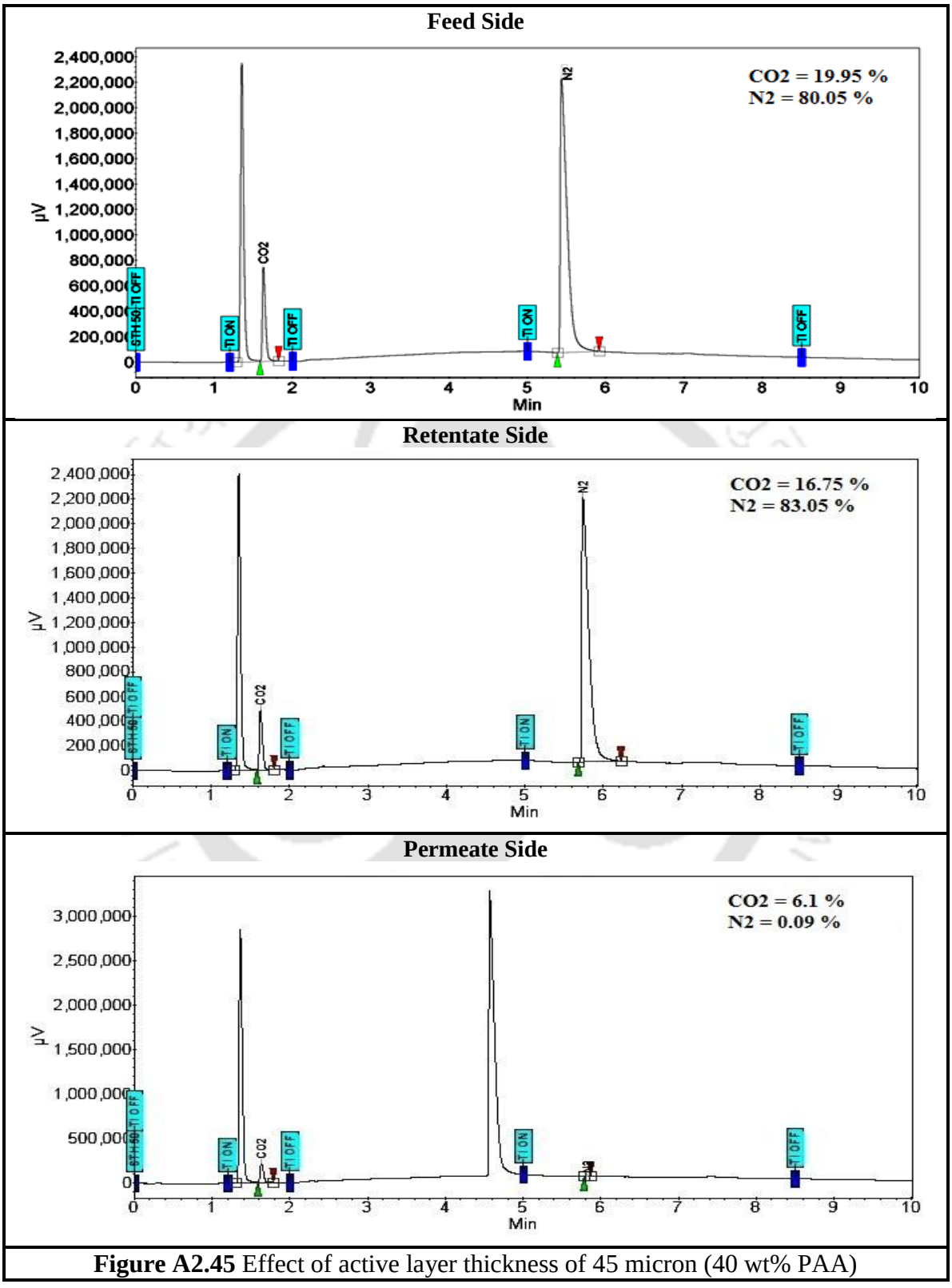

Figure A2.45 Effect of active layer thickness of 45 micron (40 wt% PAA)

A2.12 Gas Chromatography Data of Crosslinked-PVA-PVP Membrane Containing PAA and PEHA (Permeation Experiment)

Permeation experiment of 41.66 wt% PVA + 8.33 wt% PVP + 10 wt% KOH + 15 wt% PEHA + 25 wt% PAA with 60 mol% degree of cross linking by HCHO membrane with an active layer thickness of 42 micron.

Effects of Feed Pressure on Separation Performance: Feed absolute pressure was varied from 1.7 to 6.2 atm, maintaining other operating conditions constant (temperature = 100^{o}C, sweep side absolute pressure = 1.15 atm and feed side / sweep side water flow rate = 0.03 / 0.04 cm^{3}/min).

Effects of Sweep Side Water Flow Rate on Separation Performance: Sweep side water flow rate was varied from 0.02 to 0.075 cm^{3}/min, maintaining other operating conditions constant (temperature = 90^{o}C, sweep side absolute pressure = 1.15 atm and feed side water flow rates = 0.03 cm^{3}/min).

Effects of Temperature on Separation Performance: Temperature was varied from 90 to 125^{o}C, maintaining other operating conditions constant (feed / sweep side absolute pressure = 2.7 / 1.15 atm and feed / sweep side water flow rate = 0.03 / 0.04 cm^{3}/min).

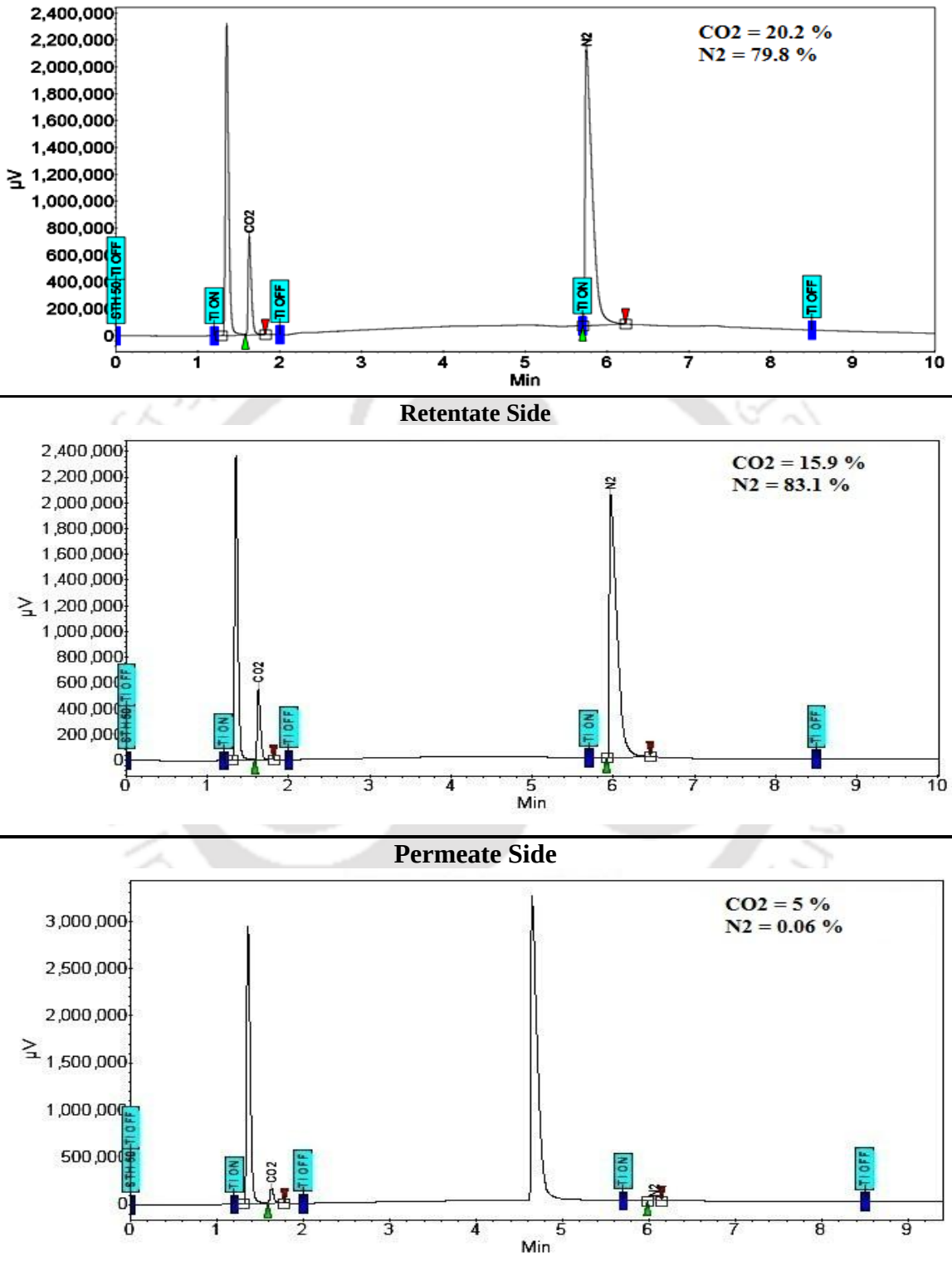

Figure A2.46 Effect of Feed Absolute Pressure = 1.71 atm, (15% PEHA+25% PAA)

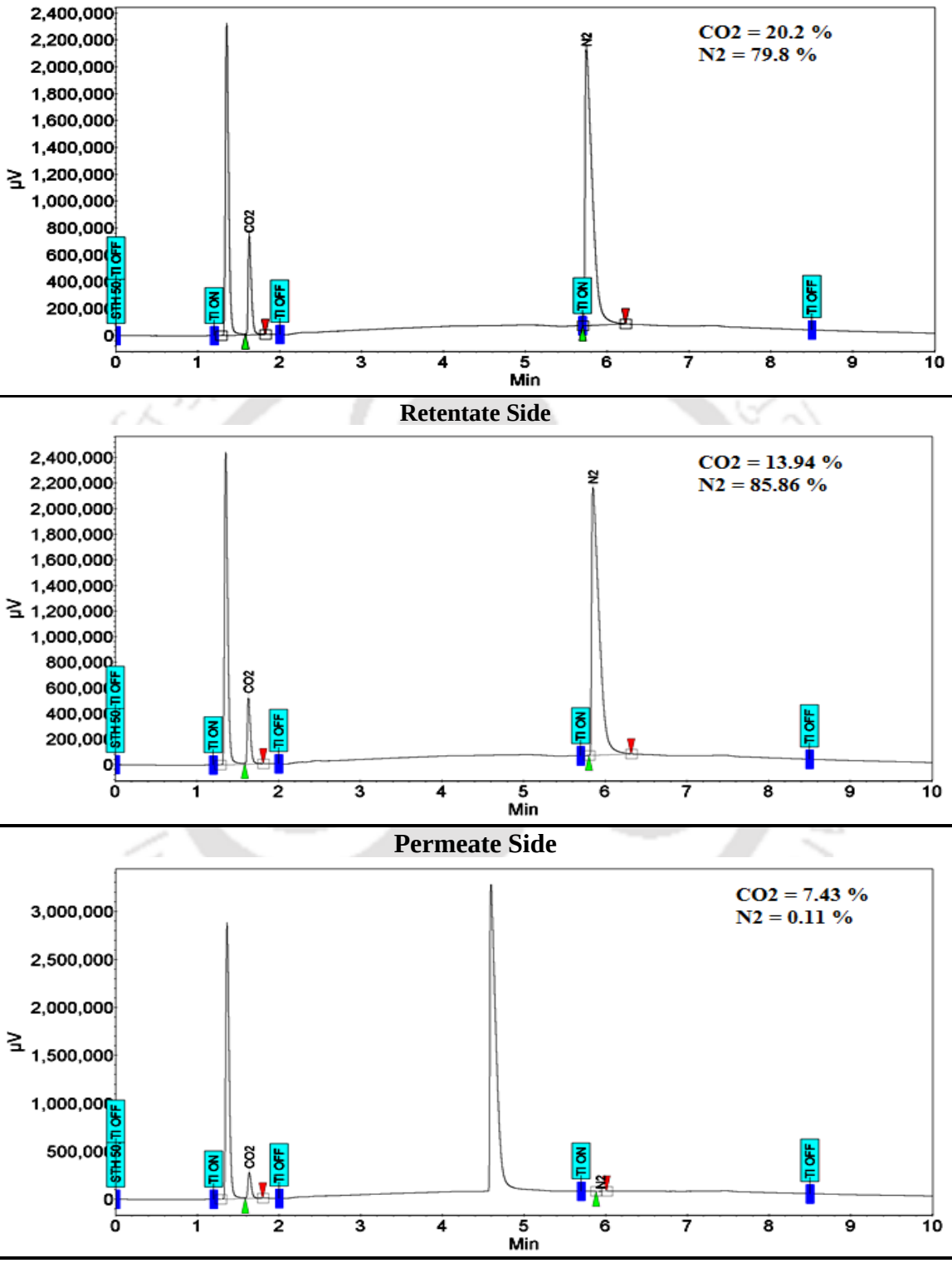

Figure A2.47 Effect of Feed Absolute Pressure = 2.76 atm, (15% PEHA+25% PAA)

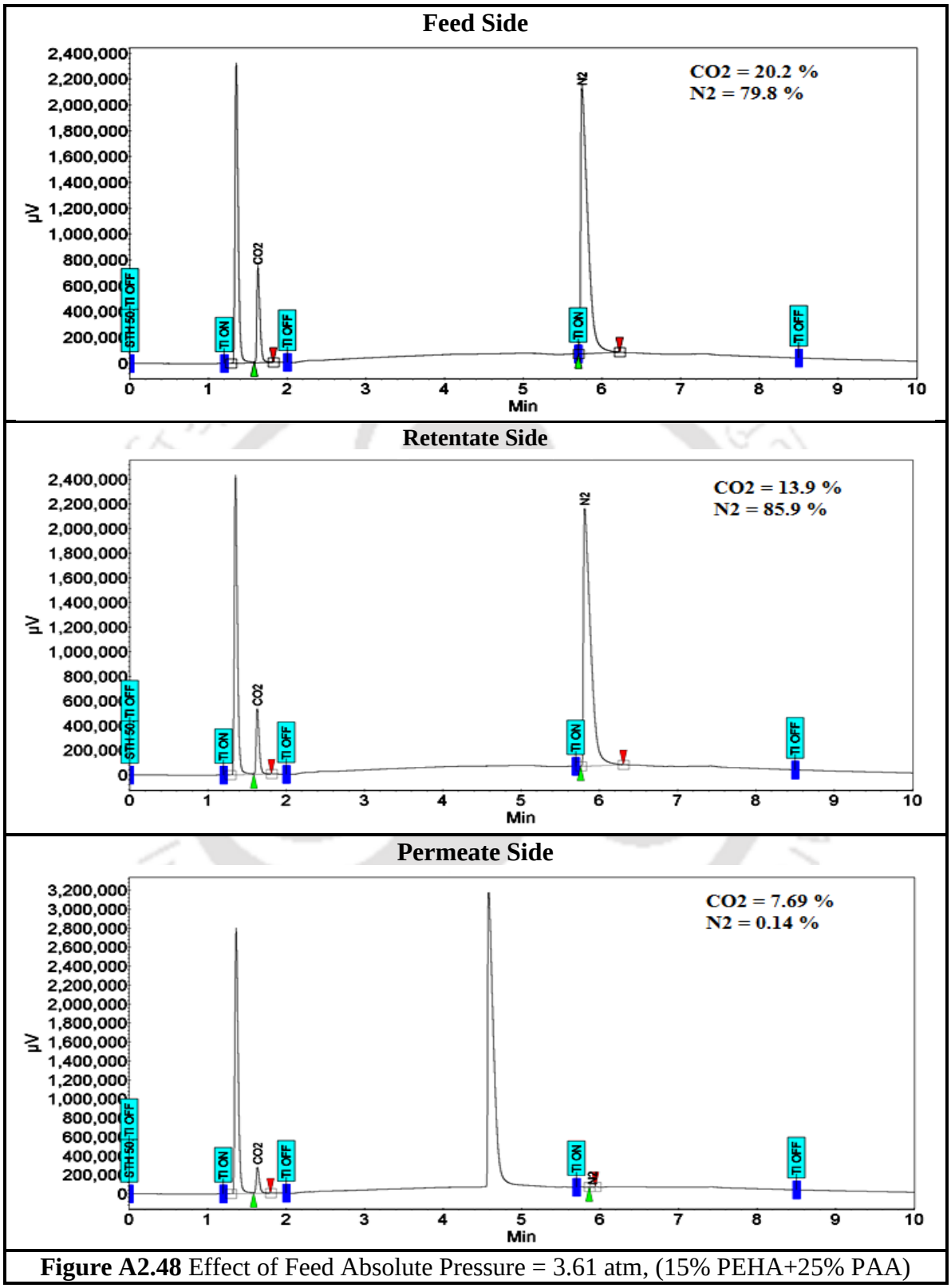

Figure A2.48 Effect of Feed Absolute Pressure = 3.61 atm, (15% PEHA+25% PAA)

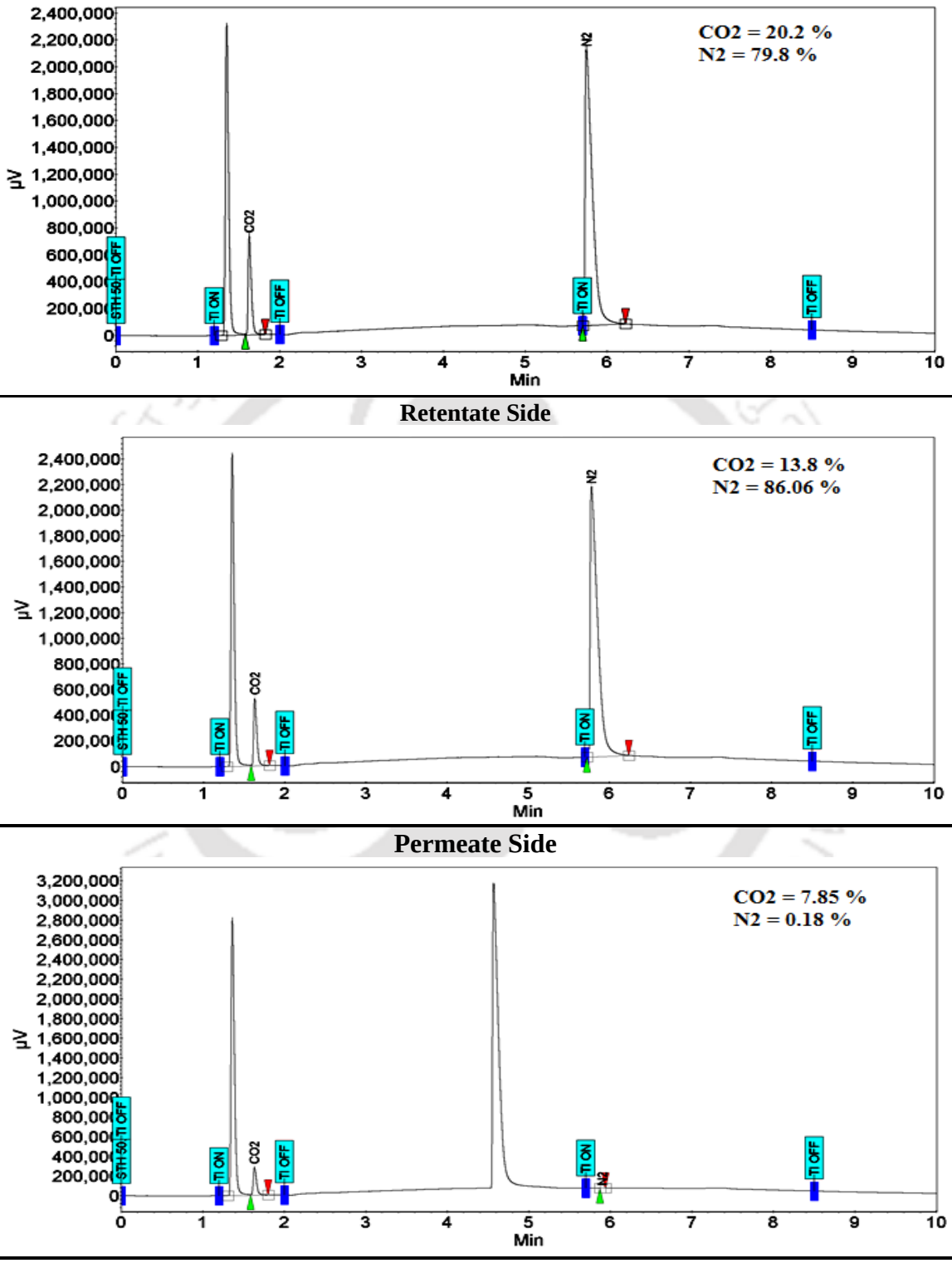

Figure A2.49 Effect of Feed Absolute Pressure = 4.94 atm, (15% PEHA+25% PAA)

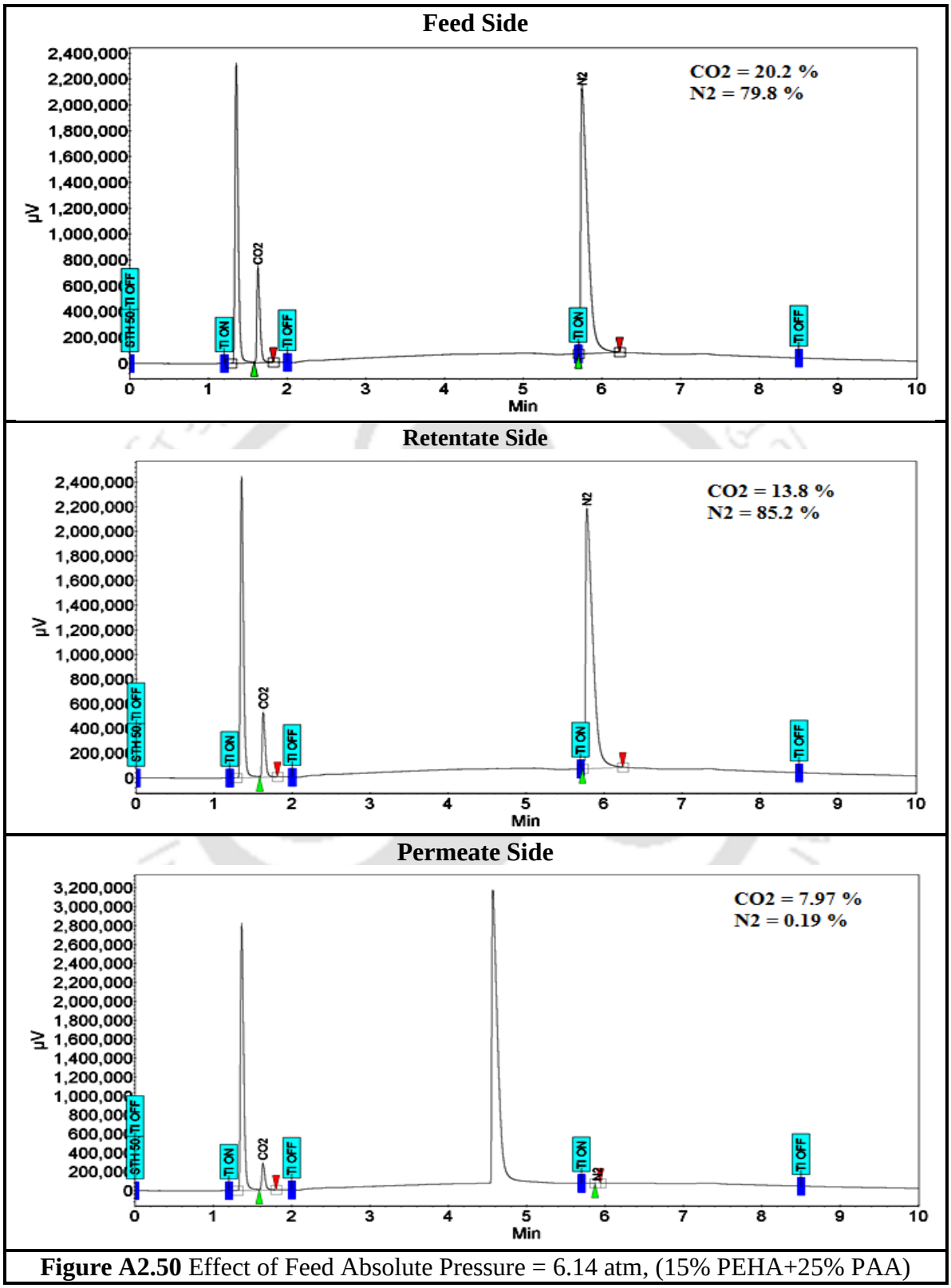

Figure A2.50 Effect of Feed Absolute Pressure = 6.14 atm, (15% PEHA+25% PAA)

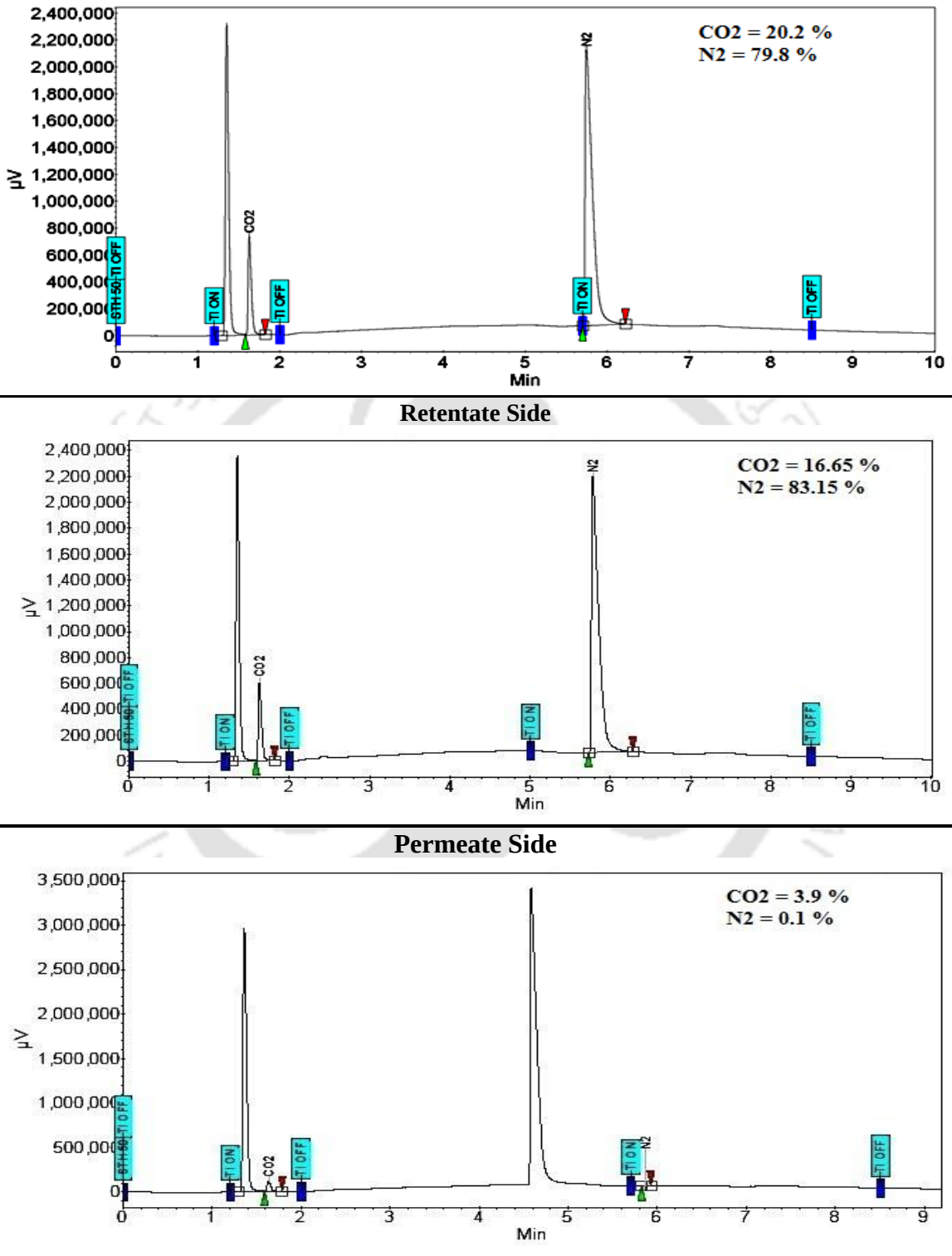

Figure A2.51 Effect of sweep side water flow rate = 0.02 ml/min, (15% PEHA+25% PAA)

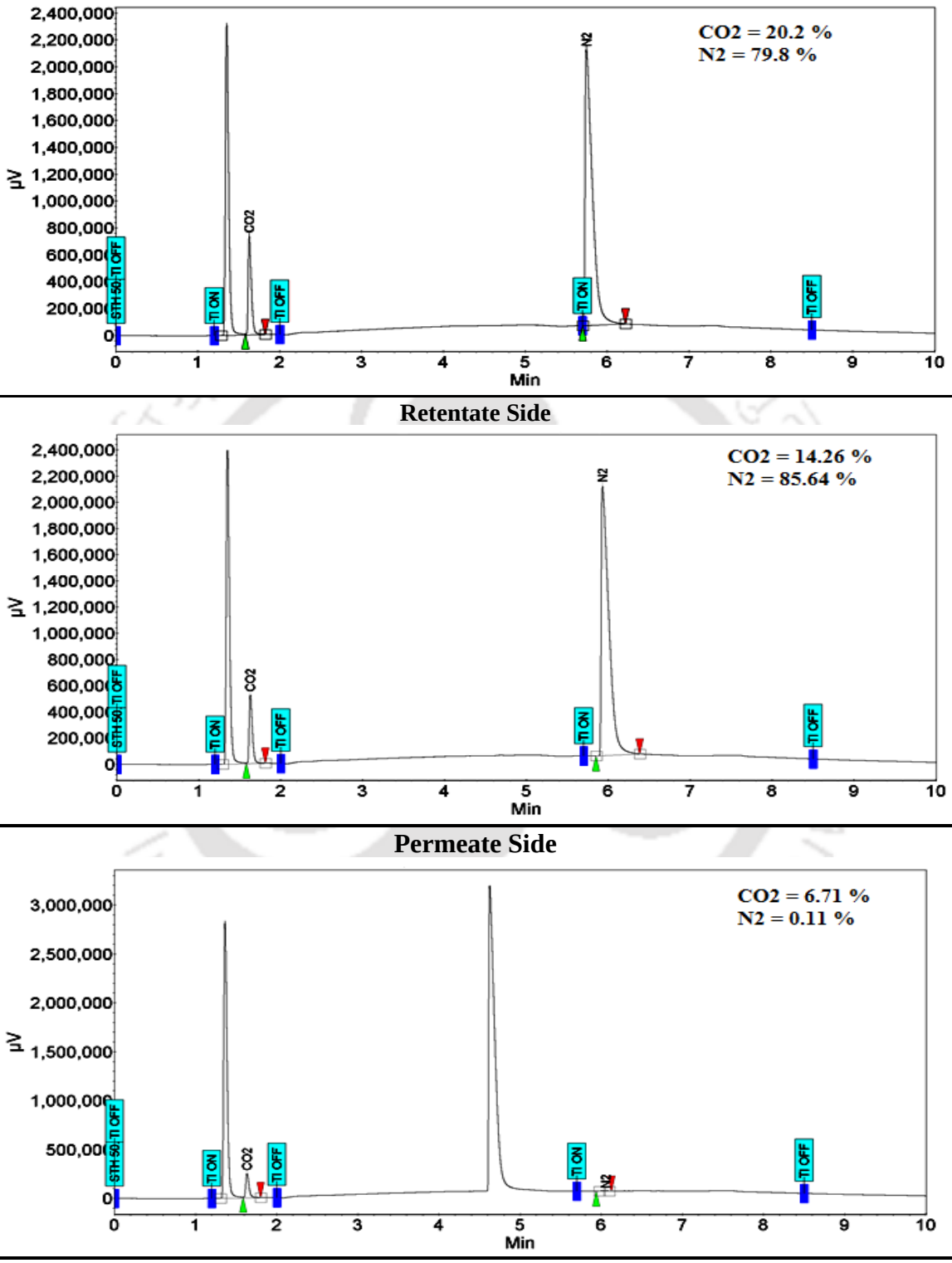

Figure A2.52 Effect of sweep side water flow rate = 0.04 ml/min, (15% PEHA+25% PAA)

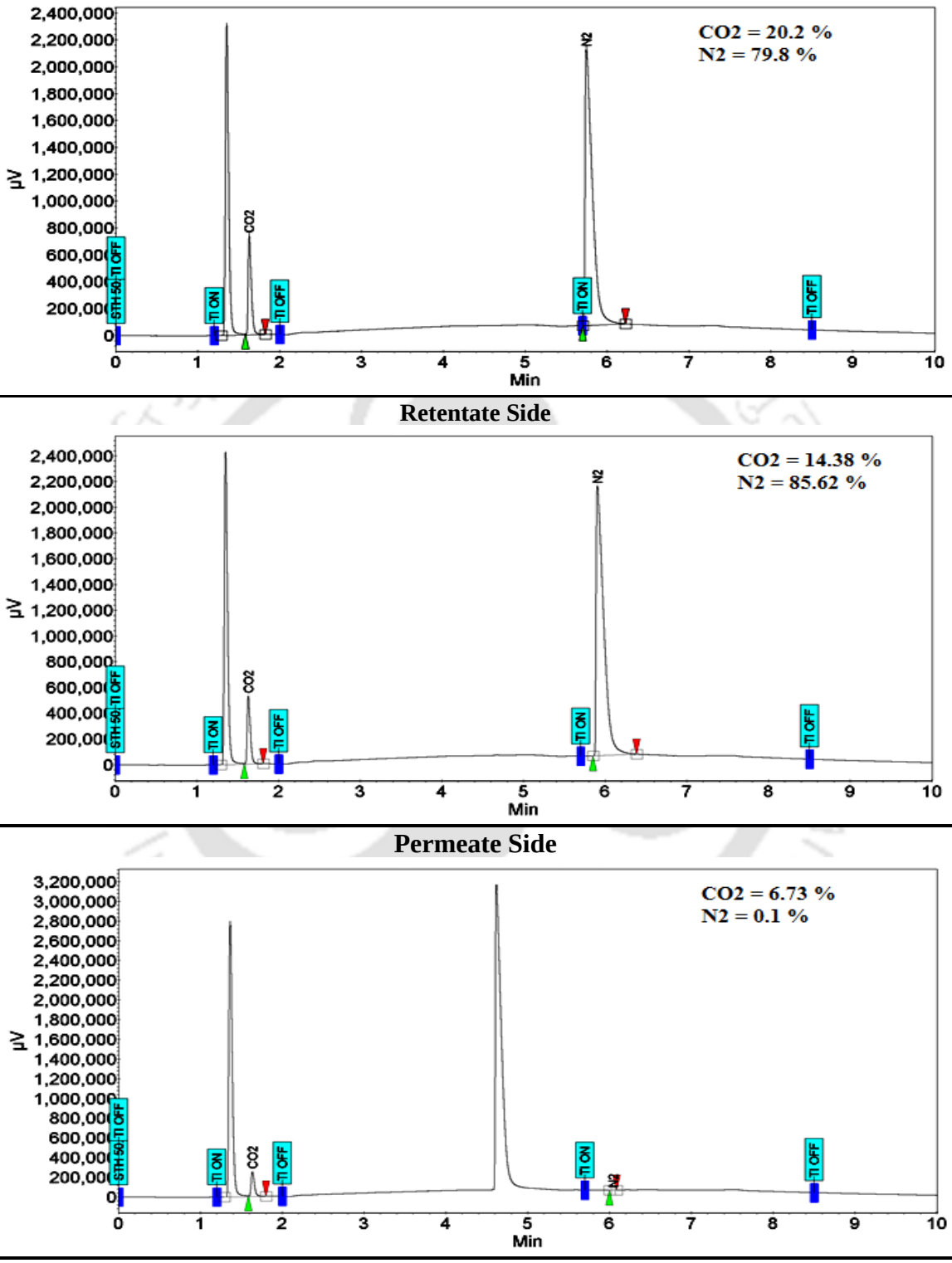

Figure A2.53 Effect of sweep side water flow rate = 0.06 ml/min, (15% PEHA+25% PAA)

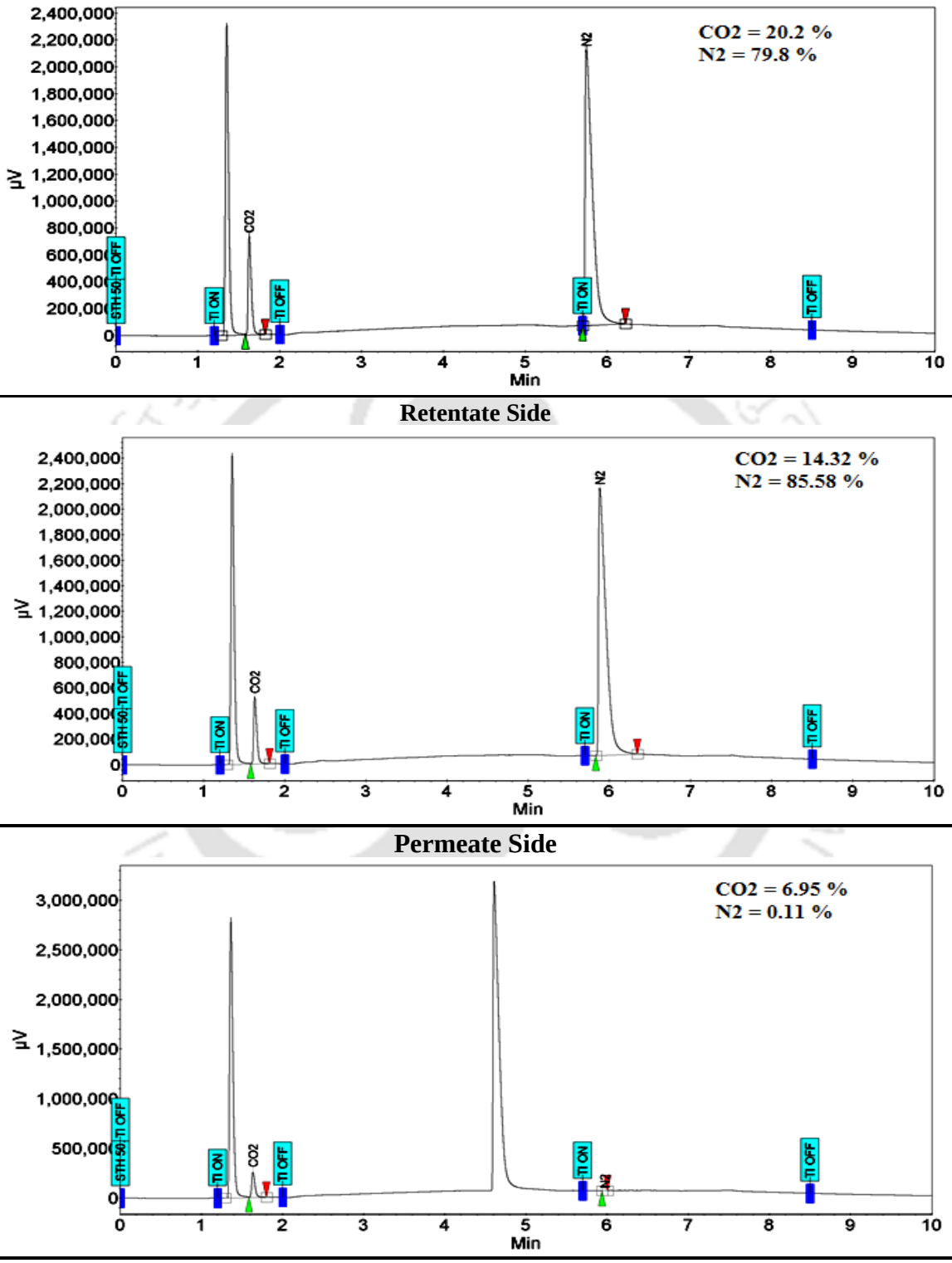

Figure A2.54 Effect of sweep side water flow rate = 0.075 ml/min, (15% PEHA+25% PAA)

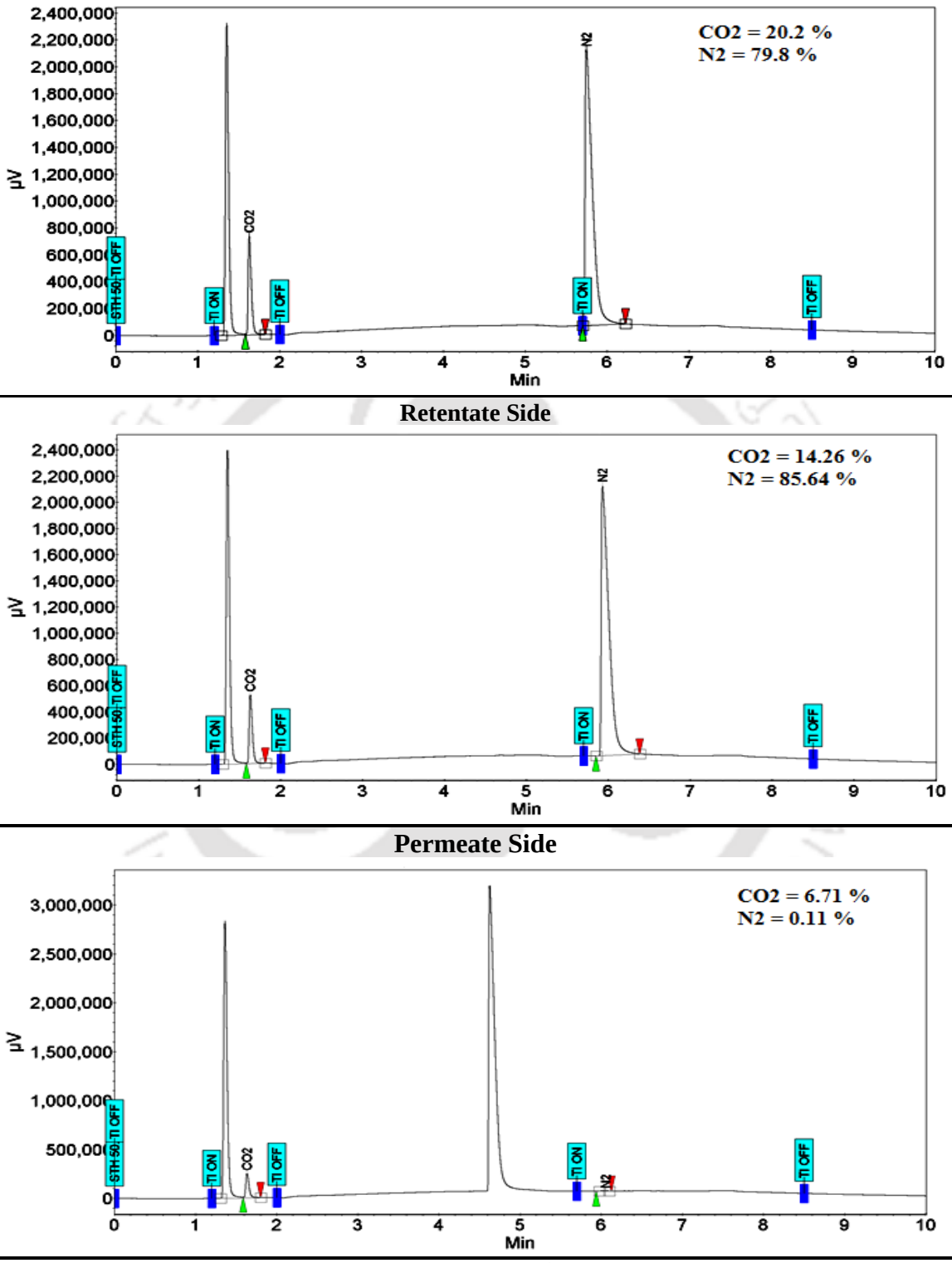

Figure A2.55 Effect of Temperature = 90°C, (15% PEHA+25% PAA)

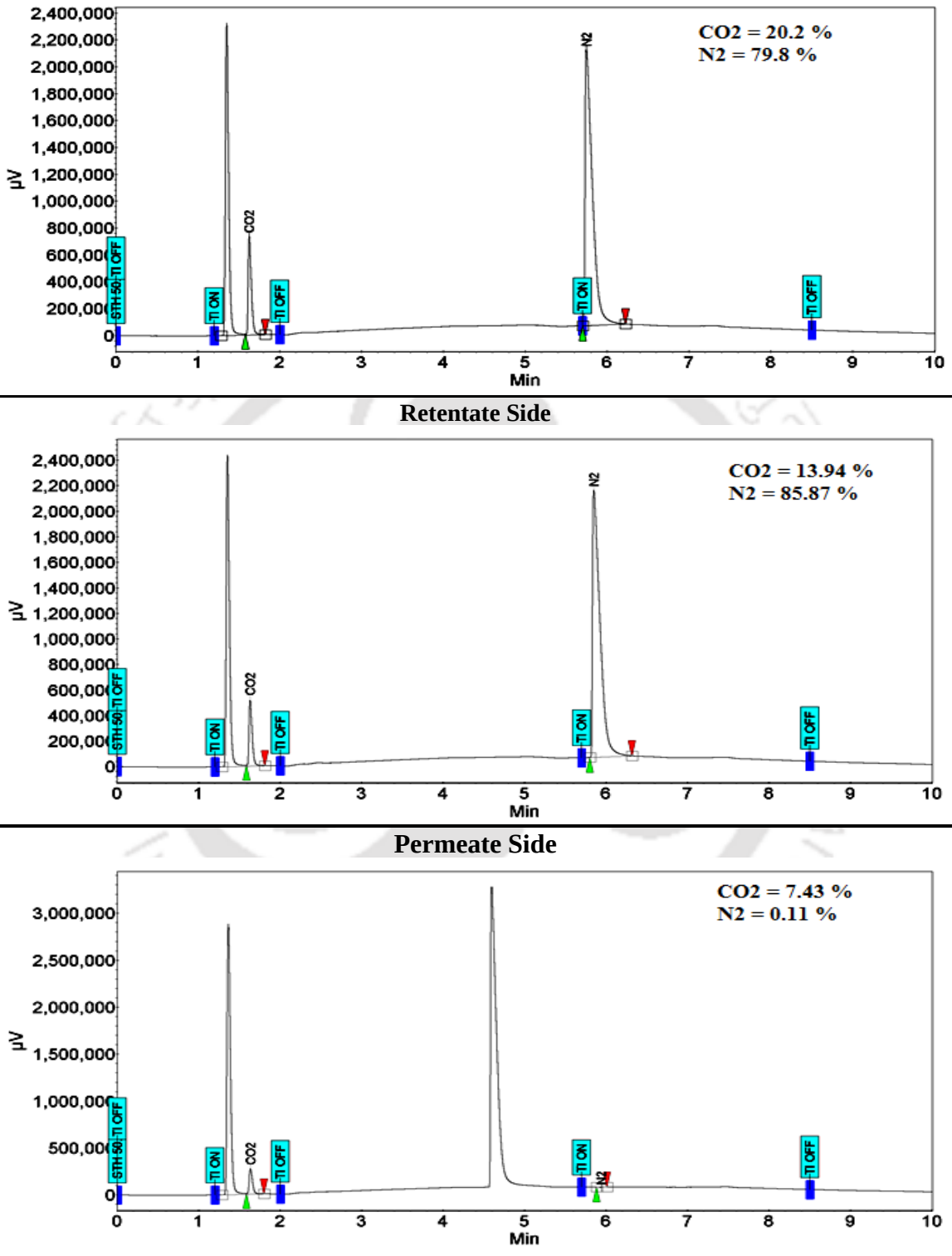

Figure A2.56 Effect of Temperature = 100^{o}C, (15% PEHA+25% PAA)

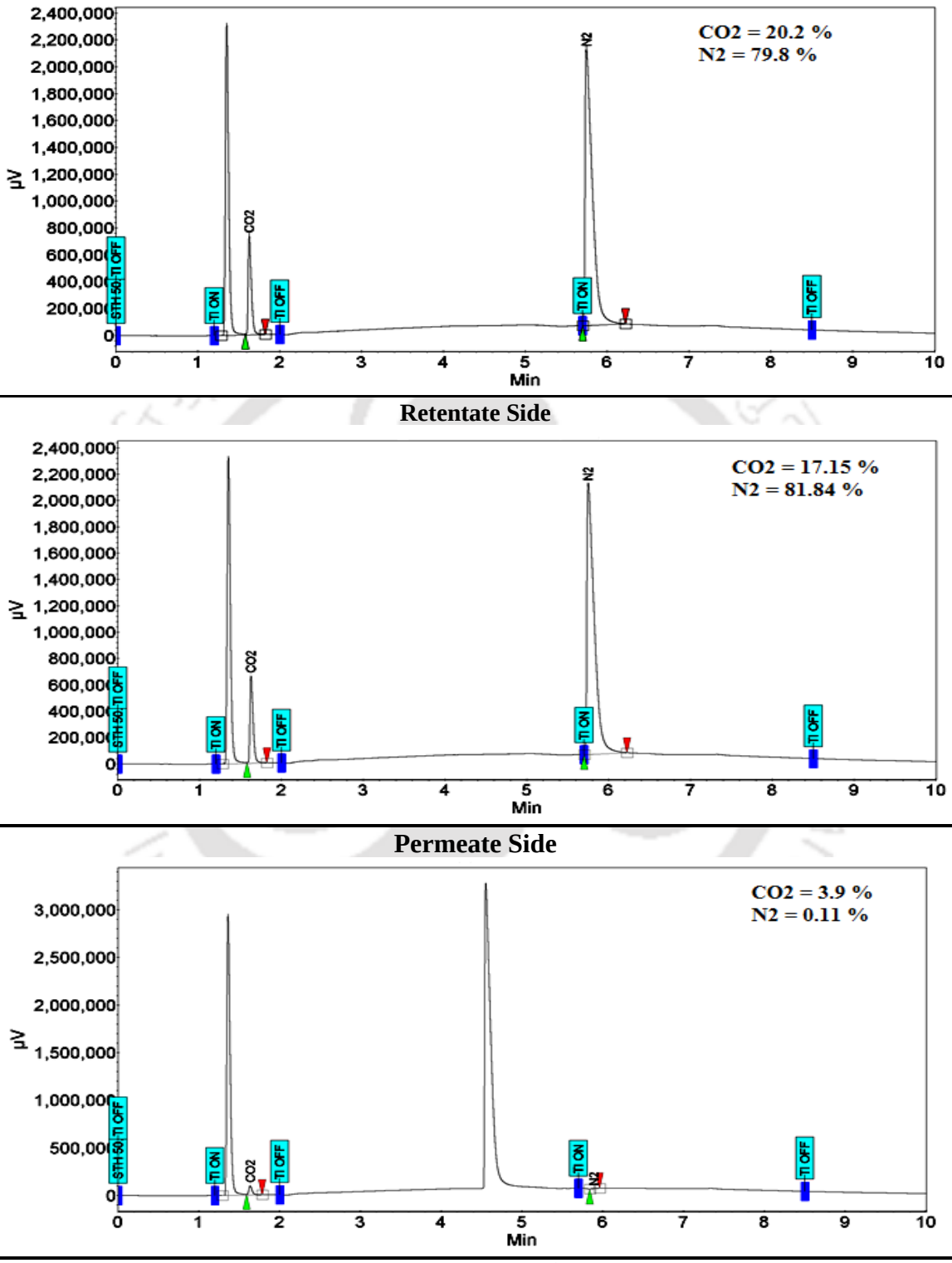

Figure A2.57 Effect of Temperature = 115^{o}C, (15% PEHA+25% PAA)

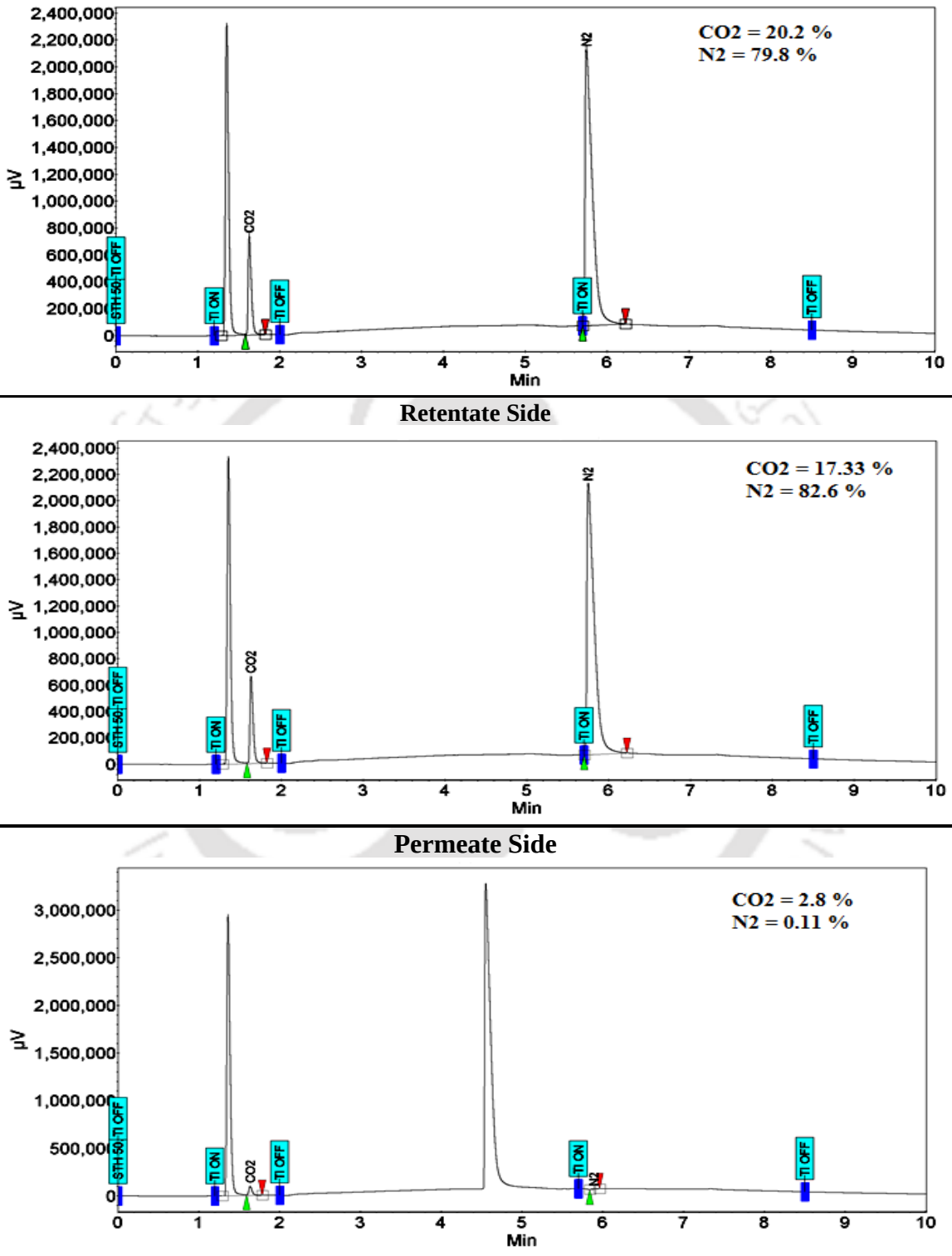

Figure A2.58 Effect of Temperature = 125^{o}C, (15% PEHA+25% PAA)

A2.13 Gas Chromatography Data of Crosslinked-PVA-PVP Membrane Containing PAA and AHPD (Effect of Thickness)

Three different active layer compositions were prepared mention below:

1. 41.66 wt% PVA + 8.33 wt% PVP + 10 wt% KOH + 25% PAA+15% AHPD with 60 mol% degree of cross linking by HCHO
2. 41.66 wt% PVA + 8.33 wt% PVP + 10 wt% KOH + 15% PAA+25% AHPD with 60 mol% degree of cross linking by HCHO
3. 41.66 wt% PVA + 8.33 wt% PVP + 10 wt% KOH + 40 wt% PAA with 60 mol% degree of cross linking by HCHO

Composition one has three different active layer membranes like 44, 58 and 80 micron. Similarly composition two has also three different active layer membranes like 43, 65 and 84 micron. And composition three has only one active layer membrane like 45 micron.

All the permeation experiment was done exactly same operating condition. Feed side and sweep side absolute pressure was maintained constant at around 2.8 and 1.15 atm, respectively. Temperature was kept constant at 95^{o}C along with constant water flow rate at both sides (feed/sweep = 0.03/0.04 cm^3/min). Both feed gas (20% CO_2 balance N_2 on dry basis) and carrier gas (Ar) flow rates were maintained at 30 cm^3/min throughout the experiment.

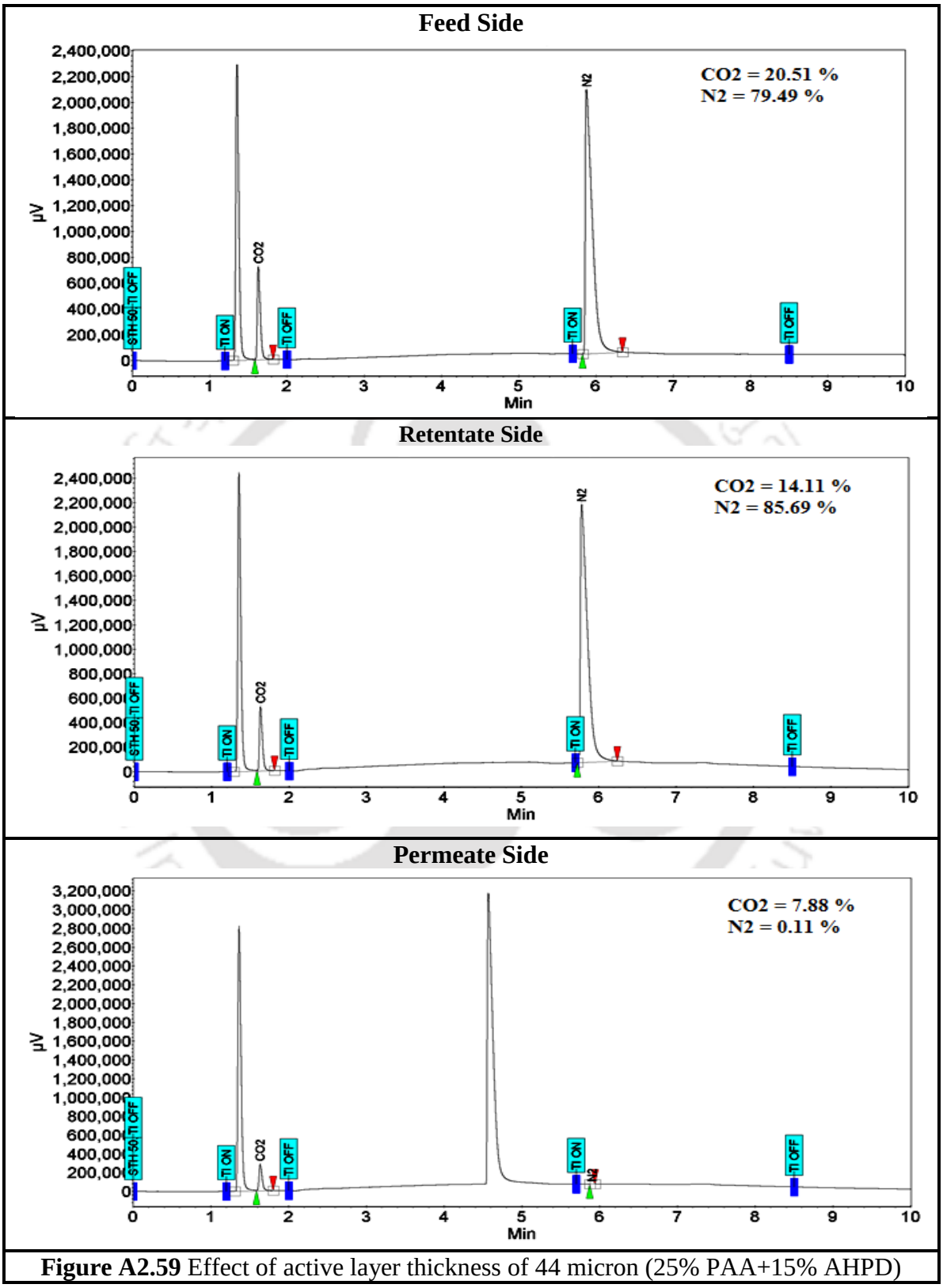

Figure A2.59 Effect of active layer thickness of 44 micron (25% PAA+15% AHPD)

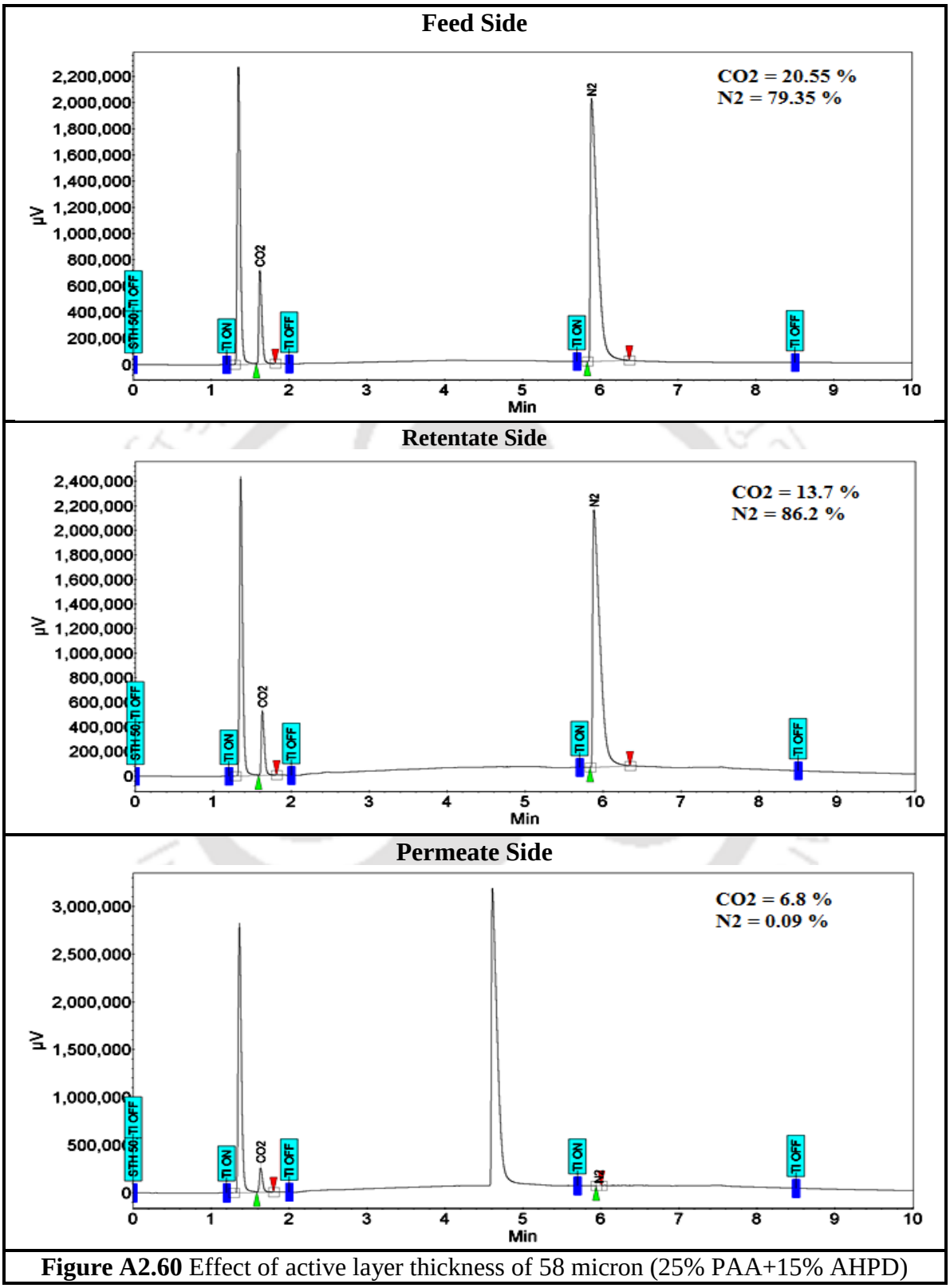

Figure A2.60 Effect of active layer thickness of 58 micron (25% PAA+15% AHPD)

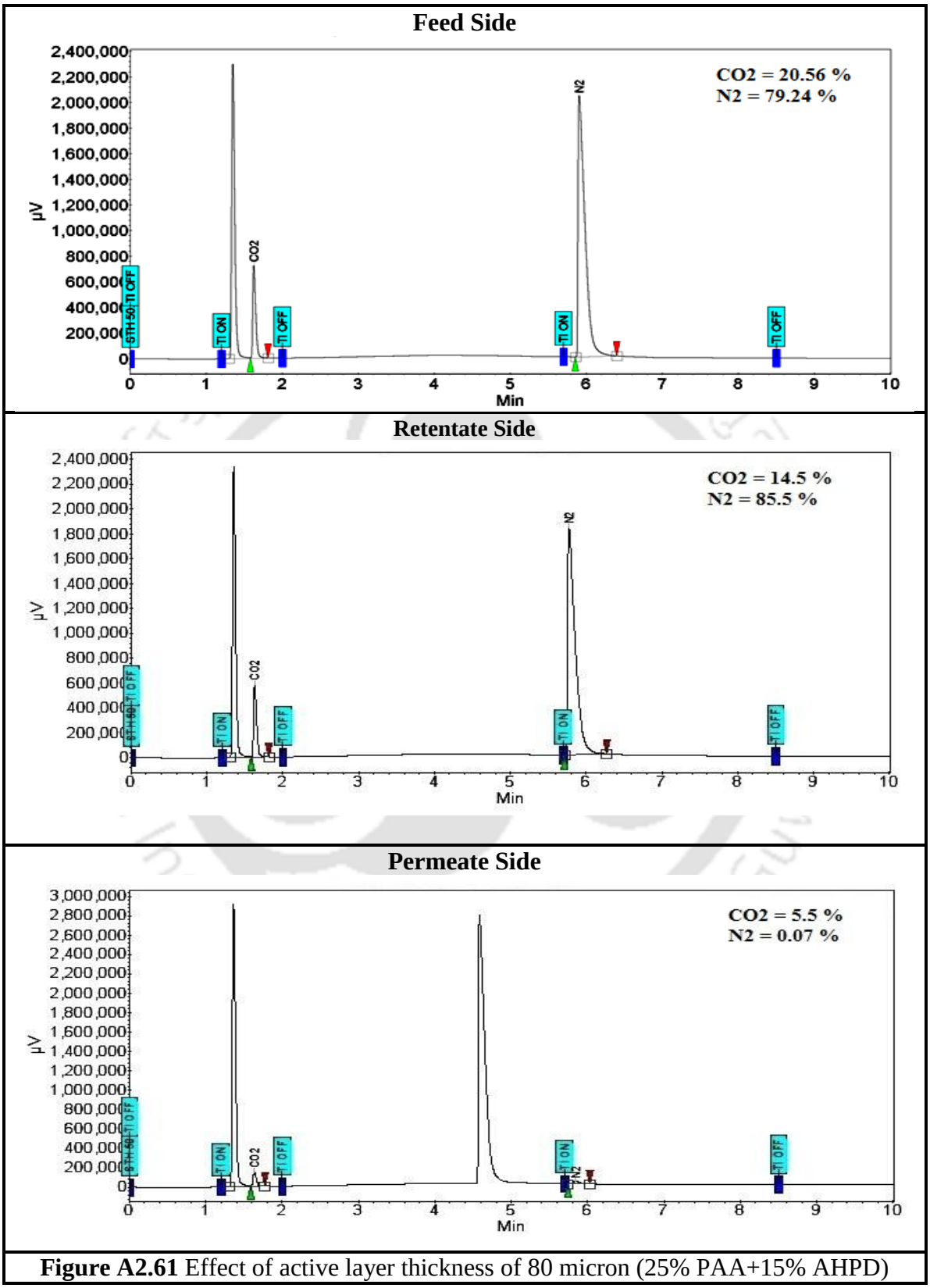

Figure A2.61 Effect of active layer thickness of 80 micron (25% PAA+15% AHPD)

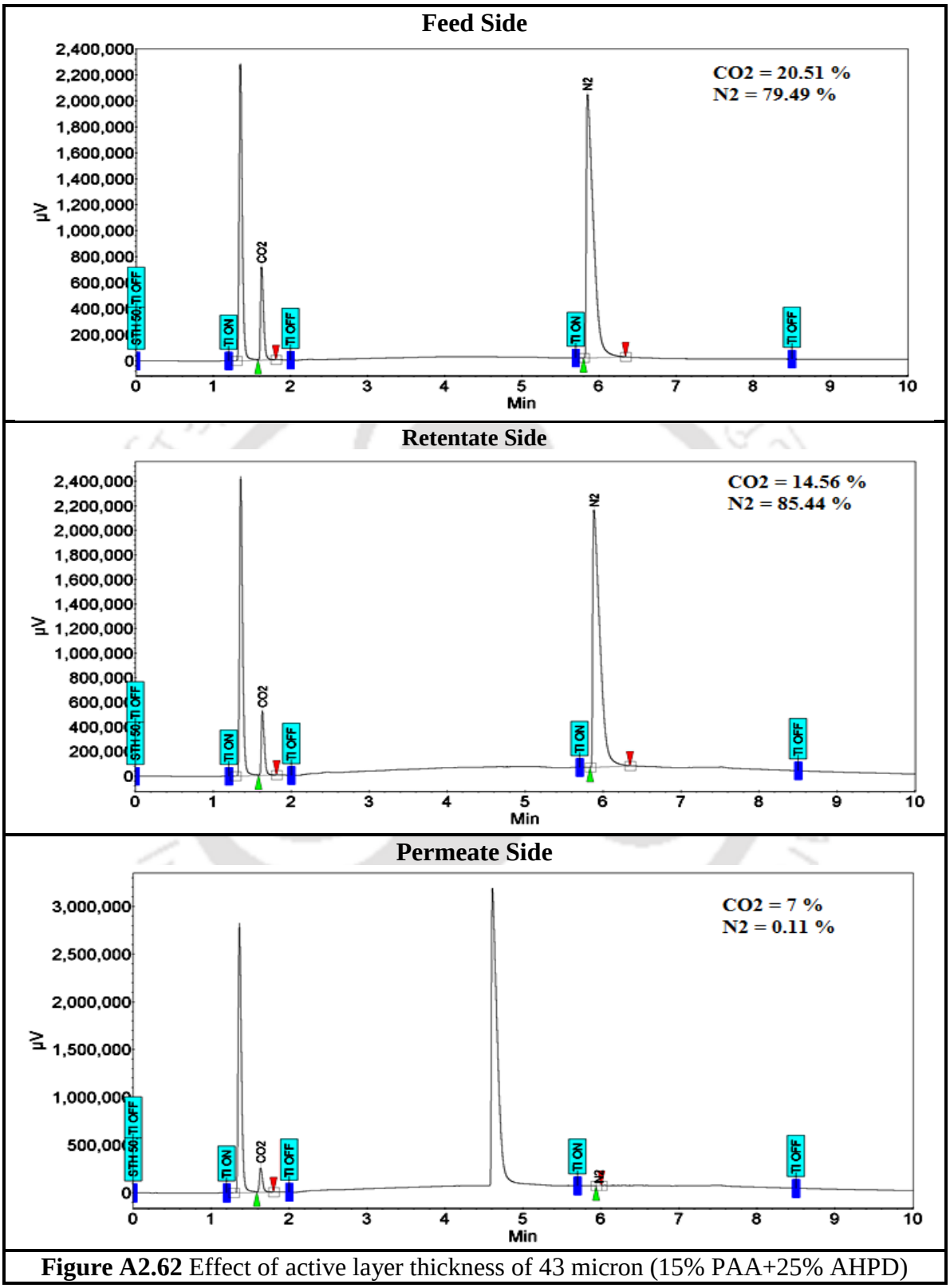

Figure A2.62 Effect of active layer thickness of 43 micron (15% PAA+25% AHPD)

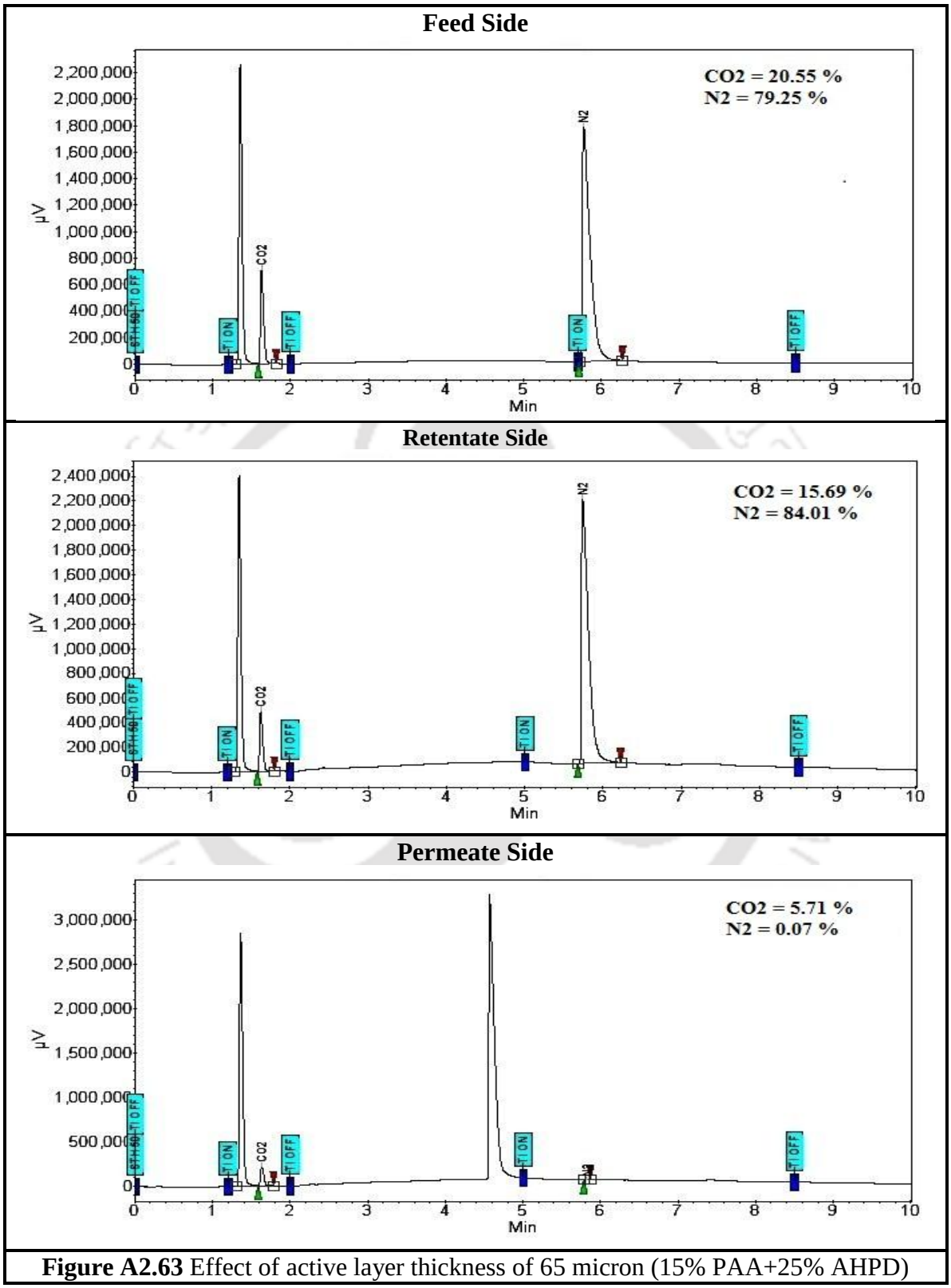

Figure A2.63 Effect of active layer thickness of 65 micron (15% PAA+25% AHPD)

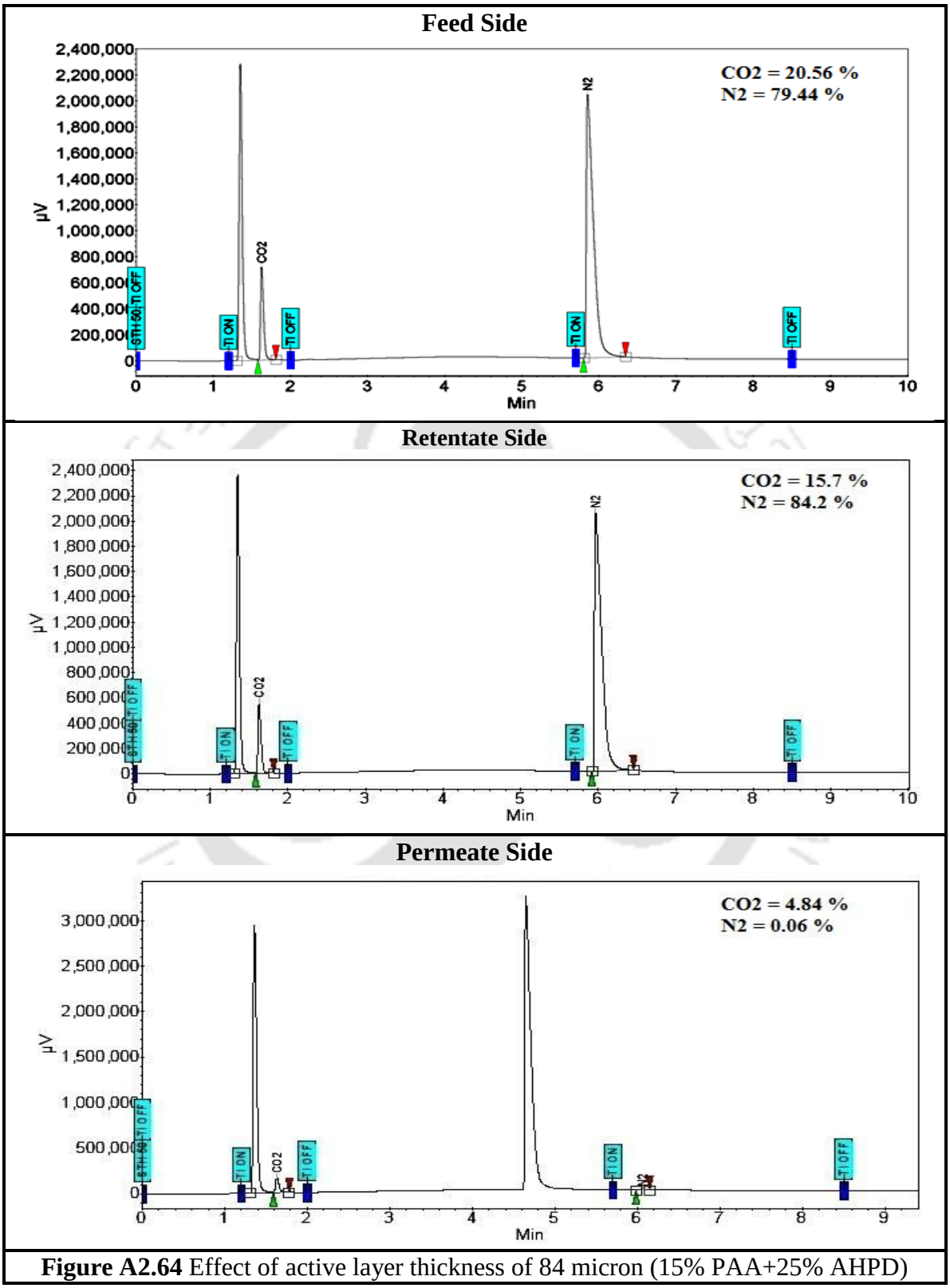

Figure A2.64 Effect of active layer thickness of 84 micron (15% PAA+25% AHPD)

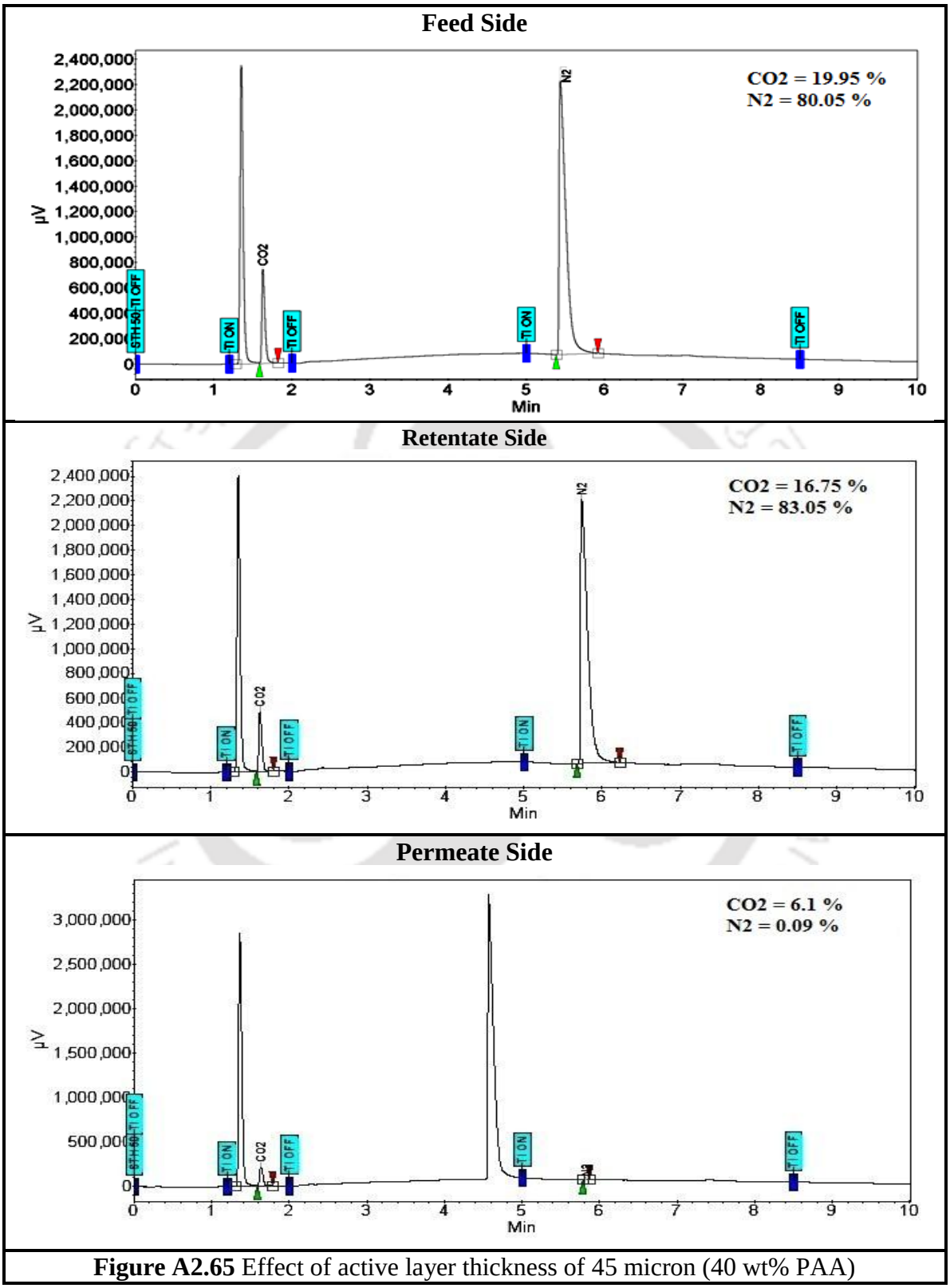

Figure A2.65 Effect of active layer thickness of 45 micron (40 wt% PAA)

A2.14 Gas Chromatography Data of Crosslinked-PVA-PVP Membrane Containing PAA and AHPD (Permeation Experiment)

Permeation experiment of 41.66 wt% PVA + 8.33 wt% PVP + 10 wt% KOH + 15 wt% AHPD + 25 wt% PAA with 60 mol% degree of cross linking by HCHO membrane with an active layer thickness of 44 micron.

Effects of Feed Pressure on Separation Performance: Feed absolute pressure was varied from 1.7 to 6.2 atm, maintaining other operating conditions constant (temperature = 100^{o}C, sweep side absolute pressure = 1.15 atm and feed side / sweep side water flow rate = 0.03 / 0.04 cm^{3}/min).

Effects of Sweep Side Water Flow Rate on Separation Performance: Sweep side water flow rate was varied from 0.02 to 0.075 cm^{3}/min, maintaining other operating conditions constant (temperature = 90^{o}C, sweep side absolute pressure = 1.15 atm and feed side water flow rates = 0.03 cm^{3}/min).

Effects of Temperature on Separation Performance: Temperature was varied from 90 to 125^{o}C, maintaining other operating conditions constant (feed / sweep side absolute pressure = 2.7 / 1.15 atm and feed / sweep side water flow rate = 0.03 / 0.04 cm^{3}/min).

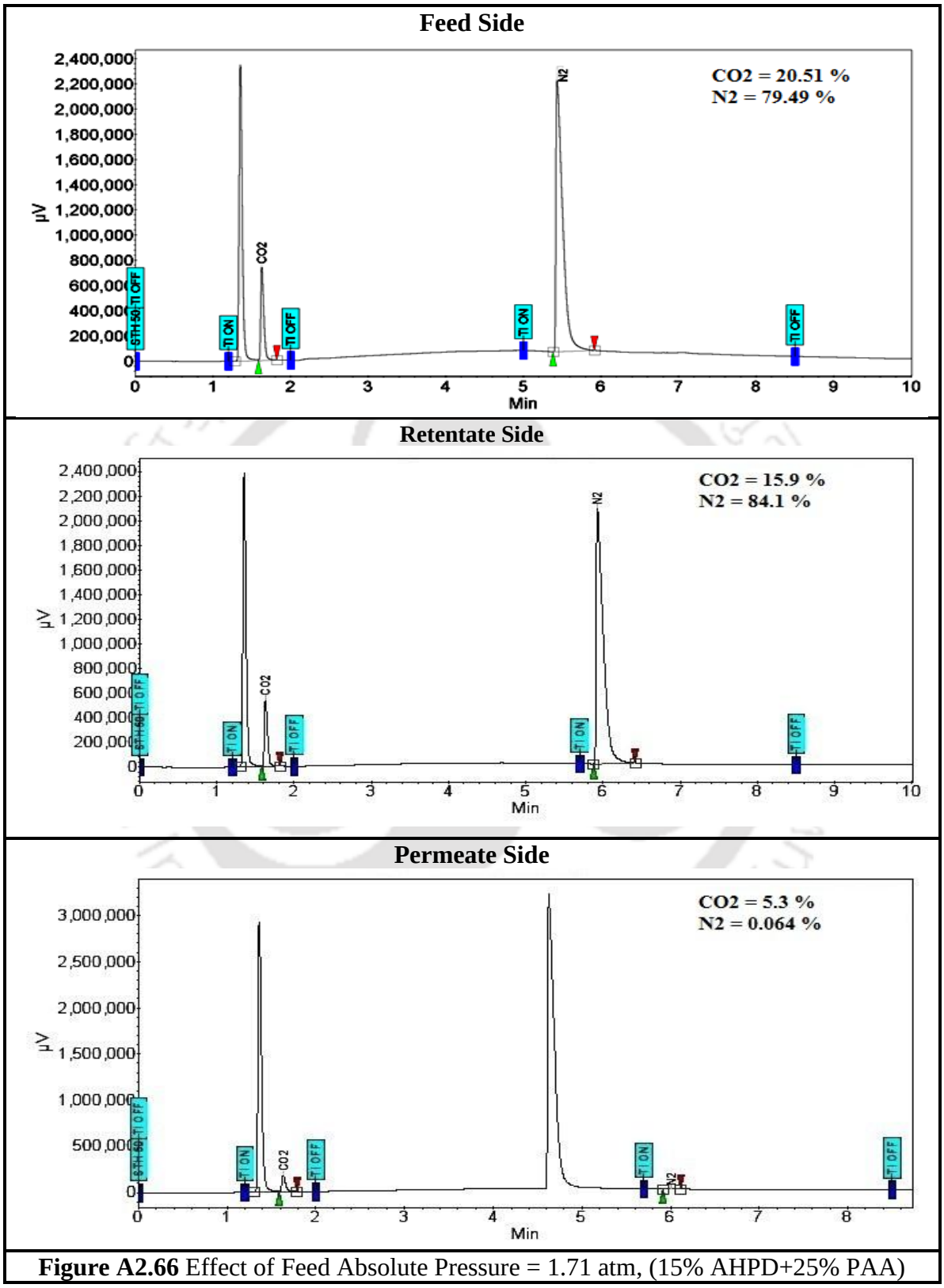

Figure A2.66 Effect of Feed Absolute Pressure = 1.71 atm, (15% AHPD+25% PAA)

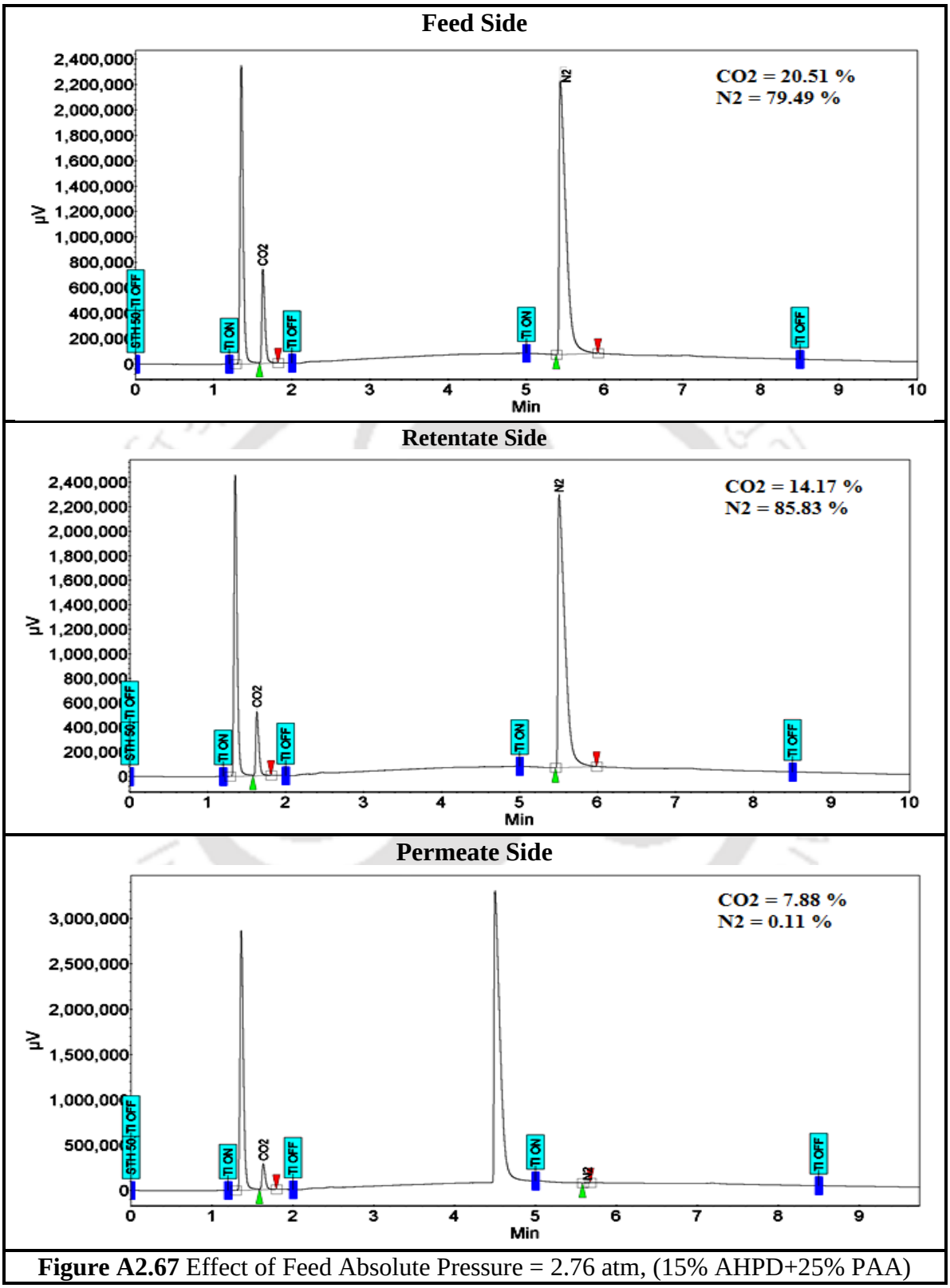

Figure A2.67 Effect of Feed Absolute Pressure = 2.76 atm, (15% AHPD+25% PAA)

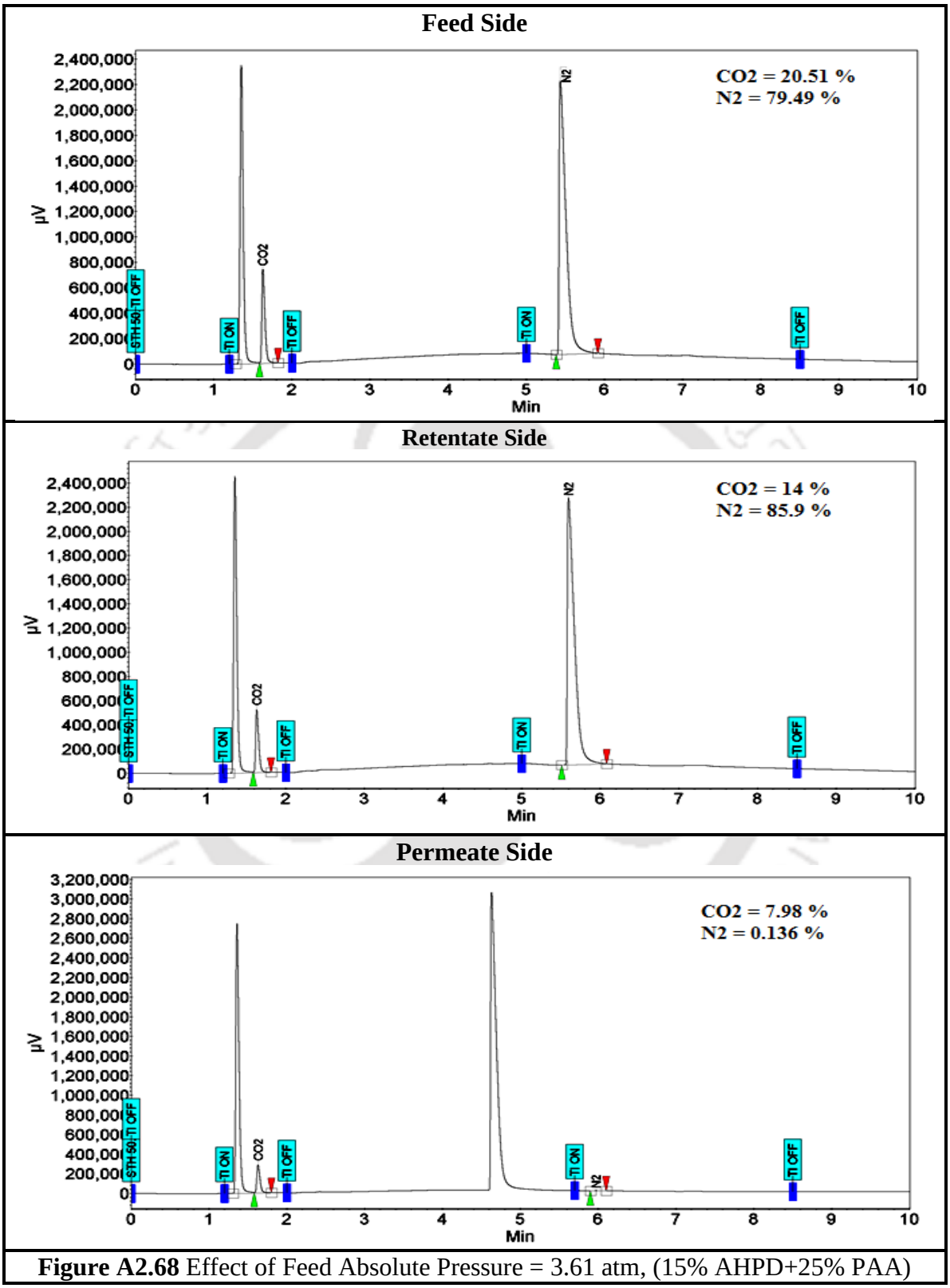

Figure A2.68 Effect of Feed Absolute Pressure = 3.61 atm, (15% AHPD+25% PAA)

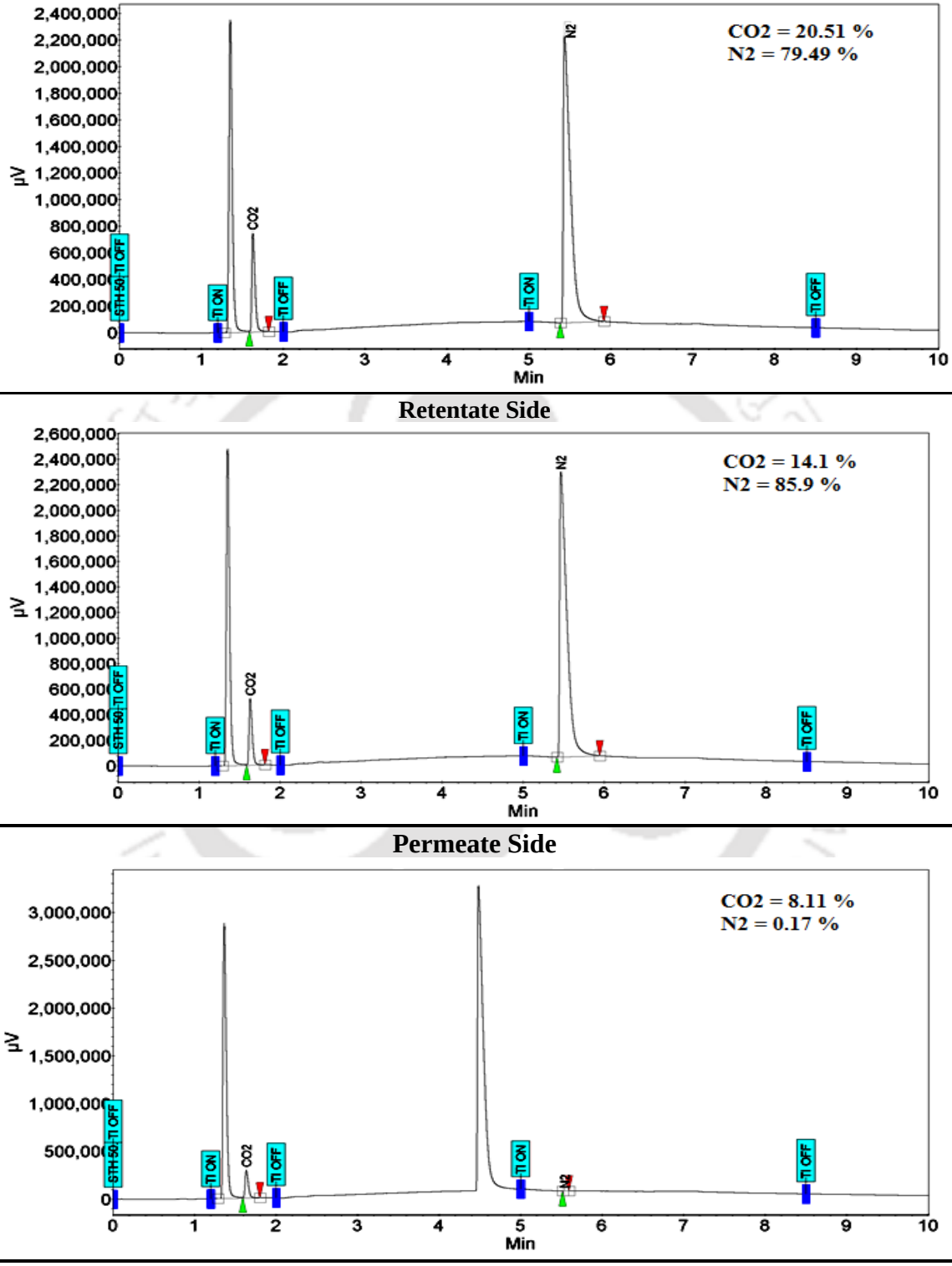

Figure A2.69 Effect of Feed Absolute Pressure = 4.94 atm, (15% AHPD+25% PAA)

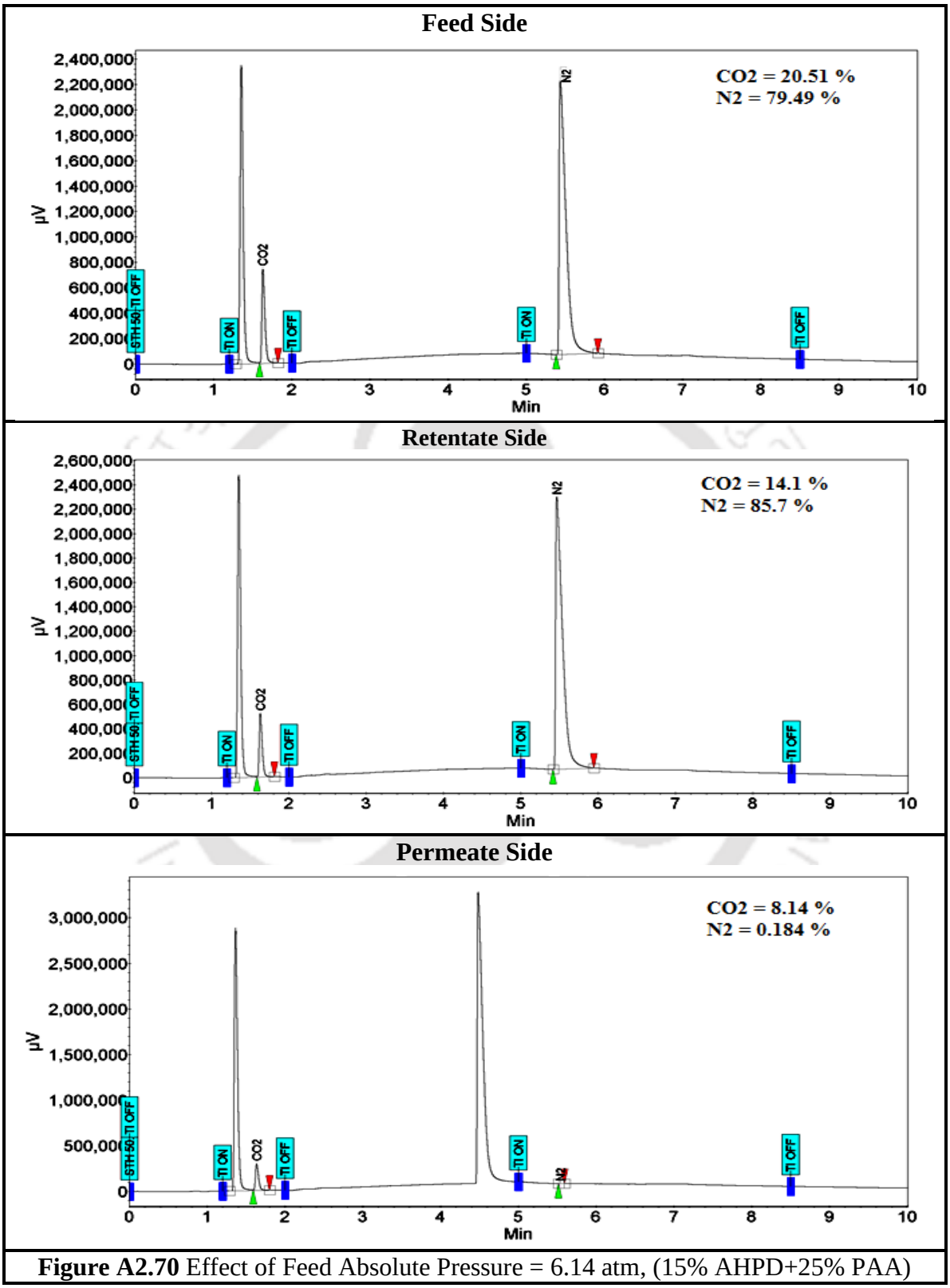

Figure A2.70 Effect of Feed Absolute Pressure = 6.14 atm, (15% AHPD+25% PAA)

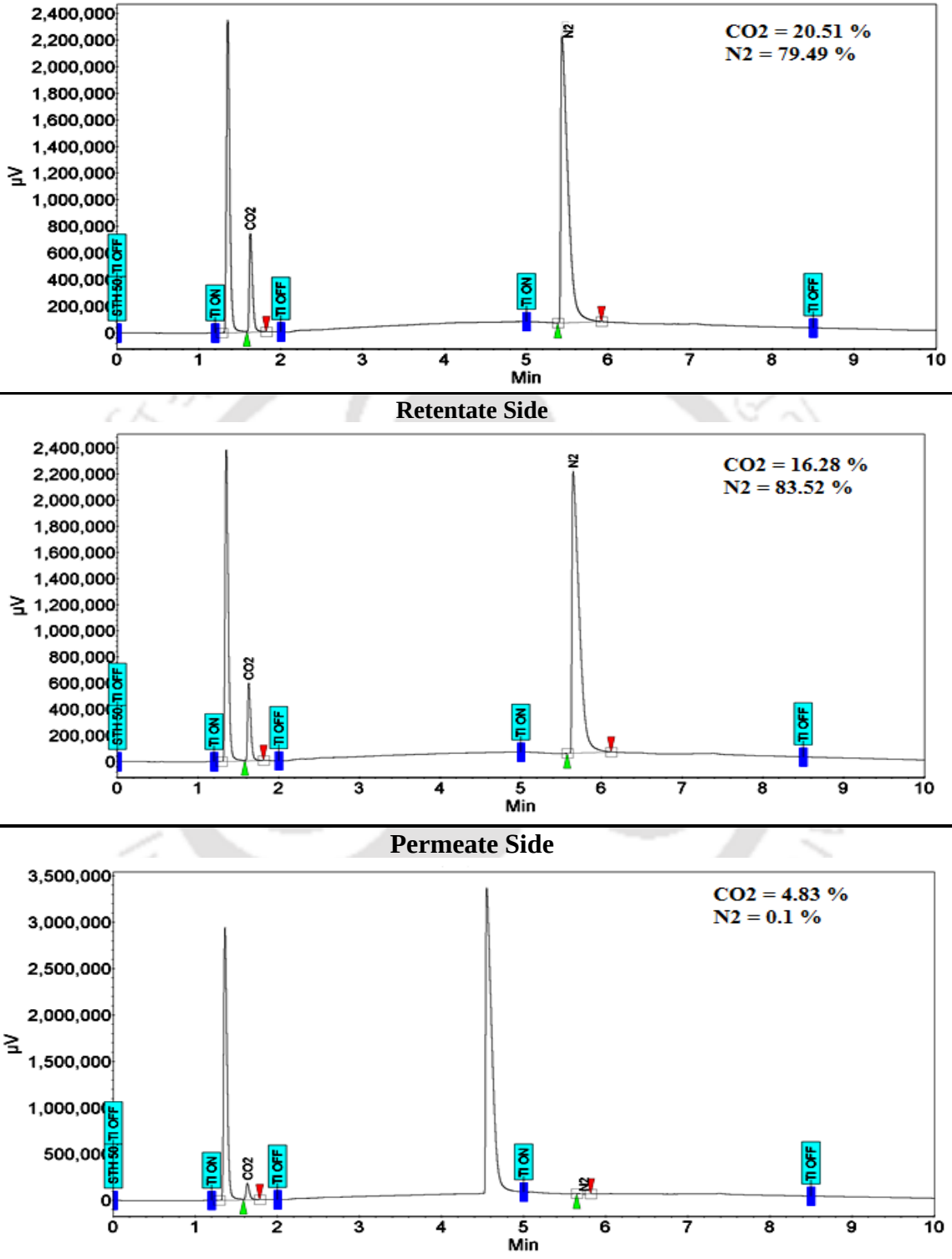

Figure A2.71 Effect of sweep side water flow rate = 0.02 ml/min, (15% AHPD+25% PAA)

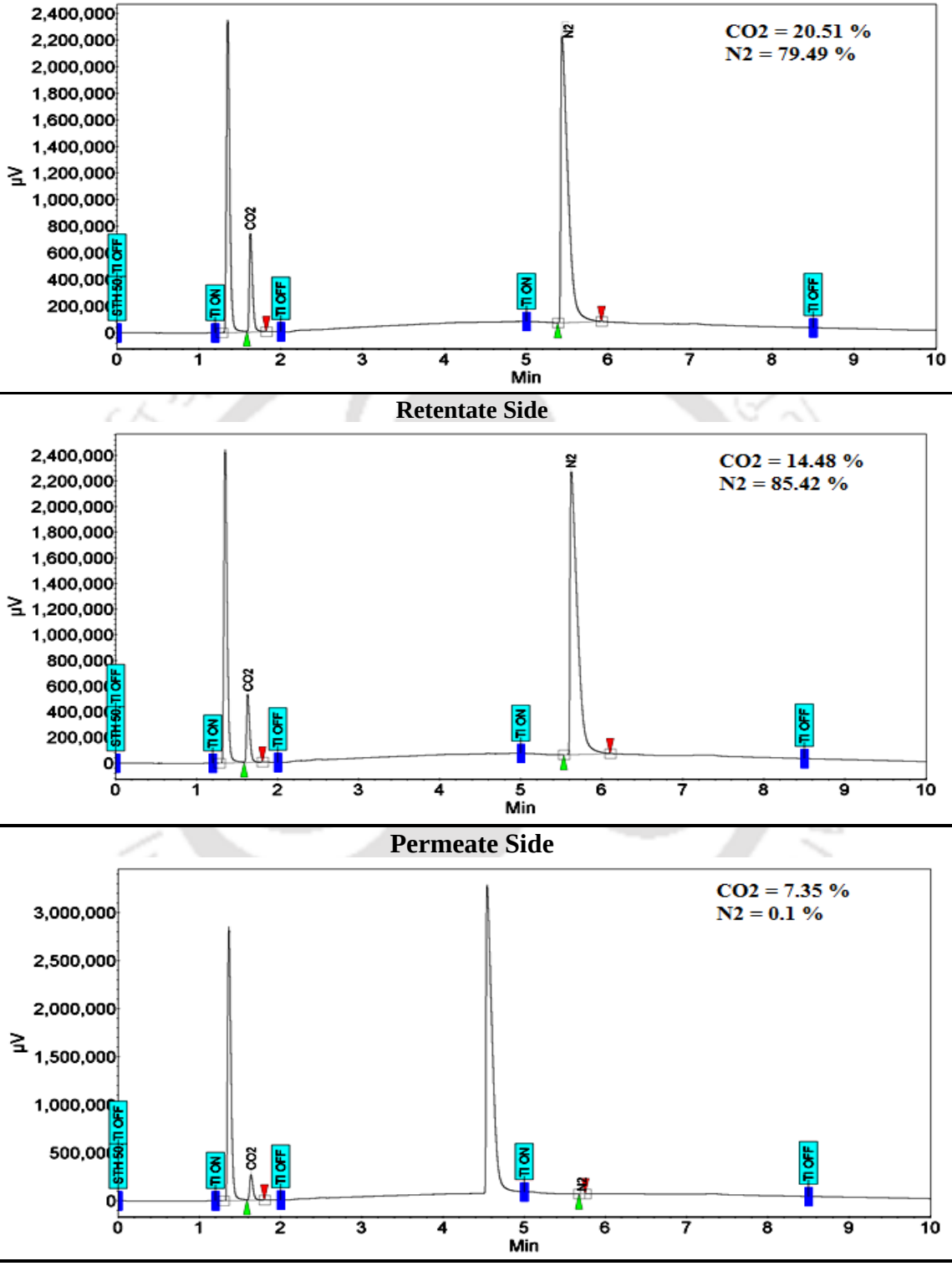

Figure A2.72 Effect of sweep side water flow rate = 0.04 ml/min, (15% AHPD+25% PAA)

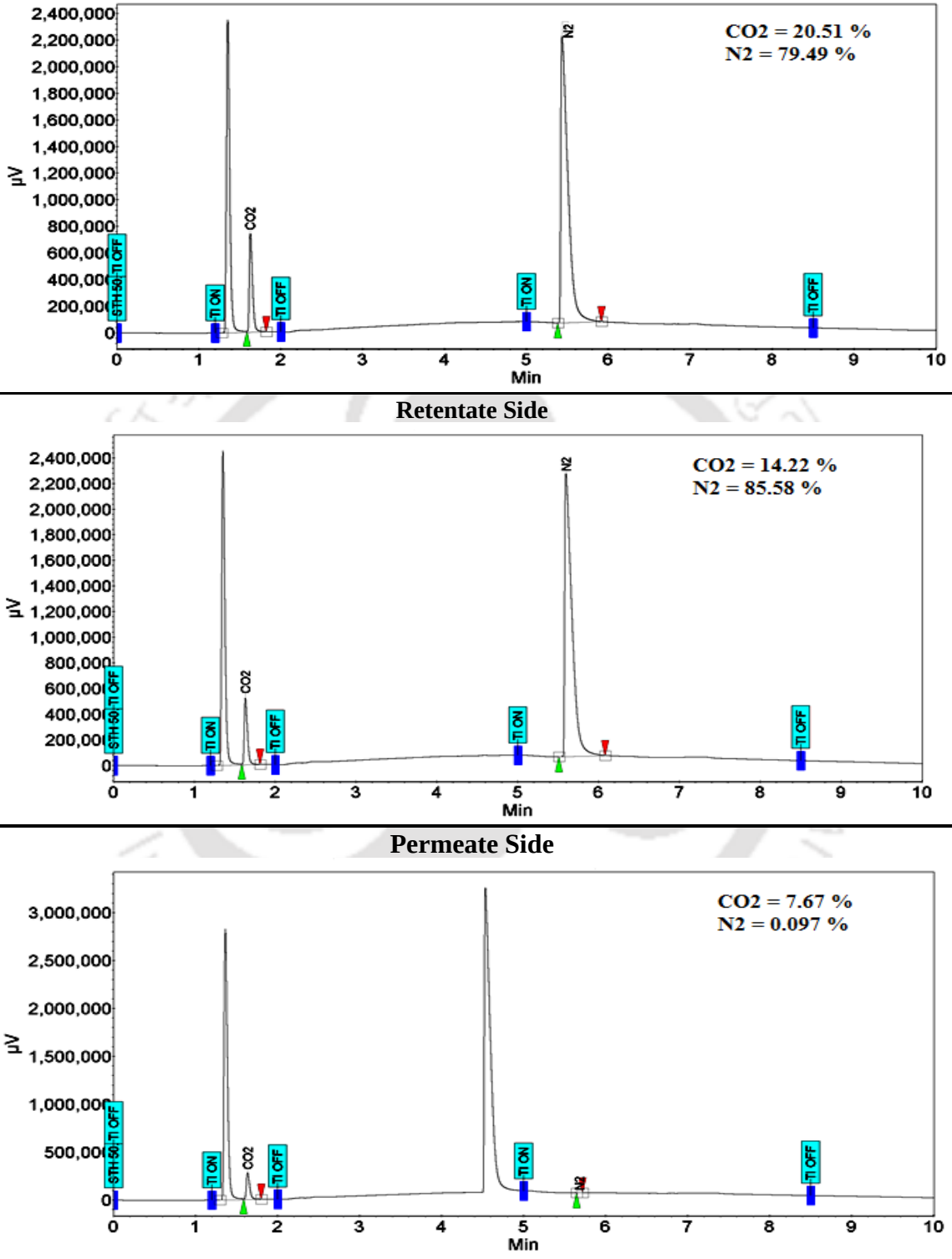

Figure A2.73 Effect of sweep side water flow rate = 0.06 ml/min, (15% AHPD+25% PAA)

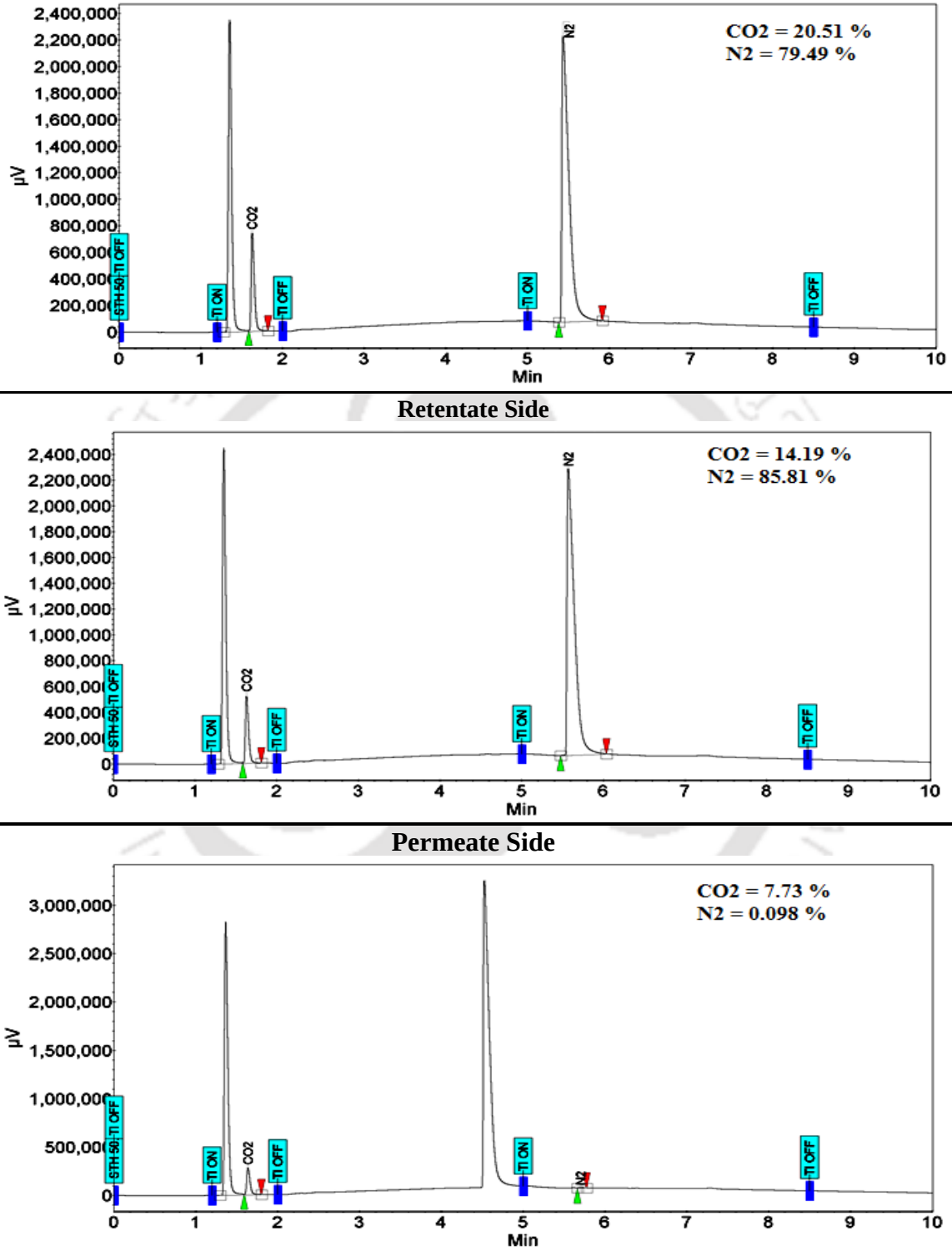

Figure A2.74 Effect of sweep side water flow rate = 0.075 ml/min, (15% AHPD+25% PAA)

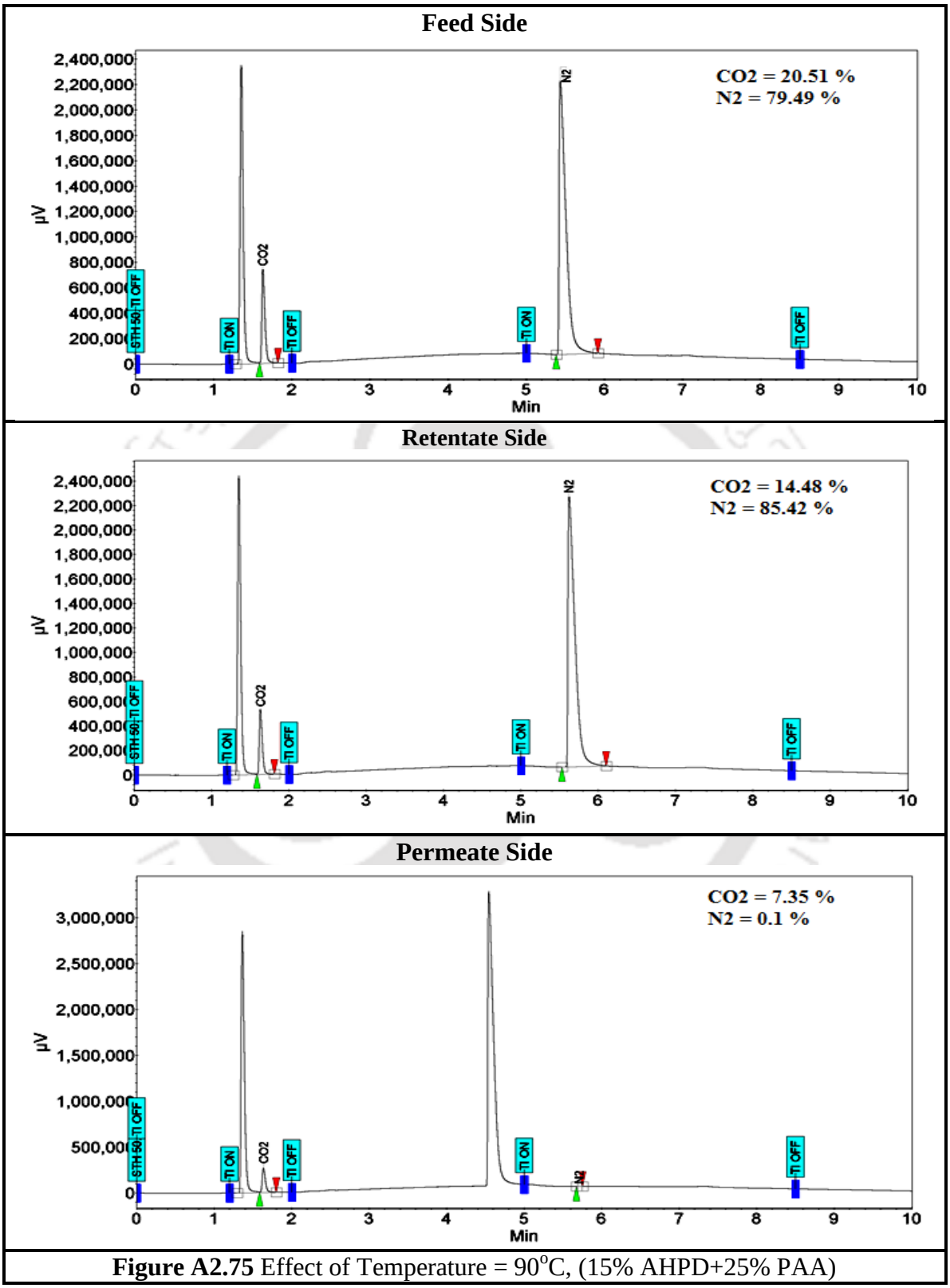

Figure A2.75 Effect of Temperature = 90°C, (15% AHPD+25% PAA)

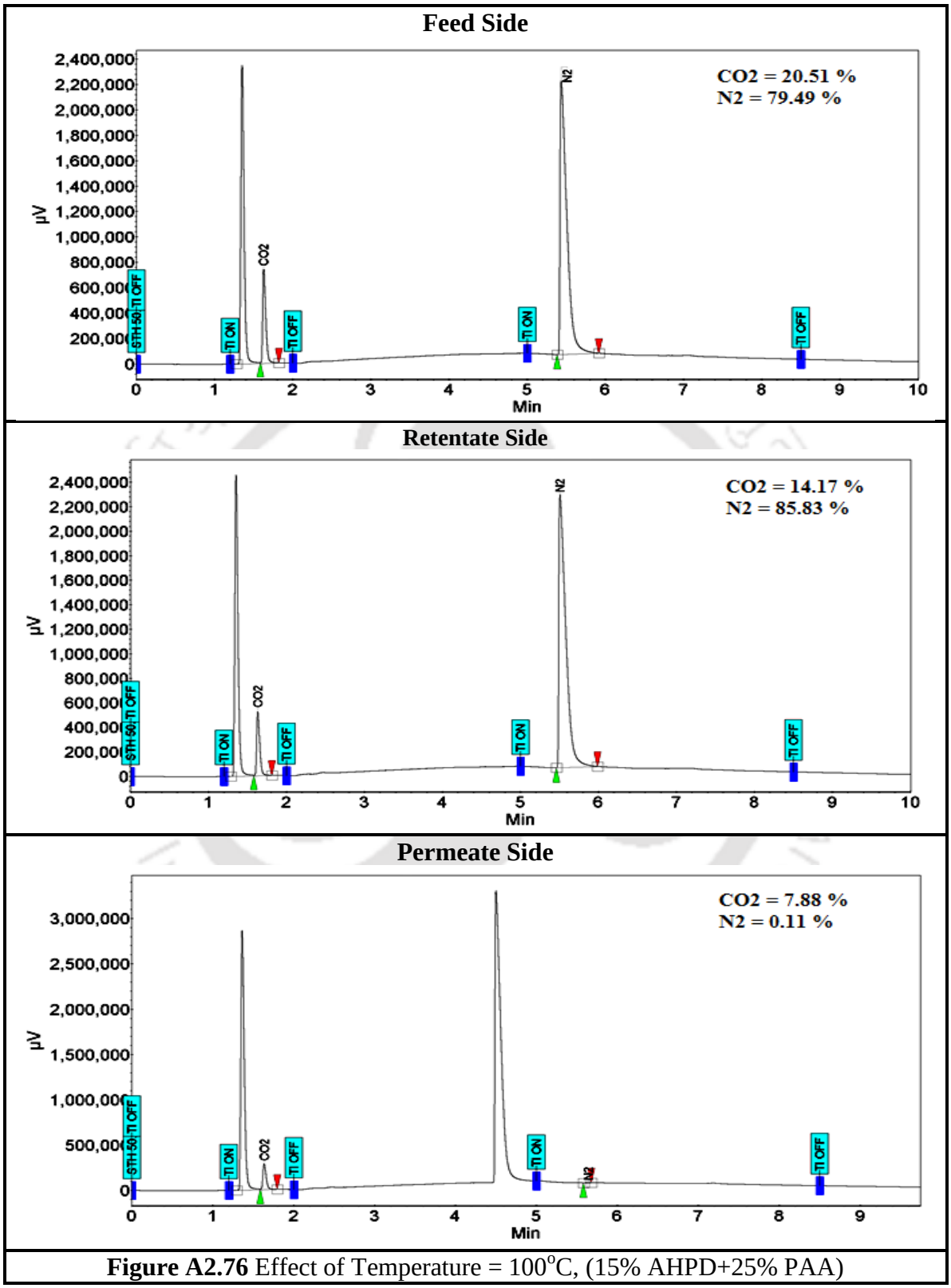

Figure A2.76 Effect of Temperature = 100^{o}C, (15% AHPD+25% PAA)

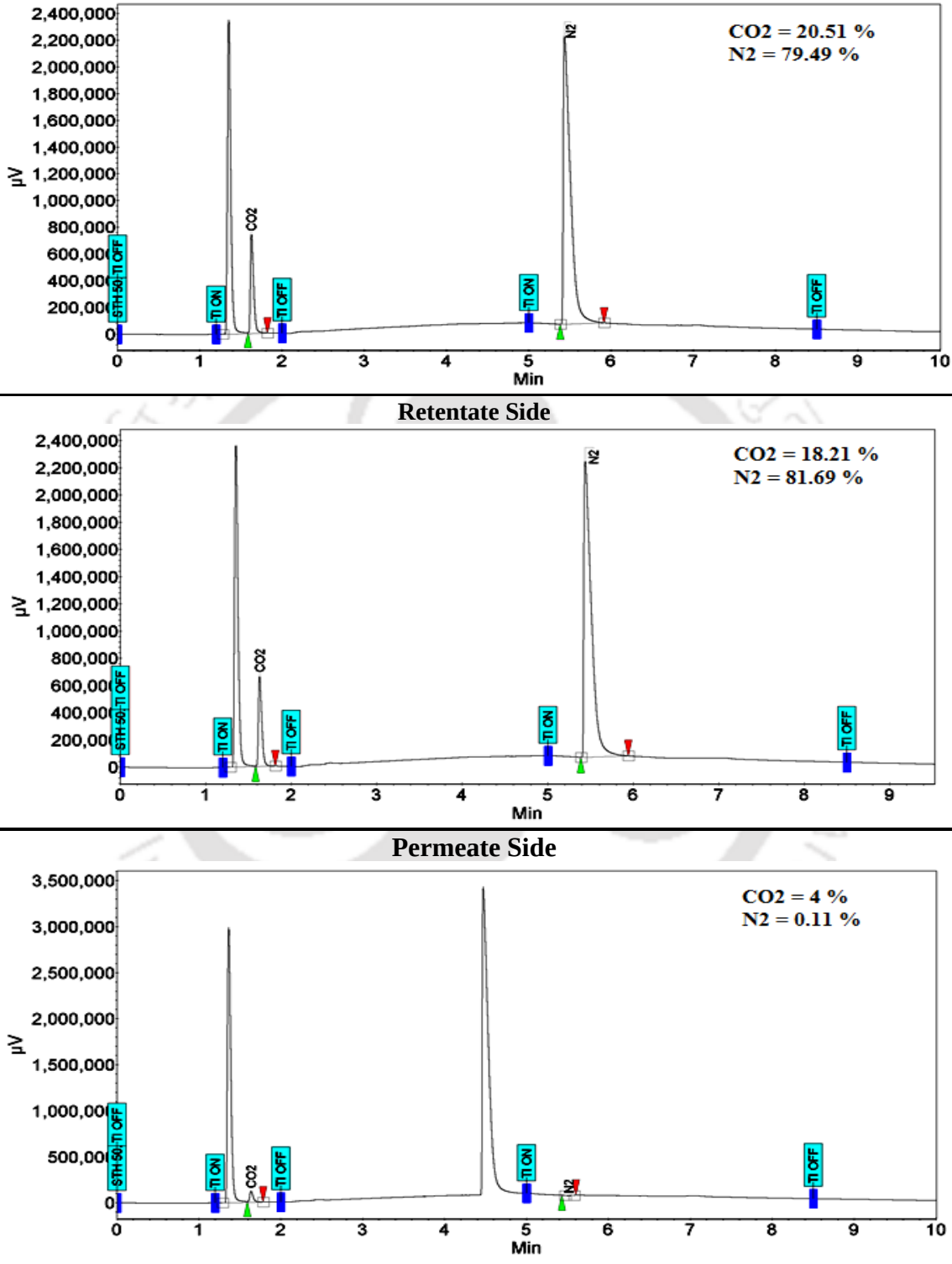

Figure A2.77 Effect of Temperature = 115^{o}C, (15% AHPD+25% PAA)

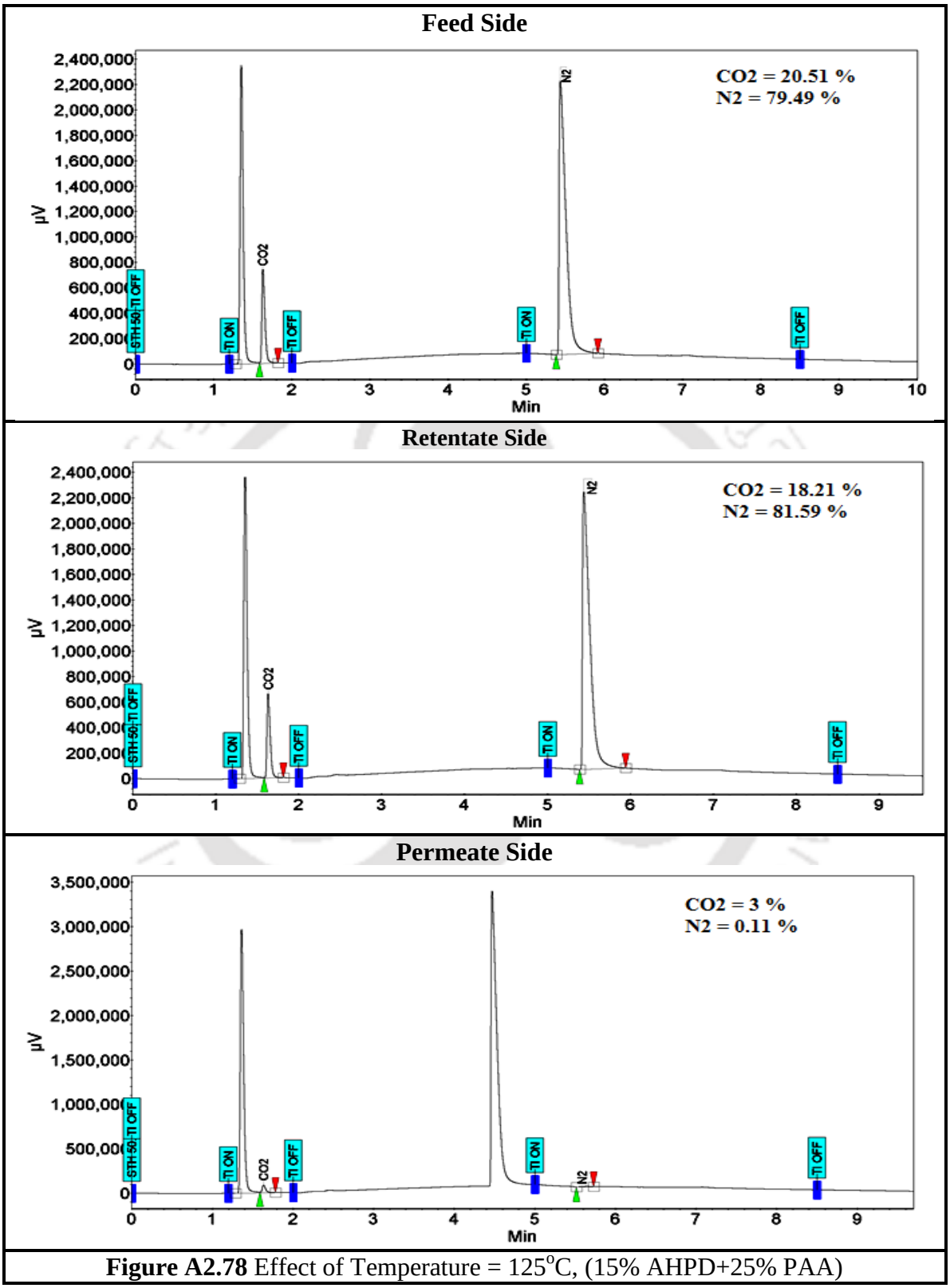

Figure A2.78 Effect of Temperature = 125°C, (15% AHPD+25% PAA)